NUREG/CR-3468
SAND84-0383
R3
Printed December 1986

Hydrogen:Air:Steam Flammability Limits and Combustion Characteristics in the FITS Vessel

Billy W. Marshall, Jr.

Prepared by
Sandia National Laboratories
Albuquerque, New Mexico 87185 and Livermore, California 94550
for the United States Department of Energy
under Contract DE-AC04-76DP00789

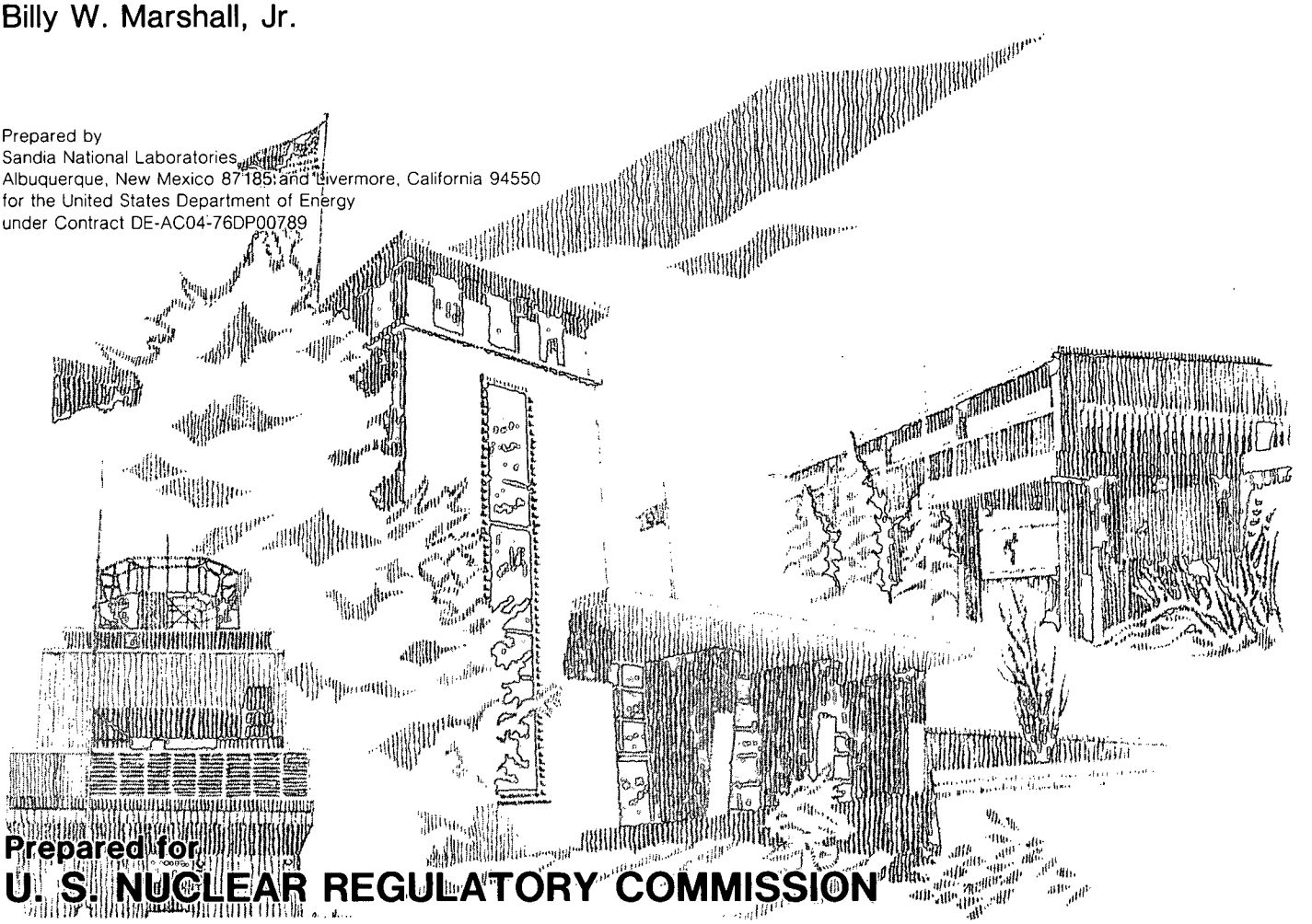

Prepared for
U. S. NUCLEAR REGULATORY COMMISSION

Available from

Superintendent of Documents
U.S. Government Printing Office
Post Office Box 37082
Washington, D.C. 20013-7982

and

National Technical Information Service
Springfield, VA 22161

NUREG/CR-3468
SAND84-0383
R3

HYDROGEN:AIR:STEAM FLAMMABILITY LIMITS AND COMBUSTION CHARACTERISTICS IN THE FITS VESSEL

by

Billy W. Marshall, Jr.

December 1986

Sandia National Laboratories
Albuquerque, New Mexico 87185
Operated by
Sandia Corporation
for the
U. S. Department of Energy

Prepared for
Division of Reactor System Safety
Accident Evaluation Branch
Office of Nuclear Regulatory Research
U. S. Nuclear Regulatory Commission
Washington, DC 20555
Under Memorandum of Understanding DOE 40-550-75
NRC FIN A1246

ABSTRACT

For the past few years, the United States Nuclear Regulatory Commission has sponsored research at Sandia National Laboratories addressing the combustion characteristics and flammability limits of combustible atmospheres that might occur inside containment during a loss-of-coolant accident inside a pressurized water reactor (PWR). Combustion of certain hydrogen:air:steam atmospheres could, at least hypothetically, threaten the integrity of the containment structure. To assist in the resolution of these issues, a series of 239 hydrogen:air:steam combustion experiments was performed in a 5.6 m^3 vessel.

Experimentally observed flammability limits of hydrogen:air:steam mixtures in both turbulent and quiescent environments were measured and a correlation developed that describes the three-component flammability limit. The newly developed correlation can be used to estimate the flammability of a mixture at these scales and larger scales to obtain approximate ignition conditions.

Transient combustion pressures of hydrogen:air mixtures were found to increase with increasing hydrogen concentrations up to ~30%, at which point a decrease was observed with further increases in the hydrogen concentration. More severe combustion environments occurred for tests initially at ambient temperature (~300 K) than for those initially at elevated temperatures (~385 K) due to decreases in the bulk gas density with increases in the gas temperature. The transient combustion-pressure data measured for the hydrogen:air:steam tests indicate that the addition of steam reduces the normalized peak combustion pressure (P_{max}/P_o) as compared to equivalent hydrogen:air burns. Furthermore, turbulence was found to affect the extent of combustion and other combustion characteristics of the lean hydrogen burns (i.e., $\leq$10% hydrogen by volume) where bouyancy governs flame propagation. However, burns containing richer hydrogen concentrations were not appreciably affect by turbulence.

The experimentally measured pressure decays were used to infer the "global" total, radiative, and convective heat transfer characteristics during the postcombustion cooling phase. Convection was found to dominate the time-integrated heat transfer (i.e., energy deposition) of the leaner (<10%) hydrogen:air burns, accounting for 50 to 70% of the postcombustion heat transfer. In contrast, radiation was slightly more prevalent than convection for the hydrogen:air burns near stoichiometry. When moderate quantities of steam were added to the environment, radiation became the dominant postcombustion (or time-integrated) cooling mechanism due to the increase in bulk gas emittance. If richer steam concentrations (i.e., >~30% by volume) were added to the environment, radiation and convection appear to be equally important heat transfer mechanisms.

TABLE OF CONTENTS

LIST OF FIGURES

ACKNOWLEDGMENTS

This work was supported by the U. S. Nuclear Regulatory Commission under the direction of Dr. P. Worthington and Dr. J. Larkins. Special thanks to A. C. Ratzel for his constructive criticisms and support during this work. The suite of computer programs developed by A. Ratzel and coworkers, referred to as SMOKE, has been extensively used to analyze many of the combustion tests described in this document. The use of this analysis tool has greatly enhanced the results and interpretations presented.

M. Turner, G. B. StClair and J. Balkenbush of the KTech Corporation assisted in the experimental work at the FITS facility. M. Turner, in particular, was instrumental in conducting these experiments and the subsequent data reduction. W. Schmidt also assisted in the posttest data processing. Without the professional attitude and expertise of these personnel, this work would not have been so successful.

M. Berman was also an important, integral part of this work. Without his continued support, enthusiasm, encouragement, and understanding during this work, it would not have been published in such an extensive format. To these and others I unintentionally failed to mention, I appreciate their constructive criticism, encouragement, and useful dialogue during this work.

EXECUTIVE SUMMARY

For the past few years, the United States Nuclear Regulatory Commission has sponsored research at Sandia National Laboratories addressing the combustion characteristics and flammability limits of combustible atmospheres that might occur inside containment during a loss-of-coolant accident inside a pressurized water reactor (PWR). Combustion of certain hydrogen:air:steam atmospheres could, at least hypothetically, threaten the integrity of the containment structure. Furthermore, the survivability of safety-related equipment and exposed cables is of concern due to the severe temperatures and heat flux conditions during and following combustion. To assist in the resolution of these issues, a series of 239 hydrogen:air:steam combustion experiments was performed in the 5.6 m^3 Fully Instrumented Test Site (FITS) vessel located at Sandia National Laboratories in Albuquerque, New Mexico. This test series incorporated air partial pressures of ~83 kPa (at the desired temperature) with both turbulent (fans on) and quiescent (fans off) preignition conditions.

This work provides an extensive data base for hydrogen:air:steam combustion characteristics and flammability limits at intermediate scale. Experimentally observed flammability limits of hydrogen:air:steam mixtures in both turbulent and quiescent environments were measured and a correlation developed that describes the three-component flammability limit. The correlation can be used to estimate the flammability of a mixture at these scales and at larger scales to obtain approximate ignition conditions.

Transient combustion pressures were measured for all experiments. The normalized peak pressure was found to increase with increasing hydrogen concentrations up to ~30%, at which point a decrease was observed with further increases in hydrogen concentration. For ambient (~300 K) and elevated temperature (~385 K) tests, the volume fractions of hydrogen, air and steam were computed at the prevailing temperature. At elevated temperatures, fewer moles of hydrogen and oxygen (or air) would be available for combustion since the densities of the gases are lower. Therefore, more severe combustion environments would be expected to occur, and did occur, for the tests at ambient temperatures. Steam was found to reduce the normalized peak combustion pressure (P_{max}/P_o) compared to equivalent hydrogen:air burns. Comparison of the experimentally measured peak pressure to the calculated Adiabatic Isochoric Complete Combustion (AICC) pressure also indicates that relatively complete combustion occurs (>95%) for hydrogen concentrations greater than ~10%. The extent of combustion for those tests containing less than about 10% hydrogen, by volume, appeared to be a strong function of the preignition turbulence. For quiescent conditions, the combustion completeness appeared to decrease as the two- and/or three-component flammability limit was approached. The level of preignition turbulence affected both the combustion completeness and general combustion characteristics of the lean hydrogen burns where buoyancy governs flame propagation in the absence of turbulence. As expected, preignition turbulence did not appear to significantly affect the extent of combustion or combustion characteristics of the richer hydrogen burns (i.e., >15% hydrogen by volume).

The experimentally measured pressure decays were used to infer the "global" postcombustion heat transfer characteristics. The term "global" implies a spatially averaged property which is inferred from the experimentally-measured pressure decay. The actual "local" conditions may be somewhat different for the lean hydrogen concentrations where relatively slow and incomplete burning may occur, although these "global" estimates appear to be representative of the actual phenomena when complete and rapid combustion occurs. The partitioning of the "global" energy deposition and peak heat flux into radiation and convection was also estimated. Convection was found to dominate the time-integrated heat transfer (i.e., energy deposition) of the leaner (<10%) hydrogen:air burns, accounting for 50 to 70% of the post-combustion heat transfer. In contrast, radiation was slightly more prevalent than convection for the hydrogen:air burns near stoichiometry. The peak heat flux results showed that radiation was the dominant early-time heat transfer mechanism for burns near stoichiometric conditions, as might be expected, while convection governed the lean hydrogen burns (<10%).

When moderate quantities of steam (<20% by volume) were added to the environment, radiation became the dominant postcombustion (or time-integrated) heat transfer mechanism due to the increase in bulk gas emittance. However, these steam concentrations did not appear to reduce the total postcombustion heat transfer, indicating that relatively complete combustion had occurred. For the very rich steam concentrations (i.e., above ~30% by volume), radiation and convection were equally important cooling mechanisms. Also, for these rich steam environments, the total energy deposition decreased slightly compared to equivalent hydrogen:air burns; e.g., evaluating these results as a function of the hydrogen-to-air ratio, the total energy deposition decreased slightly with increasingly rich steam concentrations. These results are consistent with expected trends since steam acts as an inert heat sink reducing the bulk gas temperature and, with the addition of very rich steam concentrations, the combustion of hydrogen with available oxygen would be inhibited. Finally, comparisons to the large-scale NTS results show that the radiative fraction of the total energy deposition was approximately half that observed during in the NTS tests. This is a scale phenomena and reflects the differences in radiation length-scales between the two facilities.

These data are useful for benchmarking existing computer codes such as HECTR and CONTAIN for hydrogen:air:steam combustion phenomena at these scales (~5 m^3). The "global" heat transfer data and experimentally measured pressure histories are also important for future combustion modelling and experimental analysis efforts.

1. INTRODUCTION

1.1 Background

The U. S. Nuclear Regulatory Commission and the reactor safety community have long been aware of the potential threat to containment due to the combustion of hydrogen mixtures during a hypothetical Light Water Reactor (LWR) accident. It has been postulated that combustion of hydrogen:air:steam atmospheres could lead to a breach of the containment building, due to the transient pressures and dynamic loading of the containment structure, and ultimately release radioactive material into the environment. Equally important are the extreme temperatures and heat flux conditions associated with combustion and postcombustion cooling. These harsh environments may damage important safety-related equipment, hampering the normal safety procedures used during and following an accident.

The accident at Three-Mile Island (TMI), Unit 2, is the most recent example of a loss-of-coolant accident (LOCA) in a LWR. As the fuel rods heated up, the Zircaloy metal cladding reacted with available steam to produce hydrogen, some of which remained in the primary system, was dissolved in the remaining coolant, or was released by an operator through the pressurizer into the containment building. During the accident, an estimated 280 to 370 kg of hydrogen was generated, resulting in a nearly uniform hydrogen concentration of 7.3 to 7.9% by volume [1]. At approximately 10 hours after the turbines tripped, a hydrogen burn occurred, resulting in a transient peak pressure inside containment which exceeded 190 kPa (28 psig) over a burn time of ~12 s.

During hypothetical LOCAs, hydrogen, air, and steam will be evolved producing a potentially flammable mixture of gases. The actual quantities and concentrations of each of these gases will depend upon the accident scenario considered. Other combustible gases may be present in the atmosphere but are generally assumed to be unimportant when compared to the concentrations of hydrogen [2, 3, 4]. This work considers the deflagration of mixtures of hydrogen, air and steam but does not address issues related to detonations, flame acceleration, transition from deflagration to detonation, or diffusion flames. Furthermore, since mixtures of hydrogen, air and steam are considered, the "limits of flammability" (generally referring to the two-gas flammability limit) will be broadened here to include the three-component mixture which is inerted.

1.2 Literature Review

During a hypothetical degraded-core accident, the initial conditions inside containment prior to ignition and combustion of the atmosphere will include an elevated atmospheric pressure and temperature along with various concentrations of hydrogen and steam. The flammability limits and combustion characteristics of a hydrogen:air:steam environment have been considered by numerous authors. A few of these studies are briefly reviewed below.

Figure 1 shows the work of Shapiro and Moffette [5] and Zabetakis [6] which define the regions of flammability of hydrogen:air:steam mixtures. Figures 2 and 3 show an accumulation of the flammability data by Berman and Cummings [7] for hydrogen:air:steam mixtures which have been reported by various research facilities throughout the world. (Details of the experiments comprising the data base shown in Figures 2 and 3 can be found in References 6 and 8 through 14). Note that Figure 2 shows mixtures which were in a quiescent (or fans-off) state at the time of ignition, while Figure 3 shows mixtures that were in a turbulent (or fans-on) state.

The discrepancies observed from this data base have been largely attributed to differences in initial temperature, although subtle differences in the vessel geometry (i.e., surface area and volume) and initial pressure will have an effect. These differences, especially in the "knee" region of the curve at about 10% hydrogen, make a clear definition of the lean flammability limit difficult. Furthermore, the current body of data for turbulent mixtures is somewhat incomplete and again difficult to draw conclusions from for reactor safety analysis. These data for turbulent environments are especially important in reactor safety analysis since fans and possibly sprays may be operational at the time of ignition.

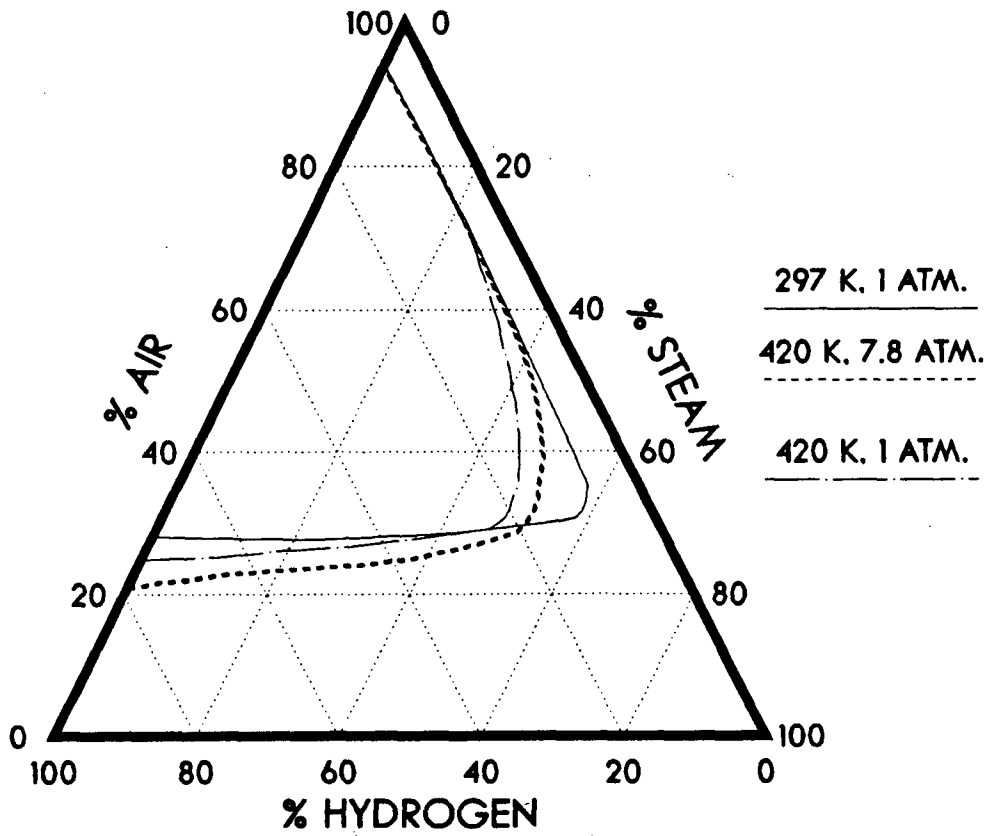

Figure 1
Flammability Limits of Hydrogen:Air:Steam
Mixtures (taken from Reference 5)

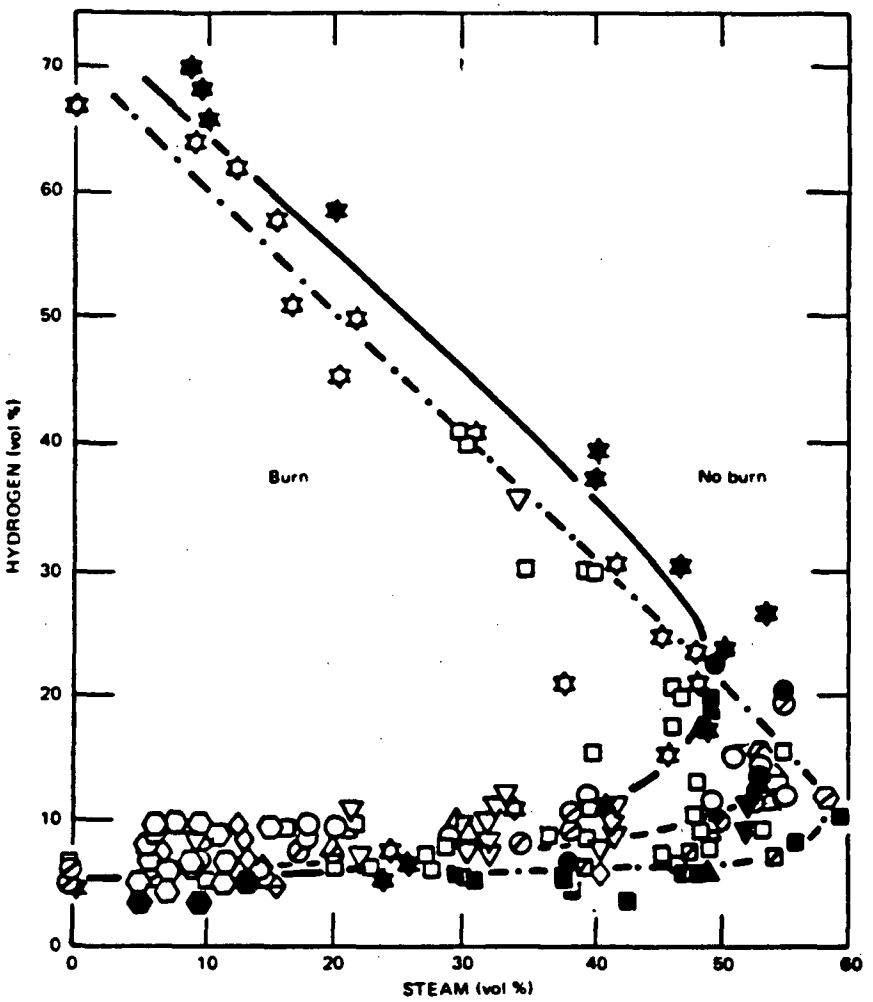

	FITS	WNRE	TVA	Fenwal	LLNL	WNRE	BM
Burn	□	○	△	◇	▽	○	✡
No burn	■	●	▲	◆	▼	●	✱
Marginal	▨	⊘	◬	◈	⩛	⊘	
T_0, K (°C)	383 (110)	353-368 (80-95)		333-473 (60-100)	T_{sat}	356 (83)	422 (149)
P_0, kPa (atm)	101 (1)	101 (1)		141.4 (1.4)	110-283 (1.1-2.8)	91-101 (0.9-1)	101 (1)

Figure 2
Flammability Limits for Hydrogen:Air:Steam Mixtures with Fans Off (taken from Reference 7). {FITS, Fully Instrumented Test Site (Sandia National Laboratories); WNRE, Whiteshell Nuclear Research Establishment (Canada); TVA, Tennessee Valley Authority; Fenwal, Fenwal, Inc.; and LLNL, Lawrence Livermore National Laboratories.}

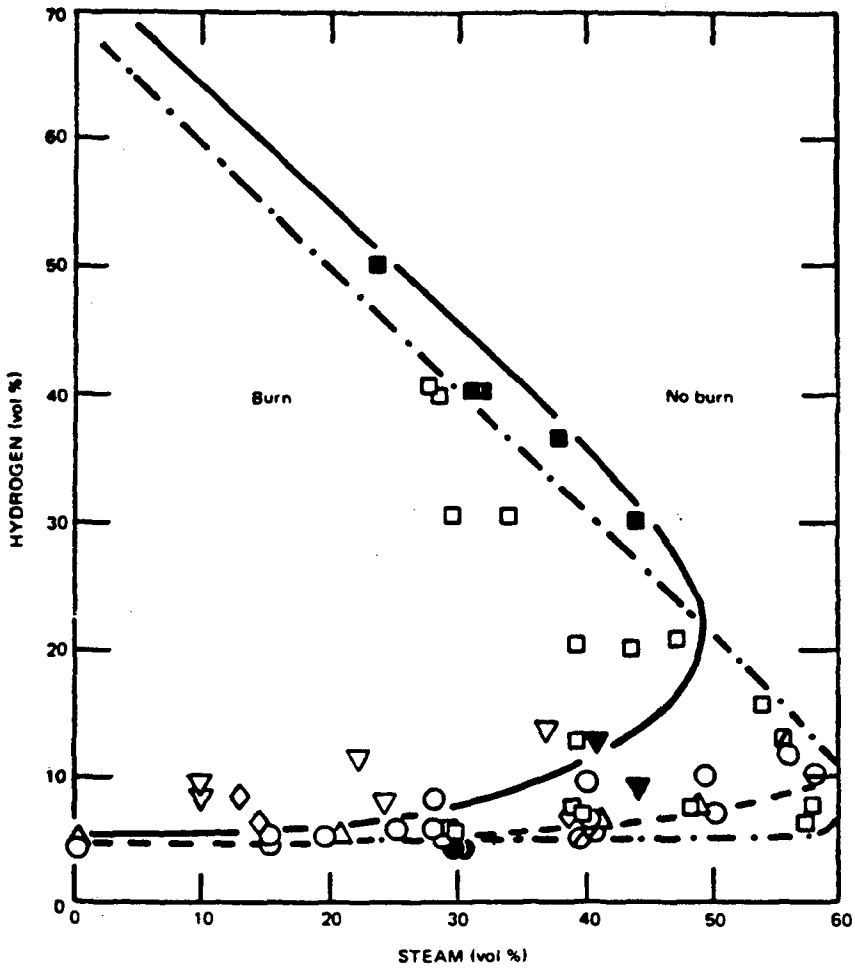

	FITS	WNRE	TVA	Fenwal	LLNL
Burn	□	○	△	◇	▽
No burn	■	●	▲	◆	▼
Marginal	⊠	⊘	⧋	◈	⧩
T_0, K (°C)	383 (110)	353-368 (80-95)		333-473 (60-100)	T_{sat}
P_0, kPa (atm)	101 (1)	101 (1)		141.4 (1.4)	110-283 (1.1-2.8)

Figure 3
Flammability Limits for Hydrogen:Air:Steam Mixtures with Fans On (taken from Reference 7). {FITS, Fully Instrumented Test Site (Sandia National Laboratories); WNRE, Whiteshell Nuclear Research Establishment (Canada); TVA, Tennessee Valley Authority; Fenwal, Fenwal, Inc.; and LLNL, Lawrence Livermore National Laboratories.}

The most complete and comprehensive work related to the flammability limits of gases available in the literature has been prepared by Coward and Jones of the Bureau of Mines [15]. This work reviews the limits of flammability for numerous combustible gases with air or oxygen (i.e., the two-component flammability limit). The flammability limits were defined in this work as:

> "the borderline composition; a slight change in one direction produces a flammable mixture, in the other direction a non-flammable mixture."

From the Coward and Jones study, the flammability limits of hydrogen:air mixtures were observed to widen as the vessel diameter increased, rapidly at first and more slowly afterward. In general, increases in the vessel diameter above 5 cm rarely showed an increase of more than a few tenths of one percent in the range of flammability. The limits were also shown to not be appreciably affected by normal variations in atmospheric pressure although they were narrowed slightly at elevated pressures. Increasing the bulk gas temperature was also observed to widen both the upper and lower hydrogen:air flammability limit. At standard conditions, the lower flammability limit for hydrogen:air mixtures was reported to be 4.0% hydrogen (by volume) while the upper limit was 75% hydrogen.

The characteristics of the hydrogen:air combustion process have been studied by numerous authors [13, 16, 17, 18, 19, 20]. One of the most recent experimental studies was performed by Benedick and coworkers who studied the combustion characteristics of hydrogen:air and hydrogen:air:carbon dioxide mixtures in the Variable Geometry Experimental System (VGES) vessel located at Sandia National Laboratories [16]. This 5-cubic-meter cylindrical vessel was used to perform eleven test series in which over 100 combustion experiments were conducted. During this study, it was observed that the combustion process of hydrogen:air mixtures containing less than ~8% hydrogen (by volume) was governed by the preignition turbulence. Higher peak pressures were observed for the turbulent (fans on) tests compared to equivalent quiescent (fans off) tests. This is probably due to the different horizontal and downward propagation limits for quiescent mixtures of the hydrogen:air. Another interesting observation was the fact that the normalized peak pressure (P_{max}/P_o) fell away from the Adiabatic Isochloric Complete Combustion (AICC) [21] calculation as the volumetric hydrogen concentrations exceeded ~10%. This is contrary to expected trends since combustion of rich hydrogen concentrations (>10%) occurs very rapidly compared to leaner (<10% hydrogen) burns, consuming most of the hydrogen and decreasing the heat transfer from the flame zone to the surroundings on the time-scale of combustion. Carbon dioxide diluent in the combustible mixture was found to reduce the peak pressures, pressure differential, burn velocity, and pressure rise time. It was also determined that 54% carbon dioxide (by volume) would inert any hydrogen:air mixture.

A study of hydrogen:air:steam combustion characteristics in a 2.3 m-diameter sphere (volume of 6.4 m^3) was performed by Kumar, Tamm, and Harrison of the Electric Power Research Institute (EPRI) [17]. This research demonstrated that at low hydrogen concentrations (4 - 9%), turbulence and gratings within the vessel significantly increased the rate and extent of

combustion. Steam was shown to decrease the extent of combustion and also the normalized peak combustion pressures. As in Benedick's work [16], turbulence did not appear to greatly enhance the combustion characteristics of atmospheres containing hydrogen concentrations greater than ~10% although turbulence did enhance the lean combustion experiments. Even when 40% steam was present, complete combustion was observed for the richer concentrations of hydrogen, although the normalized peak combustion pressure was less than those measured for comparable hydrogen:air tests.

Recently, Ratzel analyzed data collected during the EPRI/EG&G combustion studies conducted in a 2048-cubic-meter spherical hydrogen dewar located at the Nevada Test Site (NTS) [18]. Mixtures of hydrogen, air, and steam were studied, with hydrogen concentrations ranging from 5 to 13% and steam concentrations from 4 to 40%. Some of the experiments incorporated spray systems, similar to those installed in LWRs, and fans which tended to enhance the combustion rate and significantly change the postcombustion heat transfer characteristics. The measured pressures during this series of tests indicate that combustion of lean hydrogen concentrations is incomplete, with slow burning and relatively small pressure increases. As the hydrogen concentration increases, the peak combustion pressure increased while the duration of combustion decreased as observed at smaller scales. The data-reduction program SMOKE was used to infer "global" gas temperatures and radiative, convective and total heat fluxes following combustion [22]. The inferred gas temperatures compared reasonably well with measured gas temperatures. Global estimates of the total peak heat fluxes were typically less than local measurements for lean combustion and higher for mixtures above 10% hydrogen. Global estimates of the radiative heat transfer were found to be 30 to 80% of the total heat transfer depending upon the hydrogen and steam concentration. Furthermore, for hydrogen concentrations greater than ~8%, radiation dominated the early postcombustion cooling phase, especially for tests with large initial steam concentrations. Combustion completeness data were also analyzed, indicating that relatively complete combustion occurs for hydrogen concentrations above ~8%.

1.3 Combustion Experiments Conducted at FITS

Combustion studies have also been conducted and reported in the 5.6 m^3 FITS cylindrical test vessel located at Sandia National Laboratories in Albuquerque, New Mexico. Currently, three studies have been reported in the literature. In the earliest of these studies, the effects of steam and carbon dioxide as a diluent were considered [13, 23]. Flammability limits of hydrogen:air:steam mixtures were addressed, but the matrix of experiments was incomplete and could not support any rigorous conclusions. Comparisons of the experimental pressure ratios to the AICC calculations [21] revealed experimental values which exceeded the AICC results as hydrogen concentrations exceeded about 15%. This trend contradicted those observed in similar work by Benedick et al., discussed briefly above [16]. These higher than expected pressures were later attributed to instrumentation and measurement problems. In particular, the harsh thermal environment during and following combustion affected the pressure transducer diaphragm and ultimately led to the misleading data and interpretations [24].

A series of hydrogen:air:steam burns was also conducted to evaluate the response of calorimeters and some reactor safety related equipment during hydrogen combustion for the Hydrogen Burn Survival Program [25]. Gas and component temperatures from twenty-one experiments were reported and, as expected, were found to increase with increasing hydrogen concentrations. Although the experiments revealed interesting results about component response during combustion at these scales, the results could not be used to infer component survivability during combustion inside an LWR containment building. This was due to the fact that the burn times and associated heat transfer were substantially shorter in the FITS tank than would be expected during a burn inside containment. These tests were intended, however, to benchmark code simulations at small-to-intermediate scales.

Most recently, a series of hydrogen:air tests were performed to evaluate the dynamic response of three pressure transducers during combustion [24]. This work showed that the harsh environment of combustion affected the response of a Precise Sensor model 111-1 gauge while not appreciably affecting the response of the other two gauges (a Precise Sensor model 141-1 and a Kulite model XT-190). Brunswick Felt Metal 1101 was also evaluated during this study and found to serve as an excellent thermal barrier while not affecting the response of the transducer to the transient pressure signature (this observation was validated only for deflagrations and pressure rise times greater than about 10 ms).

2. EXPERIMENTAL APPARATUS

2.1 The Fully Instrumented Test Site (FITS)

All of the combustion experiments discussed in this report were conducted at the Fully Instrumented Test Site (FITS) located at Sandia National Laboratories, Albuquerque, New Mexico. This vessel was originally designed and built by an NRC-funded research program investigating Molten Fuel-Coolant Interaction phenomena. It was modified for use by the NRC-supported hydrogen combustion behavior research program in 1981 [26].

The 5.6-cubic-meter cylindrical vessel is ~3.4 m tall with a diameter of ~1.5 m as shown in Figure 4. The vessel was built to ASME codes and has a design working pressure of 2.38 Mpa with a wall thickness of 2.86 cm. There is a 1.72 MPa burst disk in place during all testing for safety reasons. The upper head is removable and is attached to the vessel with 48 3.8 cm bolts. There are twenty-five port penetrations of various sizes most of which can be used for instrumentation access and gas feedthroughs. The port fittings and flanges were designed to high-pressure boiler standards and have been tested to 2.07 MPa. The vessel was typically instrumented with pressure gauges at the C- and E-port levels. Two of these ports (C-2 and E-2) had recessed flange inserts that positioned the front surface of a pressure transducer approximately flush with the inner tank wall. In a few tests, port E-1 was used which did not have a recessed insert, resulting in the front surface of the pressure transducer being approximately 18 cm from the inner tank wall. Additionally, hydrogen, steam, carbon dioxide, and nitrogen gas feedthroughs, an igniter and gas sampling system were positioned at the F port level and a

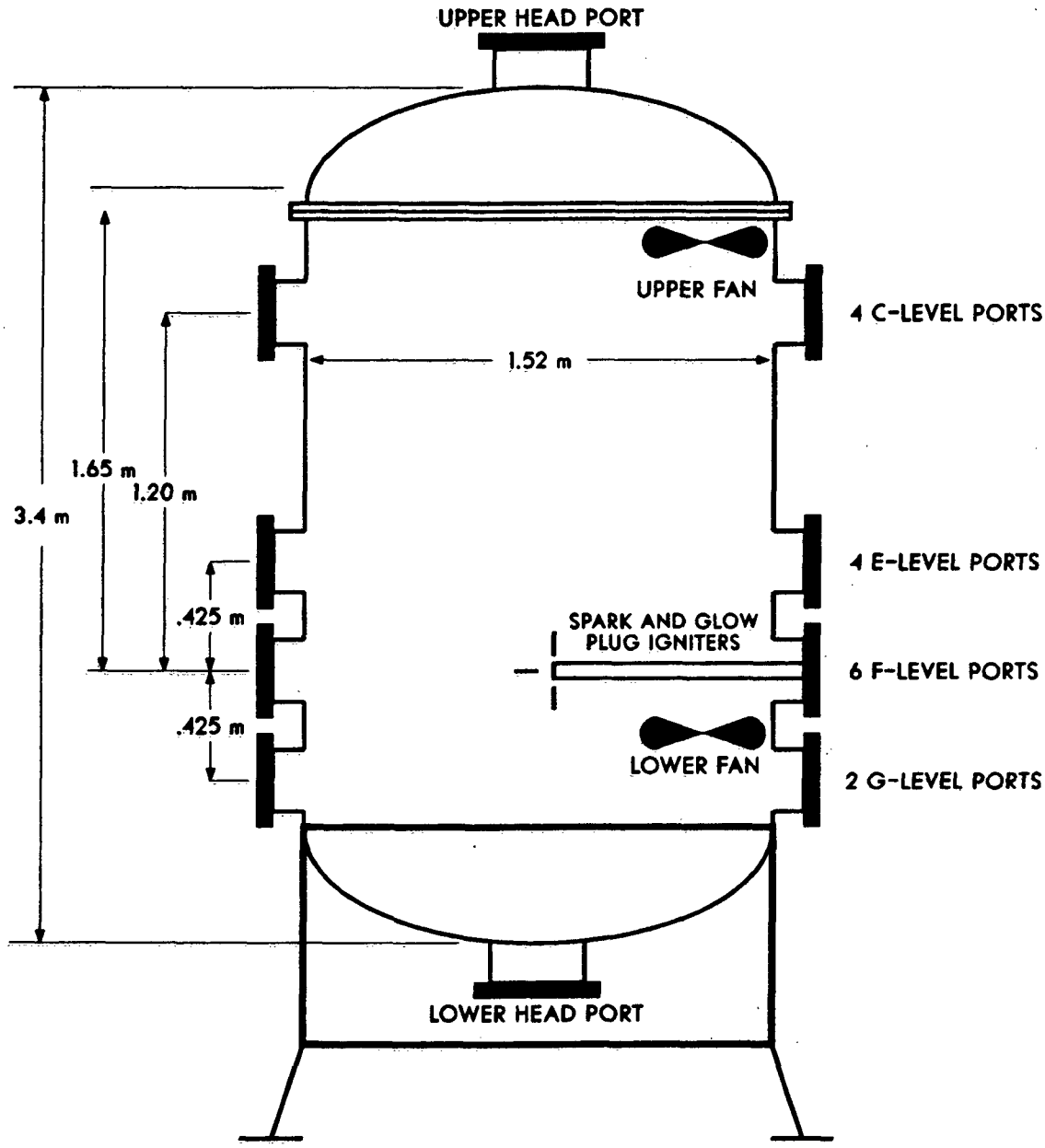

Figure 4
Schematic Drawing of the 5.6-cubic-meter FITS Vessel

liquid-ring pump at the G-level. A schematic of the facility, including the data acquisition and control room, is shown in Figure 5. Additional information on the FITS vessel and it's capabilities are available in References 13, 19, 20, 23, and 24.

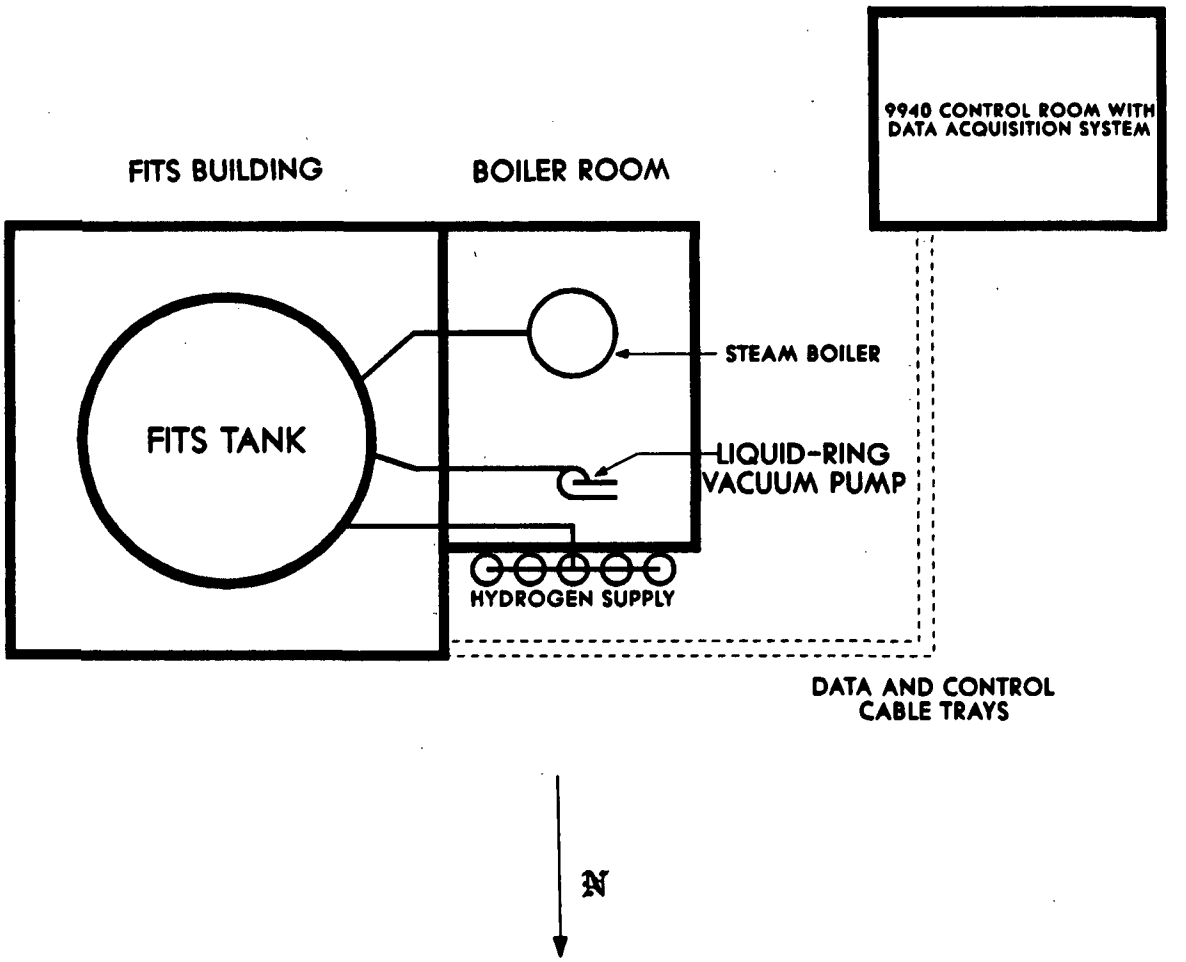

Figure 5
Schematic Drawing of the FITS Facility with Important Hardware Identified

2.2. Experimental Procedures

The hydrogen:air:steam combustion experiments were conducted in the following manner:

1. The tank was preheated to the desired temperature by injecting steam into the vessel and circulating steam around the heating coils surrounding the exterior of the vessel.

2. The tank pressure was vented out the bottom and top vents to atmospheric pressure.

3. The tank was sealed and a liquid-ring pump was used to evacuate the vessel to a pressure of ~13 kPa. The tank was then purged with atmospheric air from the top vent. This procedure (step 2 and 3) was repeated at least twice before each test.

4. The tank was sealed and allowed to come to an initial equilibrium pressure and temperature and the conditions recorded.

5. A prescribed quantity of hydrogen, determined using partial pressure calculations, was introduced and allowed to equilibrate with the air already in the vessel. Two pneumatic 14,200 LPM (500 CFM) fans were used to mix the hydrogen:air mixture. The equilibrium pressure and temperature was recorded for posttest calculations.

6. A prescribed quantity of steam (if desired) was added to the hydrogen:air mixture and mixed with the pneumatic fans. The equilibrium pressure and temperature was recorded for posttest calculations.

7. If the hydrogen:air:steam mixture was to be ignited in a quiescent state, the fans were turned off for ten minutes prior to ignition. If the mixture was to be ignited in a turbulent state, the fans were left operational throughout the experiment.

8. Once the desired initial conditions were achieved and recorded, either the glow plug or spark plug ignition source was energized remotely to initiate combustion.

9. The data acquisition system recorded the various instrumentation signals for ~5 s prior to combustion and ~30 s after ignition. The data were plotted and preliminary comparisons to the AICC and to one-another were performed before the next experiment was conducted.

Additional information about general procedures is available in References 13, 19, 20, 23, and 24.

2.3 Experimental Measurements

Two different pressure transducer models, the 141-1 gauge manufactured by Precise Sensor Inc. and the XT-190 gauge manufactured by Kulite Inc., were used to record the transient pressure signatures during these experiments. A detailed experimental study of these two gauges was performed at Sandia which indicate that these two pressure gauges record accurate pressure magnitudes and rise times for deflagration combustion experiments [24]. The Kulite XT-190, however, must be protected from the harsh thermal combustion environment (as suggested by the manufacturer) since the silicon diaphragm, on which a wheatstone bridge is bonded, is sensitive to elevated static and transient temperatures. The Kulite gauge has a perforated screen over the silicon diaphragm for protection, but is not designed for operation in transient thermal environments unless additional protection is provided. Therefore, a flame arrestor and thermal shield was used to protect these gauges. The thermal protection device incorporated Brunswick 1101 felt metal held in front of the gauge diaphragm with a steel insert. Based on the results obtained in Reference 24, felt metal serves as an excellent thermal barrier for deflagration type experiments since it does not change the transient pressure signature, the peak pressure magnitude or the pressure rise time.

The Precise Sensor 141-1 was the second gauge-type used during this experimental combustion study. This gauge is relatively insensitive to the transient thermal environment of combustion, although felt metal protection was incorporated in most experiments to ensure accurate results. The model 141-1 is a bonded strain-gauge-type transducer with the sensing element positioned approximately 5 cm from the front surface of the gauge housing. The sensing element consists of a stainless-steel diaphragm and strain-cylinder combination with a four-active-arm strain gauge permanently bonded to the cylinder. The Precise Sensor gauges were internally cooled with nitrogen gas through a baffle arrangement. A nominal inlet gauge pressure of 69 kPa was provided to the cooling manifold (resulting in a volumetric flow rate of approximately 1.42 LPM) in all experiments. The reader should refer to Reference 24 for a complete description and evaluation of the two gauges and thermal protection used in these experiments.

2.4 Data Acquisition and Analysis

2.4.1 Data Acquisition

The data acquisition system at FITS, shown in a flow chart in Figure 6, employs LeCroy ten-bit (model 8210) and twelve-bit (model 8212) transient Analog-to-Digital converters (ADCs) in a Kinetic System model 1500 Camac crate, which is controlled by an LSI 11/23 microprocessor using an RT-11 operating system. Generally, the ten bit ADCs were used to record the voltage output of the pressure transducers, since these modules recorded approximately 8200 points of data over the thirty second time interval. The period of data acquisition for each ADC module was controlled with LeCroy 8501 programmable 3-speed clock generators, allowing sample rates of 20 Hz to 2 MHz.

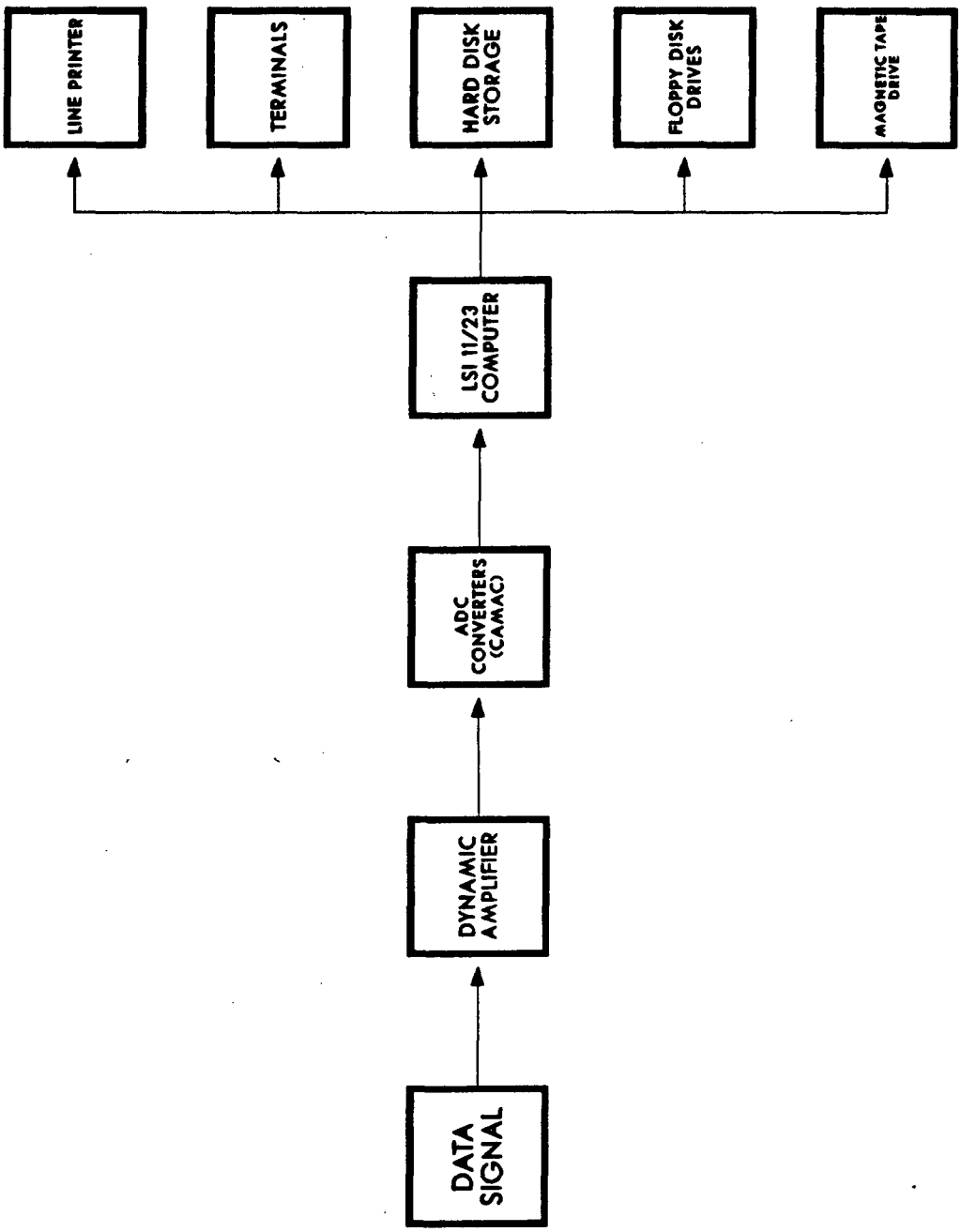

Figure 6
Flow Chart Showing the Data Acquisition System at the FITS Facility

Approximately 12 percent (one eighth) of the available module memory was allocated to preignition data and the remainder was used to record the postignition data. The ADC modules were triggered using a Transiac model 1020 amplifier/trigger source. This trigger was accomplished by monitoring (through the transiac) the output voltage of a pressure transducer. When a preset voltage level was detected, a TTL "trigger signal" was sent to the clock generators and ADCs, designating time zero, and the combustion data were recorded.

The voltage signals generated by a pressure transducer were amplified using Dynamic series 7600 differential amplifiers that incorporated model 7860-A strain-gauge conditioners. These amplifiers have a variable gain switch in addition to a multiturn variable gain control, which allows the exact gains to be calibrated and set.

2.4.2 Data Analysis Using SMOKE

The experimentally measured combustion-pressure transient can be used to infer "global" heat transfer characteristics of the postcombustion cooling phase. The term "global" implies a spatially averaged property that is inferred from a transient pressure-decay measurement. The actual "local" conditions may be somewhat different than these "global" estimates, especially near the flammability limits where relatively slow and incomplete combustion can occur. However, for burns in which rapid and relatively complete combustion occurs, the inferred "global" heat transfer results are considered representative of the actual "local" phenomena.

The partitioning of the "global" total energy deposition and peak heat flux rate into radiation and convection can be estimated from the experimentally measured pressure decay. The total heat flux rate is obtained using the expression

$$\dot{q}_T = - \frac{C_v}{R} \cdot \frac{V}{A} \cdot \frac{dP}{dt} \qquad (2.1)$$

and the radiative heat transfer from,

$$\dot{q}_R = \epsilon_g \sigma T_g^4 - \alpha_g \sigma T_w^4 \qquad (2.2)$$

where

$\dot{q}_T$ = the total heat flux rate (W/m^2)
$\dot{q}_R$ = the radiative heat flux rate (W/m^2)

C_v = the specific heat capacity at constant volume (J/kg-K)
R = the ideal gas constant ($kPa\text{-}m^3/kg\text{-}K$)
V = the vessel volume = 5.6 m^3

A = the surface area of the vessel = 19.5 m^2
ϵ_g = the total hemispherical gas emittance
σ = the Stefan-Boltzmann constant for radiation (W/m^2-K^4)
T_g = the bulk gas temperature (K)
α_g = the total hemispherical absorptance of the gas
T_w = the vessel wall temperature (K)

and

$\frac{dP}{dt}$ = the first time derivative of the measured pressure decay.

The heat transfer inside the vessel includes both convection and radiation. In this report, the convective heat transfer is assumed to be the difference between the total and radiative heat transfer. The energy depositions are estimated by numerically integrating the respective heat flux rates expressed in Equations (2.1) and (2.2), over time. A suite of computer codes, referred to as SMOKE, was developed by A. Ratzel and coworkers at Sandia to analyze experimentally measured combustion data [18, 22]. A summary of these computer codes and their functions will be briefly reviewed here for convenience. For additional information, the reader should consult these cited References.

SMOKE is a series of computer codes developed at SNLA to analyze combustion data taken at FITS, VGES, and the NTS hydrogen combustion dewar. A two-step process was used to reduce the combustion data. In the first step, the raw data was smoothed and curve fit such that continuous first derivatives could be calculated from the experimentally-measured pressure signals. In the second step, the desired modules of SMOKE were run on the "smoothed" data and the results stored for review. Each of these processes will be briefly reviewed here.

Preliminary Reduction using SMOOTH

The data collected at the FITS facility was prepared for data processing in SMOKE in two steps. The first step was to selectively cull and format the data into 300 to 500 time-voltage pairs. These data pairs were then smoothed using the computer code SMOOTH to provide continuous signals and first derivatives needed for processing.

The computer code SMOOTH operates on the data using a smoothing filter such as a Hanning filter or a rational function fit. The rational function fitter was particularly useful for obtaining continuous first derivatives of the postcombustion pressure data which was used to estimate the "global" total and radiative heat transfer characteristics.

SMOKE

Upon completion of the smoothing and filtering processes, the suite of computer codes comprising SMOKE was used to analyze the data. The version of SMOKE used to analyze these data consisted of two separate computer modules, MERGE and PRESS, which are briefly discussed below.

MERGE

MERGE is the initialization code which gathers information about the experiment, such as initial concentrations of the gases, initial gas temperature and pressure, the type of instrumentation

and their respective locations, amplifier gains, any associated calibration, and other pertinent information important to the processing of the signals. MERGE then configures this information into data files for further use by the remaining modules of SMOKE. Adiabatic Isochloric Combustion (AIC) calculations were also performed in the MERGE module and stored for comparison with the experimental data.

PRESS

The code PRESS is capable of processing up to three pressure transducer signals. Basically, PRESS uses the information obtained in MERGE to calculate the associated pressure in engineering units and then estimates the "global" radiative and total peak heat fluxes and cumulative energy deposition from the pressure decay. Output from PRESS include the absolute peak pressure and rise time, the absolute peak temperature which is inferred from the peak pressure, ratio of the peak to initial pressure, ratio of the peak to AIC peak pressure, and the "global" total and radiative postcombustion heat transfer conditions. "Hot-wall" (no condensation occurs) and "cold-wall" (condensation is allowed to occur) analyses were also incorporated in PRESS.

Of the 239 burns conducted during this test series, 120 were processed with SMOKE. For a burn to be processed with SMOKE, it had to have a relatively noise-free pressure gauge signal which recorded an overpressure due to combustion of greater than ~35 kPa (5 psig). Of the 120 burns processed, 82 were hydrogen:air burns and 38 were hydrogen:air:steam burns.

3. INITIAL GAS CONCENTRATIONS

The initial gas concentrations were calculated using partial pressure approximations. Generally, for a mixture of hydrogen, air, and steam, the compositions are calculated as;

$$\%H_2 = \frac{P_2 - P_1}{P_3} \times 100 = \frac{\Delta P_{hyd}}{P_3} \times 100 \qquad (3.1)$$

and

$$\%Steam = \frac{P_3 - P_2}{P_3} \times 100 = \frac{\Delta P_{steam}}{P_3} \times 100 \qquad (3.2)$$

where

$\%H_2$ = the volumetric percentage of hydrogen,
%Steam = the volumetric percentage of steam,
P_1 = the beginning absolute pressure of air, kPa
P_2 = the absolute pressure after hydrogen is added, kPa
P_3 = the absolute pressure after steam is added, kPa
ΔP_{hyd} = the pressurization due to the addition of hydrogen, kPa
ΔP_{steam} = the pressurization due to the addition of steam, kPa.

These equations are accurate as long as the temperature within the fixed volume remains constant and the behavior of the gases can be represented using ideal gas laws.

Experimentally, the temperature of the gases within the FITS vessel may change in time for the "hot-walled" tests where heat transfer from the vessel walls becomes important. To provide more accurate determinations of the precombustion gas concentrations in the vessel, the change in pressure due to these temperature fluctuations during the filling process was accounted for.

Assuming ideal gas laws apply, the pressure in the chamber after the first fill (state 2) can be expressed as,

$$P_2 = C\, n_2 T_2, \qquad C = R/V \tag{3.3}$$

where the number of moles in the second state is given by

$$n_2 = n_{hyd} + n_{air} \,. \tag{3.4}$$

The initial number of moles of air in the volume (state 1) can be written as

$$n_{air} = \frac{P_1}{C\, T_1} \tag{3.5}$$

Substituting Equation (3.4) and (3.5) into Equation (3.3) and rearranging, gives the following expression for the number of moles of hydrogen:

$$n_{hyd} = \frac{1}{C}\left[\frac{P_2}{T_2} - \frac{P_1}{T_1}\right] \,. \tag{3.6}$$

Similarly, the number of moles of hydrogen can be written in terms of the partial pressure of hydrogen as

$$n_{hyd} = \frac{\Delta P_{hyd}}{C\, T_2} \,. \tag{3.7}$$

Substitution of Equation (3.7) into Equation (3.6), yields the following expression:

$$\Delta P_{hyd} = \left[\frac{P_2}{T_2} - \frac{P_1}{T_1}\right] T_2 \,. \tag{3.8}$$

In a similar manner, the pressure in the vessel due to steam can be developed as

$$\Delta P_{steam} = \left[\frac{P_3}{T_3} - \frac{P_2}{T_2} \right] T_3 \quad . \tag{3.9}$$

The corrected partial pressures for hydrogen and steam addition can now be used to obtain accurate concentrations of the gases using Equations (3.1) and (3.2), respectively. The pressure and temperature used in these calculations were taken from the preignition experimental data after each fill process and after a steady-state condition was achieved. The initial hydrogen and steam concentrations for each experiment have been calculated using this technique and the results are presented in Appendix 1. These corrected concentrations are reported throughout this text. The corresponding uncertainty in these calculations is addressed in Appendix 2. In general, the uncertainty of these calculated initial volumetric percentages for hydrogen and steam was less than $\pm$7.5% and $\pm$2.2%, respectively, of the calculated concentrations.

4. EXPERIMENTAL RESULTS AND INTERPRETATIONS

For convenience, the presentation of the results from the FITS testing has been split into four major sections. In the first section, the flammability limits of hydrogen:air:steam are discussed. The second and third sections present the combustion pressure and heat transfer results for the hydrogen:air and hydrogen:air:steam burns, respectively. In the final section, the combustion completeness data is presented.

4.1 Hydrogen:Air:Steam Flammability Results

One of the goals of this work was to provide a more complete data base for the flammability limits for hydrogen:air:steam mixtures, both in quiescent and turbulent environments, at intermediate-scale. Experimentally, a mixture was classified as a "no-burn" if no appreciable pressure rise was detected (generally much less than 6 kPa), while a mixture was classified a "marginal burn" if the measured overpressure was less than 10% of the AICC calculated overpressure for the same initial conditions. (This definition is somewhat arbitrary, but gives a consistent method of defining a "marginal burn.") Those tests in which the combustion overpressure exceeded 10% of the AICC calculated overpressure were classified "burns."

In Figure 7 the three-component flammability results are shown for quiescent (fans off) mixtures of hydrogen, air and steam with air partial pressures of one Albuquerque atmosphere (~ 83 kPa) and an initial temperature of approximately 110°C. The shaded symbols represent a mixture which did not ignite, the unshaded symbols represent one which ignited and the crossed symbols represent the marginal burns according to the definition above.

The experimental procedure used to define the flammability of a mixture was as follows:

1. Attempt to ignite the mixture with a spark plug ignition source. If no ignition (i.e., pressure rise) was detected, two more spark ignitions were attempted.

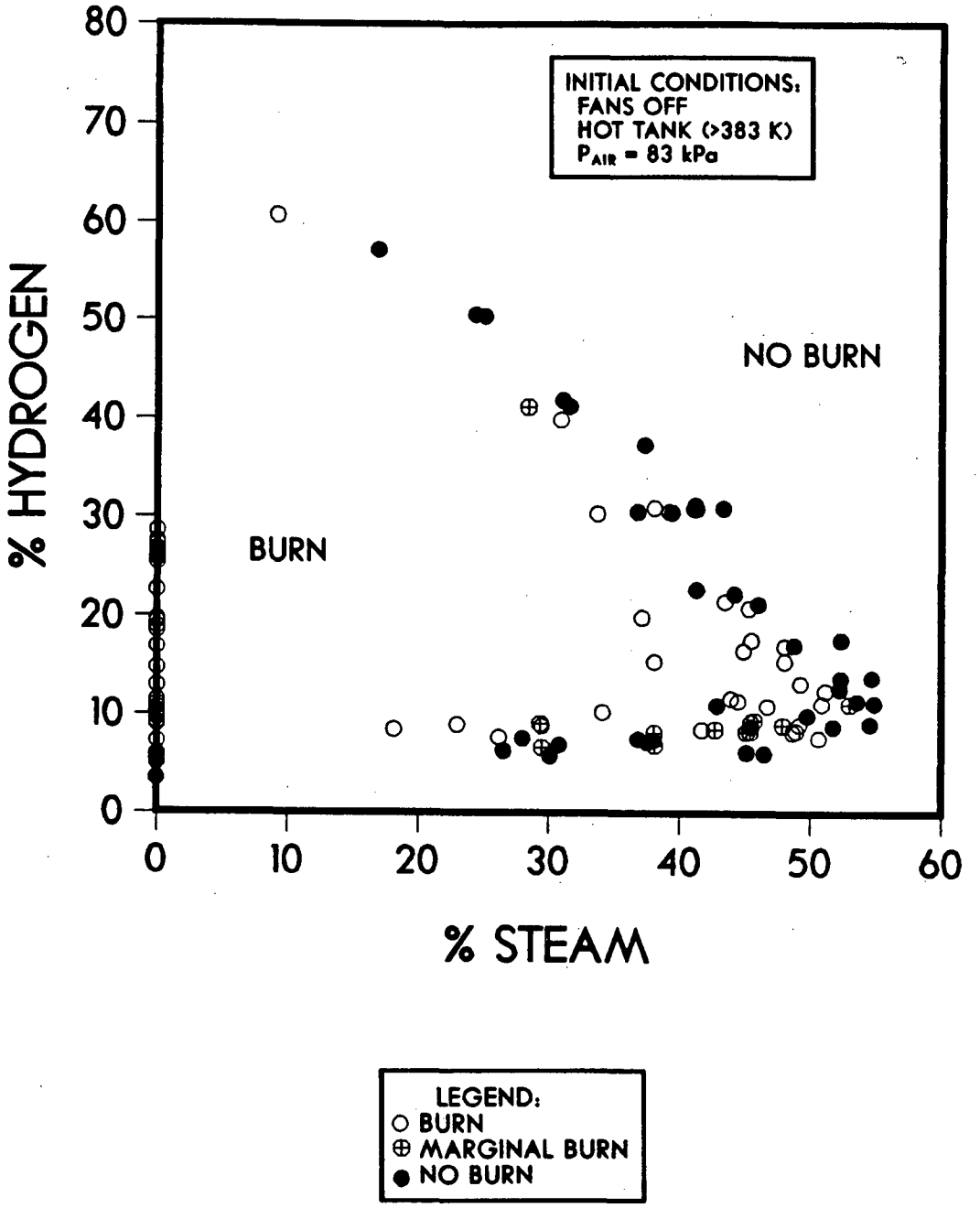

Figure 7
Hydrogen:Air:Steam Flammability Data with Fans Off

2. If no ignition was detected with the spark plug source, a glow plug was energized for ~1 min.

3. If still no ignition was detected, the fans were turned on and a spark ignition attempted one more time. If no ignition was observed, one final ignition was attempted with the glow plug energized for ~1 minute while the fans were operational.

Following this procedure, an inert mixture was defined for both turbulent and quiescent conditions. In one case, ignition occurred in a turbulent environment while no ignition occurred in the quiescent environment (i.e., steps 1 and 2). This result has been included as a "no-burn" in the quiescent flammability data base while it was classified as a "burn" or "marginal-burn," which ever the case, in the turbulent data base.

The results shown in Figure 7 also indicate that any combustible hydrogen: air mixture is inerted in the FITS vessel with ~52% steam by volume. This is relatively close to the 54% carbon dioxide inerting percentage found in the VGES tank which is of comparable volume [16].

In Figure 8, the flammability results of hydrogen, air and steam mixtures in a turbulent (fans on) environment are presented. Similar to the quiescent mixtures shown in Figure 7, the air partial pressure was ~83 kPa with an initial precombustion temperature of ~110°C. These results also indicate that complete inerting occurs at around 52% steam.

The flammability limits are a function of one or more of several initial and boundary conditions. These conditions included, the initial temperature and pressure, the presence of suspended liquid droplets, the preignition turbulence and the strength and location of the ignition source. Comparing Figures 7 and 8, the importance of preignition turbulence is apparent near the flammability limit; very few marginal burns are observed for a turbulent environment, while numerous burns are observed for the quiescent environment. Buoyancy-driven flame propagation is the dominant process governing the combustion of quiescent mixtures near the flammability limits. If a mixture is capable of local ignition, preignition turbulence results in more extensive flame propagation and larger fractions of hydrogen being consumed. Preignition turbulence affects the combustion completeness and, therefore, the chamber pressurization of the lean hydrogen concentrations near the flammability limits. Thus, qualitatively different characteristics would be expected for turbulent versus quiescent mixtures near their respective flammability limits.

The scatter in the marginal and no-burn flammability data shown in Figure 7 and 8 are unavoidable at these scales. Marginal burns appear to be random in nature and their appearance cannot be correlated to any one initial or boundary condition, except possibly preignition turbulence. If a mixture is capable of "marginal" flame propagation in a quiescent environment, preignition turbulence allows the flame to propagate resulting in a "burn" classification. Furthermore, the scatter in the data may also be a result of small variation in one or all of the initial and boundary conditions mentioned above. Generally, these deviations from desired conditions are small and unavoidable at these scales.

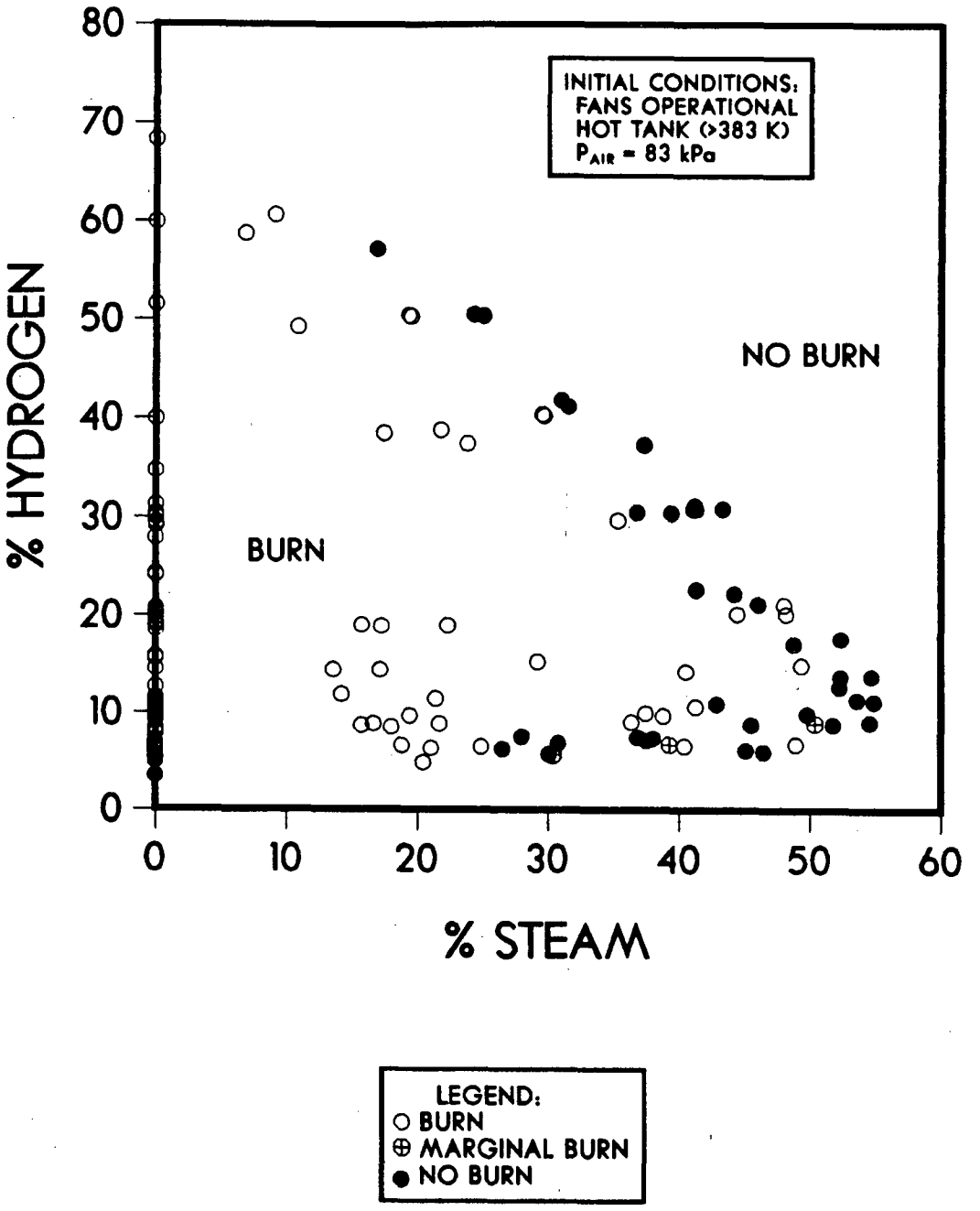

Figure 8
Hydrogen:Air:Steam Flammability Data with Fans Operational

Finally, the flammability limits of hydrogen:air and a diluent may be directly related to the heat capacity (and therefore the molecular structure) of the diluent gas. Steam is a triatomic gas that may suppress the combustion process more effectively than a diatomic gas such as nitrogen. In Figure 9, the hydrogen:air:steam flammability correlation developed in the next section is shown plotted against the flammability curve for nitrogen as reported by Drell and Belles in 1975 [27]. Also, inerting limits similar to those shown for steam were experimentally observed by Benedick et al., [16] for carbon dioxide in a similar sized vessel. The nitrogen curve, shown in Figure 9, indicates that larger concentrations of the diatomic gas are needed to inhibit the combustion process. Furthermore, it appears likely that if a monatomic gas such as helium were used as the diluent gas, the three-component flammability limits would approach the lean oxygen and hydrogen flammability limits. Hence, not only are the flammability limits affected by initial and boundary conditions, they are also governed by the heat capacity of the diluent gas.

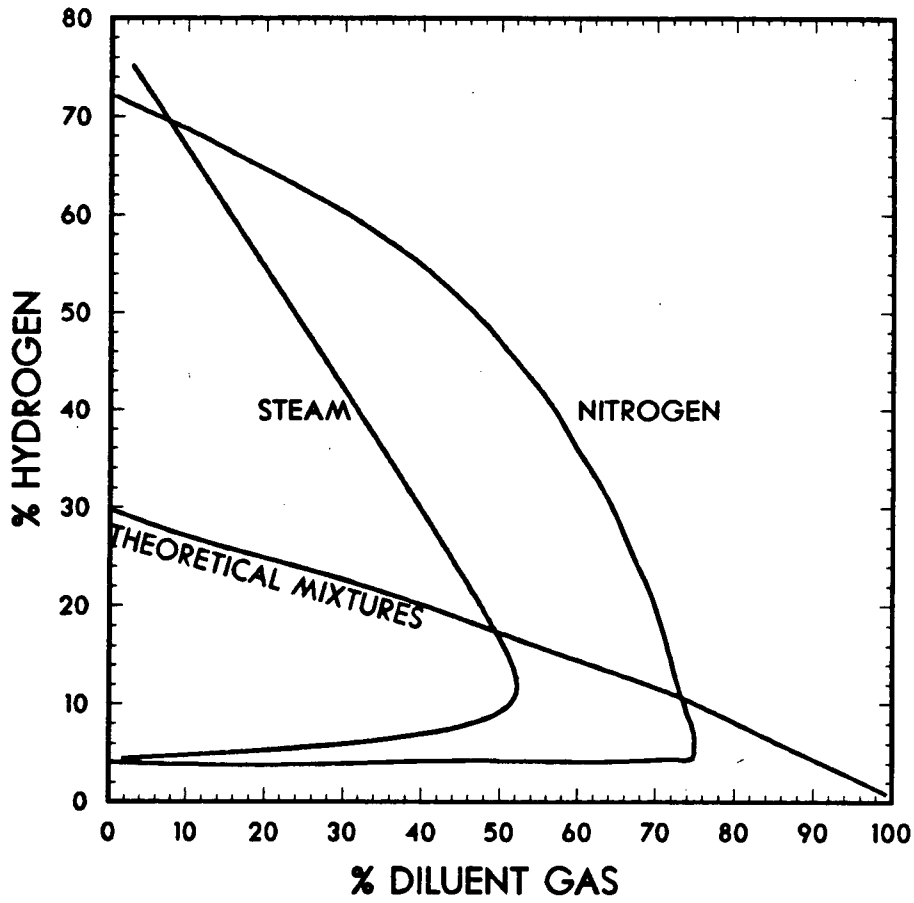

Figure 9
Hydrogen:Air:Steam Flammability Limits for
Steam and Nitrogen

4.1.1 Development of a Correlation for the Hydrogen:Air:Steam Flammability Limits

One of the contributions of this work, other than adding to the existing data base, is the ability to curve fit these flammability results with an exponential-type equation. This was achieved by using a piecewise exponential curve fitting technique resulting in a single exponential equation which describes the entire region of flammability. The technique is briefly described below.

As is well known, if an exponential such as

$$Y(x) = A\ e^{-Bx} \qquad (4.1)$$

is plotted on a linear-log scale, a straight line results and the constants A and B can be defined using a standard linear regression curve-fitting technique.. In Figure 10 the initial air concentration is plotted on a linear-log grid against the hydrogen concentration for the inert mixtures. From this plot, the influence of two distinct exponential are observed; one over the range of 0 - 10% hydrogen and a second for hydrogen concentrations greater than 15%.

A computer program was written which incorporated a linear regression routine to fit the data presented in Figure 10. Hydrogen and air concentrations from the different "no-burn" flammability tests were used to calculate a conservative expression for the three-component flammability limit.

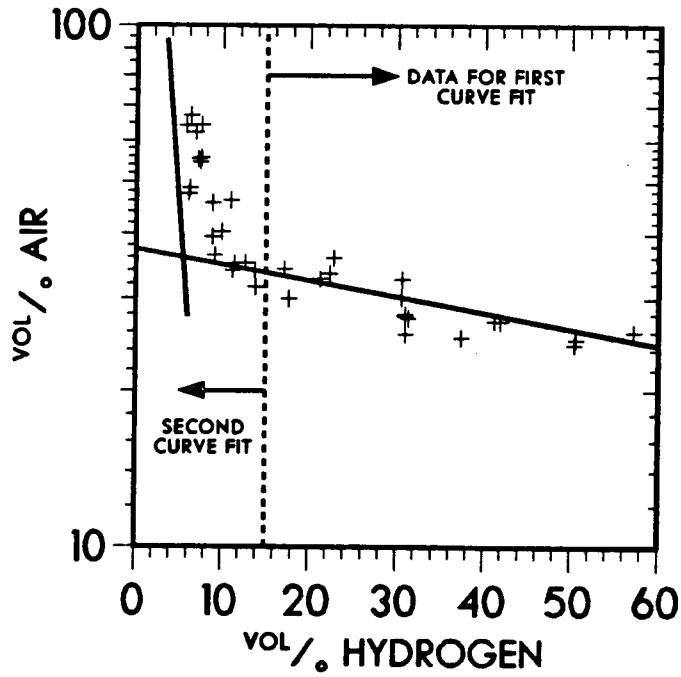

Figure 10
Exponential Check using the Inert Mixtures of
Hydrogen, Air, and Steam

The first least-squares curve fit incorporated data greater than 15% hydrogen and resulted in the following expression:

$$\ln(\%Air_1) = 3.62 - 0.007\%H_2 \ . \tag{4.2}$$

The influence of this exponential term was subtracted from the data base and a second fit calculated using the data between 0 and 10% hydrogen resulting in the expression:

$$\ln(\%Air_2) = 6.25 - 0.488\%H_2 \ . \tag{4.3}$$

Combining these two equations and accounting for the fact that the combustible atmosphere consists of only hydrogen, air and steam, the steam content can be expressed in terms of the hydrogen concentration as follows;

$$\%Steam = 100-\%H_2-37.3\ e^{-0.007\%H_2} - 518.0\ e^{-0.488\%H_2} \tag{4.4}$$

The approximate flammability of a mixture can be determined with this correlation given a volumetric concentration of hydrogen. In Figures 11A and 11B, this correlation is plotted with the experimental data previously reported in Figures 7 and 8, respectively. As shown, the correlation provides a relatively good fit over the entire flammability region. Even at the knee of the curve, the correlation compares reasonably well with the scatter in the data. Furthermore, this single correlation provides a conservative approximation of the flammability limits for both quiescent and turbulent conditions since only the "no-burn" data was used.

Comparison of this correlation to the curves proposed by Zabetakis [6] and Tamm, et al., [9] are shown in Figure 12. The correlation compares reasonably well with the fans-on curve fit of Tamm for the lean hydrogen concentrations. However, the correlation overpredicts the flammability limits with fans-off as proposed by Tamm or the curve introduce by Zabetakis. These differences may be attributed to geometric differences such as the characteristics length scales of the different vessels, the volume-to-surface area ratio of the vessel, and the location and ignition energy of the igniters.

Zabetakis was the first to propose a curve for the entire region of flammability, but his curve is significantly different than that developed in this and other work. It predicts much narrower flammability limits in the knee region of the curve around 10% hydrogen. The curves proposed by Zabetakis and Tamm were generated using engineering judgement to "hand-fit" the data base. The technique described in this report defines a method of curve fitting the data base with an expression using existing techniques. This method does not require engineering judgment to fit the curve and, therefore, should yield more credence to the resulting curves.

An expression of the type defined in Equation (4.4) could be easily implemented into currently available reactor safety analysis tools such as HECTR [28,29] and MAAP [30]. However, before an expression of this type is used in such codes, an expression of the current world's data base should be developed using this technique. Note that care must be taken in choosing the

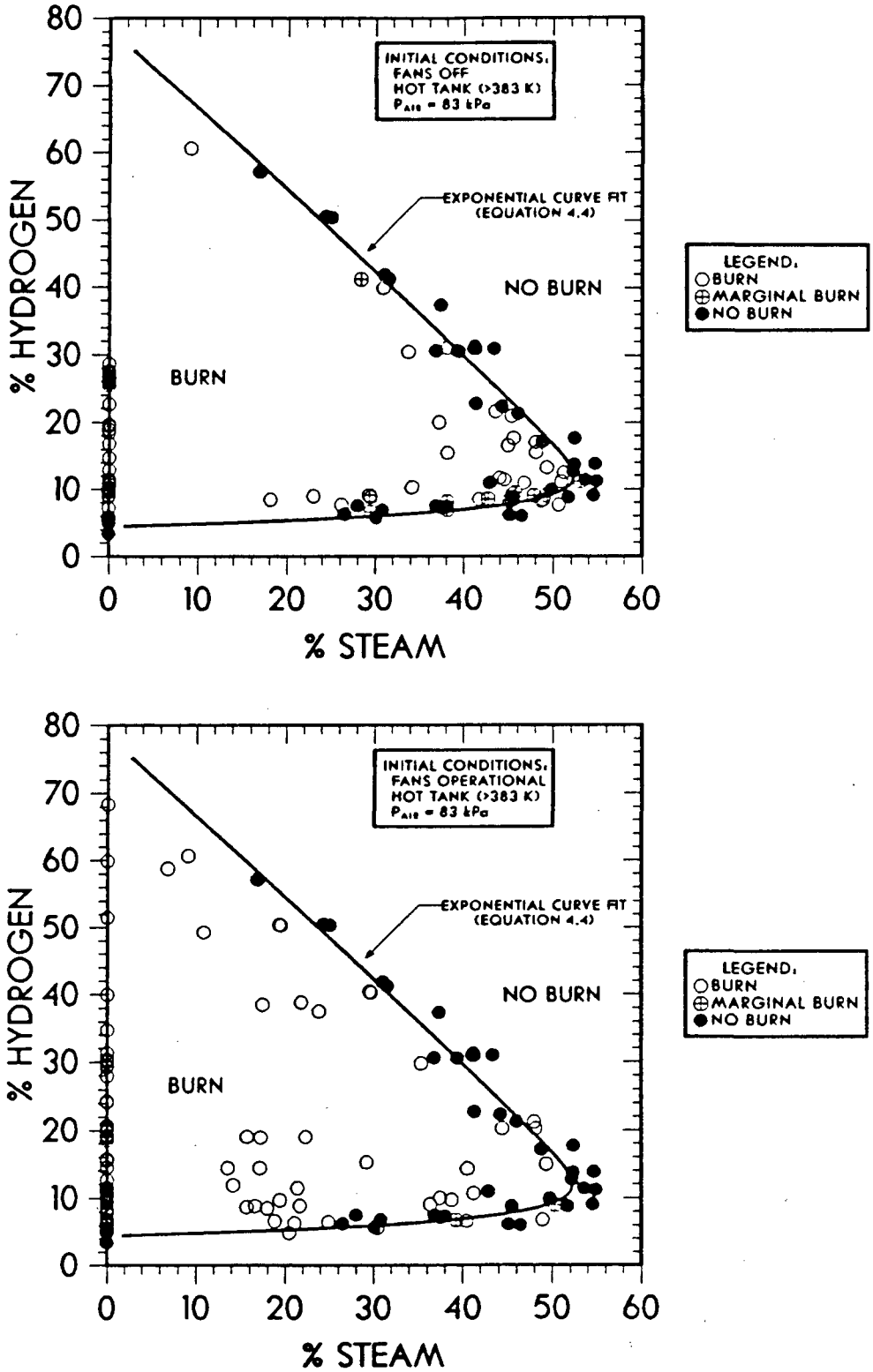

Figure 11
Hydrogen:Air:Steam Flammability Data with Fans On and Off Shown with the Exponential Curve Fit.

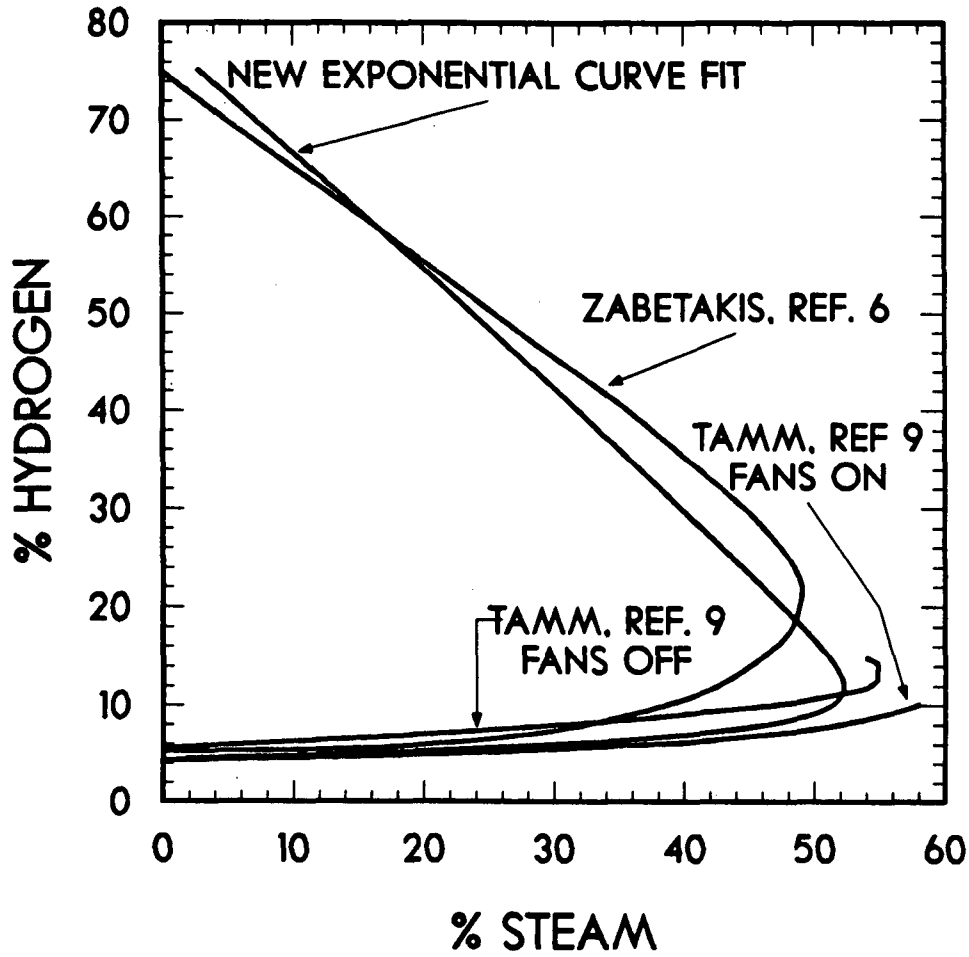

Figure 12
Comparison of the Flammability Curve Fit with those
Proposed by Zabetakis [6] and Tamm, et al., [9]

largest vessel geometries available from the existing data base to provide a representative correlation for containment sized volumes. The expression provided in this work will provide a much more accurate representation of the flammability limits than currently exists in most of these combustion codes.

4.2 Hydrogen:Air Combustion Results

4.2.1 Combustion Pressure Results

The experimental combustion peak pressure data for each of the hydrogen:air burns are included in Appendix 3 along with the Adiabatic Isochloric Complete Combustion (AICC) theoretical maximum pressures for reference. Also, representative pressure signatures are included in Appendix 7 for each combustion experiment. Graphical representation of these results will be presented and discussed in this section.

Figure 13 shows the ratio of the peak-to-initial pressure as a function of the initial hydrogen concentration for both the quiescent and turbulent burns in cold-wall and hot-wall tests. As observed by other investigators [16,17], preignition turbulence tends to promote more complete burning for lean (<10%) hydrogen concentrations while preignition turbulence is relatively unimportant for the richer burns. For lean quiescent burns, incomplete burning is most likely a result of the downward and horizontal flame propagation limits; e.g., the flame kernel is able to propagate only upward due to buoyancy effects. In contrast, turbulence induced by fans causes unburned gases to be "fed" into the flame zone, burning gases which otherwise might not be combusted. For the richer burns (>10% hydrogen), the flame is able to propagate uniformly in all directions independent of the preignition turbulence eliminating this dependence.

The normalized peak pressure was also observed to increase to a maximum at about 30% hydrogen by volume and then decreases with increasing hydrogen concentration. For hydrogen concentrations greater than stoichiometry, the mixture becomes oxygen lean and is unable to react with all the available hydrogen. Thus, the extra hydrogen acts as a diluent, similar to nitrogen, reducing the combustion peak pressures. Furthermore, preignition turbulence was found to be unimportant for these rich hydrogen concentrations; i.e., the data for quiescent burns are with the scatter of the turbulent burn results.

The importance of the preignition gas temperature is also evident when the results from these two figures are compared. At stoichiometry, a decrease of ~20% in the normalized peak combustion pressure is observed for burns at elevated preignition temperatures (~385 K, referred to as hot-wall) compared to equivalent burns at ambient temperatures (~300 K, referred to as cold-wall). This is essentially due to the decreased quantity of hydrogen and oxygen available for combustion. At elevated temperatures, fewer mole of hydrogen and oxygen (or air) are available for combustion since the densities of the gases are lowered as the temperature is increased. Therefore, more severe combustion environments would be expected to occur, and did occur, for the tests at ambient temperature.

Comparisons of the experimental peak pressures to the AICC theoretical maximums are shown in Figure 14. These plots indicate that as the hydrogen concentration increases from ~5% to ~10%, the ratio of the experimental to AICC peak pressure also increases. For hydrogen concentrations richer than ~10%, this ratio tends to level off between 0.9 and 1.0 and then begins a slight decrease for hydrogen concentrations exceeding about 30%.

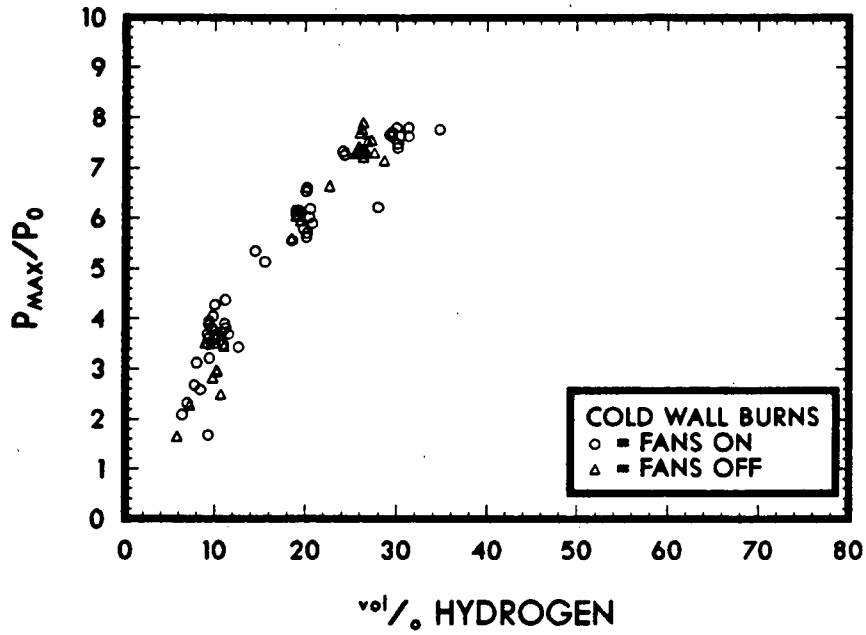

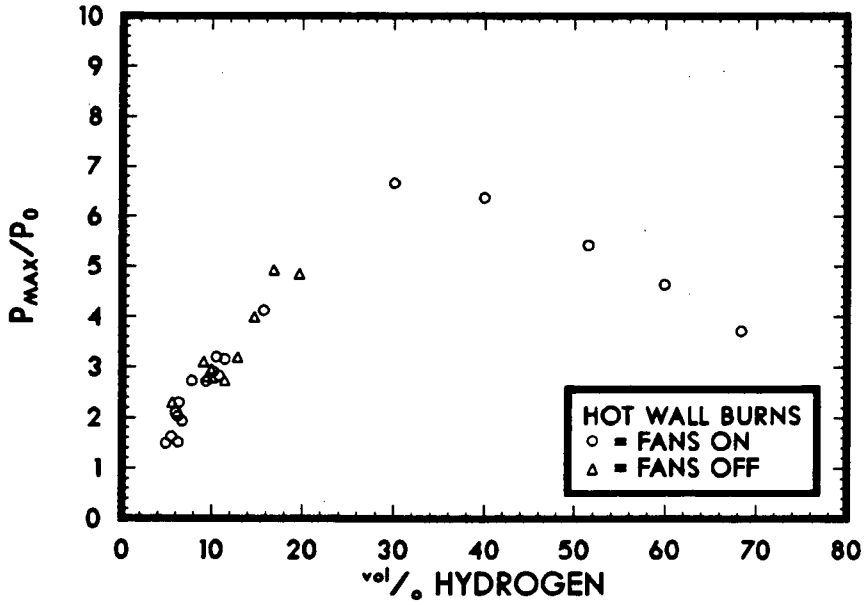

Figure 13
Normalized Peak Combustion Pressure for the Cold- and Hot-wall Hydrogen:Air Burns

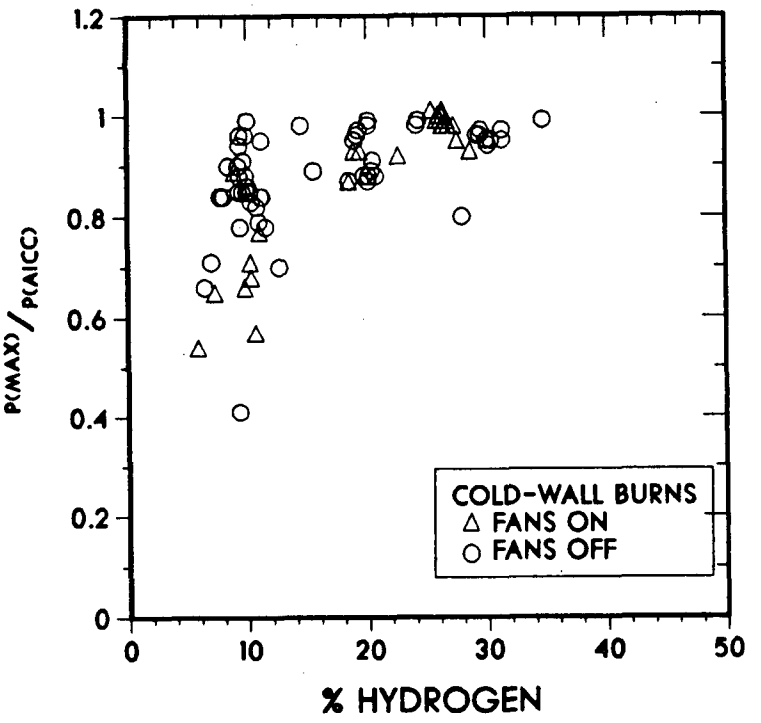

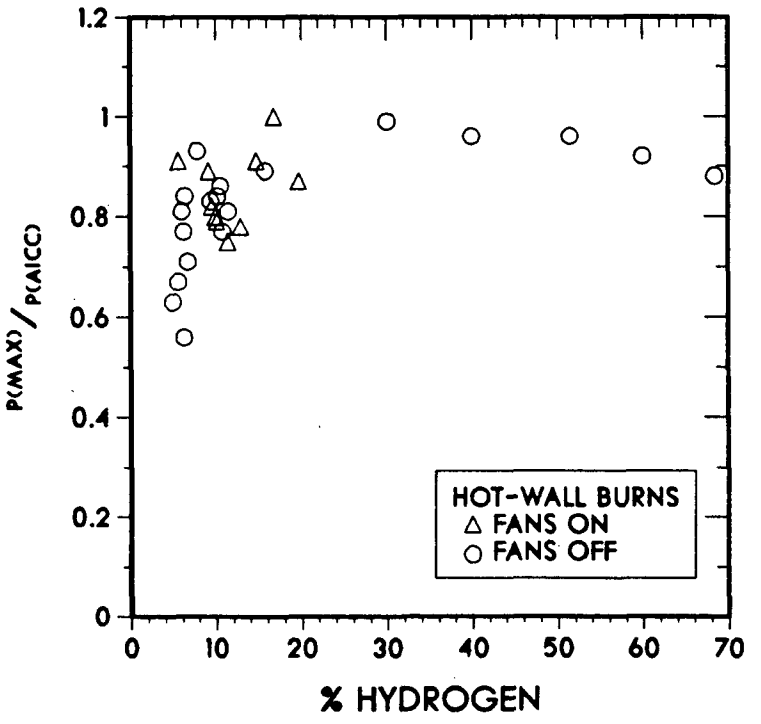

Figure 14
Comparison of the Experimental Peak Pressures to the AICC Calculated Peak Pressure for the Cold- and Hot-wall Hydrogen:Air Burns

The duration of combustion, as measured by the time from combustion initiation to the time of peak pressure, is plotted in Figure 15 against the initial hydrogen concentration and is shown in tabular form in Appendix 3. Here, the hot- and cold-wall tests are shown together for both quiescent and turbulent burns. As expected, the duration of combustion is significantly longer for the lean quiescent burns compared to similar turbulent burns. This observation is more clearly shown in Figure 16 where the pressure signatures of two nominally 9.5% hydrogen:air burns are shown. The most striking difference is the overall pressure signature recorded for these two experiments. For the quiescent burn, the initial pressure rise from the preignition pressure to the first "bump" in the signature is probably due to flame propagation in essentially an upward direction. Once the flame reaches the top of the vessel, it then propagates down the vessel walls, burning some (or all) of the remaining gases. Downward and horizontal flame propagation probably also occurred during the initial pressure rise but moved very slowly compared to the upward moving flame kernel. Furthermore, any upward movement of the bulk gases would retard the propagation of the flame in the downward direction until the top of the vessel is reached.

Another measure of the combustion severity can be obtained by considering the mean pressure derivative (calculated as the measured overpressure divided by the pressure rise time) as a function of the initial concentration of hydrogen, as shown in Figure 17. These results indicate that there is very little difference between the turbulent and quiescent burns near stoichiometry. However, more distinct differences are observed for those hydrogen burns containing less than 10%; the mean pressure derivative is greater for the turbulent burns than for the quiescent burns, indicating that the chemical energy release rate is higher for turbulent burns than for quiescent burns. Additionally, the mean pressure derivative for the burns at ambient temperature are generally greater than for the burns at elevated temperature, indicating again that more energy is released and combustion is generally more severe at the lower initial temperature. These trends are consistent with those already presented and serve as an additional check point for the observations and conclusions discussed previously.

4.2.2 Peak Gas Temperature Results

The "global" peak gas temperatures inferred from the pressure signals using SMOKE have also been provided in Appendix 3 with the combustion pressure results for reference. In Figures 18A and 18B, the normalized peak gas temperatures are shown for the combustion experiments at ambient and elevated initial temperatures, respectively. For these results, there appears to be very little difference in the peak gas temperature between the turbulent and quiescent burns, although some differences would be expected in the very lean hydrogen burns. There is, however, a significant dependence of the results upon the preignition temperature as might be expected from the previous discussion. The burns initially at ambient temperature (cold-wall) generally achieve higher peak gas temperatures than do comparable burns at elevated temperature (hot-wall). These results again suggest that the heat fluxes and energy depositions are more severe during cold-wall burns than during hot-wall combustion due, as noted before, to the larger quantities of hydrogen available for combustion in the cold-wall burns.

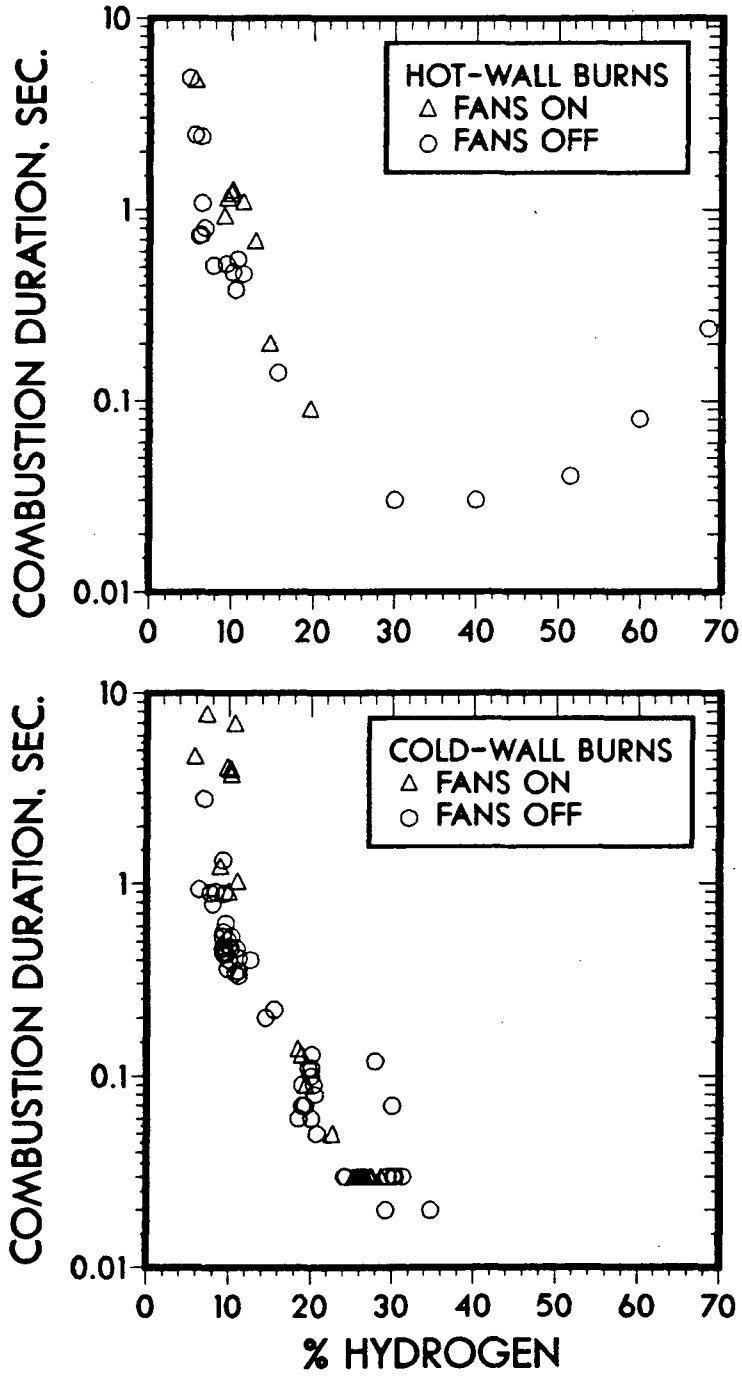

Figure 15
Combustion Duration for the Cold- and Hot-wall
Hydrogen:Air Burns

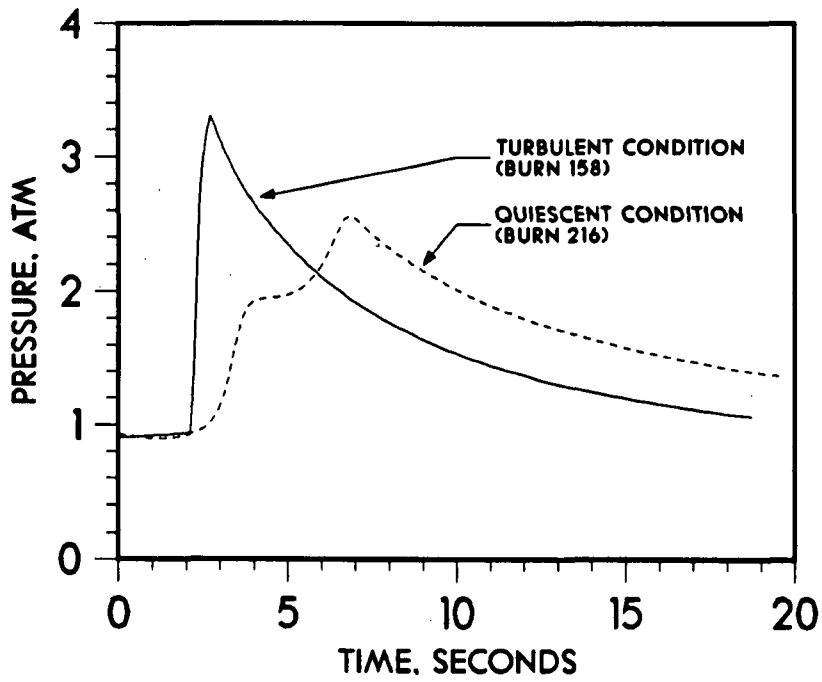

Figure 16
Comparison of Two Nominally 9.5% Hydrogen Burns with and without Fans Operational

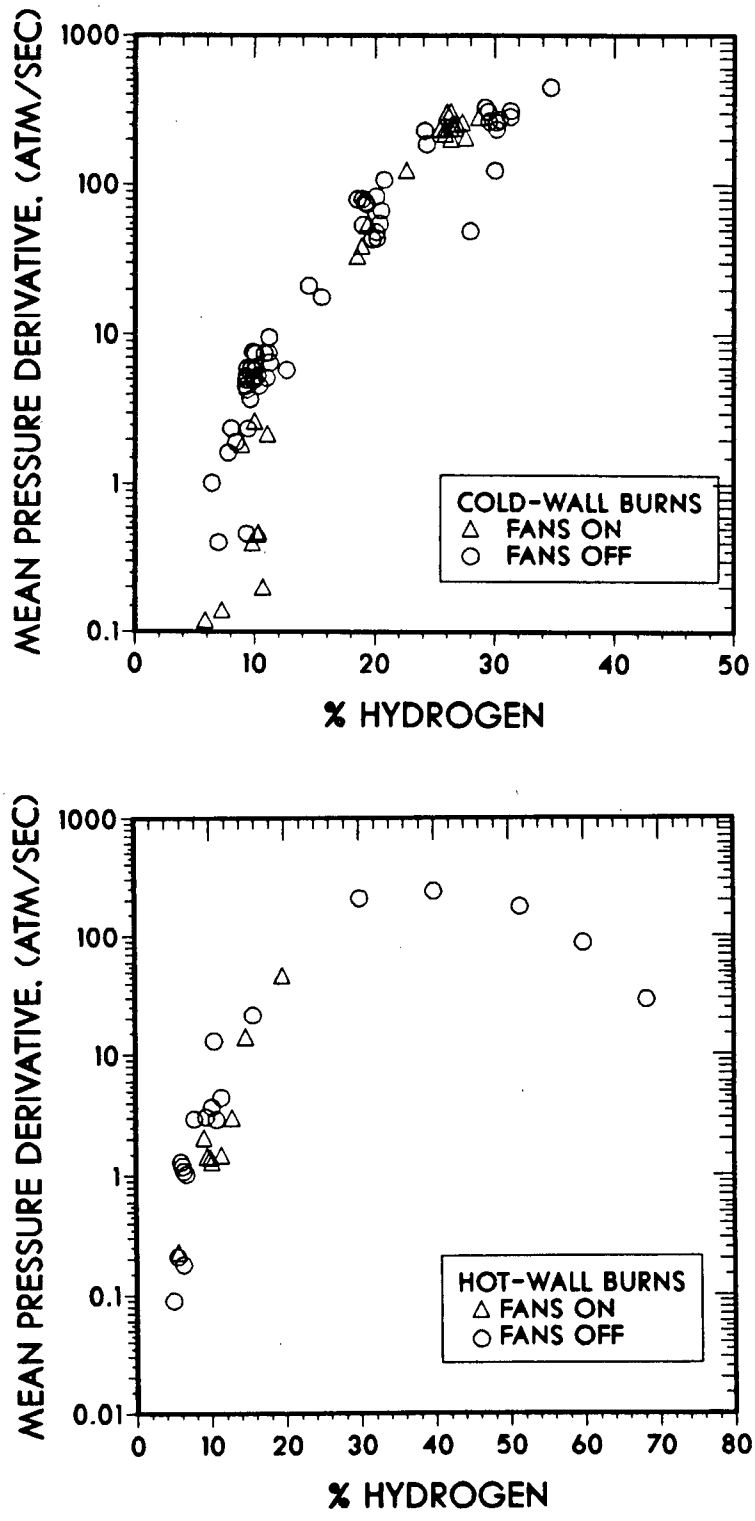

Figure 17
Mean Pressure Derivative for the Cold- and Hot-wall Hydrogen:Air Burns

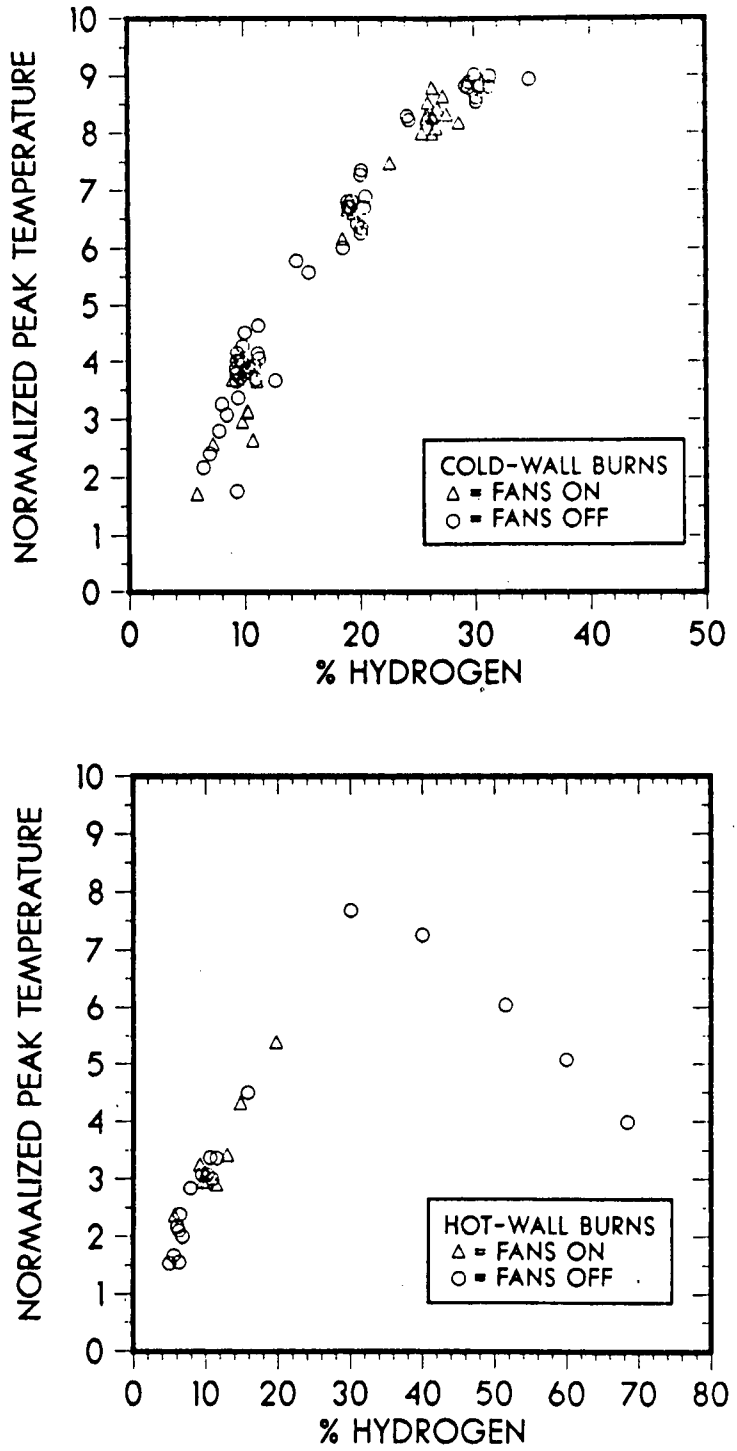

Figure 18
Normalized Peak "Global" Gas Temperature for the
Cold- and Hot-wall Hydrogen:Air Burns

4.2.3 Heat Transfer Results

The "global" heat flux and energy depositions have been inferred from the pressure signals using the suite of computer programs referred to as SMOKE and are reported in tabular form in Appendix 4. In Figure 19, the "global" total peak heat fluxes for the combustion experiments at elevated (hot-wall) and ambient (cold-wall) preignition temperatures are shown. Comparing the lean (~10%) and stoichiometric precombustion conditions, the total peak heat flux increases by a factor of ~10 for the hot-wall burns and by ~12 for the cold-wall burns. Furthermore, stoichiometric cold-wall burns are ~20% more severe than comparable hot-wall combustion tests. This is a further evidence that combustion severity increases as the preignition temperature decreases.

Analyses show that the heat transfer processes during and after combustion are dominated by convection and radiation. Results from SMOKE indicate, as shown in Figure 20, that during and immediately following combustion, heat transfer is governed by radiation for hydrogen concentrations greater than ~20%, while convection becomes more important for burns with less than 10% hydrogen. For the lean burns, the ratio of the radiative to the total peak heat flux is generally less than 50% indicating that postcombustion heat transfer is dominated by convection. This observation occurs at both elevated and ambient preignition temperatures, implying that the mechanisms of heat transfer at early times after combustion are unaffected by the initial gas temperature, at least for the lean cases (<10%). Near stoichiometry, radiation accounts for ~90% of the early postcombustion heat transfer for the cold-wall tests and ~75% for similar hot-wall burns. Radiation dominated heat transfer would be expected for the rich hydrogen burns since radiation is proportional to the fourth-power of the gas temperature and is more significant at elevated gas temperatures than convection which is proportional to the first-power of the gas temperature. Thus, although similar trends in the heat transfer mechanisms are observed for lean burns at both ambient and elevated preignition temperatures, some differences do exist between the two at concentrations near stoichiometry.

Results from the large-scale NTS combustion tests [18] appear similar to these reported here. Ratzel reported that the ratio of the peak radiative to total heat flux varied from 0.34 at 6.0% hydrogen (test NTSP9P) to 0.56 at 9.9% hydrogen (test NTSP15). It should be noted that a dramatic increase in this ratio was observed for concentrations near 8%. Specifically, for test NTSP00 with 6.6% hydrogen, the ratio of the two peak heat fluxes was 0.31 while for test NTSP13 with 7.8% hydrogen, the ratio increased to 0.53. Although the number of "dry" burns in the NTS series was relatively small, these four tests seem to fall within the general scatter of the results obtained from the combustion experiments in the FITS vessel. However, due to the increased vessel geometry and the characteristic radiation length-scale, the integrated radiation heat transfer would be expected to be more significant in the NTS combustion dewar than in the FITS vessel [31].

The time-integral of the heat flux, or cumulative energy deposition, has also been estimated using SMOKE. The cumulative energy deposition is an integral measure of the postcombustion heat transfer and indicates the total

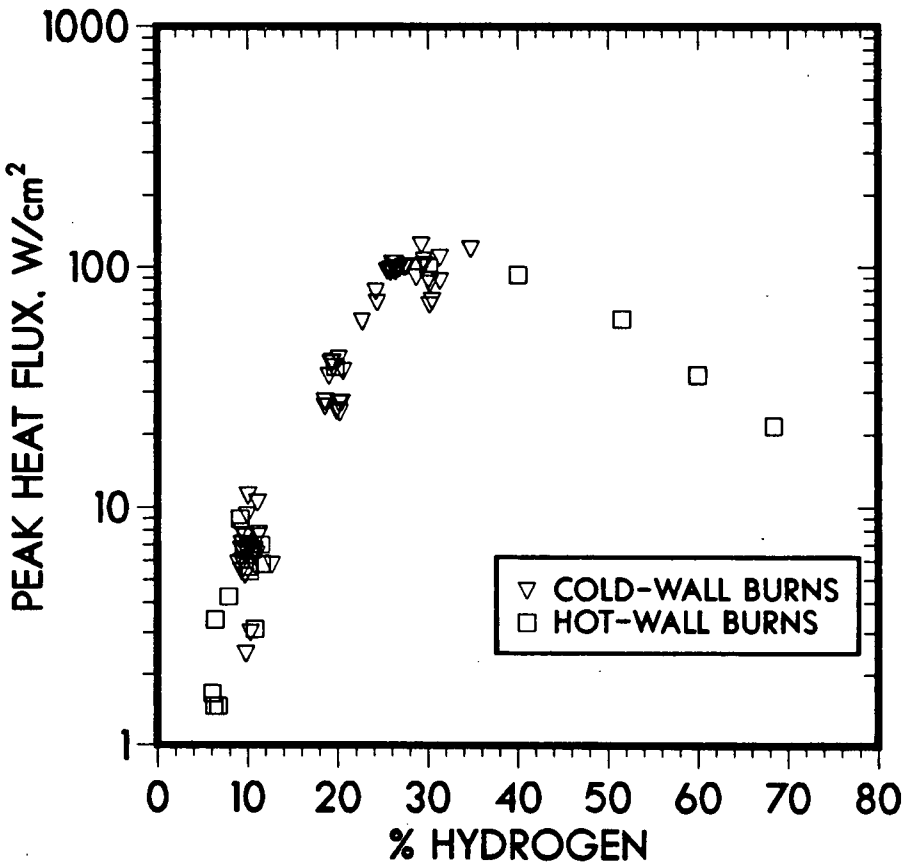

Figure 19
"Global" Total Peak Heat Fluxes for the Cold- and Hot-wall Hydrogen:Air Burns

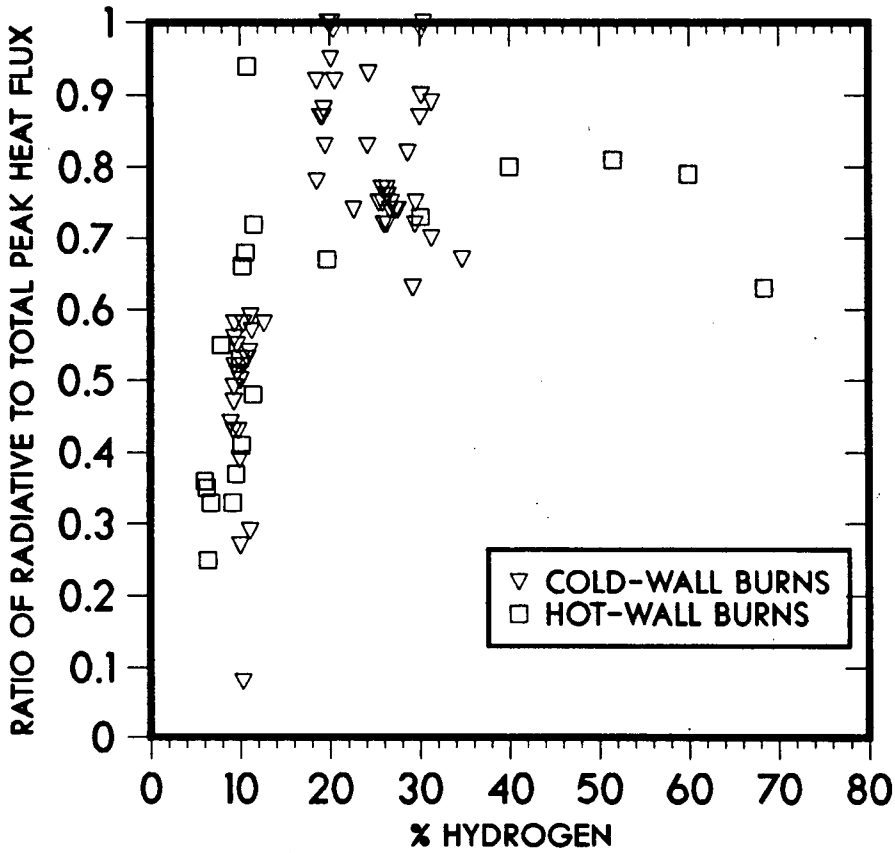

Figure 20
Ratio of the "Global" Peak Radiative to Total Peak
Heat Flux for the Hydrogen:Air Burns

energy absorbed by the vessel surfaces over the data recording period (~30 s). The time-rate of energy deposition (i.e., heat flux profiles) may also be an important parameter when considering the heat transfer phenomena associated with combustion, but is not presented here. It is safe to say, however, that the decay of the heat flux with time is directly related to the pressure decay since this decay represents the cooling processes within the vessel. However, the "local" conditions may be somewhat different from the "global" conditions, especially for lean hydrogen burns where relatively slow, incomplete and localized burning can occur. If relatively uniform combustion occurs, the differences between the local and global postcombustion heat transfer should diminish.

If the cumulative total energy deposition is plotted as a function of the initial hydrogen concentration, as shown in Figure 21, the difference in postcombustion heat transfer due to the initial precombustion gas temperature is evident. An increase of ~30% in the total energy deposition is observed for burns at ambient temperature compared to equivalent burns at elevated temperature and at hydrogen concentrations near stoichiometry. The total energy depositions for the hot-wall combustion experiments were observed to increase from ~10 J/cm^2 near the lean flammability limit (~5% hydrogen) to ~80 J/cm^2 near stoichiometric (~30% hydrogen) while the cold-wall counterparts increased from ~15 J/cm^2 to ~95 J/cm^2 over the same range. As observed before, this is a result of more hydrogen and oxygen available for combustion at lower preignition temperatures.

If the ratio of the radiative to total energy deposition is considered as a function of the initial volumetric hydrogen concentration, as shown in Figure 22, convection is observed to be the dominant integral postcombustion heat transfer mechanism for mixtures less than ~10% hydrogen. Thus, at this scale, postcombustion heat transfer for the lean hydrogen burns is governed by convection during both early and late periods after combustion. Radiation and convection were found to play approximately equal roles in the postcombustion cooling process for burns greater than 15%. Furthermore, this trend continues for the very rich hydrogen burns (>30%) indicating that the excess hydrogen does not greatly influence the postcombustion cooling heat transfer mechanisms. These integral heat transfer results are true in spite of the fact that radiation was observed to be the dominant mechanism of heat transfer shortly after combustion for the rich burns (refer back to the peak heat flux results). Convection is the dominant mechanism of heat transfer at late times after combustion, for both rich and lean hydrogen concentrations, since it is proportional to the gas temperature difference and radiation is weakly proportional to the fourth-power of the gas temperature. Thus, as the bulk gas temperature decreases, convection will ultimately become the dominate mode of heat transfer.

If these experimental results are compared to the large-scale NTS data, some differences become apparent. Ratzel reported that the ratio of the cumulative radiative to total energy deposition varied from 0.33 at 6.0% hydrogen (test NTSP9P) to 0.47 at 9.9% hydrogen (test NTSP15). If these NTS-inferred results are compared to the FITS results, radiation accounts for a larger partition of the total heat transfer at large-scale than at intermediate scales. As evident from Figure 22, the NTS data are approximately twice that of the FITS data. Thus, although convection mechanisms will eventually dominate the postcombustion heat transfer

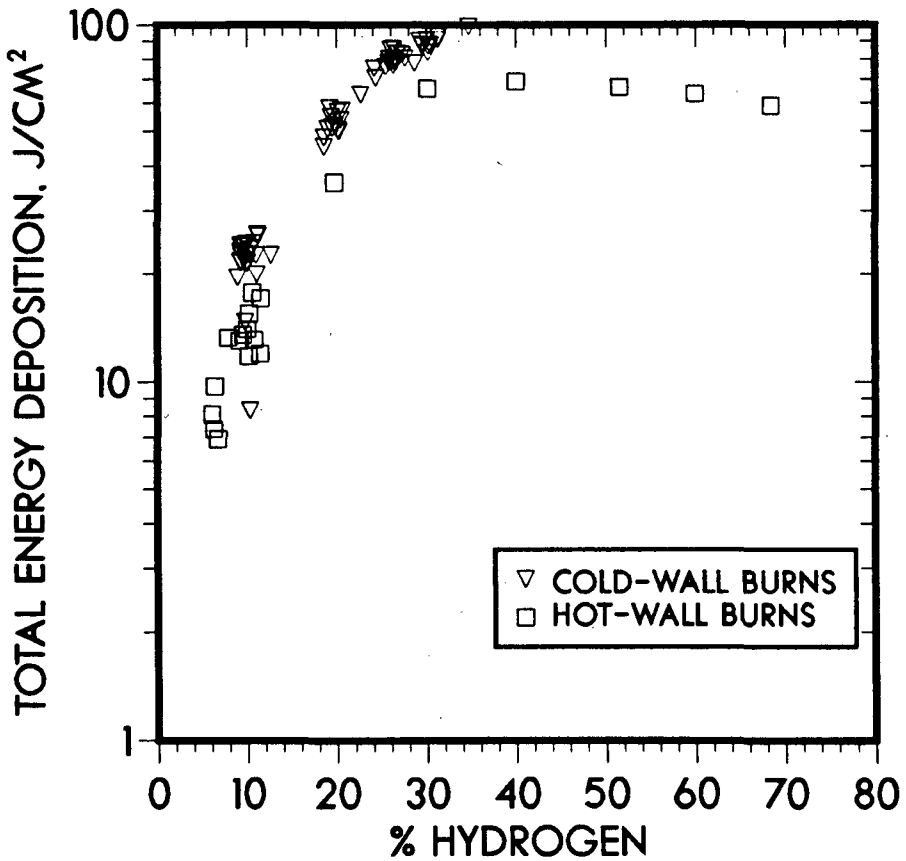

Figure 21
Cumulative Total "Global" Energy Deposition for
the Hydrogen:Air Burns

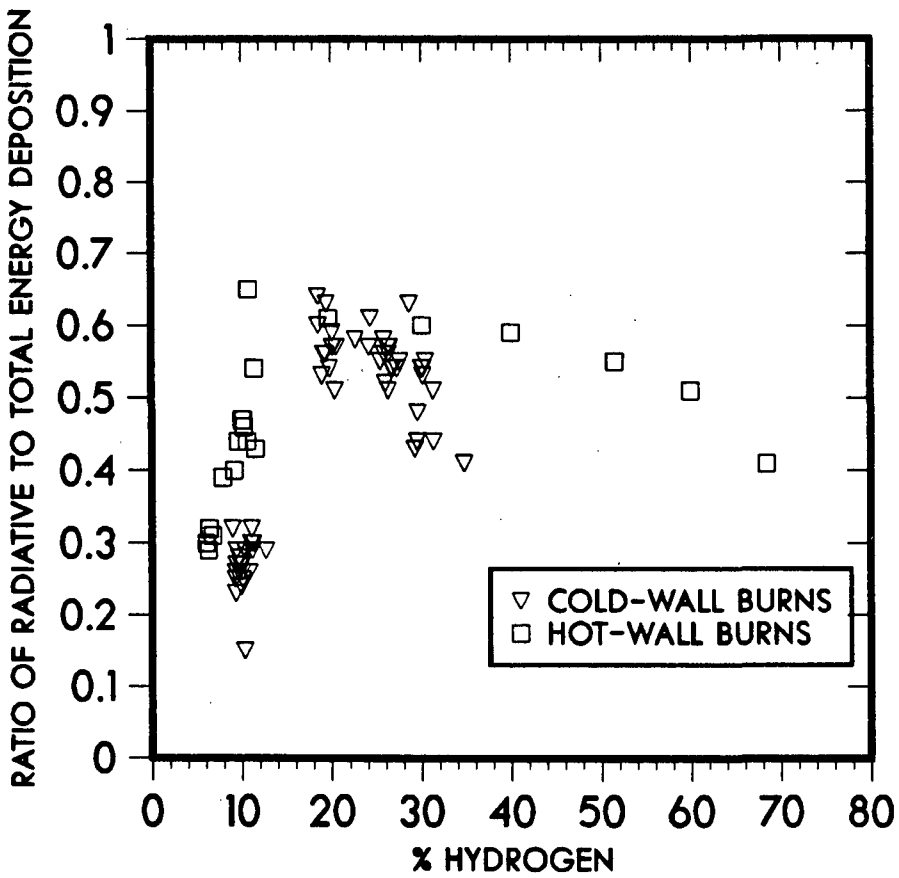

Figure 22
Ratio of the Cumulative Radiative to Total Energy Depositions for the Hydrogen:Air Burns

processes, the importance of radiation during the postcombustion cooling phase must increase relative to the vessel volume. These observations have also been observed and reported by Ratzel and Shepherd [31]. Briefly, the radiative heat transfer is directly related to the characteristic length scale for radiation; in particular, the effective emittance of the gases in the volume increases as the vessel size increases. Due to the large differences in vessel volume and geometry, the emittance would be expected to increase by a factor of ~2 resulting in an approximate equal increase in the radiative heat transfer for the NTS combustion tests [31] and [32]. Therefore, the differences between the FITS data and the large-scale NTS data are attributed solely to the differences in scale.

4.3 Hydrogen:Air:Steam Combustion Results

4.3.1 Combustion Pressure Results

The experimentally measured peak pressures and AICC calculated peak pressures for each of the hydrogen:air:steam experiments are presented in Appendix 5. Also, representative pressure signatures are presented in Appendix 7 for each combustion experiment for future reference. These results are presented graphically in this section and are discussed in detail.

The measured pressures during combustion of the hydrogen:air:steam mixtures indicate that the normalized peak pressure (i.e., the ratio of the peak-to-initial pressure) decreases with increasing steam, as shown in Figure 23. (Note that in this figure and those to follow, comparisons of the burns with and without steam are made relative to the hydrogen concentration in hydrogen:air only. Comparison on a volumetric basis will be presented in a later part of this section.) Turbulent lean burns are affected by the addition of steam compared to the hydrogen:air counterpart, although not as much as the quiescent burns; up to a 50% reduction is observed for the quiescent burns. This again implies that preignition turbulence may be one of the most important condition determining the combustion characteristics of lean mixtures of hydrogen with and without steam. Furthermore, steam was found to affect the combustion pressurization of the richer hydrogen concentrations (>15%) for both turbulent and quiescent conditions; a reduction in the normalized peak pressure of up to ~50% was observed depending upon the steam concentration. Thus, as might be expected, steam acts as an inert heat sink and reduces the bulk gas temperatures and chamber pressurization during combustion of the available hydrogen with oxygen.

As the hydrogen concentration increases away from a particular hydrogen:air:steam flammability limit, increasing fractions of hydrogen are consumed during the combustion process. This general trend is shown in Figure 24 as the ratio of the measured peak to AICC calculated peak pressure. Substantial decreases in this ratio are observed for the quiescent lean burns indicating decreasing amounts of hydrogen are consumed during combustion as the steam concentration increases. The turbulent burns, on the other hand, appear to be less affected by the addition of moderate concentrations of steam; again preignition turbulence is an important factor. The combustion of near-stoichiometric concentrations also appear to be affected by moderate to high concentrations of steam for both turbulent and quiescent environments.

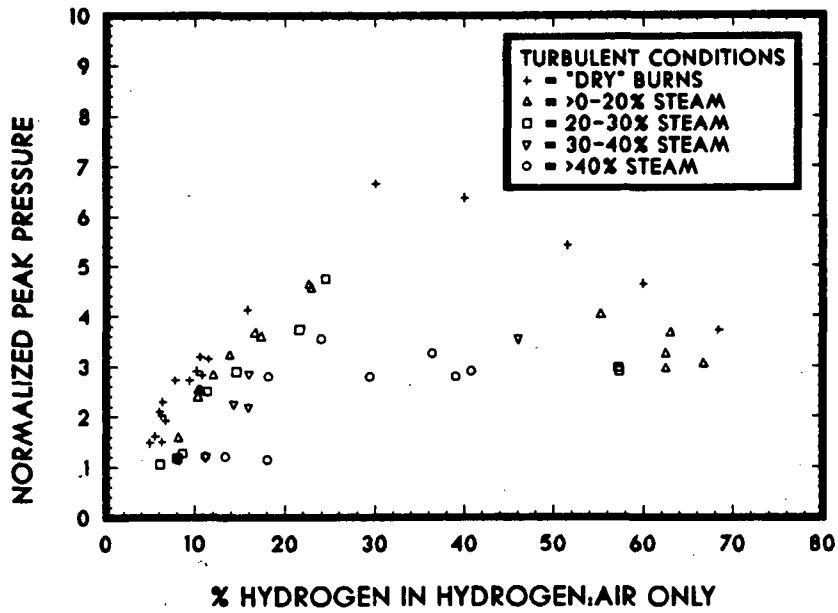

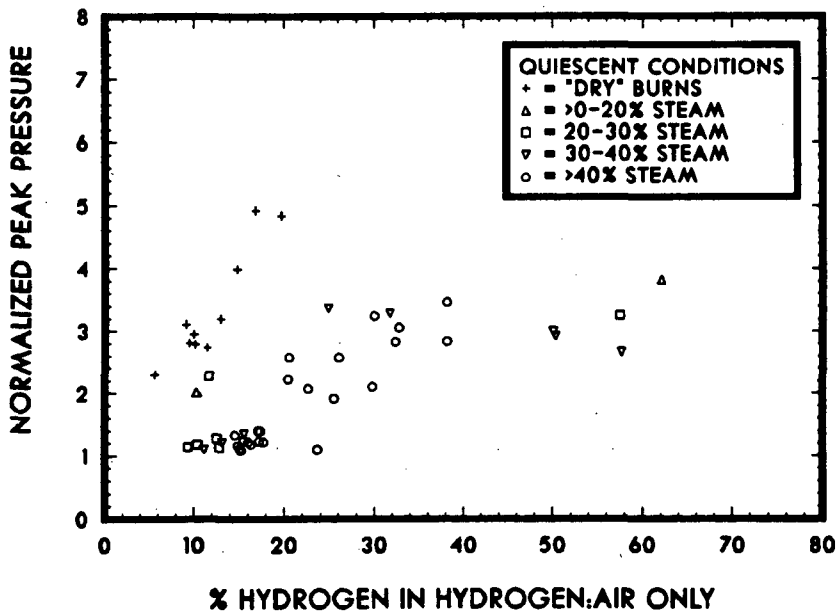

Figure 23
Normalized Peak Combustion Pressure for the Hydrogen:Air:Steam Burns, with fans on and off, as a Function of the Hydrogen Concentration in Hydrogen:Air only

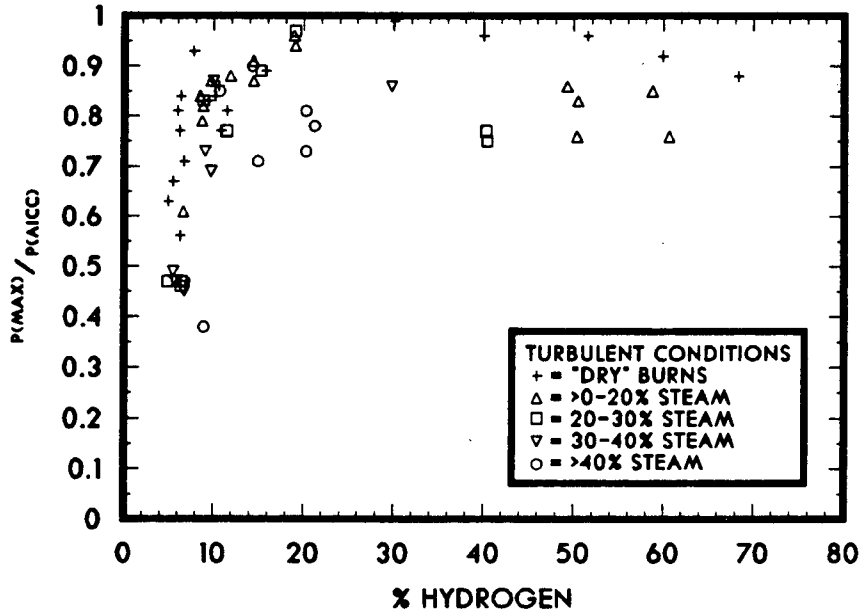

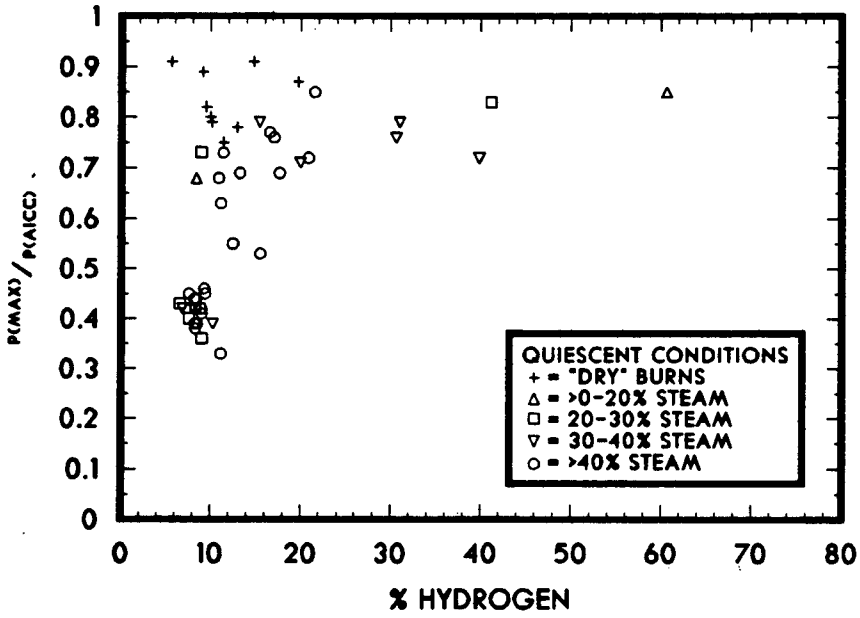

Figure 24
Ratio of the Experimental Peak to AICC Calculated
Peak Pressure for the Hydrogen:Air:Steam Burns

The results presented in Figures 23 and 24 show that if the hydrogen concentration is considered on a hydrogen-in-air basis only, steam affects the combustion of hydrogen with oxygen for both turbulent and quiescent conditions. If, however, these data are considered as a function of the volumetric hydrogen concentration as shown in Figure 25, relatively small differences exist between the lean turbulent burns with and without steam. The quiescent burns, on the other hand, are affected. Buoyancy is thought to dominate the flame propagation of lean hydrogen burns in a quiescent environment, while similar turbulent burns are less affected. For turbulent preignition conditions, steam acts only as an inert gas, similar to nitrogen in air, and combustion properties are similar to those observed for similar hydrogen:air burns with the same total volumetric hydrogen concentrations. For example, a turbulent burn containing (by volume) ~8% hydrogen and 20% steam would be similar to one containing no steam and ~8% hydrogen. Therefore, on a volumetric basis, the combustion characteristics of lean turbulent mixtures containing steam are not significantly affected by the addition of moderate quantities of steam compared to similar hydrogen:air burns. For the richer burns, however, buoyancy is not the dominant role of flame propagation and steam acts as a diluent, equally reducing the combustion pressures of quiescent and turbulent burns.

The duration of combustion was found to increase with increasing steam content compared to equivalent hydrogen:air burns. As shown in Figure 26, the quiescent burns are more influenced by the addition of steam than turbulent burns. The duration of combustion increases for the lean hydrogen:air concentrations in both turbulent and quiescent burns. Quiescent burns containing more than ~10% hydrogen in air seem to be most affected by the addition of steam, increasing the duration of combustion by as much as two orders-of-magnitude. Similar turbulent burns do not appear to be as affected unless rich steam concentrations (>40%) are present. Thus, the duration of combustion for hydrogen:air:steam burns is related not only to the quantities of steam available in the volume but also to the preignition turbulence.

4.3.2 Peak Gas Temperature Results

The "global" normalized peak gas temperatures were obtained from the hydrogen:air:steam burns processed with SMOKE and are presented in Appendix 5 with the combustion pressure results for reference. These results are shown in Figure 27. For the lean turbulent burns with steam, the normalized peak gas temperatures are generally equal to or slightly less than equivalent hydrogen:air burns. Quiescent lean burns are, however, significantly affected by the addition of steam. In both cases, the very rich hydrogen burns are more dramatically affected by the addition of steam, lack of sufficient oxygen for combustion, and diffusion rate of oxygen and hydrogen.

4.3.3 Heat Transfer Results

The "global" heat flux and energy deposition results have been calculated using SMOKE for the hydrogen:air:steam burns. The numerical results are presented in Appendix 6. The total peak heat flux results, shown in Figure 28, indicate that early-time combustion heat transfer is significantly reduced

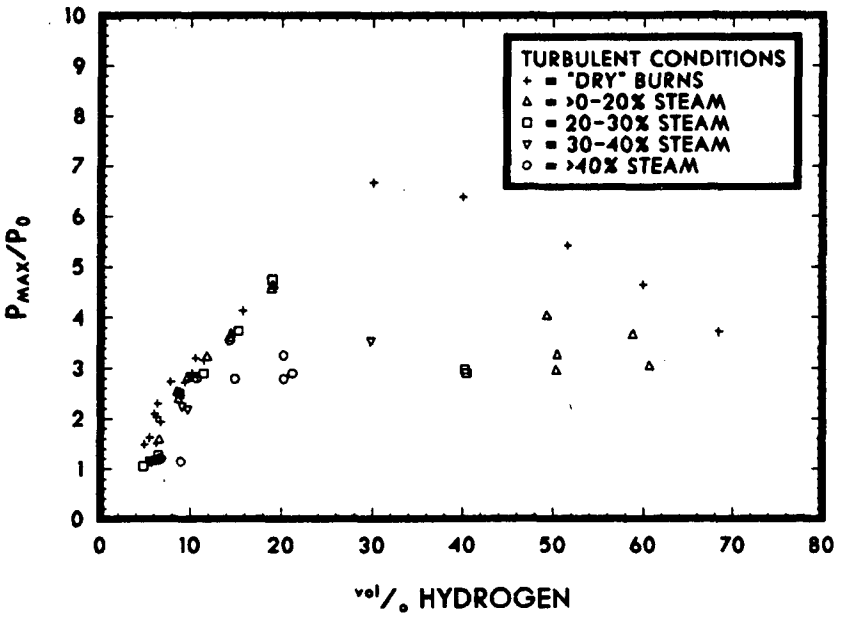

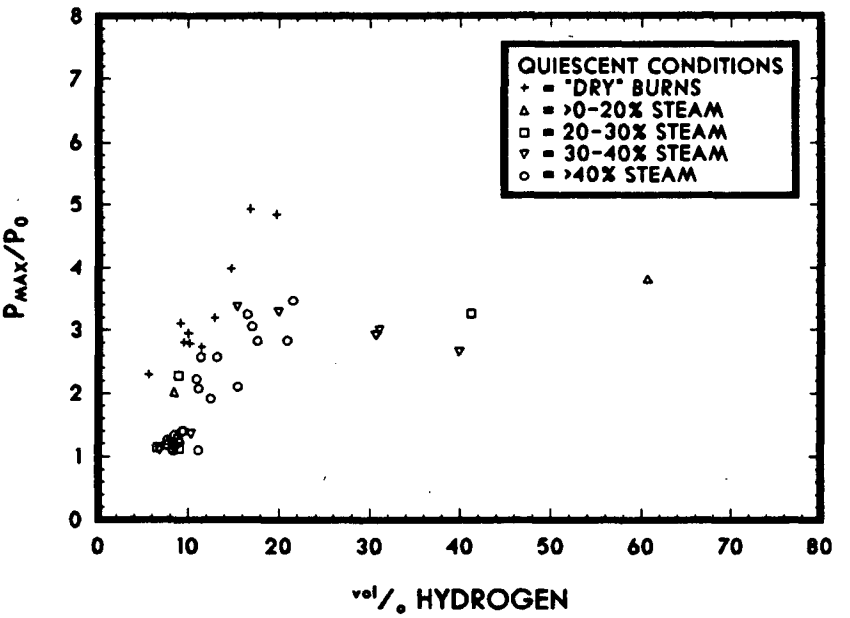

Figure 25
Normalized Peak Combustion Pressure for the Hydrogen:Air:Steam Burns, with fans on and off, as a Function of the Volumetric Hydrogen Concentration

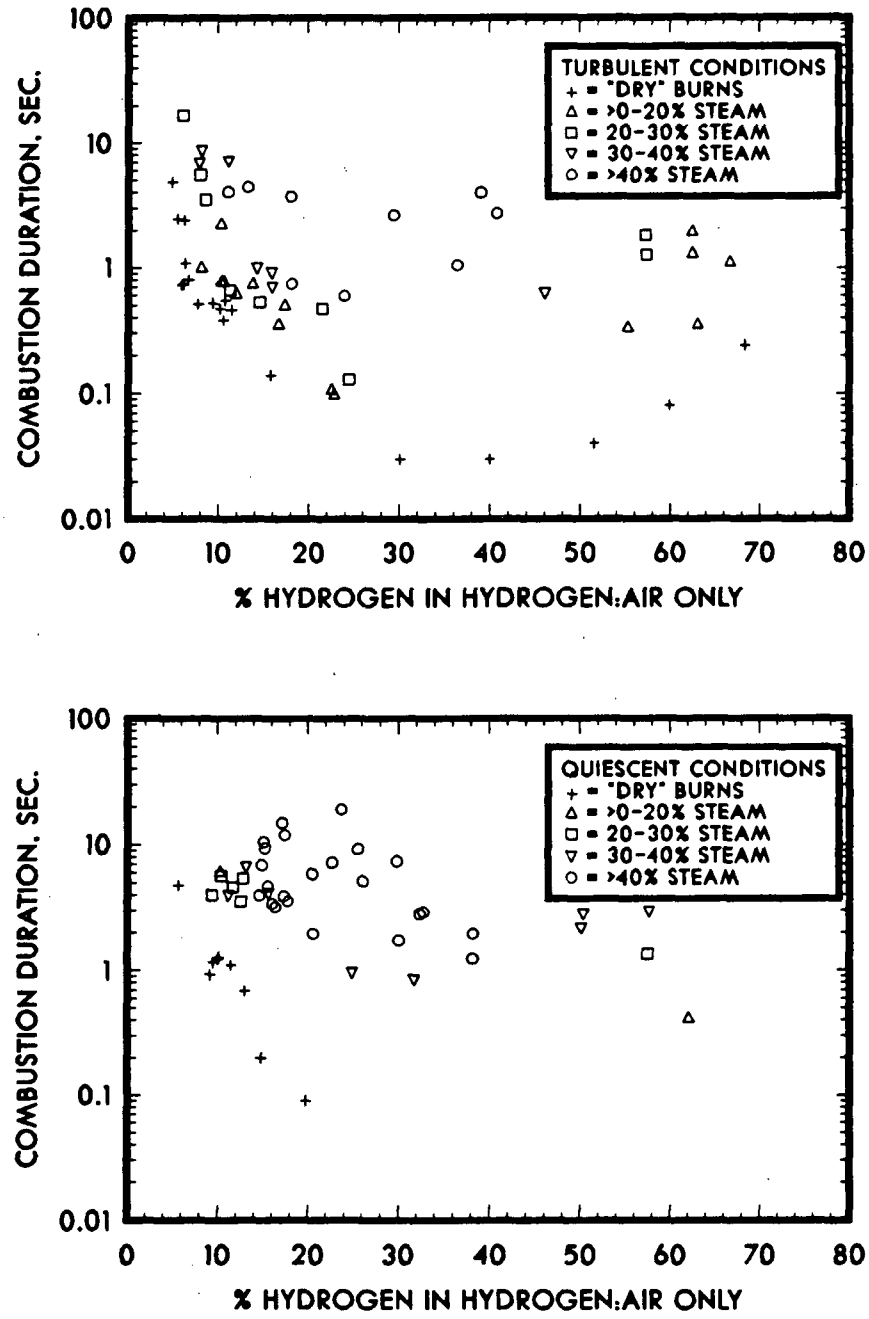

Figure 26
Combustion Duration for the Hydrogen:Air:Steam
Burns with and without Fans Operational

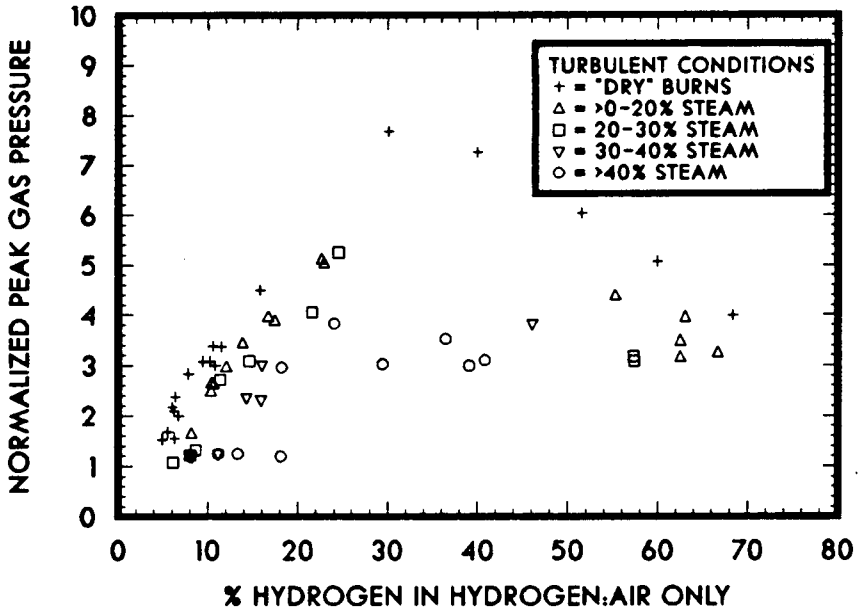

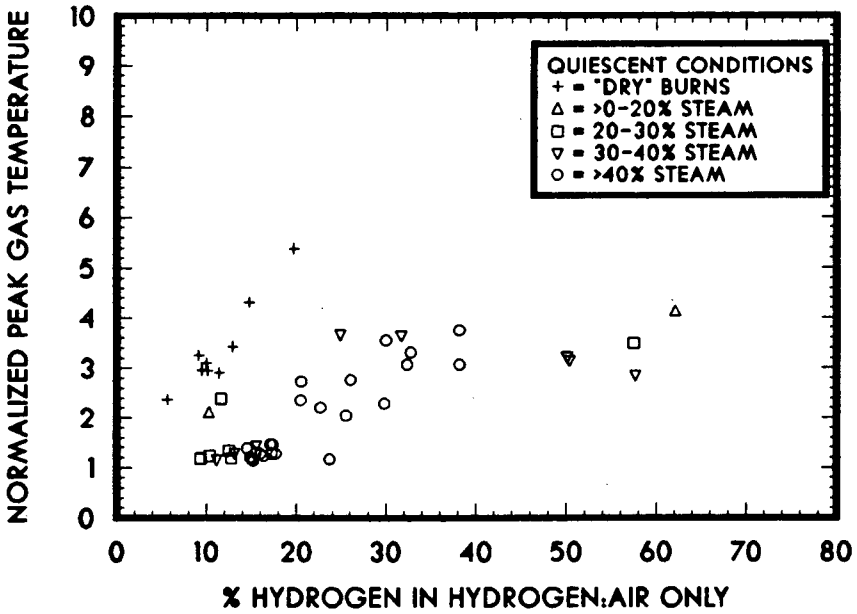

Figure 27
Normalized Peak "Global" Gas Temperature for the
Hydrogen:Air:Steam Burns with and without Fans Operational

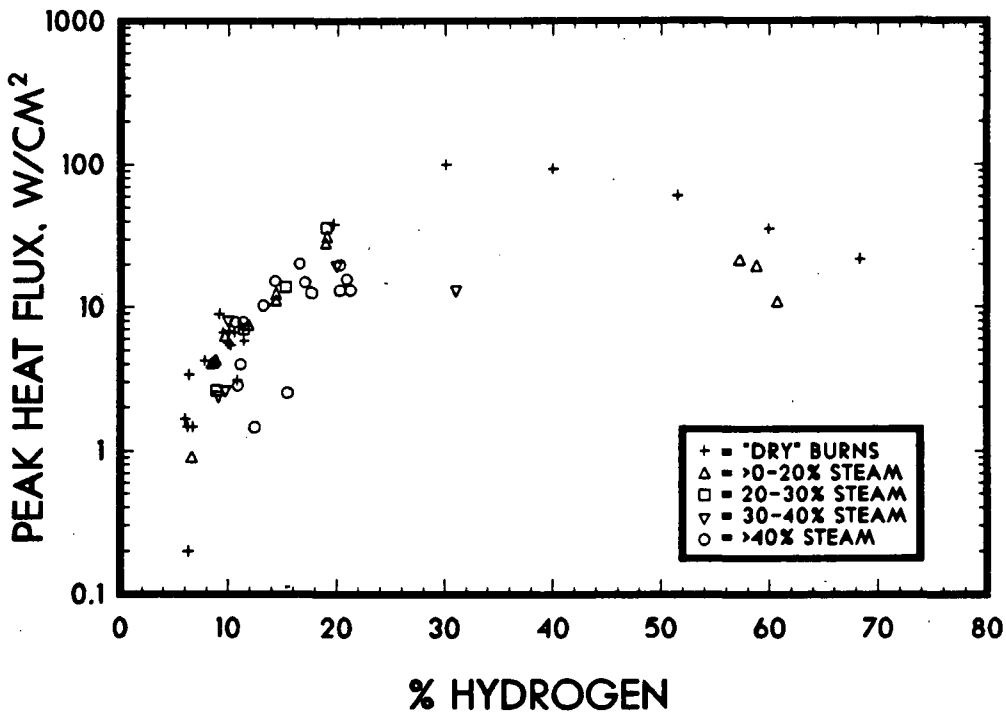

Figure 28
"Global" Peak Heat Flux for the Hydrogen:Air:Steam
Burns with and without the Fans Operational

by the addition of relatively large concentrations of steam. There are, however, numerous lean hydrogen burns in which the addition of moderate quantities of steam have increased the peak heat fluxes. As discussed earlier, the severity of a hydrogen:air:steam burn is clearly related to the hydrogen concentration relative to air (or more correctly the oxygen). If the total peak heat flux is plotted against the hydrogen percentage in air, as shown in Figure 29, a decrease in the peak heat flux due to the addition of steam is observed for all cases. This is consistent with expected trends. Steam provides a formidable heat sink, reducing the bulk gas temperature and retarding the normal combustion of hydrogen with oxygen. The partitioning of the early-time heat transfer (i.e., ratio of the radiative-to-total peak heat flux) is shown in Figure 30 plotted against the hydrogen concentration in air for the burns with and without steam. Here we observe that heat transfer shortly after combustion of a lean hydrogen:air environment is dominated by convection. With the addition of steam to the atmosphere, radiation begins to play a larger role in the early-time postcombustion heat transfer process due to the increased gas emittance and absorptance. However, as the hydrogen:air:steam flammability limits are approached by the addition of very rich steam concentrations, convection again becomes the prevalent heat transfer mechanism due to the reduced combustion severity and lower post-

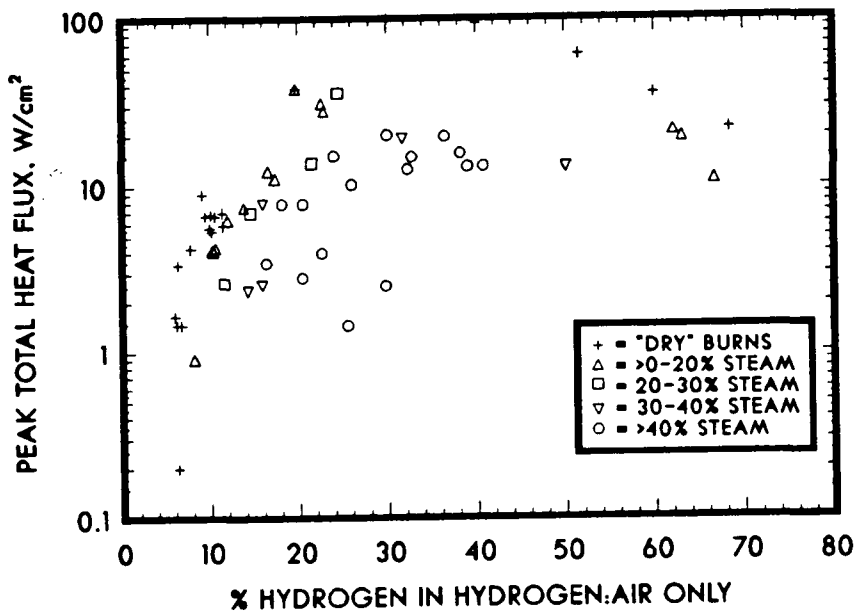

Figure 29
"Global" Peak Heat Flux for the Hydrogen:Air:Steam Burns Shown as a Function of the Hydrogen Concentration in Hydrogen:Air only

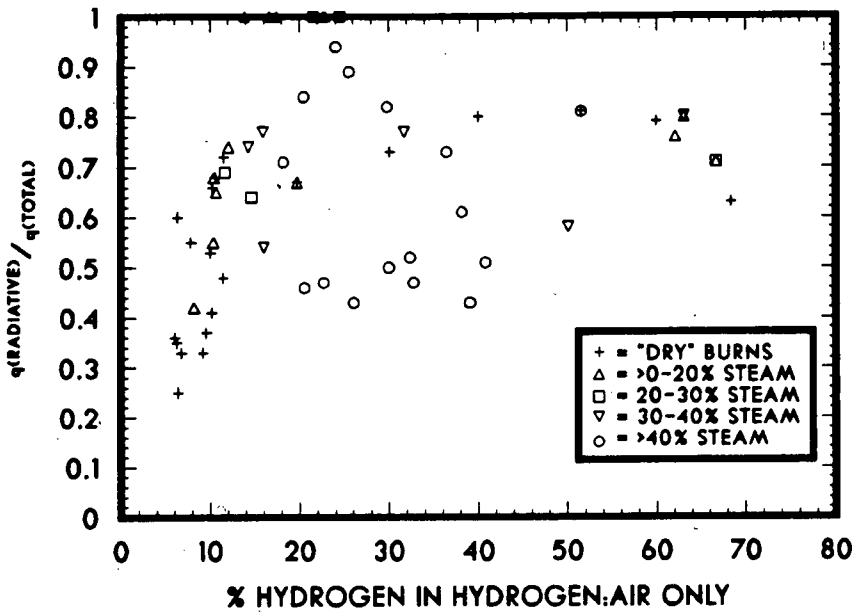

Figure 30
Ratio of the "Global" Peak Radiative to Total Peak Heat Flux for the Hydrogen:Air:Steam Burns shown as a Function of the Hydrogen Concentration in Hydrogen:Air only

combustion gas temperatures. Therefore, for a particular hydrogen concentration relative to air, the partitioning of the early postcombustion heat transfer is governed by the extent of combustion and the quantity of steam in the volume.

In Figure 31 the total energy deposition (i.e., the time-integrals of the calculated heat fluxes) for the hydrogen:air:steam burns is shown plotted against the volumetric hydrogen concentration. From this plot, the combustion severity again appears to increase with increasing steam content, especially for burns containing less than ~25% hydrogen by volume. Furthermore, the burns containing more than 40% steam by volume resulted in the greatest total energy depositions. If the same data are plotted against the hydrogen concentration in air, as shown in Figure 32, the influence of steam is less obvious. For moderate quantities of steam, the integral heat transfer is not appreciably changed since combustion is not significantly inhibited; i.e., approximately the same combustion energy is released for these burns as the "dry" burns. However, the rich steam quantities begin to inhibit the normal

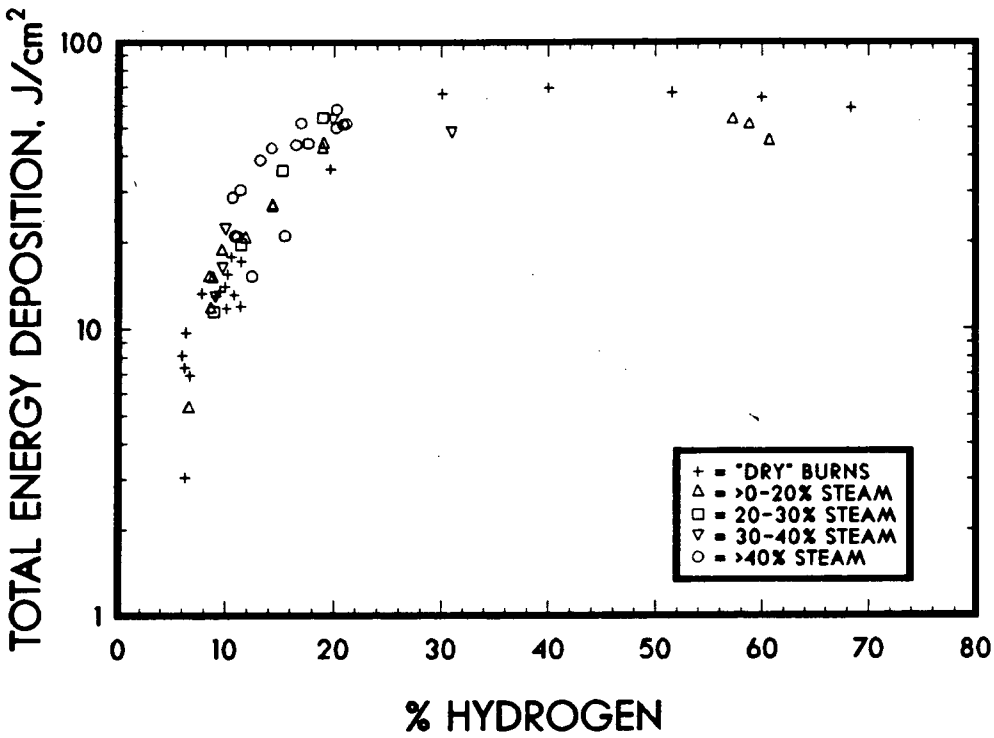

Figure 31
"Global" Cumulative Total Energy Deposition for the Hydrogen:Air: Steam Burns with and without the Fans Operational

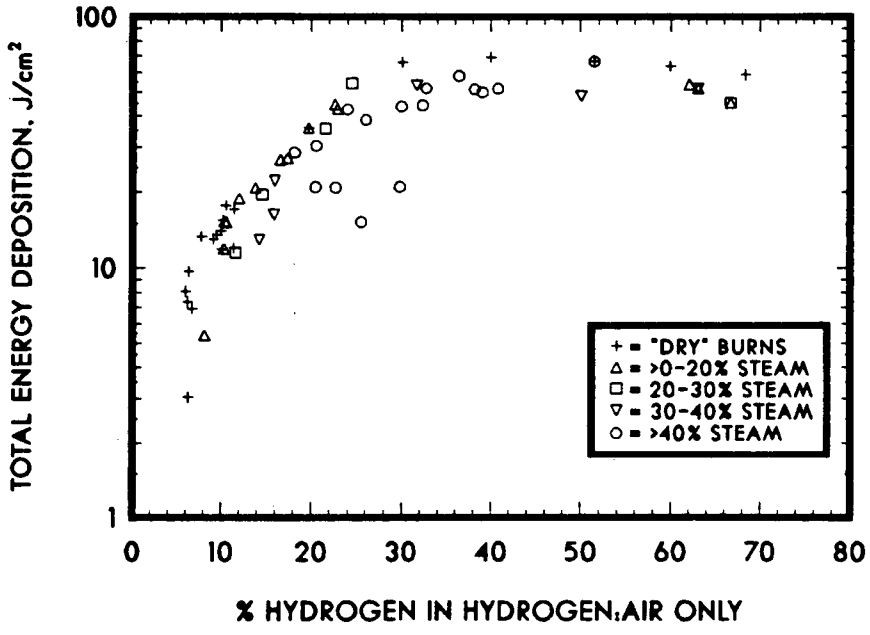

Figure 32
"Global" Cumulative Total Energy Deposition for the Hydrogen:Air: Steam Burns shown as a Function of the Hydrogen Concentration in Hydrogen:Air only

combustion process and the total energy released (or equally the total energy deposition) is correspondingly less. As an example, around stoichiometry the addition of more than ~40% steam reduces the energy deposition from ~70 J/cm^2 to ~50 J/cm^2.

The partitioning of the heat transfer is significantly changed by the addition of steam, as shown in Figure 33 where the ratio of the radiative to total heat transfer quantities are shown against the volumetric hydrogen concentration. The addition of steam greatly influences the radiative heat transfer mechanisms during the postcombustion cooling processes. For burns containing less than ~10% hydrogen, the radiative heat transfer increases from ~50% of the total transfer for burns without steam to as much as ~70% for those with steam. Thus, radiation heat transfer is the dominant gas cooling mechanism following combustion of the lean burns with steam, although natural convection would be expected to ultimately dominate the late-time heat transfer process.

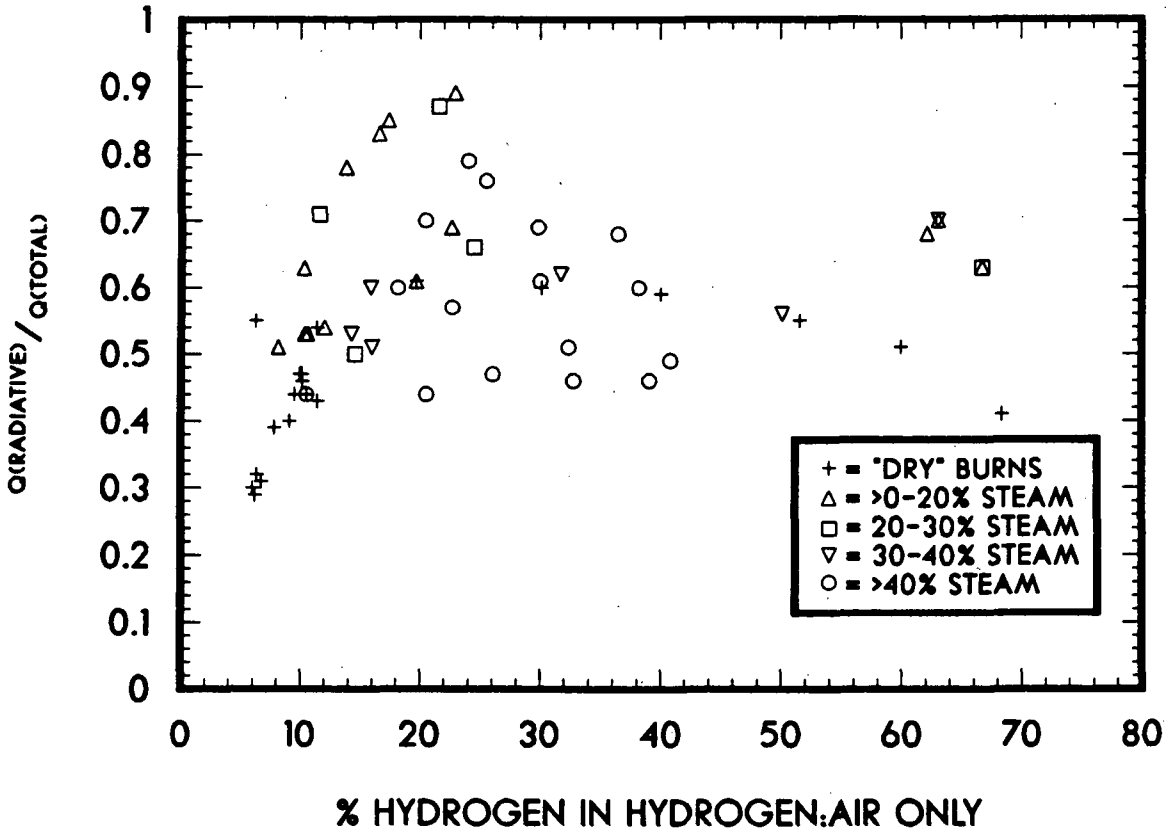

Figure 33
Ratio of the "Global" Radiative to Total Energy
Deposition for the Hydrogen:Air:Steam Burns

In general, we see from the FITS data that steam reduces the overall heat transfer compared to equivalent hydrogen:air burns at these scales. Steam does affect the partitioning of the heat transfer mechanisms compared to the "dry" hydrogen:air burns; i.e., radiation becomes the dominant heat transfer mechanism for the lean hydrogen burns with rich steam concentrations. The important parameter which must be accounted for when considering the effect of steam as a diluent is the quantity of hydrogen relative to the available air. If the volumetric concentrations are considered alone when analyzing these data, misleading conclusions about the effect of steam on the postcombustion heat transfer processes and general combustion characteristics could result.

4.4 Combustion Completeness

Gas samples were taken in a few of the combustion experiments reported here. These gas samples were taken before and after the burns and were analyzed with a gas chromatograph. However, due to systematic problems with the sampling procedure, gas samples were not taken in all of the experiments. Furthermore, the data obtained and reported in this section is used only to compute the fraction burned and not for quantitative interpretation of the initial gas concentrations. The difficulty in obtaining accurate pre and posttest "grab samples" has plagued numerous experimentalist in the field [16, 23]. Desirable alternatives include a dynamic system capable of on-line analysis of the gas concentrations inside the FITS chamber. One possibility would be a mass spectrometer, giving rapid and potentially accurate results with relatively little maintenance or disturbance from condensables such as steam.

The gas samples taken during this series are shown in Table 1. As with other facilities, a 10 to 15% difference occurred between the partial pressure calculations and the gas analysis which is attributed to systematic problems. Therefore, the gas sample analysis was used only to compute the approximate percent fraction burned during combustion according to:

$$\text{fraction burned} = \frac{(\%H_2)_i - (\%H_2)_f \left[\dfrac{(\%N_2)_i}{(\%N_2)_f} \right]}{(\%H_2)_i} \tag{4.5}$$

where $(\%H_2)_i$ = the preburn hydrogen concentration,
$(\%H_2)_f$ = the postburn hydrogen concentration,
$(\%N_2)_i$ = the preburn nitrogen concentration, and
$(\%N_2)_f$ = the postburn nitrogen concentration.

These results are shown in Figure 34 and generally show that as the steam fraction increases, the extent of the burn decreases. Furthermore, most of the burns above ~8% hydrogen by volume appear to be relatively complete, although the data are sparse and should not be over emphasized.

Table 1
Pre and Posttest Gas Sample Analysis for 14 Combustion Tests.

Burn Number	Test ID	%H_2 Precombustion	%N_2 Precombustion	%H_2 Postcombustion	%N_2 Postcombustion	Fraction Burned
129	HECTR5	6.25	73.53	5.45	74.03	0.13
130	HECTR6	7.11	75.97	5.73	74.41	0.18
131	HECTR7	11.41	69.18	TRACE	85.89	1.00
132	HECTR8	13.18	67.91	N.D.	84.85	1.00
133	HECTR9	13.43	67.89	3.55	83.77	0.85
134	HECT10	16.58	65.53	N.D.	87.44	1.00
137	HECT13	5.40	75.09	0.68	80.01	0.88
138	HECT14	7.80	73.47	N.D.	81.96	1.00
139	HECT15	10.04	70.43	N.D.	82.94	1.00
140	HECT16	7.01	74.24	3.95	76.71	0.46
142	HECT18	10.93	70.27	TRACE	82.73	1.00
143	HECT19	13.52	68.55	N.D.	86.10	1.00
144	HECT20	14.03	67.28	2.35	81.86	0.86
145	HECT21	17.06	65.91	N.D.	87.75	1.00

TRACE = Trace amounts were detected in the sample.
N.D. = None detected

- Results are based on H_2 +(O_2+AR) + N_2 = 100%
- These gas analyses were performed by Sandia's Analytical Chemistry Division and do not account for any water vapor present in the sample (i.e., dry gas analysis).

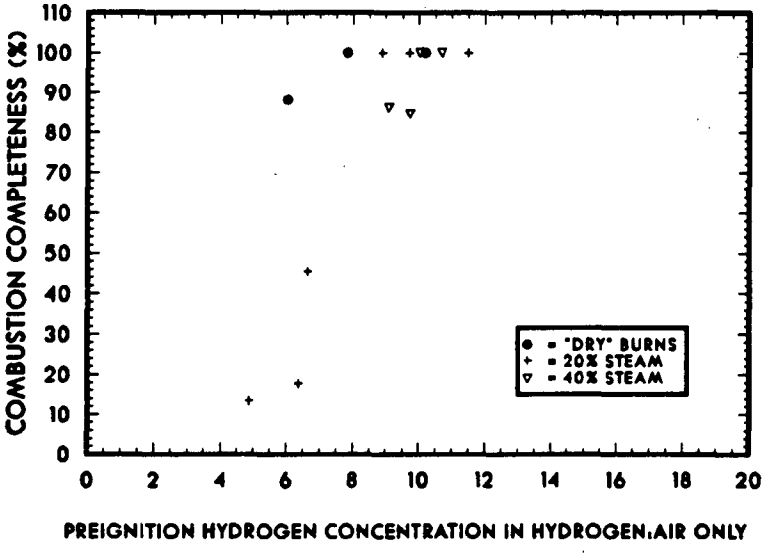

Figure 34
Combustion Completeness Data shown Plotted against the Precombustion Volumetric Hydrogen Concentration

5. CONCLUSIONS

This work has provided a complete data base for hydrogen:air:steam combustion characteristics and flammability limits at intermediate scale. Experimentally observed flammability limits for hydrogen:air:steam mixtures in turbulent and quiescent environments were measured to within an average of $\pm$7.5 and $\pm$2.2% of the calculated hydrogen and steam concentration, respectively. An exponential peeling routine was used to define a correlation for these data which describes the entire region of flammability and is given by;

$$\%\text{Steam} = 100 - \%H_2 - 37.3 \cdot e^{-0.007\%H_2} - 518.0 \cdot e^{-0.488\%H_2} \qquad (5.1)$$

This correlation may be used in reactor safety analysis codes for determining the flammability of a calculated mixture. It could also be used to estimate the earliest time into an accident sequence that ignition of a hydrogen:air: steam environment could occur assuming an ignition source were available.

Transient combustion pressures have been measured for most of these experiments. The normalized combustion peak pressure (P_{max}/P_o) was found to increase with increasing hydrogen concentrations of up to ~30%, at which point a decrease was observed for further increases in hydrogen concentration. Steam was found to decrease the normalized peak pressures compared to the hydrogen:air counterpart. Comparison of the experimentally measured peak pressure to the AICC calculated peak indicates that relatively complete combustion occurs (>95%) for hydrogen concentrations greater than ~10%, while lesser quantities of hydrogen are burned as the lean hydrogen:air flammability limit is approached. Turbulence was found to increase the extent of combustion and combustion characteristics of the lean burns, while not appreciably affecting the combustion characteristics of rich burns. Ambient preignition temperatures of ~300 K resulted in more severe combustion environments than equivalent burns at elevated temperature (~385 K). This result is directly related to the decrease in hydrogen and oxygen mass as the bulk temperature increases for a given fixed volume (e.g., for a fixed volume and air partial pressure, increases in the bulk gas temperature result in lesser quantities of hydrogen being introduced into the vessel to achieve the same partial pressure condition). Thus, as we observed, more severe burns for combustion experiments at lower preignition temperatures would be expected.

The experimental pressure signatures were used to infer the "global" total, convective and radiative postcombustion energy deposition (or thermal loading) and peak heat fluxes. These results indicate that burns at lower preignition temperatures tended to be more severe than those at elevated temperatures. Convection was found to play the dominant role in the leaner (<15%) hydrogen:air burns, accounting for 70 to 90% of the postcombustion heat transfer while radiation and convection played equal roles near stoichiometry. Steam was found to increase the total energy deposition and peak heat fluxes if considered as a function of the volumetric hydrogen concentration, especially for hydrogen concentrations of 25% or less. If, however, the heat transfer results are considered as a function of the hydrogen concentration in

air, the addition of steam tends to decrease the total energy deposition and peak heat fluxes. Thus, the postcombustion heat transfer characteristics are governed by the hydrogen concentration in air.

Radiation was found to dominate the postcombustion heat transfer processes for lean hydrogen burns containing steam. Furthermore, comparisons to the large-scale NTS results show that the radiative fraction of the total energy deposition at this scale was approximately half that observed at large-scale. This result is a scaling phenomena; the partitioning of the radiative heat transfer is directly related to the characteristic length-scale for radiation. In particular, the gas emittance would be expected to approximately double due to the increased radiation length scale; e.g., an increase in the radiation length scale will effectively increase the gas emittance. Based on differences in vessel geometry and volume, the bulk gas emittance and radiative partition in the NTS tests would be expected to increase by approximately twice the values observed in the FITS vessel.

Generally, the combustion pressures, "global" gas temperatures, and "global" heat transfer data provided in this report should be useful in assessing the importance of hydrogen:air:steam flammability limits and combustion characteristics for nuclear reactor safety analyses. The data provide useful reference points for benchmarking existing and newly developed computer codes for hydrogen:air:steam combustion characteristics and for containment response modelling. These data should also provide useful information for determining the response of safety-related equipment to hydrogen burns.

6. References

1. R. G. Zalosh et al., Analysis of the Hydrogen Burn in the TMI-2 Containment, EPRI NP-3975, Factory Mutual Research Corporation, Massachusetts, April 1985.

2. Core-Meltdown Experimental Review, NUREG/CR-0205, SAND 74-0382 (Revision), Sandia National Laboratories, Albuquerque, NM, March 1977.

3. M. P. Sherman et al., The Behavior of Hydrogen During Accidents in Light Water Reactors, NUREG/CR-1561, SAND80-1495, Sandia National Laboratories, Albuquerque, NM, August 1980.

4. A. L. Camp et al., Light Water Reactor Hydrogen Manual, NUREG/CR-2726, SAND82-1137, Sandia National Laboratories, Albuquerque, NM, August 1983.

5. A. M. Shapiro and T. R. Moffette, Hydrogen Flammability Data and Applications to PWR LOCA, WARD-SC-545 Bettis Plant, 1957.

6. M. G. Zabetakis, Research on the Combustion and Explosion Hazards of Hydrogen-Water Vapor-Air Mixtures, Bureau of Mines, Pittsburgh, Pennsylvania, AECU-3327, September 1956.

7. M. Berman and J. C. Cummings, "Hydrogen Behavior in Light Water Reactors," Nuclear Safety, Vol. 25, No. 1, January-February 1984.

8. M. Berman et al., Light Water Rector Safety Research Program Semiannual Report, April-September 1982, NUREG/CR-3407, SAND83-1576, Sandia National Laboratories, Albuquerque, NM, October 1983.

9. H. Tamm et al., "A Review of Recent Experiments at WNRE on Hydrogen Combustion," Proceedings of the Second International Conference on the Impact of Hydrogen on Water Reactor Safety, M. Berman, J. Carey, J. Larkins, and L. Thompson (technical program committee), NUREG/CP-0038, EPRI RP 1932-35, SAND82-2456.

10. W. E. Lowry et al., Final Results of the Hydrogen Igniter Experimental Program, NUREG/CR-2486, UCRL-53036, February 1982.

11. Tennessee Valley Authority, Sequoyah Nuclear Plant, Research Program on Hydrogen Combustion and Control Quarterly Report #3, Appendix A.2, June 1981.

12. D. Renfro et al., "Development and Testing of Hydrogen Ignition Devices," Proceedings of the Second International Conference on the Impact of Hydrogen on Water Reactor Safety, M. Berman, J. Carey, J. Larkins, and L. Thompson (technical program committee), NUREG/CP-0038, EPRI RP 1932-35, SAND82-2456.

13. S. F. Roller et al., "Medium-Scale Tests of H2:Air:Steam Systems," Proceedings of the Second International Conference on the Impact of Hydrogen on Water Reactor Safety, M. Berman, J. Carey, J. Larkins, and L. Thompson (technical program committee), NUREG/CP-0038, EPRI RP 1932-35, SAND82-2456.

14. D. D. S. Liu et al., Canadian Combustion Studies Related to Nuclear Reactor Safety Assessment, Available as Atomic Energy of Canada Report AECL-6994, October 1980.

15. H. F. Coward and G. W. Jones, Limits of Flammability of Gases and Vapors, Bulletin 503, U. S. Bureau of Mines, Washington D. C., 1952.

16. W. B. Benedick et al., Combustion of Hydrogen:Air Mixtures in the VGES Cylindrical Tank, NUREG/CR-3273, SAND83-1022, Sandia National Laboratories, Albuquerque, NM, May 1984.

17. R. K. Kumar et al., Intermediate-Scale Combustion Studies of Hydrogen-Air-Steam Mixtures, EPRI NP-2955, Electric Power Research Institute, June 1984.

18. A. C. Ratzel, Data Analyses for Nevada Test Site (NTS) Premixed Combustion Tests, NUREG/CR-4138, SAND85-0135, Sandia National Laboratories, Albuquerque, NM, May 1985.

19. B. W. Marshall, Jr., Flammability Limits and Combustion Characteristics of Hydrogen:Air:Steam at Intermediate Scale, Proceedings of the ANS/ENS Topical Meeting on the Operability of Nuclear Power Systems in Normal and Adverse Environments, Albuquerque, NM, September 29 - October 3, 1986.

20. B. W. Marshall, Jr., Hydrogen:Air:Steam Flammability Limits and Combustion Results at Intermediate Scale, Presented at the 1986 Spring Technical Meeting of The Combustion Institute, Banff, Alberta, Canada, April 28 - 30, 1986.

21. S. Gordon and B. J. McBride, Computer Program for Calculation of Complex Chemical Equilibrium Compositions, Rocket Performance, Indicent and Reflected Shocks, and Chapman-Jouguet Detonations, NASA SP-273, Washington DC: Scientific and Technical Info Ofc, NASA, 1971.

22. A. C. Ratzel, S. N. Kempka, J. E. Shepherd, and A. W. Reed, SMOKE: A Data Reduction Package for Analysis of Combustion Experiments," NUREG/CR-4136, SAND83-2657, Sandia National Laboratories, Albuquerque, NM, September 1985.

23. S. F. Roller, Pressure Measurements in a Hydrogen Combustion Environment: Hydrogen-Air Combustion Test Series 1 and 2 in the FITS Tank, NUREG/CR-3721 (1 of 2), SAND83-2621 (1 of 2), Sandia National Laboratories, Albuquerque, NM, March 1985.

24. B. W. Marshall, Jr. and A. C. Ratzel III, Pressure Measurements in a Hydrogen Combustion Environment: An Evaluation of Three Pressure Transducers, NUREG/CR-3721 (2 of 2), SAND83-2621 (2 of 2), Sandia National Laboratories, Albuquerque, NM, May 1984.

25. E. H. Richards and J. J. Aragon, Hydrogen-Burn Survival Experiments at Fully Instrumented Test Site (FITS), NUREG/CR-3521, SAND83-1715, Sandia National Laboratories, Albuquerque, NM, August 1984.

26. M. Berman, ed., Light Water Reactor Safety Research Program Semiannual Report, April-September 1981, NUREG/CR-2481, SAND82-0006, Sandia National Laboratories, Albuquerque, NM, October 1982.

27. I. L. Drell and F. E. Belles, Survey of Hydrogen Combustion Properties, National Advisory Committee for Aeronautics, Report 1383, 1958, Update 1975.

28. C. C. Wong, HECTR Development and Assessment, SAND85-1792C, Proceedings of the 13th Water Reactor Safety Research Information Meeting, Gaithersburg, MD, October 1985.

29. A. L. Camp, M. J. Wester, and S. E. Dingman, HECTR Version 1.0 User's Manual, NUREG/CR-3913, SAND84-1522, Sandia National Laboratories, Albuquerque, NM, February 1985.

30. R. E. Henry, et al., Technical Report 16.2-3 MAAP Modular Accident Analysis Program User's Manual-Vol. I, Industry Degraded Core Rulemaking Program, August 1983.

31. A. C. Ratzel and J. E. Shepherd, "Heat Transfer Resulting from Premixed Combustion," Heat Transfer and Fire and Combustion Systems, HTD-Vol. 45, Published by ASME, SAND84-2262C, August 1985, pp 191-202.

32. S. N. Kempka, A. C. Ratzel, A. W. Reed, and J. E. Shepherd, Postcombustion Convection in an Intermediate-Scale Vessel, Proceedings of the joint ANS/ASME conference on design, construction, and operation of Nuclear Power Plants, Portland, Oregan, SAND83-2180C, August 1984.

APPENDIX 1

Corrected Initial Data

This appendix presents the corrected initial precombustion gas concentrations of hydrogen and steam as well as the initial temperature and pressure for each of the 239 burns performed in this test series. For convenience, the burn have been numbered to provide a method of correlating the initial data to the combustion pressure and "global" heat transfer results presented in subsequent appendices and throughout this report. The type of ignition for each test was classified according to the following:

S = Spark plug ignition;
G = Glow plug ignition;
M = Marginal ignition (i.e., $\Delta P/\Delta P_{aicc} \leq 0.1$);
N = No detectable ignition.

The preignition gas turbulence is either given a fans-on designation ('O') or a fans-off designation ('F') depending upon the condition of the fans at the time of ignition.

BURN	TEST ID	% H_2	%H_2O	P_0 (atm)	T_0 (K)	IGN.	FAN
1	H06S30	7.67	26.16	1.18	368.85	S	F
2	S30H06	6.61	29.46	1.23	370.75	M	F
3	S30H05	5.74	30.07	1.21	379.35	N	0
4	S30H05	6.26	26.51	1.18	363.85	M	F
5	S30H05	6.51	24.88	1.15	355.45	B	F
6	30S05H	6.87	30.78	1.25	373.45	N	0
7	30S05H	7.52	27.98	1.21	367.25	N	0
8	30S06H	9.04	29.33	1.26	379.65	M	F
9	30S07H	8.84	29.43	1.25	379.25	S	F
10	H07S40	10.25	34.10	1.40	366.45	S	F
11	07H40S	8.13	38.07	1.47	379.65	M	F
12	06HS40	6.89	38.08	1.42	379.85	M	F
13	05HS40	7.37	38.03	1.41	380.35	N	F
14	H05S40	7.17	37.51	1.40	374.05	N	0
15	H05S40	7.49	36.84	1.37	374.45	N	0
16	H07S50	9.00	47.86	1.76	392.55	M	F
17	H06S50	8.26	45.11	1.63	378.45	M	F
18	S50H06	8.51	42.71	1.61	369.35	M	F
19	S50H05	8.31	45.38	1.67	381.05	M	F
20	05H50S	6.17	45.11	1.64	379.15	N	0
21	05H50S	8.47	41.70	1.67	364.85	S	F
22	50SH05	6.03	46.44	1.67	382.75	N	0
23	H08S50	9.32	45.54	1.76	383.15	G	F
24	S50H08	9.44	45.71	1.80	382.35	M	F
25	H10S50	11.66	43.91	1.82	379.25	G	F
26	H13S50	15.41	38.06	1.70	376.45	G	F
27	H10S55	11.41	44.45	1.80	375.95	G	F
28	H10S60	9.92	49.75	1.94	378.35	N	0
29	H10S60	7.65	50.61	1.87	381.05	G	F
30	10H60S	8.97	50.33	1.91	378.45	M	0
31	HH10	9.97	0.00	0.89	359.45	S	F
32	S55H08	8.81	45.48	1.75	379.65	M	F
33	H20S45	19.94	37.11	1.95	379.85	S	F
34	H20S50	22.75	41.30	2.17	384.55	M	F
35	S50H20	22.33	44.20	2.43	382.55	N	0
36	S50H20	21.28	46.01	2.38	381.95	N	0
37	H20S48	21.57	43.47	2.25	378.85	G	F
38	S48H20	20.88	45.29	2.27	383.45	G	F
39	H30S43	30.92	41.07	2.76	385.95	N	0
40	H30S43	31.28	41.17	2.75	386.25	N	0
41	H30S40	30.53	39.39	2.52	376.05	N	0
42	H30S38	30.60	36.77	2.35	386.35	N	0
43	10H20S	8.96	22.96	1.13	382.05	S	F
44	H30S35	30.41	33.67	2.18	375.35	G	F
45	40S30H	31.02	38.04	2.48	384.35	G	F
46	S45H30	30.97	43.30	2.98	385.75	N	0

BURN	TEST ID	% H_2	%H_2O	P_0 (atm)	T_0 (K)	IGN.	FAN
47	43SH30	30.91	41.27	2.75	388.55	N	0
48	30HS40	30.62	39.18	2.54	375.85	G	F
49	H40S30	39.89	30.83	2.60	395.65	G	F
50	H40S35	37.37	37.31	3.01	391.75	N	0
51	10HS15	8.44	18.13	1.08	395.75	S	F
52	40H33S	41.87	30.99	2.80	386.55	N	0
53	30SH40	41.20	28.33	2.47	381.05	M	F
54	33SH40	41.25	31.53	2.77	385.25	N	0
55	06HS30	5.72	30.45	1.24	384.95	M	0
56	30SH06	5.54	30.38	1.24	385.55	G	0
57	07HS40	6.77	39.28	1.46	377.45	M	0
58	S4007H	6.64	40.42	1.48	385.75	S	0
59	50SH07	6.81	48.91	1.79	383.55	S	0
60	H50S25	50.39	25.03	3.12	387.35	N	0
61	S30H40	21.23	47.97	2.52	382.85	G	0
62	S3040H	40.44	29.52	2.59	381.65	G	0
63	30HS35	29.80	35.30	2.26	387.05	G	0
64	S4520H	20.26	44.40	2.21	388.65	G	0
65	H4030S	40.29	29.66	2.58	382.65	G	0
66	50SH20	20.26	48.12	2.50	379.95	G	0
67	S50H15	14.92	49.32	2.17	389.75	G	0
68	15H40S	14.29	40.52	1.71	387.15	S	0
69	30S15H	15.27	29.18	1.42	391.35	G	0
70	50HS10	49.29	10.83	1.99	391.25	G	0
71	H50S20	50.46	19.30	2.59	384.65	G	0
72	50HS20	50.36	19.47	2.62	392.45	G	0
73	15S15H	14.40	17.14	1.17	391.15	S	0
74	S10H15	14.40	13.56	1.11	403.05	S	0
75	H2015S	18.94	17.22	1.25	397.55	S	0
76	10S13H	11.89	14.18	1.07	392.75	S	0
77	H5HF	3.44	0.00	0.84	384.75	N	0
78	HH5F	5.03	0.00	0.83	406.15	N	0
79	H6HF	5.54	0.00	0.83	393.75	S	0
80	HF5H	5.00	0.00	0.83	394.45	N	0
81	HF5H	5.60	0.00	0.83	389.35	N	0
82	8HFW	6.96	0.00	0.84	311.55	S	0
83	8HWF	7.77	0.00	0.85	352.25	S	0
84	60H10S	60.67	9.07	2.64	393.25	G	0
85	H60S5	58.77	6.80	2.27	396.35	G	0
86	H5025S	50.56	24.30	3.08	393.55	N	0
87	FW8H	8.43	0.00	0.88	311.05	S	0
88	H6010S	57.23	7.85	2.41	382.55	G	F
89	10HH	9.41	0.00	0.92	392.05	S	0
90	H60S15	57.18	16.86	3.10	377.85	N	F

BURN	TEST ID	% H_2	%H_2O	P_0 (atm)	T_0 (K)	IGN.	FAN
91	S5010H	10.95	42.85	1.81	385.55	N	0
92	H1010S	8.70	15.68	1.12	392.65	S	0
93	GC06	5.86	0.00	0.86	292.65	S	F
94	GC08	7.24	0.00	0.87	293.85	S	F
95	INIT1	9.30	0.00	0.90	296.25	S	0
96	INIT2	9.43	0.00	0.94	296.85	S	0
97	INIT3	11.55	0.00	0.98	296.25	S	0
98	INIT4	10.02	0.00	0.90	293.85	S	0
99	INIT5	14.49	0.00	0.95	296.25	S	0
100	INIT6	20.17	0.00	1.02	298.55	S	0
101	INIT7	6.41	0.00	0.86	302.75	S	0
102	INIT8	9.83	0.00	0.90	296.25	S	0
103	INIT9	11.19	0.00	0.92	298.05	S	0
104	FLAMM1	10.91	46.68	2.06	393.85	S	F
105	FLAMM2	11.41	53.56	2.40	382.05	N	0
106	FLAMM3	11.15	50.85	2.22	392.65	S	F
107	FLAMM4	11.14	52.97	2.28	384.35	M	F
108	FLAMM5	11.20	54.85	2.43	384.95	N	0
109	FLAMM6	13.80	54.67	2.64	393.85	N	0
110	FLAMM7	13.72	52.31	2.44	384.35	N	0
111	FLAMM8	12.48	51.12	2.26	398.55	G	F
112	FLAMM9	12.66	52.23	2.36	392.65	N	0
113	FLAM10	13.23	49.22	2.24	384.95	G	F
114	FLAM11	15.50	48.01	2.30	395.05	G	F
115	FLAM12	16.54	44.87	2.13	387.35	G	F
116	FLAM13	17.12	48.75	2.44	396.25	N	0
117	FLAM14	17.64	45.48	2.26	386.75	G	F
118	FLAM15	17.67	52.35	2.84	404.45	N	0
119	FLAM16	17.04	48.01	2.34	380.85	G	F
120	FLAM17	8.23	48.63	1.94	396.25	G	F
121	FLAM18	8.37	48.88	1.97	400.35	G	F
122	FLAM19	9.03	49.12	1.98	390.85	G	F
123	FLAM20	9.09	54.53	2.38	392.65	N	0
124	FLAM21	8.83	51.72	2.11	390.25	N	0
125	HECTR1	6.28	0.00	0.87	374.35	G	0
126	HECTR2	4.94	0.00	0.84	373.15	G	0
127	HECTR3	6.38	0.00	0.85	373.15	G	0
128	HECTR4	10.80	0.00	0.95	380.85	G	0
129	HECTR5	4.86	20.44	1.11	384.35	G	0
130	HECTR6	6.36	21.04	1.12	382.55	G	0
131	HECTR7	8.88	21.65	1.16	384.35	G	0
132	HECTR8	11.47	21.37	1.21	368.95	G	0
133	HECTR9	9.73	38.77	1.57	387.95	G	0
134	HECT10	10.68	41.23	1.69	390.85	G	0
135	HECT11	6.24	0.00	0.88	383.15	G	0
136	HECT12	6.74	0.00	0.88	393.85	G	0

BURN	TEST ID	% H_2	%H_2O	P_0 (atm)	T_0 (K)	IGN.	FAN
137	HECT13	6.03	0.00	0.87	383.75	G	0
138	HECT14	7.83	0.00	0.88	393.85	G	0
139	HECT15	10.19	0.00	0.91	392.65	G	0
140	HECT16	6.63	18.81	1.08	387.35	G	0
141	HECT17	8.53	17.97	1.10	384.35	G	0
142	HECT18	8.87	16.62	1.09	389.65	G	0
143	HECT19	9.70	19.39	1.14	388.55	G	0
144	HECT20	9.09	36.34	1.46	385.55	G	0
145	HECT21	10.01	37.43	1.53	383.75	G	0
146	H2OHD	16.85	0.00	0.98	384.35	S	F
147	ART1	5.62	0.00	0.84	376.65	S	F
148	ART2	12.91	0.00	0.95	377.25	S	F
149	ART3	14.74	0.00	0.96	387.35	S	F
150	ART4	15.76	0.00	0.96	377.85	S	0
151	ART5	8.02	0.00	0.87	295.65	S	0
152	ART6	15.56	0.00	0.95	295.05	S	0
153	PRES1	9.90	0.00	0.91	296.85	S	0
154	PRES2	18.95	0.00	1.01	298.05	S	0
155	PRES3	29.53	0.00	1.14	300.95	S	0
156	PRES4	9.29	0.00	0.89	306.25	S	0
157	PRES5	19.31	0.00	1.02	306.85	S	0
158	PRES6	9.36	0.00	0.91	296.85	S	0
159	PRES7	20.52	0.00	1.03	297.45	S	0
160	PRES8	31.32	0.00	1.17	300.35	S	0
161	PRES9	10.26	0.00	0.92	305.65	S	0
162	PRES10	11.05	0.00	0.91	305.65	S	F
163	PRES11	19.45	0.00	1.01	305.65	S	F
164	PRES12	9.67	0.00	0.89	298.05	S	0
165	PRES13	10.36	0.00	0.91	295.05	S	0
166	PRES14	9.25	0.00	0.90	296.85	S	0
167	PRES15	9.62	0.00	0.91	298.55	S	0
168	PRES16	22.65	0.00	1.06	296.25	S	F
169	PRES17	11.47	0.00	0.94	370.75	S	0
170	PRES18	9.53	0.00	0.94	374.35	S	F
171	PRES19	10.12	0.00	0.93	379.05	S	F
172	PRES20	9.13	0.00	0.92	355.35	S	F
173	PRES21	19.69	0.00	1.05	359.55	S	F
174	PRES22	11.43	0.00	0.94	398.55	S	F
175	PRH10A	9.34	0.00	0.87	293.25	S	0
176	PRH10B	9.36	0.00	0.86	296.85	S	0
177	PRH20A	20.09	0.00	0.96	297.45	S	0
178	PRH20B	18.98	0.00	0.94	300.35	S	0
179	PRH25A	24.32	0.00	1.01	303.35	S	0
180	PRH25B	24.16	0.00	1.05	295.05	S	0
181	PRH30A	29.23	0.00	1.13	299.15	S	0
182	PRH30B	29.47	0.00	1.16	303.35	S	0

BURN	TEST ID	% H_2	%H_2O	P_0 (atm)	T_0 (K)	IGN.	FAN
183	PRH10C	10.98	0.00	0.96	308.65	S	0
184	PRH20C	19.18	0.00	1.10	307.45	S	0
185	PRH10D	11.24	0.00	0.94	301.55	S	0
186	PRH30C	31.33	0.00	1.22	301.55	S	0
187	PRH35A	34.74	0.00	1.32	306.85	S	0
188	PRH10H	10.55	0.00	0.92	370.15	S	0
189	PRH20S	19.03	22.27	1.39	382.55	S	0
190	PRSH20	19.06	15.71	1.21	384.95	S	0
191	PRH50A	51.53	0.00	1.64	377.25	S	0
192	PRH60A	59.93	0.00	2.02	378.45	S	0
193	PRH30D	30.08	0.00	1.17	358.95	S	0
194	PRH40A	39.99	0.00	1.37	355.95	S	0
195	PRH40S	37.53	23.78	2.04	382.55	S	0
196	PRSH40	38.86	21.76	2.05	393.25	S	0
197	PR40HS	38.52	17.41	1.82	389.65	S	0
198	PRH70A	68.37	0.00	2.58	392.05	S	0
199	H10HD	7.09	0.00	0.87	390.85	S	F
200	LAST1	10.21	0.00	0.93	306.85	G	F
201	LAST2	10.68	0.00	0.92	305.65	G	F
202	LAST3	26.18	0.00	1.12	293.85	S	F
203	LAST4	27.58	0.00	1.12	306.25	S	F
204	LAST5	26.34	0.00	1.12	296.25	S	F
205	LAST6	27.28	0.00	1.12	302.15	S	F
206	LAST7	25.86	0.00	1.12	305.65	S	F
207	LAST8	26.43	0.00	1.12	310.45	G	F
208	LAST9	28.65	0.00	1.15	313.95	G	F
209	LAST10	25.99	0.00	1.14	298.55	G	F
210	LAST11	26.82	0.00	1.14	303.95	S	F
211	LAST12	25.83	0.00	1.12	308.65	G	F
212	LAST13	26.34	0.00	1.13	310.45	S	F
213	LAST14	26.69	0.00	1.14	315.15	G	F
214	LAST15	25.43	0.00	1.12	318.15	G	F
215	LAST16	26.35	0.00	1.14	318.75	G	F
216	RANGE1	9.78	0.00	0.90	293.15	S	F
217	RANGE2	18.51	0.00	1.01	292.65	S	F
218	RANGE3	10.28	0.00	0.91	296.25	S	F
219	RANGE4	8.94	0.00	0.89	296.25	S	F
220	RANGE5	18.93	0.00	1.00	296.85	S	F
221	RANGE6	9.97	0.00	0.90	293.25	S	F
222	RANGE7	11.14	0.00	0.91	296.25	S	0
223	RANGE8	18.53	0.00	1.02	300.95	S	0
224	RANGE9	27.97	0.00	1.14	300.95	S	0
225	RANG10	10.06	0.00	0.91	304.55	S	0
226	RANG11	20.76	0.00	1.03	303.95	S	0
227	RANG12	30.16	0.00	1.18	306.85	S	0
228	RANG13	10.80	0.00	0.93	296.25	S	0

BURN	TEST ID	% H_2	%H_2O	P_0 (atm)	T_0 (K)	IGN.	FAN
229	RANG14	20.41	0.00	1.04	296.25	S	0
230	RANG15	30.42	0.00	1.18	300.35	S	0
231	RANG16	12.65	0.00	0.95	305.65	S	0
232	RANG17	20.16	0.00	1.04	308.05	S	0
233	RANG18	9.31	0.00	0.91	297.45	S	0
234	RANG19	19.79	0.00	1.04	298.55	S	0
235	RANG20	30.17	0.00	1.19	302.75	S	0
236	RANG21	9.99	0.00	0.92	308.65	S	0
237	RANG22	20.11	0.00	1.04	309.25	S	0
238	RANG23	30.02	0.00	1.19	294.45	S	0
239	RANG24	9.98	0.00	0.92	302.15	S	0

APPENDIX 2
Experimental Uncertainty Analysis

As discussed in Section 3 of this report, the volumetric gas compositions were calculated using partial pressure calculations. The error or uncertainty associated with these calculations can be estimated using a Kline-McClintock uncertainty analysis [2.1]. In this analysis, the uncertainty associated with a calculated results r can be estimated as

$$w_r = \left\{ \left[\frac{\partial r}{\partial x1} w_{x1} \right] + \left[\frac{\partial r}{\partial x2} w_{x2} \right] + \ldots + \left[\frac{\partial r}{\partial xn} w_{xn} \right] \right\}^{0.5} \qquad \text{(A2-1)}$$

where x_1, x_2, ..., and x_n are the independent variables and w_{x1}, w_{x2}, ..., and w_{xn} are the uncertainties associated with each experimental measurement.

Using this technique, the uncertainty associated with the partial pressure calculations defined by Equations (3.1), (3.2), (3.8), and (3.9) can be estimated. If this technique is applied to the equation defining the hydrogen partial pressure (Equation (3.8)), the uncertainty associated with this calculation is given by;

$$w_{P_{hyd}} = \left\{ \left[1 + \left(\frac{T_3}{T_2} \right)^2 \right] \cdot \left[w_p^2 + \left(\frac{P_2}{T_2} \right)^2 w_{T_2}^2 \right] \right\}^{0.5} \qquad \text{(A2-2)}$$

In a like manner, the uncertainty associated with the steam partial pressure calculation (Equation (3.9)) is

$$w_{P_{stm}} = \left\{ \left[1 + \left(\frac{T_3}{T_2} \right)^2 \right] \cdot \left[w_P^2 + \left(\frac{P_2}{T_2} \right)^2 w_T^2 \right] \right\}^{0.5} \qquad \text{(A2-3)}$$

If the hydrogen and steam concentrations are calculated using Equations (3.1) and (3.2), respectively, then the uncertainty associated with these calculated results can be expressed as

$$w_{\%hyd} = \left\{ \left[\frac{w_{P_{hyd}}}{P_{stm}} \right]^2 + \left[\frac{-w_{P_{air}}}{P_{stm}} \right]^2 + \left[\frac{P_{hyd} - P_{air}}{P_{stm}} w_{P_{stm}} \right]^2 \right\}^{0.5} \qquad \text{(A2-4)}$$

and

$$w_{\%stm} = \left\{ \left[- \frac{w_{P_{hyd}}}{P_{stm}} \right]^2 + \left[\left(\frac{P_{hyd}}{P_{stm}} \right) \cdot w_{P_{stm}} \right]^2 \right\}^{0.5} \qquad \text{(A2-5)}$$

Therefore, the uncertainty associated with these calculations can be estimated if the uncertainty of each measurement is known.

For this analysis, the uncertainty of the experimental measurements are assumed to be $\pm$1°C for the temperature measurements and $\pm$0.0073 kPa (0.5 psia) of the static pressure measurement. On the average, the uncertainty of the calculated initial volumetric percentages for hydrogen and steam were within $\pm$7.5 % and $\pm$2.2 %, respectively, of the calculated concentration.

The experimental error of the dynamic pressure measurements can be estimated by considering each component in the data acquisition system at the facility. Generally, the pressure gauges used during this experimental series were found to be accurate to within $\pm$ ~5% over the entire range of the gauge response. The dynamic amplifiers are reported as being accurate to within 0.1% of the gain setting which has been checked and calibrated during the course of testing. The ADCs are accurate to within $\pm$9.8 mV (equivalent to one-bit of resolution) of the actual voltage which was generally small compared to the actual voltage reading and should introduce relatively small errors (i.e., < 1%). Thus, the integral error associated with the transient combustion pressure measurements were estimated to be within ~10%.

The uncertainty associated with the heat transfer calculations as inferred from the pressure signals has not been addressed in this work, but the reader should refer to Reference 2.2 for information pertaining to these codes.

References

2.1. J. P. Holman, Experimental Methods for Engineers, Third Edition, McGraw-Hill Book Company, 1978.

2.2. A. C. Ratzel, S. N. Kempka, J. E. Shepherd, and A. W. Reed, SMOKE: A Data Reduction Package for Analysis of Combustion Experiments," NUREG/CR-4136, SAND83-2657, Sandia National Laboratories, Albuquerque, NM, September 1985.

APPENDIX 3

Combustion Pressure Data for the Hydrogen:Air Burns

This appendix presents combustion pressure data for each of the hydrogen: air burns conducted. Included are the normalized peak pressures, the ratio of the measured peak to AICC calculated peak pressure, the combustion duration (measured as the time from ignition to the peak pressure), the mean pressure derivative, and the "global" bulk gas temperature as inferred from the computer programs referred to as SMOKE. Note that if the experimental data were not available due to hardware failures or experimental difficulties, the columns are appropriately marked with "NA" (Not Available). If the test was not processed using the suite of computer programs referred to as SMOKE, the gas temperature column is appropriately label with "NP." Also, the burn number is given and Appendix 1 should be referenced for the initial conditions of the burns reported.

Burn	$\%H_2$	$\%H_2$ in air	$\%H_2O$	$\frac{P_{max}}{P_0}$	$\frac{P_{max}}{P_{aicc}}$	Δt (s)	$\frac{\Delta P(atm)}{\Delta t(s)}$	$\frac{T_{max}}{T_0}$
31	9.97	9.97	0.00	2.95	0.81	1.22	1.43	3.11
79	5.54	5.54	0.00	1.62	0.67	2.45	0.21	1.67
82	6.96	6.96	0.00	2.32	0.71	2.79	0.40	2.41
83	7.77	7.77	0.00	2.68	0.84	0.89	1.61	2.80
87	8.43	8.43	0.00	2.59	0.80	0.90	1.90	3.08
89	9.41	9.41	0.00	2.72	0.83	0.52	3.08	2.86
93	5.86	5.86	0.00	1.66	0.54	4.70	0.12	1.72
94	7.24	7.24	0.00	2.28	0.65	7.84	0.14	2.58
95	9.30	9.30	0.00	1.68	0.41	1.32	0.46	1.76
96	9.43	9.43	0.00	3.21	0.78	0.88	2.35	3.37
97	11.55	11.55	0.00	3.69	0.78	NA	NA	NP
98	10.02	10.02	0.00	4.28	0.99	0.40	7.44	4.51
99	14.49	14.49	0.00	5.35	0.98	0.20	21.06	5.78
100	20.17	20.17	0.00	6.61	0.99	0.13	44.00	7.36
101	6.41	6.41	0.00	2.09	0.66	9.30	1.01	2.17
102	9.83	9.83	0.00	4.05	0.96	0.36	7.60	4.27
103	11.19	11.19	0.00	4.38	0.95	0.33	9.51	4.64
125	6.28	6.28	0.00	1.51	0.56	2.40	0.18	1.55
126	4.94	4.94	0.00	1.49	0.63	4.84	0.09	1.53
127	6.38	6.38	0.00	2.30	0.84	1.08	1.09	2.38
128	10.80	10.80	0.00	2.83	0.77	0.55	2.93	3.00
135	6.24	6.24	0.00	2.03	0.77	0.74	1.20	2.10
136	6.74	6.74	0.00	1.93	0.72	0.80	1.03	2.00
137	6.03	6.03	0.00	2.10	0.81	0.73	1.30	2.17
138	7.83	7.83	0.00	2.73	0.93	0.51	2.96	2.84
139	10.19	10.19	0.00	2.91	0.84	0.47	3.71	3.08
146	16.85	16.85	0.00	4.93	1.00	NA	NA	NP
147	5.62	5.62	0.00	2.30	0.91	4.77	0.23	2.37
148	12.91	12.91	0.00	3.20	0.78	0.69	3.03	3.43
149	14.74	14.74	0.00	3.99	0.91	0.20	14.16	4.32
150	15.76	15.76	0.00	4.13	0.89	0.14	21.46	4.50
151	8.02	8.02	0.00	3.12	0.84	0.78	2.36	3.26
152	15.56	15.56	0.00	5.14	0.89	0.22	17.62	5.58
153	9.90	9.90	0.00	3.76	0.88	0.51	4.93	3.96
154	18.95	18.95	0.00	6.15	0.95	0.07	80.00	6.81
155	29.53	29.53	0.00	7.71	0.97	0.03	263.8	8.89
156	9.29	9.29	0.00	3.60	0.90	0.46	4.99	3.78
157	19.31	19.31	0.00	6.15	0.97	0.07	73.77	6.82
158	9.36	9.36	0.00	3.62	0.88	0.56	4.28	3.81
159	20.52	20.52	0.00	6.19	0.91	0.08	66.96	6.90
160	31.32	31.32	0.00	7.80	0.97	0.03	283.9	9.00
161	10.26	10.26	0.00	3.63	0.85	0.46	5.27	3.83
162	11.05	11.05	0.00	3.45	0.77	1.03	2.17	3.66
163	19.45	19.45	0.00	5.96	0.93	0.09	55.67	6.62
164	9.67	9.67	0.00	3.81	0.91	0.43	5.88	4.01

Burn	$\%H_2$	$\%H_2$ in air	$\%H_2O$	$\frac{P_{max}}{P_0}$	$\frac{P_{max}}{P_{aicc}}$	Δt (s)	$\frac{\Delta P(atm)}{\Delta t(s)}$	$\frac{T_{max}}{T_0}$
165	10.36	10.36	0.00	3.67	0.83	0.53	4.55	3.88
166	9.25	9.25	0.00	3.69	0.91	0.53	4.53	3.88
167	9.62	9.62	0.00	3.53	0.85	0.62	3.70	3.71
168	22.65	22.65	0.00	6.65	0.92	0.05	125.8	7.49
169	11.47	11.47	0.00	3.16	0.81	0.46	4.47	3.37
170	9.53	9.53	0.00	2.81	0.82	1.16	1.46	2.96
171	10.12	10.12	0.00	2.79	0.79	1.27	1.31	2.95
172	9.13	9.13	0.00	3.11	0.89	0.93	2.08	3.26
173	19.69	19.69	0.00	4.85	0.87	0.09	47.03	5.39
174	11.43	11.43	0.00	2.74	0.75	1.10	1.49	2.91
175	9.43	9.34	0.00	3.88	0.94	0.47	5.20	4.01
176	9.36	9.36	0.00	3.95	0.96	0.43	5.90	4.15
177	20.09	20.09	0.00	6.54	0.98	0.06	83.13	7.28
178	18.98	18.98	0.00	6.07	0.95	0.09	53.60	6.72
179	24.32	24.32	0.00	7.26	0.99	0.03	185.9	8.23
180	24.16	24.16	0.00	7.33	0.98	0.03	229.0	8.30
181	29.23	29.23	0.00	7.66	0.96	0.02	327.4	8.83
182	29.47	29.47	0.00	7.63	0.96	0.03	307.6	8.80
183	10.98	10.98	0.00	3.48	0.79	0.46	5.14	3.69
184	19.18	19.18	0.00	6.06	0.96	0.07	76.30	6.72
185	11.24	11.24	0.00	3.81	0.84	0.41	6.44	4.05
186	31.33	31.33	0.00	7.63	0.95	0.03	310.8	8.81
187	34.74	34.74	0.00	7.76	0.99	0.02	447.8	8.94
188	10.55	10.55	0.00	3.20	0.86	0.38	13.08	3.38
191	51.53	51.53	0.00	5.42	0.96	0.04	176.7	6.04
192	59.93	59.93	0.00	4.64	0.92	0.08	88.00	5.08
193	30.08	30.08	0.00	6.66	0.99	0.03	207.4	7.68
194	39.99	39.99	0.00	6.37	0.96	0.03	238.2	7.26
198	68.37	68.37	0.00	3.72	0.88	0.24	29.09	3.99
199	11.46	11.46	0.00	2.89	0.78	NA	NA	NA
200	10.21	10.21	0.00	2.98	0.71	4.01	0.46	3.15
201	10.68	10.68	0.00	2.50	0.57	7.00	0.20	2.65
202	26.18	26.18	0.00	7.78	0.99	NA	NA	NA
203	27.58	27.58	0.00	7.31	0.95	0.03	207.9	8.33
204	26.34	26.34	0.00	7.90	1.01	0.03	309.1	8.80
205	27.28	27.28	0.00	7.56	0.98	0.03	262.4	8.65
206	25.86	25.86	0.00	7.43	0.99	0.03	218.2	8.33
207	26.43	26.43	0.00	7.33	0.98	0.03	253.2	8.30
208	28.65	28.65	0.00	7.16	0.93	0.03	283.4	8.19
209	25.99	25.99	0.00	7.70	1.00	0.03	305.5	8.54
210	26.82	26.82	0.00	7.53	0.98	0.03	256.7	8.44
211	25.83	25.83	0.00	7.34	0.99	0.03	236.7	8.26
212	26.34	26.34	0.00	7.29	0.98	0.04	203.1	8.29
213	26.69	26.69	0.00	7.31	0.99	0.03	239.9	8.09
214	25.43	25.43	0.00	7.29	1.01	0.03	234.7	8.01

Burn	$\%H_2$	$\%H_2$ in air	$\%H_2O$	$\frac{P_{max}}{P_0}$	$\frac{P_{max}}{P_{aicc}}$	Δt (s)	$\frac{\Delta P(atm)}{\Delta t(s)}$	$\frac{T_{max}}{T_0}$
215	26.35	26.35	0.00	7.22	1.00	0.03	236.3	8.00
216	9.78	9.78	0.00	2.83	0.66	4.10	0.40	2.97
217	18.51	18.51	0.00	5.60	0.87	0.14	33.34	6.18
218	10.28	10.28	0.00	2.96	0.68	3.78	0.47	3.13
219	8.94	8.94	0.00	3.52	0.89	1.23	1.83	3.69
220	18.93	18.93	0.00	6.04	0.94	0.13	38.99	6.68
221	9.97	9.97	0.00	3.68	0.85	0.91	2.65	3.88
222	11.14	11.14	0.00	3.90	0.84	0.35	7.49	4.14
223	18.53	18.53	0.00	5.56	0.87	0.06	79.65	6.01
224	27.97	27.97	0.00	6.22	0.80	0.12	49.18	NP
225	10.06	10.06	0.00	3.62	0.86	0.40	6.00	3.82
226	20.76	20.76	0.00	5.90	0.88	0.05	107.4	NP
227	30.16	30.16	0.00	7.40	0.94	0.03	260.7	8.55
228	10.80	10.80	0.00	3.71	0.82	0.34	7.42	3.93
229	20.41	20.41	0.00	6.02	0.89	0.09	54.77	6.71
230	30.42	30.42	0.00	7.63	0.95	0.03	270.9	8.82
231	12.65	12.65	0.00	3.43	0.70	0.40	5.77	3.67
232	20.16	20.16	0.00	5.71	0.88	0.11	43.74	6.36
233	9.31	9.31	0.00	3.48	0.85	0.44	5.21	3.65
234	19.79	19.79	0.00	5.79	0.88	0.12	43.30	6.43
235	30.17	30.17	0.00	7.48	0.94	0.03	233.5	8.63
236	9.99	9.99	0.00	3.50	0.85	0.40	5.72	3.70
237	20.11	20.11	0.00	5.63	0.88	0.10	48.20	6.27
238	30.02	30.02	0.00	7.80	0.95	0.07	124.5	9.02
239	9.98	9.98	0.00	3.58	0.85	0.47	5.10	3.78

APPENDIX 4

Global Heat Transfer Data for the Hydrogen:Air Burns Processed with SMOKE

This appendix presents the "global" heat transfer data for the hydrogen: air burns processed with the suite of computer program referred to as SMOKE. Included are data for the total and radiative peak heat flux and cumulative energy depositions. Note that the maximum energy deposition calculated using adiabatic isochoric combustion conditions are presented for each burn processed for comparison. Also shown are comparisons (i.e., ratios) of the radiative and total energy depositions and peak heat fluxes, indicating the partitioning of the postcombustion heat transfer. The burn number for each test is given and Appendix 1 should be referenced for the initial conditions of the burns reported.

Burn	%H_2	Q(AIC)	Q(TOT)	Q(RAD)	Q(RAD)/Q(TOT)	q(TOT)	q(RAD)	q(RAD)/q(TOT)
		J/cm^2				W/cm^2		
31	9.97	25.61	14.01	6.54	0.47	5.62	2.96	0.53
125	6.28	15.12	3.05	1.69	0.55	0.20	0.12	0.60
127	6.38	15.96	9.72	3.16	0.33	3.39	0.84	0.25
128	10.80	26.00	13.13	8.49	0.65	3.09	2.91	0.94
135	6.24	14.27	7.36	2.11	0.29	1.47	0.51	0.35
136	6.74	15.52	6.90	2.13	0.31	1.47	0.48	0.33
137	6.03	13.96	8.10	2.44	0.30	1.66	0.59	0.36
138	7.83	18.00	13.30	5.17	0.39	4.24	2.35	0.55
139	10.19	24.43	15.50	7.13	0.46	5.41	3.57	0.66
153	9.90	31.12	24.11	5.84	0.24	9.27	3.59	0.39
155	29.53	100.8	87.48	41.63	0.48	101.7	75.90	0.75
156	9.29	27.76	21.65	5.63	0.26	6.66	3.26	0.49
157	19.31	64.58	54.90	30.61	0.56	39.88	34.90	0.88
158	9.36	29.54	22.56	6.01	0.27	5.92	3.07	0.52
159	20.52	71.40	57.16	32.61	0.57	36.57	33.76	0.92
160	31.32	105.4	90.96	39.74	0.44	109.6	76.97	0.70
161	10.26	32.07	22.65	6.49	0.29	6.89	3.60	0.52
162	11.05	34.02	19.95	6.30	0.32	10.45	3.03	0.29
163	19.45	64.98	51.20	32.20	0.63	38.06	31.45	0.83
164	9.67	29.84	23.79	6.18	0.26	7.51	3.80	0.51
165	10.36	32.74	23.36	6.88	0.30	5.99	3.46	0.58
166	9.25	28.88	23.02	5.74	0.25	7.91	3.38	0.43
167	9.62	30.05	21.82	6.08	0.28	5.20	2.88	0.55
168	22.65	80.20	63.27	36.89	0.58	58.90	43.61	0.74
169	11.47	30.22	17.11	7.45	0.44	5.82	4.19	0.72
170	9.53	24.54	13.55	6.00	0.44	6.67	2.44	0.37
171	10.12	25.62	11.81	5.58	0.47	6.79	2.76	0.41
172	9.13	24.29	13.02	5.15	0.40	8.95	2.96	0.33
173	19.69	57.78	35.88	21.84	0.61	38.17	25.59	0.67
174	11.43	27.80	12.00	6.48	0.54	6.99	3.36	0.48
175	9.34	28.24	23.77	6.43	0.27	6.54	3.65	0.56
176	9.36	27.95	23.99	6.89	0.29	7.00	4.09	0.58
177	20.09	65.19	56.74	33.51	0.59	41.12	39.15	0.95
178	18.98	60.13	50.75	26.80	0.53	34.94	30.37	0.87
179	24.32	78.75	70.60	43.10	0.61	70.72	65.93	0.93
180	24.16	84.02	75.36	43.24	0.57	78.76	65.01	0.83
181	29.23	96.57	90.19	38.69	0.43	123.5	77.57	0.63
182	29.47	101.7	87.96	39.03	0.44	106.4	76.18	0.72
183	10.98	35.23	22.49	6.79	0.30	6.35	3.46	0.55
184	19.18	69.41	58.04	32.60	0.56	39.46	34.18	0.87
185	11.24	35.92	25.50	7.72	0.30	7.74	4.45	0.58
186	31.33	109.5	92.80	47.54	0.51	87.13	77.46	0.89
187	34.74	116.0	98.96	40.34	0.41	118.6	79.31	0.67
188	10.55	27.37	17.76	7.85	0.44	6.65	4.49	0.68
191	51.53	92.30	66.45	36.89	0.56	60.38	48.87	0.81

Burn	%H_2	Q(AIC)	Q(TOT)	Q(RAD)	Q(RAD)/Q(TOT)	q(TOT)	q(RAD)	q(RAD)/q(TOT)
		J/cm^2				W/cm^2		
192	59.93	94.73	63.69	32.16	0.51	35.30	27.99	0.79
193	30.08	86.60	65.93	39.74	0.60	99.81	73.29	0.73
194	39.99	98.05	69.02	40.85	0.59	92.71	74.07	0.80
198	68.37	91.18	58.79	24.29	0.41	21.74	13.62	0.63
203	27.58	94.28	80.64	44.01	0.55	100.5	74.15	0.74
204	26.34	94.72	85.88	43.67	0.51	102.9	74.32	0.72
205	27.28	95.03	82.57	44.67	0.54	99.82	74.28	0.74
206	25.86	90.69	80.29	44.96	0.56	97.23	73.06	0.75
207	26.43	90.40	78.63	44.43	0.57	96.36	73.21	0.76
208	28.65	96.19	77.93	49.25	0.63	90.38	74.29	0.82
209	25.99	94.90	85.42	44.86	0.53	103.4	74.17	0.72
210	26.82	95.06	83.24	45.36	0.55	98.79	74.31	0.75
211	25.83	89.52	78.39	45.13	0.58	94.82	72.77	0.77
212	26.34	90.99	79.26	44.73	0.56	95.57	73.18	0.77
213	26.69	91.27	78.84	42.99	0.54	98.72	73.54	0.75
214	25.43	85.78	76.09	41.98	0.55	96.01	72.14	0.75
215	26.35	89.51	76.76	43.34	0.57	96.79	73.14	0.76
216	9.78	31.02	14.69	3.93	0.27	2.43	1.04	0.43
217	18.51	64.38	48.13	30.92	0.64	26.12	24.05	0.92
218	10.28	32.67	8.30	1.23	0.15	2.98	0.25	0.08
219	8.94	27.60	19.55	6.30	0.32	5.84	2.57	0.44
221	9.97	31.55	21.55	5.90	0.27	11.18	3.04	0.27
222	11.14	36.10	25.70	7.53	0.29	7.54	4.45	0.59
223	18.53	63.58	45.19	26.89	0.60	27.47	21.34	0.78
225	10.06	31.10	22.64	5.72	0.25	6.94	3.46	0.50
227	30.16	103.5	83.70	44.72	0.53	69.28	68.86	0.99
228	10.80	34.92	24.29	6.28	0.26	6.62	3.51	0.53
229	20.41	71.67	53.83	27.34	0.51	27.19	26.99	0.99
230	30.42	106.3	87.86	48.11	0.55	72.18	71.92	1.00
231	12.65	40.52	22.50	6.47	0.29	5.76	3.32	0.58
232	20.16	68.49	49.93	28.36	0.57	24.77	24.77	1.00
233	9.31	29.20	21.46	4.89	0.23	5.41	2.55	0.47
234	19.79	69.46	51.84	27.76	0.54	25.22	25.15	1.00
235	30.17	105.8	87.47	47.60	0.54	85.19	76.27	0.90
236	9.99	30.66	21.33	5.63	0.26	6.37	3.20	0.50
237	20.11	67.92	50.37	28.59	0.57	26.94	26.94	1.00
238	30.02	108.9	90.73	49.30	0.54	88.22	76.86	0.87

APPENDIX 5

Combustion Pressure Data for the Hydrogen:Air:Steam Burns

This appendix presents the combustion pressure information for each of the hydrogen:air:steam burns which were conducted in this test series. Included are the normalized peak pressures, the ratio of the measured peak to AICC calculated peak pressure, the combustion duration (measured as the time from ignition to the peak pressure), the mean pressure derivative, and the "global" bulk gas temperature as inferred from the suite of computer programs referred to as SMOKE. Note that if the experimental data were not available due to hardware failures or experimental difficulties, the columns are appropriately marked with "NA" (Not Available). If the test was not processed using the suite of computer programs referred to as SMOKE, the gas temperature column is appropriately label with "NP." As in the previous appendices, the burn number is given and Appendix 1 should be referenced for the initial conditions of the burns reported.

Results for burns with 0 to 20% steam by volume

Burn	%H_2	%H_2 in air	%H_2O	$\frac{P_{max}}{P_0}$	$\frac{P_{max}}{P_{aicc}}$	Δt (s)	$\frac{\Delta P(atm)}{\Delta t(s)}$	$\frac{T_{max}}{T_0}$
51	8.44	10.30	18.13	2.02	0.68	6.21	0.18	2.12
70	49.29	55.28	10.83	4.04	0.86	0.34	17.99	4.41
71	50.46	62.54	19.30	3.27	0.83	1.33	4.44	3.50
72	50.36	62.53	19.47	2.97	0.76	2.00	2.59	3.18
73	14.40	17.37	17.14	3.61	0.87	0.51	5.98	3.90
74	14.40	16.66	13.56	3.69	0.91	0.36	8.39	3.98
75	18.94	22.88	17.22	4.58	0.96	0.10	43.82	5.06
76	11.89	13.85	14.18	3.25	0.88	0.76	3.18	3.46
84	60.67	66.72	9.07	3.06	0.76	1.12	4.87	3.27
85	58.77	63.05	6.80	3.68	0.85	0.36	16.86	3.97
88	60.67	62.10	9.07	3.82	0.85	0.42	16.19	4.14
92	8.70	10.32	15.68	2.40	0.79	2.30	0.68	2.51
140	6.63	8.17	18.81	1.60	0.61	1.02	0.64	1.66
141	8.53	10.40	17.97	2.55	0.84	0.80	2.15	2.67
142	8.87	10.64	16.62	2.54	0.82	0.79	2.15	2.65
143	9.70	12.03	19.39	2.84	0.87	0.63	3.33	2.99
190	19.06	22.61	15.71	4.65	0.94	0.12	48.91	5.14
197	38.52	46.64	17.41	NA	NA	NA	NA	NP

Results for burns with 20-30% steam by volume

Burn	%H_2	%H_2 in air	%H_2O	$\frac{P_{max}}{P_0}$	$\frac{P_{max}}{P_{aicc}}$	Δt (s)	$\frac{\Delta P(atm)}{\Delta t(s)}$	$\frac{T_{max}}{T_0}$
1	7.67	10.39	26.16	1.18	0.40	5.65	0.04	1.23
2	6.61	9.36	29.46	1.14	0.43	3.98	0.12	1.18
5	6.51	8.66	24.88	1.28	0.47	3.52	0.09	1.32
8	9.04	12.79	29.33	1.13	0.36	5.43	0.03	1.19
9	8.84	12.52	29.43	1.28	0.42	3.56	0.10	1.34
43	8.96	11.63	22.96	2.28	0.73	4.59	0.31	2.39
53	41.20	57.48	28.33	3.26	0.83	1.34	4.15	3.49
62	40.44	57.38	29.52	2.90	0.75	1.26	3.87	3.09
65	40.29	57.29	29.66	2.97	0.77	1.81	2.81	3.18
69	15.27	21.56	29.18	3.74	0.90	0.47	8.28	4.06
129	4.86	6.11	20.44	1.06	0.47	16.83	0.004	1.08
130	6.36	8.05	21.04	1.18	0.46	5.54	0.04	1.22
131	8.88	11.34	21.65	2.50	0.83	0.65	2.67	2.72
132	11.47	14.59	21.37	2.90	0.78	0.53	4.05	3.09
189	19.03	24.48	22.27	4.75	0.97	0.13	41.07	5.26
195	37.53	49.24	23.78	NA	NA	NA	NA	NP
196	38.86	49.66	21.76	NA	NA	NA	NA	NP

Results for burn with 30-40% steam by volume

Burn	$\%H_2$	$\%H_2$ in air	$\%H_2O$	$\frac{P_{max}}{P_0}$	$\frac{P_{max}}{P_{aicc}}$	Δt (s)	$\frac{\Delta P(atm)}{\Delta t(s)}$	$\frac{T_{max}}{T_0}$
10	10.25	15.55	34.10	1.35	0.39	4.06	0.12	1.43
11	8.13	13.12	38.07	1.21	0.42	6.62	0.05	1.27
12	6.89	11.12	38.08	1.10	0.42	3.92	0.04	1.14
26	15.41	24.88	38.06	3.37	0.79	0.95	4.24	3.65
33	19.94	31.71	37.11	3.29	0.71	0.84	5.31	3.63
44	30.41	45.86	33.67	NA	NA	NA	NA	NP
45	31.02	50.07	38.04	3.00	0.79	2.15	2.31	3.21
48	30.62	50.34	39.18	2.92	0.77	2.78	1.76	3.13
49	39.89	57.66	30.83	2.66	0.72	2.91	1.49	2.84
55	5.72	8.22	30.45	1.13	0.47	8.54	0.02	1.17
56	5.54	7.95	30.38	1.15	0.49	6.83	0.03	1.18
57	6.77	11.15	39.28	1.18	0.45	7.05	0.04	1.22
63	29.80	46.07	35.30	3.52	0.86	0.62	5.70	3.80
133	9.73	15.89	38.77	2.17	0.69	0.90	1.94	2.29
144	9.09	14.28	36.34	2.23	0.73	0.98	1.84	2.34
145	10.01	16.00	37.43	2.83	0.87	0.69	4.05	2.99

Results for burns with greater than 40% steam by volume

Burn	$\%H_2$	$\%H_2$ in air	$\%H_2O$	$\frac{P_{max}}{P_0}$	$\frac{P_{max}}{P_{aicc}}$	Δt (s)	$\frac{\Delta P(atm)}{\Delta t(s)}$	$\frac{T_{max}}{T_0}$
16	9.00	17.26	47.86	1.23	0.42	3.92	0.10	1.29
17	8.26	15.04	45.11	1.12	0.39	10.50	0.02	1.17
18	8.51	14.86	42.71	1.16	0.39	6.91	0.04	1.21
19	8.31	15.21	45.38	1.09	0.38	9.40	0.02	1.14
21	8.47	14.53	41.70	1.33	0.44	4.00	0.14	1.39
23	9.32	17.11	45.44	1.40	0.46	14.84	0.05	1.47
24	9.44	17.38	45.71	1.40	0.45	11.93	0.06	1.47
25	11.66	20.78	43.91	NA	NA	NA	NA	NP
27	11.41	20.54	44.45	2.58	0.73	1.97	1.45	2.74
29	7.65	15.49	50.61	1.25	0.45	4.70	0.10	1.30
30	8.97	18.07	50.33	1.15	0.38	3.74	0.07	1.20
37	21.57	38.16	43.47	3.47	0.85	1.24	4.46	3.75
38	20.88	38.17	45.29	2.84	0.72	1.97	2.13	3.07
58	6.64	11.14	40.42	1.21	0.48	4.06	0.08	1.25
59	6.81	13.33	48.91	1.21	0.47	4.45	0.08	1.25
61	21.23	40.80	47.97	2.90	0.78	2.74	1.75	3.11
64	20.26	36.44	44.40	3.26	0.81	1.05	4.76	3.53
66	20.26	39.06	48.12	2.79	0.73	4.02	1.12	3.00
67	14.92	29.44	49.32	2.79	0.71	2.65	1.47	3.03
68	14.29	24.03	40.52	3.55	0.90	0.60	7.31	3.83
104	10.91	20.46	46.68	2.23	0.68	5.88	0.43	2.36
106	11.15	22.68	50.85	2.08	0.63	7.25	0.33	2.21
107	11.14	23.70	52.97	1.10	0.33	19.05	0.01	1.17
111	12.48	25.53	51.12	1.90	0.54	9.29	0.22	2.03
113	13.23	26.05	49.22	2.58	0.69	5.16	0.69	2.77
114	15.50	29.82	48.01	2.11	0.53	7.40	0.35	2.29
115	16.54	30.00	44.87	3.25	0.77	1.74	2.77	3.55
117	17.64	32.36	45.48	2.83	0.69	2.84	1.46	3.07
119	17.04	32.77	48.01	3.06	0.76	2.93	1.65	3.31
120	8.23	16.03	48.63	1.22	0.44	3.40	0.13	1.28
121	8.37	16.37	48.88	1.18	0.42	3.21	0.11	1.24
122	9.03	17.74	49.12	1.22	0.41	3.57	0.12	1.28
134	10.68	18.17	41.23	2.80	0.85	0.75	3.94	2.97

APPENDIX 6

Global Heat Transfer Data for the Hydrogen:Air:Steam Burns Processed with SMOKE

This appendix presents the "global" heat transfer data for the hydrogen: air:steam burns processed with the suite of computer program referred to as SMOKE. Included are data for the total and radiative peak heat flux and cumulative energy depositions. Note that the maximum energy deposition calculated using adiabatic isochoric combustion conditions are presented for each burn processed for comparison. Also shown are comparisons (i.e., ratios) of the radiative and total energy depositions and peak heat fluxes, indicating the partitioning of the postcombustion heat transfer. Furthermore, as in the previous appendices, the burn number for each test is given and Appendix 1 should be referenced for the initial conditions of the burns reported.

Results for burns with 0 to 20% steam by volume

Burn	$\%H_2$	$\%H_2$ in air	$\%H_2O$	Q(AIC)	Q(TOT)	Q(RAD)	Q(RAD)/Q(TOT)	q(TOT)	q(RAD)	q(RAD)/q(TOT)
					J/cm^2			W/cm^2		
73	14.40	17.37	17.14	46.14	27.21	23.22	0.85	11.13	11.13	1.00
74	14.40	16.60	13.56	42.11	26.87	22.40	0.83	12.39	12.39	1.00
75	18.94	22.88	17.22	62.88	42.82	38.17	0.89	28.19	28.19	1.00
76	11.89	13.85	14.18	34.73	20.89	16.30	0.78	7.53	7.53	1.00
84	60.67	66.72	9.07	90.38	45.31	28.54	0.63	10.84	7.64	0.70
85	58.77	63.05	6.80	87.86	51.68	35.94	0.70	19.42	15.49	0.80
88	57.23	62.10	7.85	98.17	53.78	36.71	0.68	21.32	16.30	0.77
92	8.70	10.32	15.68	26.35	11.92	7.55	0.63	4.17	2.28	0.55
140	6.63	8.17	18.81	19.50	5.40	2.73	0.51	0.91	0.38	0.42
141	8.53	10.40	17.97	26.08	15.29	8.14	0.53	4.09	2.76	0.68
142	8.87	10.64	16.62	26.74	15.18	8.01	0.53	4.29	2.77	0.65
143	9.70	12.03	19.39	30.70	18.92	10.21	0.54	6.34	4.66	0.74
190	19.06	22.61	15.71	63.39	44.64	30.62	0.69	31.42	31.42	1.00

Results for burns with 20-30% steam by volume

Burn	$\%H_2$	$\%H_2$ in air	$\%H_2O$	Q(AIC)	Q(TOT)	Q(RAD)	Q(RAD)/Q(TOT)	q(TOT)	q(RAD)	q(RAD)/q(TOT)
					J/cm^2			W/cm^2		
43	8.96	11.63	22.96	28.45	11.49	8.13	0.71	2.62	1.81	0.69
69	15.27	21.56	29.18	60.87	35.54	30.92	0.87	13.77	13.77	1.00
132	11.47	14.59	21.37	37.93	19.63	9.85	0.50	7.00	4.48	0.64
189	19.03	24.48	22.27	74.02	54.29	35.77	0.66	36.03	36.03	1.00

Results for burns with 30-40% steam by volume

Burn	$\%H_2$	$\%H_2$ in air	$\%H_2O$	Q(AIC)	Q(TOT)	Q(RAD)	Q(RAD)/Q(TOT)	q(TOT)	q(RAD)	q(RAD)/q(TOT)
				J/cm^2				W/cm^2		
45	31.02	50.07	38.04	93.43	48.20	26.80	0.56	12.83	7.48	0.58
133	9.73	15.89	38.77	41.39	16.31	9.78	0.60	2.56	1.98	0.77
144	9.09	14.28	36.34	38.11	12.91	6.79	0.53	2.35	1.73	0.74
145	10.01	16.00	37.43	44.06	22.22	11.27	0.51	7.89	4.22	0.54

Results for burns with greater than 40% steam by volume

Burn	$\%H_2$	$\%H_2$ in air	$\%H_2O$	Q(AIC)	Q(TOT)	Q(RAD)	Q(RAD)/Q(TOT)	q(TOT)	q(RAD)	q(RAD)/q(TOT)
				J/cm^2				W/cm^2		
27	11.41	20.54	44.45	61.02	30.47	13.55	0.45	7.87	3.61	0.46
38	20.88	38.17	45.29	95.29	51.48	30.65	0.60	15.65	9.58	0.61
61	21.23	40.80	47.97	95.94	51.79	25.36	0.49	13.11	6.66	0.50
64	20.26	36.44	44.40	94.99	58.17	39.30	0.68	19.73	14.47	0.73
66	20.26	39.06	48.12	98.37	50.11	22.91	0.46	13.06	5.65	0.43
68	14.29	24.03	40.52	70.51	42.59	33.88	0.80	15.16	14.20	0.94
104	10.91	20.46	46.68	63.77	21.02	14.64	0.70	2.83	2.37	0.84
106	11.15	22.68	50.85	71.44	20.92	11.85	0.57	3.98	1.89	0.48
111	12.48	25.53	51.12	80.16	15.25	11.62	0.76	1.46	1.30	0.89
113	13.23	26.05	49.22	86.64	38.65	18.08	0.47	10.25	4.42	0.43
114	15.50	29.82	48.01	101.2	21.07	14.62	0.69	2.52	2.06	0.82
115	16.54	30.00	44.87	101.1	43.72	26.70	0.61	20.16	10.01	0.50
117	17.64	32.36	45.48	102.3	44.22	22.66	0.51	12.57	6.58	0.52
119	17.04	32.77	48.01	102.2	51.98	23.94	0.46	14.88	7.01	0.47
121	8.37	16.37	48.88	45.91	9.43	2.26	0.24	3.47	0.19	0.06
134	10.68	18.17	41.23	49.80	28.65	17.22	0.60	7.88	5.63	0.71

APPENDIX 7

Representative Pressure Signatures for each of the Combustion Tests

In this appendix, representative pressure signatures from two types of gauges (the Precise Sensor model 141-1 and the Kulite model XT-190) are shown for comparison and reference. For all of the tests in which combustion occurred and the data is available for posttest processing, the pressure transients are shown for the two gauge types whenever possible. The two gauge types are distinguished using a solid line to represent the pressure transient recorded by a Precise Sensor Model 141-1 and a dashed line to represent that recorded by a Kulite Model XT-190. Both gauge types were not available in all tests, but comparisons of the two are presented whenever possible. Also note that in some cases, a small offset in time between the two curves is apparent. This is simply due to the fact that the entire data set is plotted on these curves (i.e., time on these plots is relative) and in many cases the data for the two gauges were recorded on two different digitizing modules. Therefore, the number of pretrigger data points were generally different resulting in the small time shift. However, comparison of the two pressure transients from the time of ignition (i.e., the first deviation from the baseline) generally reveals identical combustion-pressure signatures and magnitudes.

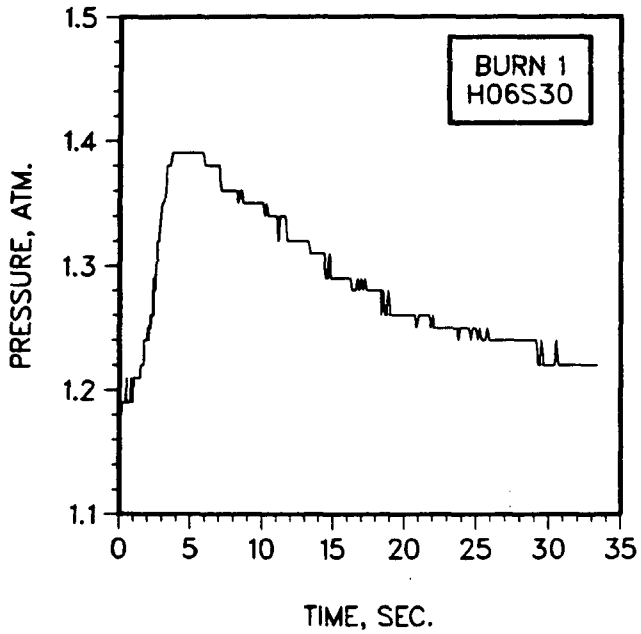
BURN 1
H06S30
PRESSURE, ATM.
1.5
1.4
1.3
1.2
1.1
0
5
10
15
20
25
30
35
TIME, SEC.

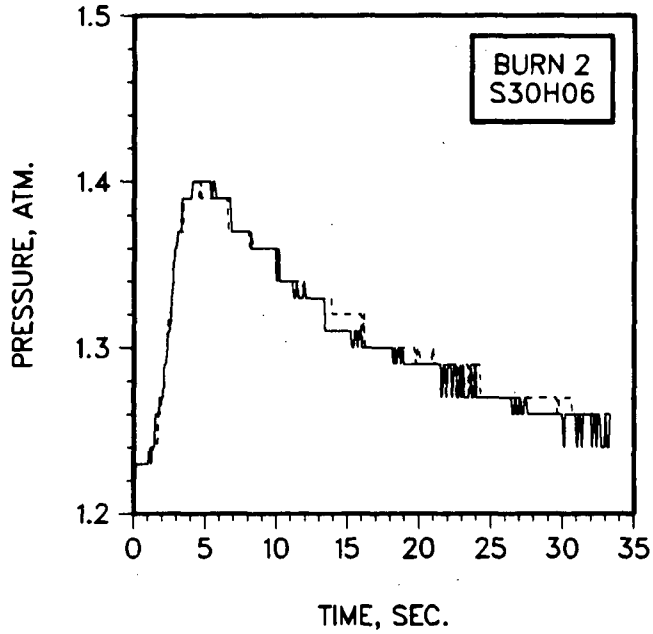
BURN 2
S30H06
PRESSURE, ATM.
1.5
1.4
1.3
1.2
0
5
10
15
20
25
30
35
TIME, SEC.

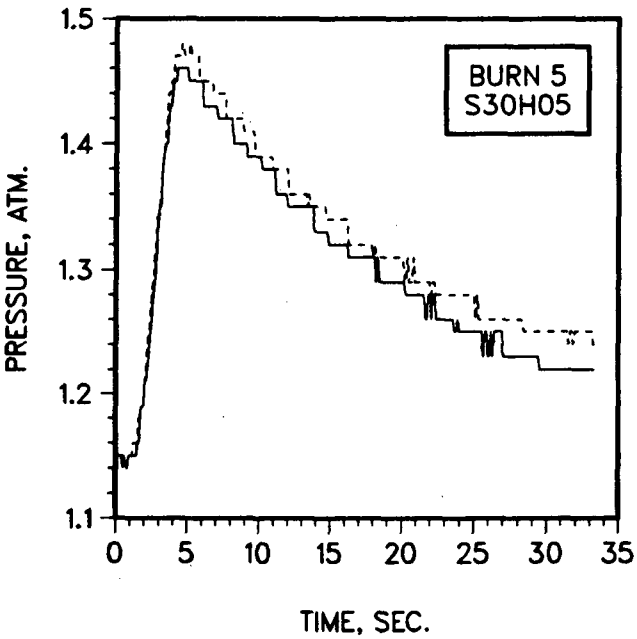
BURN 5
S30H05
PRESSURE, ATM.
1.5
1.4
1.3
1.2
1.1
0
5
10
15
20
25
30
35
TIME, SEC.

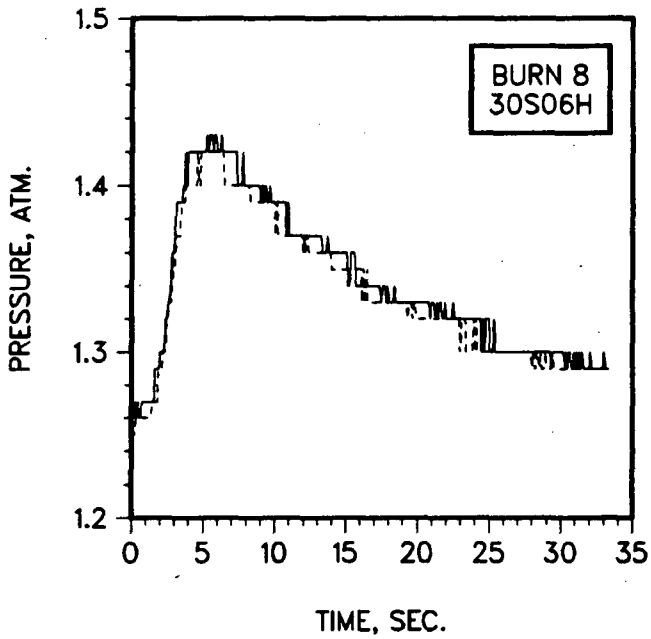
BURN 8
30S06H
PRESSURE, ATM.
1.5
1.4
1.3
1.2
0
5
10
15
20
25
30
35
TIME, SEC.

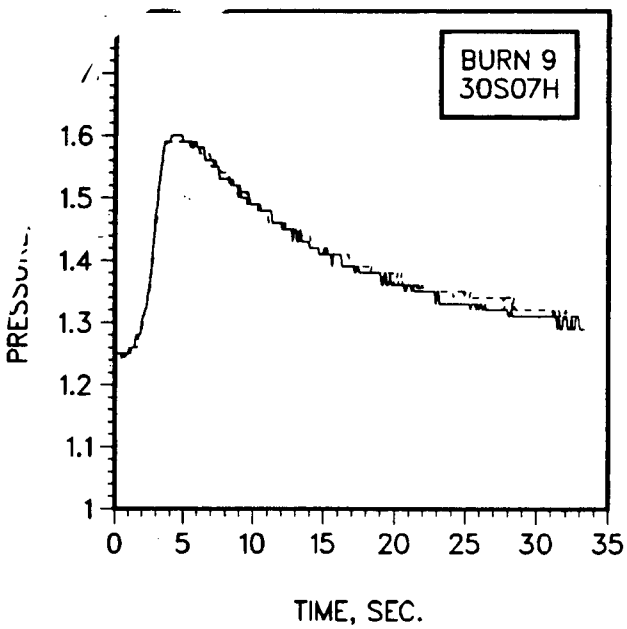
BURN 9
30S07H
1.6
1.5
1.4
1.3
1.2
1.1
1
0 5 10 15 20 25 30 35
TIME, SEC.

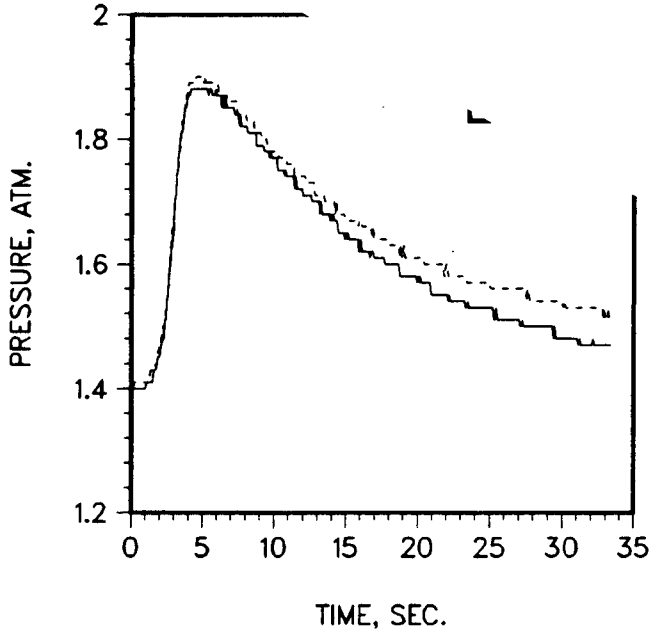
2
1.8
1.6
1.4
1.2
PRESSURE, ATM.
0 5 10 15 20 25 30 35
TIME, SEC.

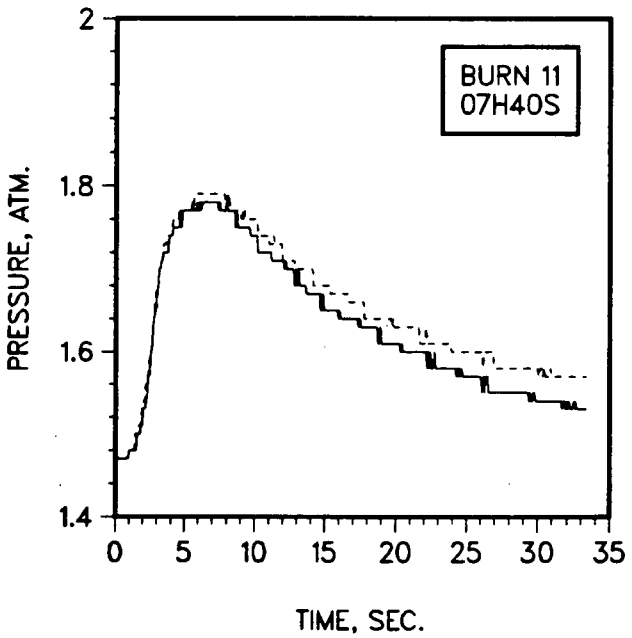
BURN 11
07H40S
2
1.8
1.6
1.4
PRESSURE, ATM.
0 5 10 15 20 25 30 35
TIME, SEC.

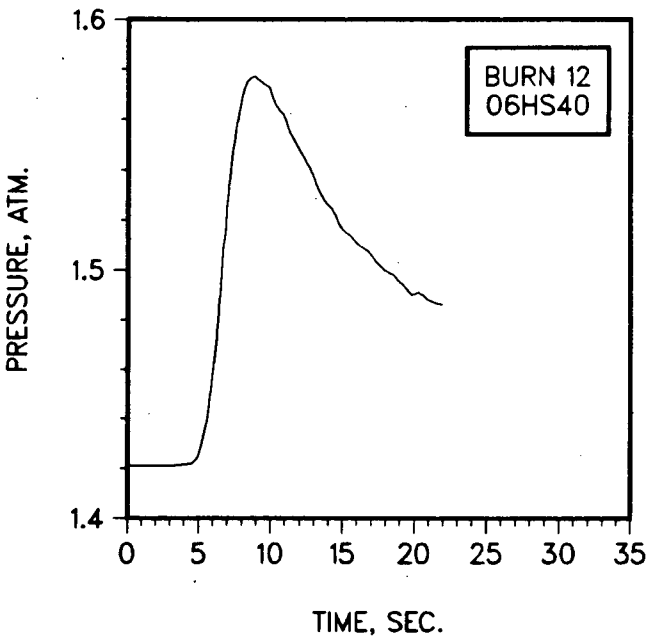
BURN 12
06HS40
1.6
1.5
1.4
PRESSURE, ATM.
0 5 10 15 20 25 30 35
TIME, SEC.

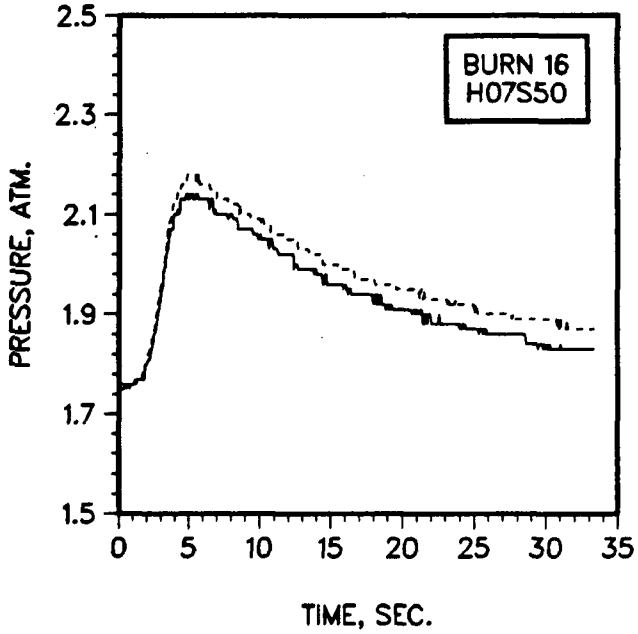
BURN 16
H07S50
PRESSURE, ATM.
2.5
2.3
2.1
1.9
1.7
1.5
0
5
10
15
20
25
30
35
TIME, SEC.

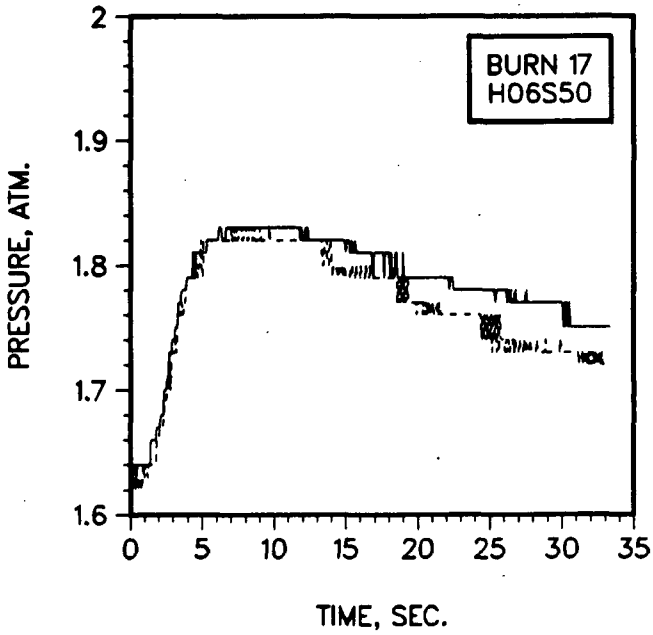
BURN 17
H06S50
PRESSURE, ATM.
2
1.9
1.8
1.7
1.6
0
5
10
15
20
25
30
35
TIME, SEC.

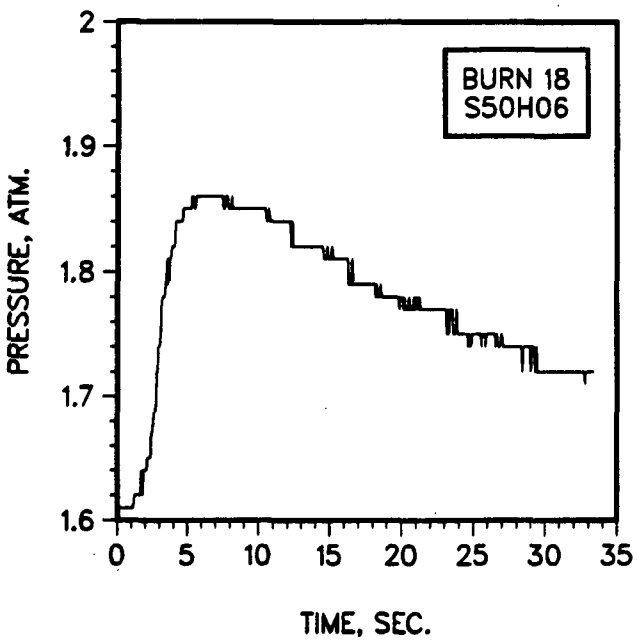
BURN 18
S50H06
PRESSURE, ATM.
2
1.9
1.8
1.7
1.6
0
5
10
15
20
25
30
35
TIME, SEC.

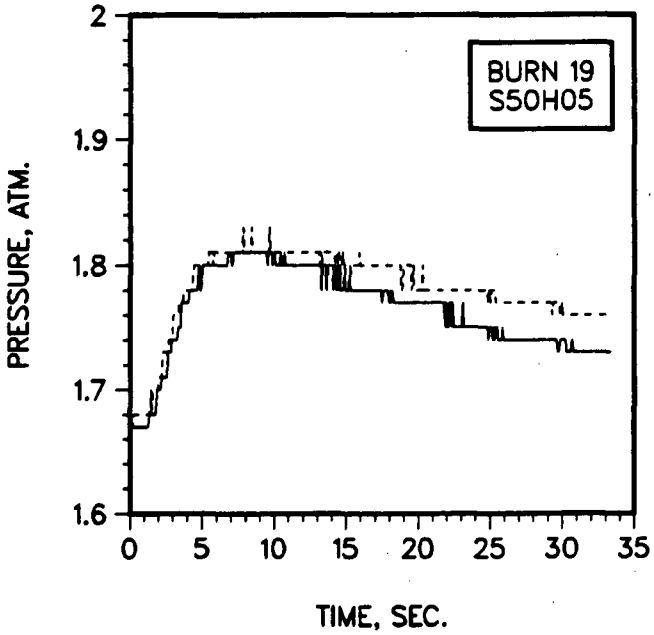
BURN 19
S50H05
PRESSURE, ATM.
2
1.9
1.8
1.7
1.6
0
5
10
15
20
25
30
35
TIME, SEC.

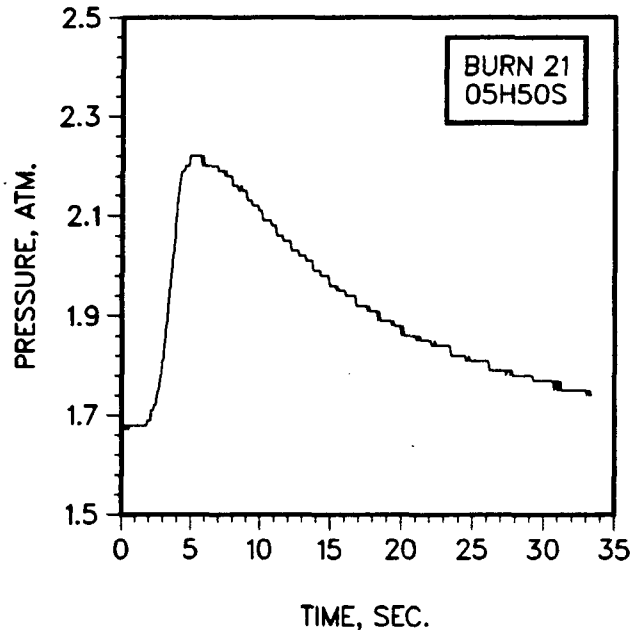
BURN 21
05H50S
PRESSURE, ATM.
2.5
2.3
2.1
1.9
1.7
1.5
0
5
10
15
20
25
30
35
TIME, SEC.

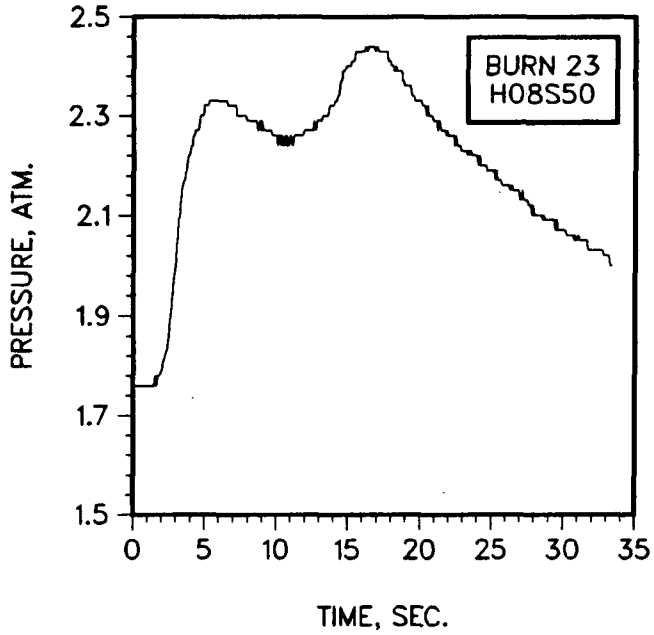
BURN 23
H08S50
PRESSURE, ATM.
2.5
2.3
2.1
1.9
1.7
1.5
0
5
10
15
20
25
30
35
TIME, SEC.

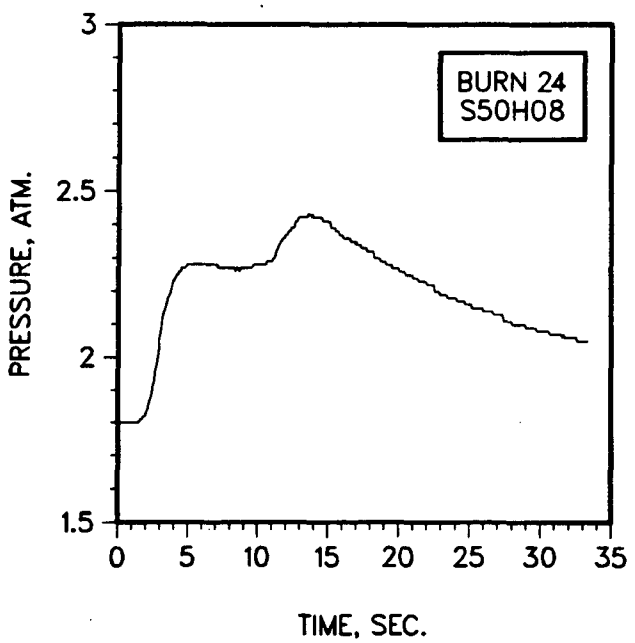
BURN 24
S50H08
PRESSURE, ATM.
3
2.5
2
1.5
0
5
10
15
20
25
30
35
TIME, SEC.

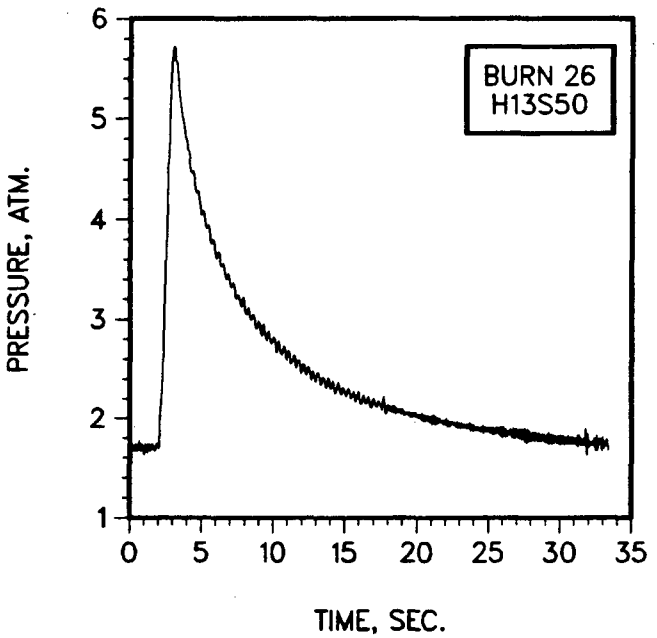
BURN 26
H13S50
PRESSURE, ATM.
6
5
4
3
2
1
0
5
10
15
20
25
30
35
TIME, SEC.

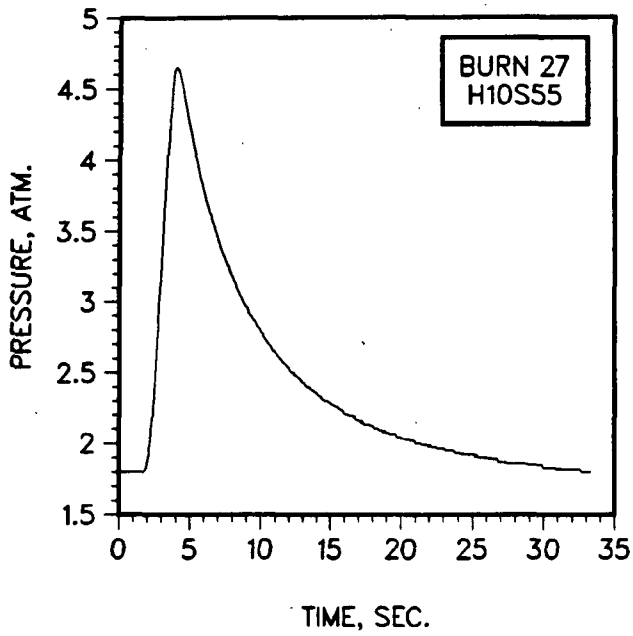
BURN 27
H10S55
PRESSURE, ATM.
TIME, SEC.
5
4.5
4
3.5
3
2.5
2
1.5
0
5
10
15
20
25
30
35

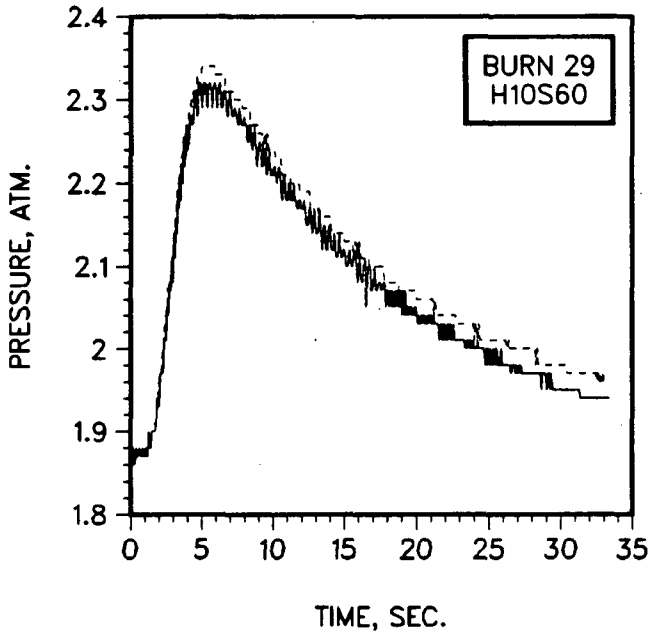
BURN 29
H10S60
PRESSURE, ATM.
TIME, SEC.
2.4
2.3
2.2
2.1
2
1.9
1.8
0
5
10
15
20
25
30
35

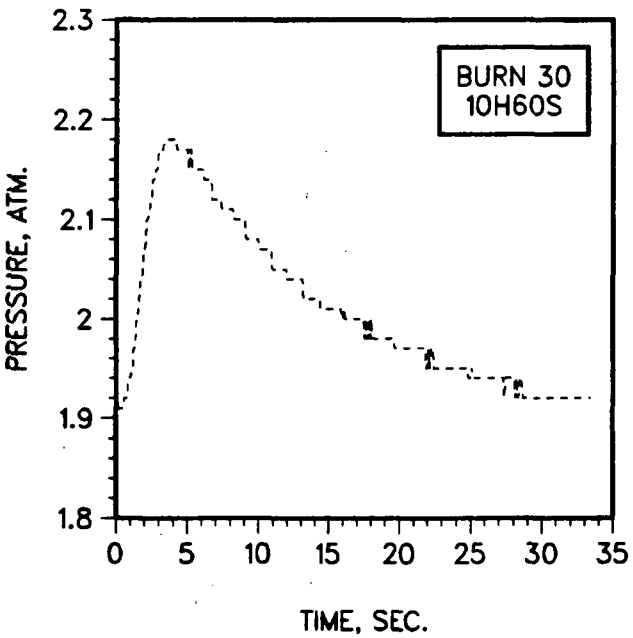
BURN 30
10H60S
PRESSURE, ATM.
TIME, SEC.
2.3
2.2
2.1
2
1.9
1.8
0
5
10
15
20
25
30
35

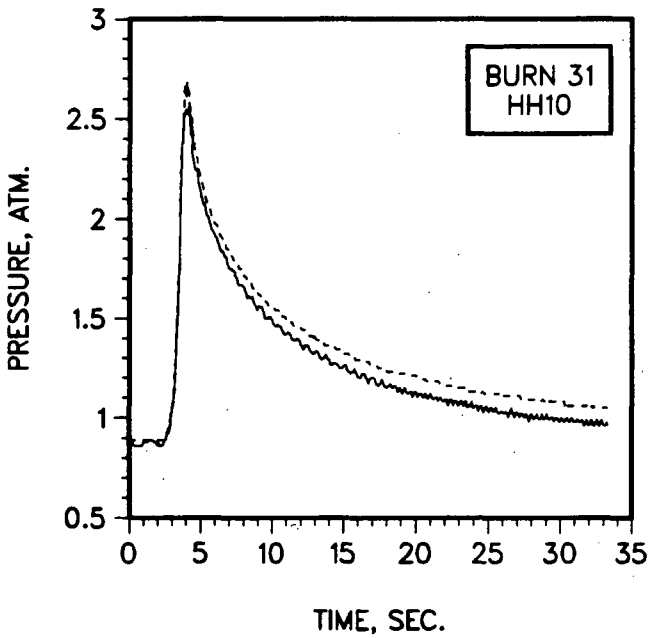
BURN 31
HH10
PRESSURE, ATM.
TIME, SEC.
3
2.5
2
1.5
1
0.5
0
5
10
15
20
25
30
35

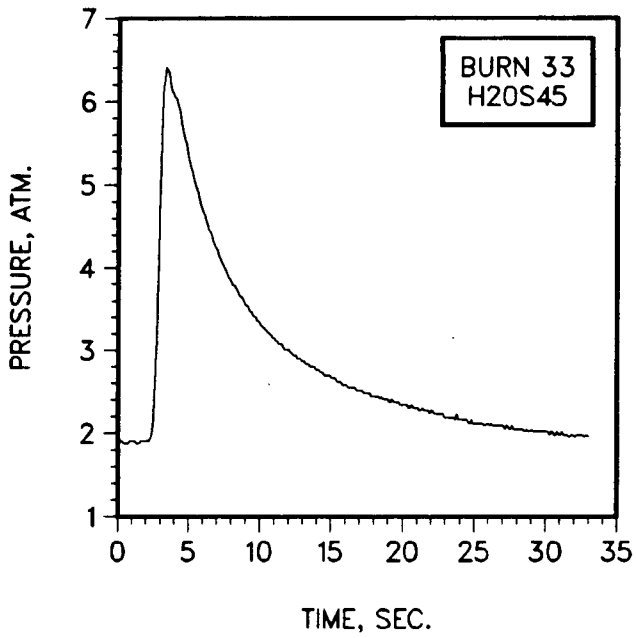
BURN 33
H20S45
PRESSURE, ATM.
TIME, SEC.
1
2
3
4
5
6
7
0
5
10
15
20
25
30
35

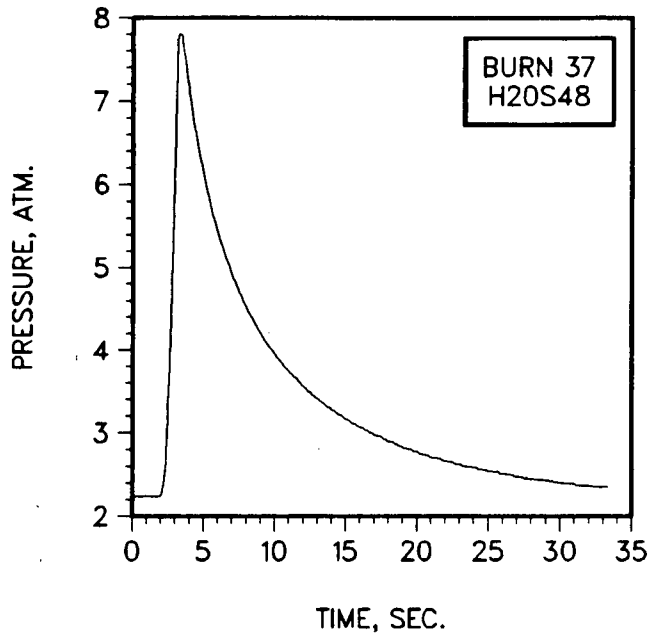
BURN 37
H20S48
PRESSURE, ATM.
TIME, SEC.
2
3
4
5
6
7
8
0
5
10
15
20
25
30
35

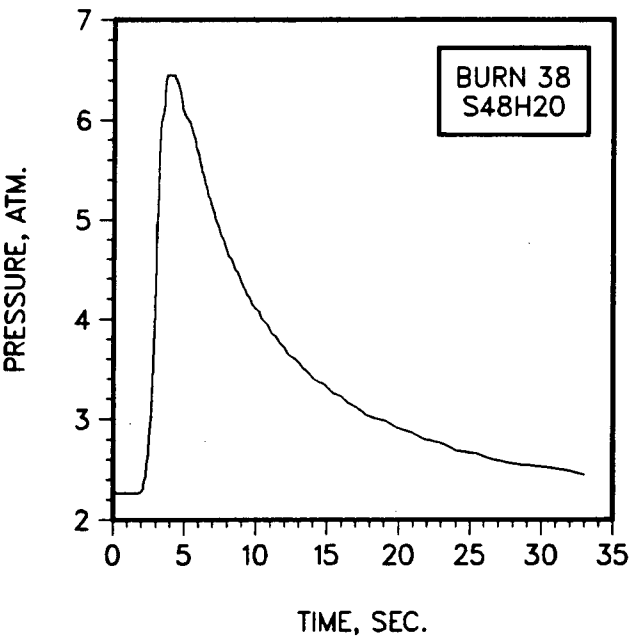
BURN 38
S48H20
PRESSURE, ATM.
TIME, SEC.
2
3
4
5
6
7
0
5
10
15
20
25
30
35

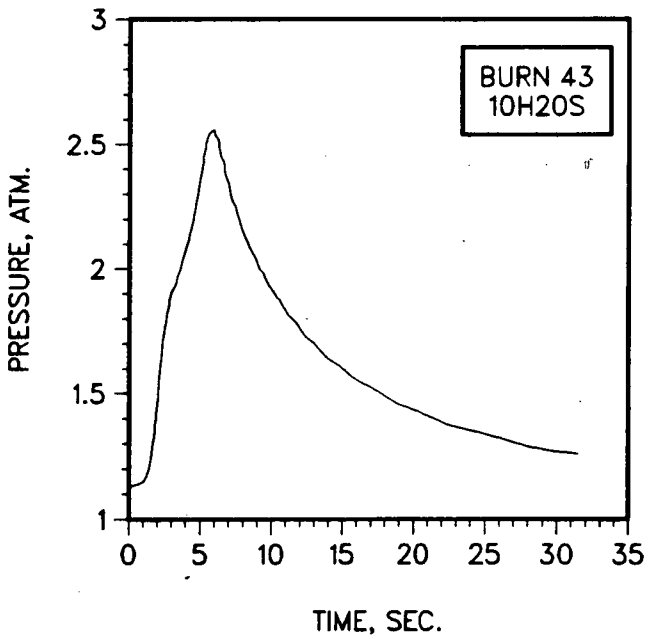
BURN 43
10H20S
PRESSURE, ATM.
TIME, SEC.
1
1.5
2
2.5
3
0
5
10
15
20
25
30
35

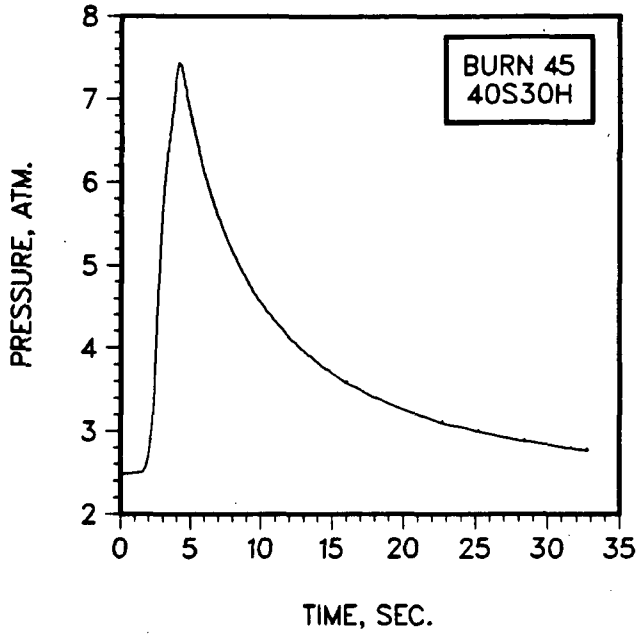
BURN 45
40S30H
PRESSURE, ATM.
TIME, SEC.
8
7
6
5
4
3
2
0
5
10
15
20
25
30
35

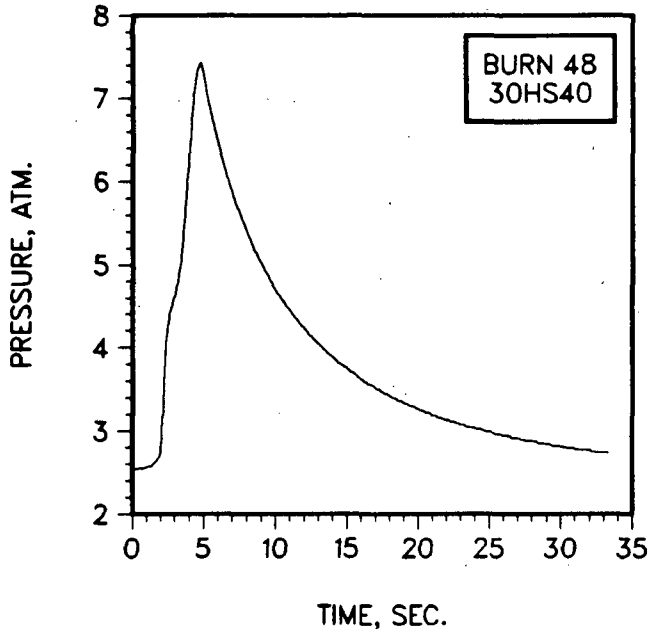
BURN 48
30HS40
PRESSURE, ATM.
TIME, SEC.
8
7
6
5
4
3
2
0
5
10
15
20
25
30
35

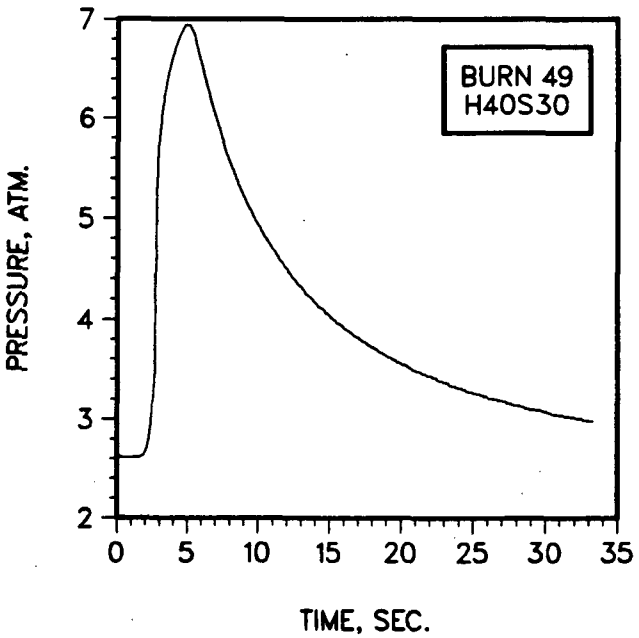
BURN 49
H40S30
PRESSURE, ATM.
TIME, SEC.
7
6
5
4
3
2
0
5
10
15
20
25
30
35

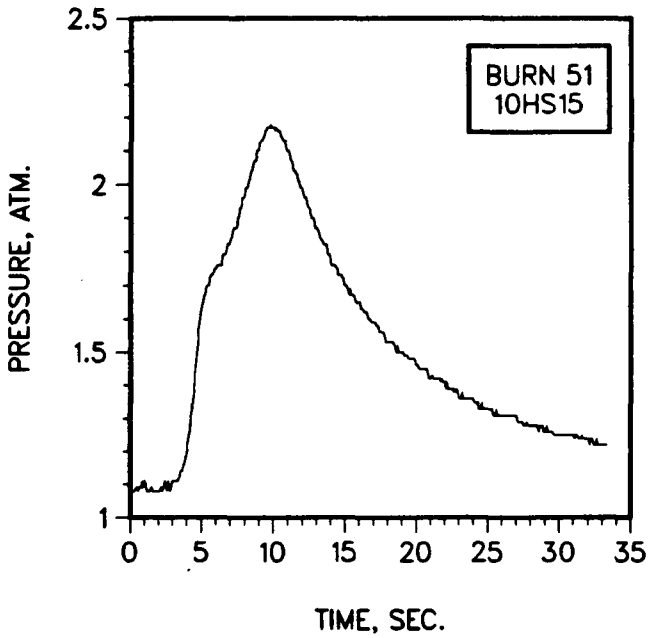
BURN 51
10HS15
PRESSURE, ATM.
TIME, SEC.
2.5
2
1.5
1
0
5
10
15
20
25
30
35

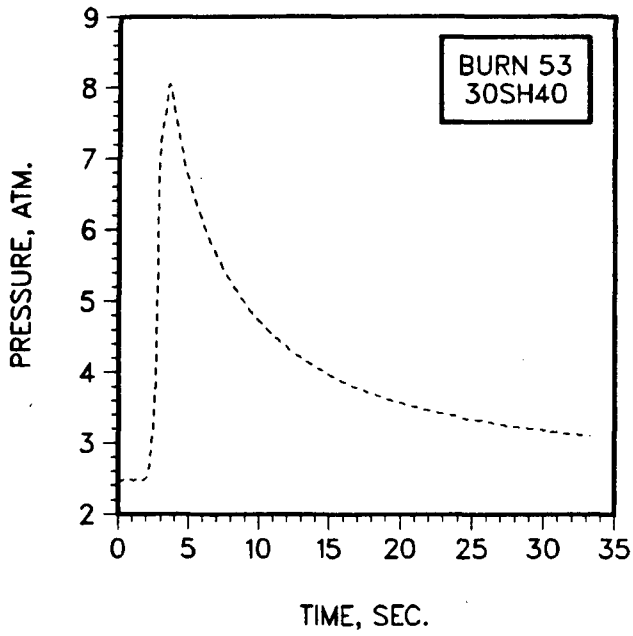
BURN 53
30SH40
PRESSURE, ATM.
TIME, SEC.
9
8
7
6
5
4
3
2
0
5
10
15
20
25
30
35

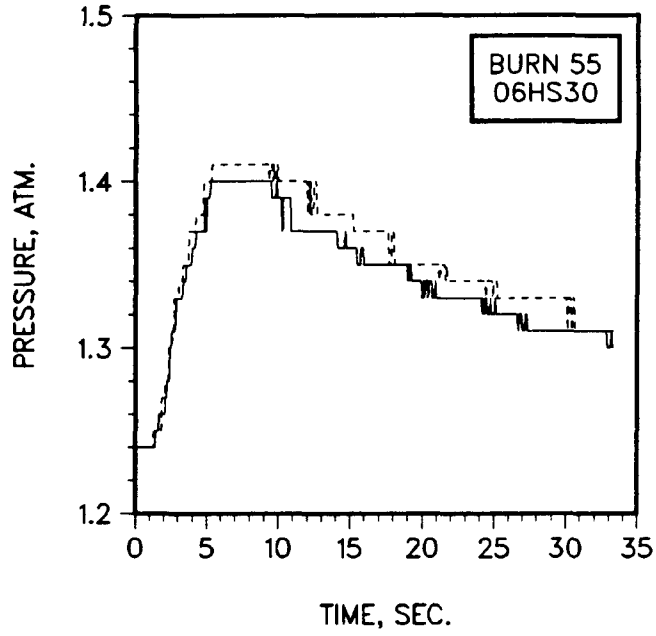
BURN 55
06HS30
PRESSURE, ATM.
TIME, SEC.
1.5
1.4
1.3
1.2
0
5
10
15
20
25
30
35

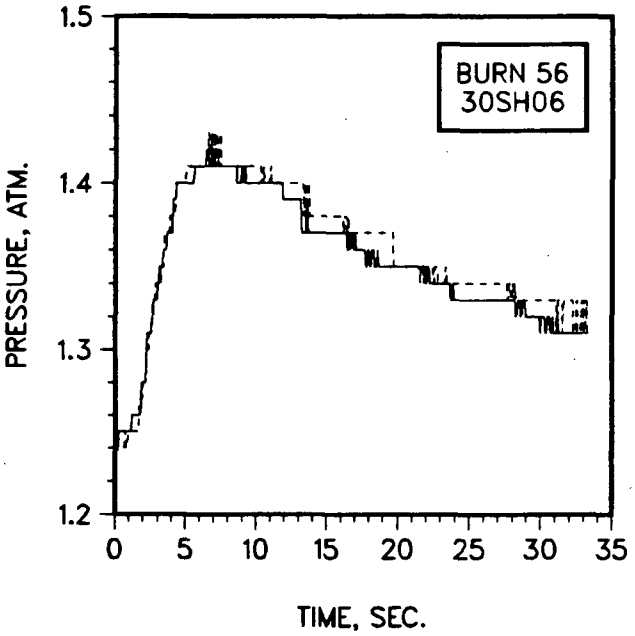
BURN 56
30SH06
PRESSURE, ATM.
TIME, SEC.
1.5
1.4
1.3
1.2
0
5
10
15
20
25
30
35

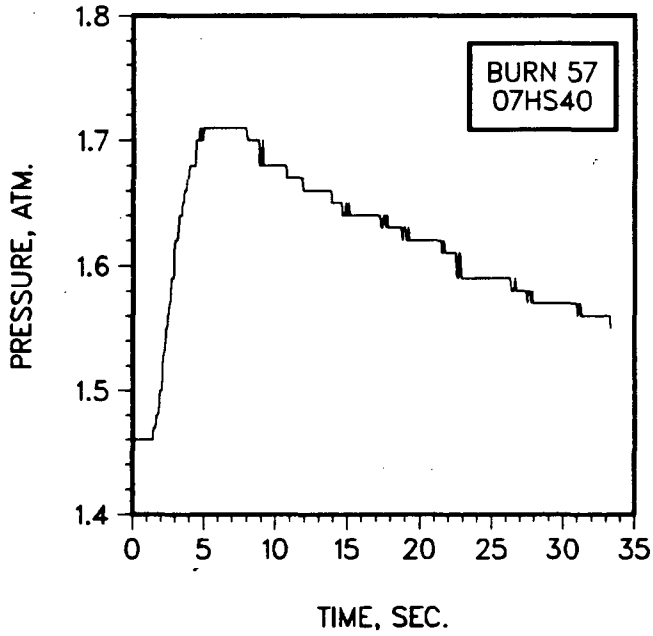
BURN 57
07HS40
PRESSURE, ATM.
TIME, SEC.
1.8
1.7
1.6
1.5
1.4
0
5
10
15
20
25
30
35

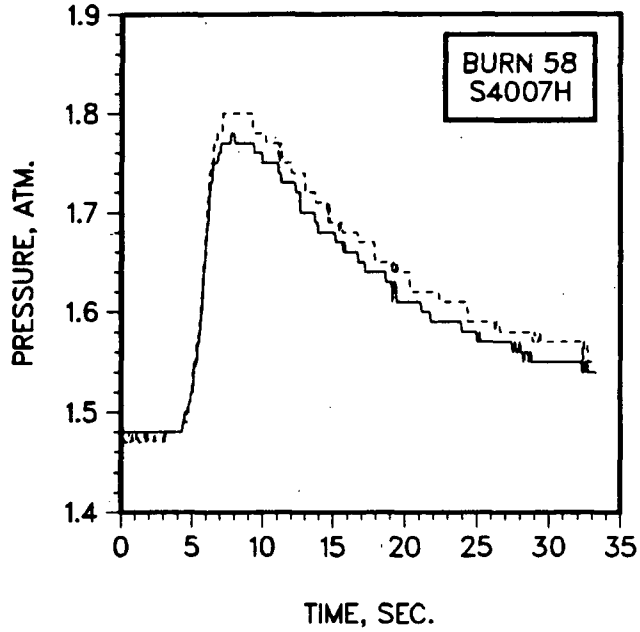
BURN 58
S4007H
PRESSURE, ATM.
TIME, SEC.
1.9
1.8
1.7
1.6
1.5
1.4
0
5
10
15
20
25
30
35

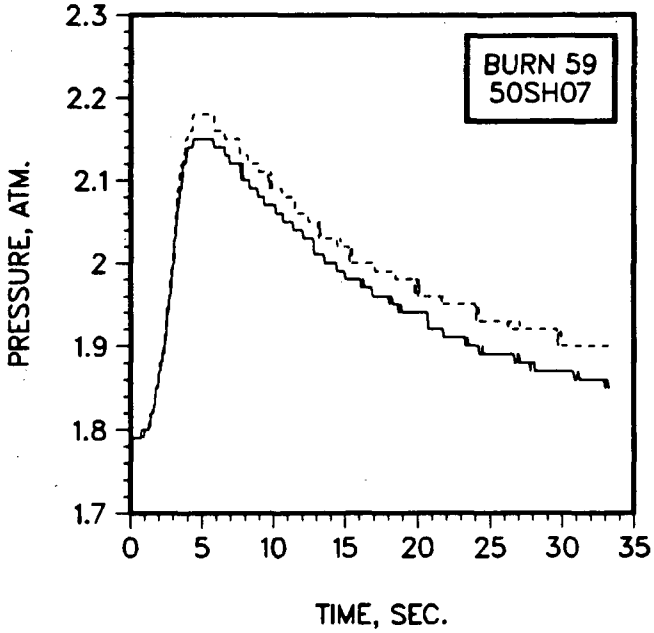
BURN 59
50SH07
PRESSURE, ATM.
TIME, SEC.
2.3
2.2
2.1
2
1.9
1.8
1.7
0
5
10
15
20
25
30
35

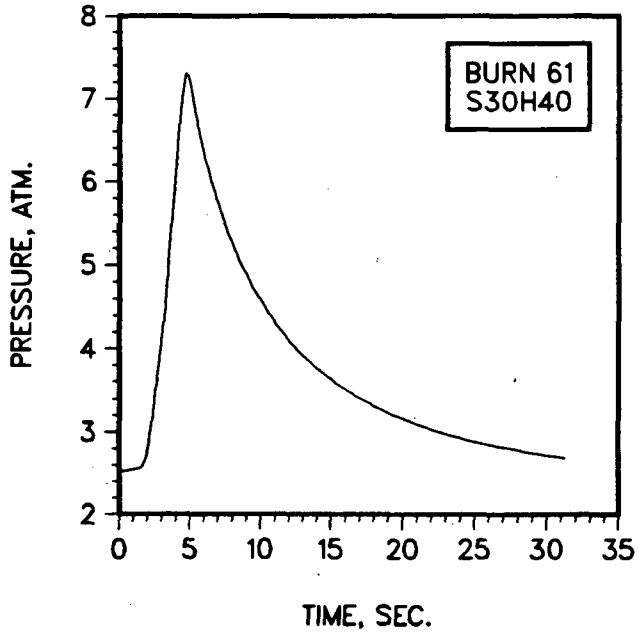
BURN 61
S30H40
PRESSURE, ATM.
TIME, SEC.
8
7
6
5
4
3
2
0
5
10
15
20
25
30
35

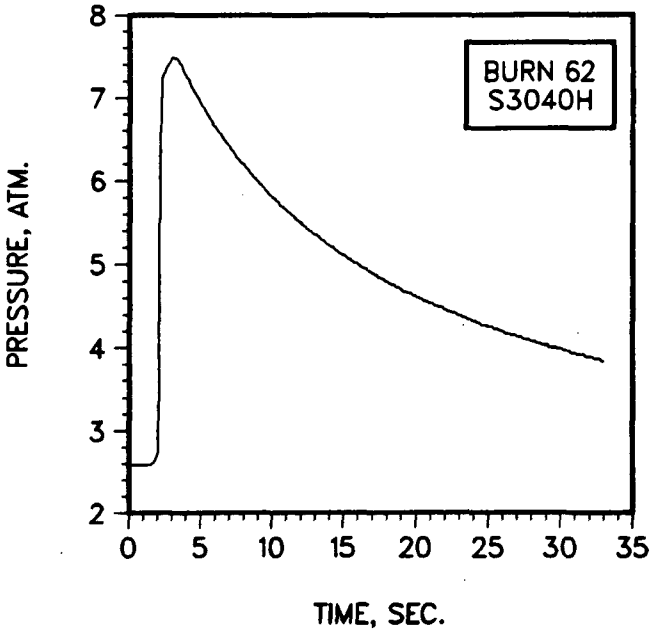
BURN 62
S3040H
PRESSURE, ATM.
TIME, SEC.
8
7
6
5
4
3
2
0
5
10
15
20
25
30
35

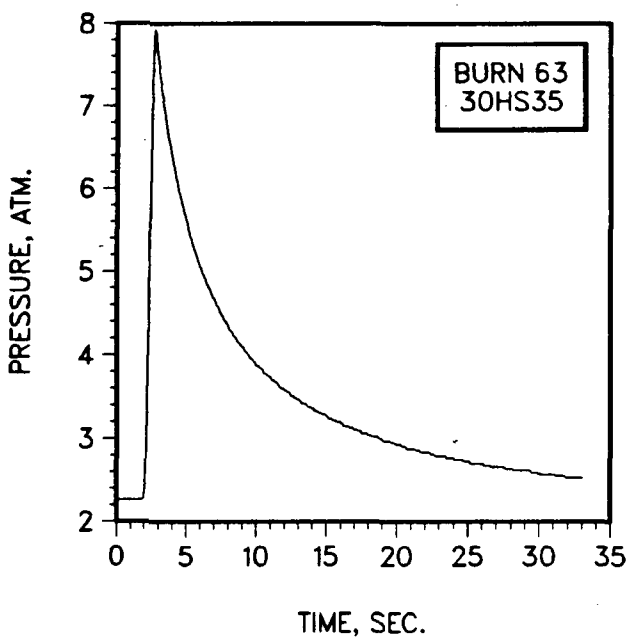
BURN 63
30HS35
PRESSURE, ATM.
TIME, SEC.

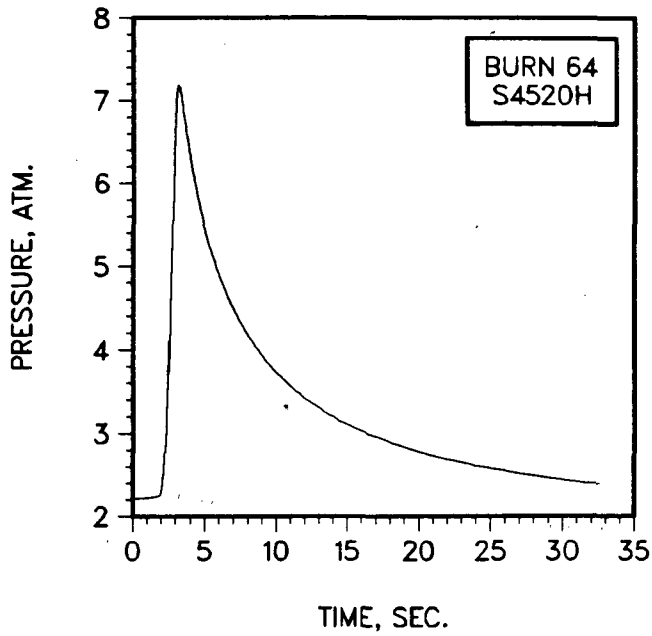
BURN 64
S4520H
PRESSURE, ATM.
TIME, SEC.

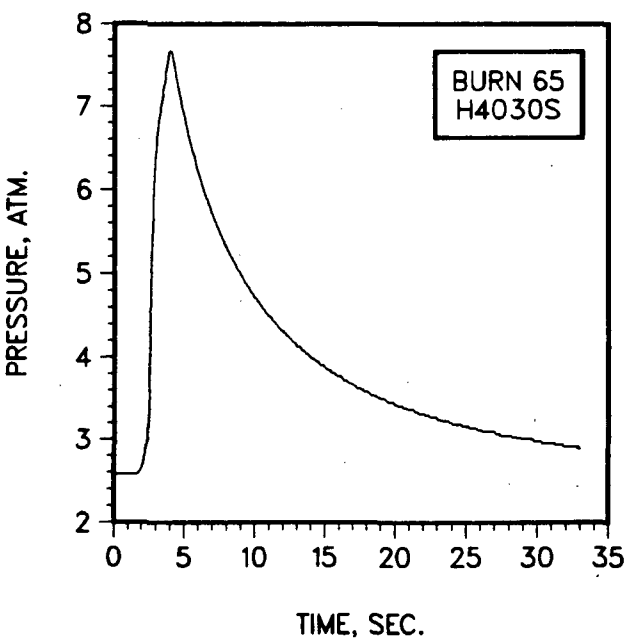
BURN 65
H4030S
PRESSURE, ATM.
TIME, SEC.

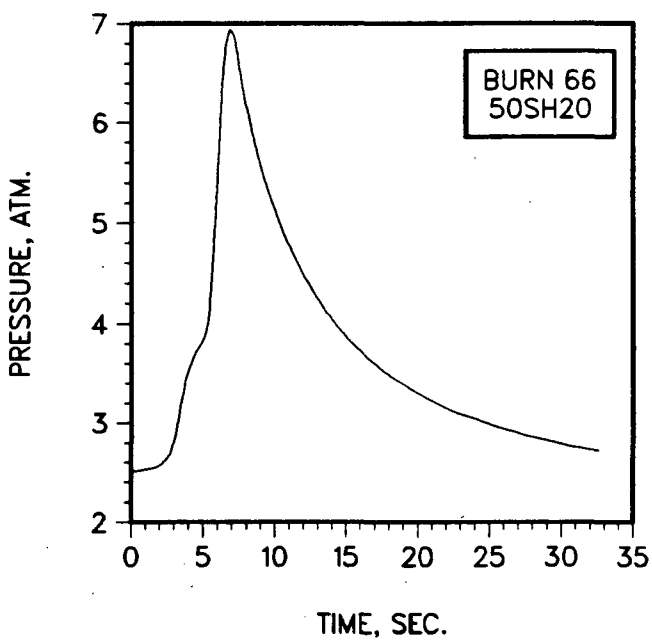
BURN 66
50SH20
PRESSURE, ATM.
TIME, SEC.

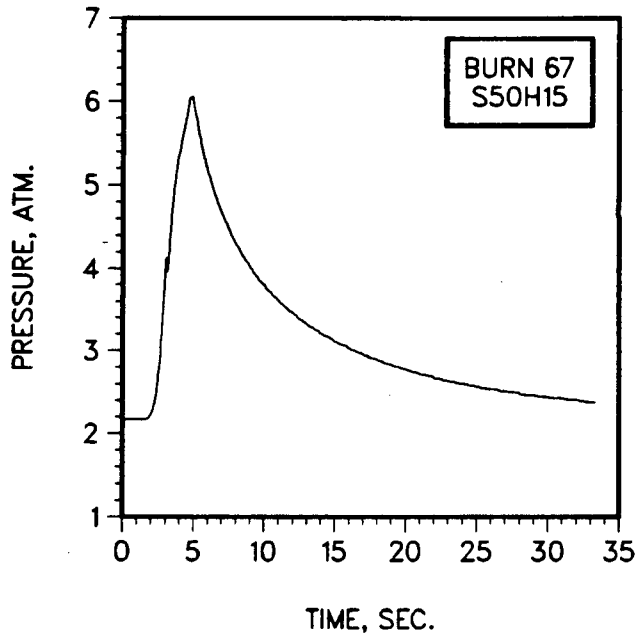
BURN 67
S50H15
PRESSURE, ATM.
TIME, SEC.

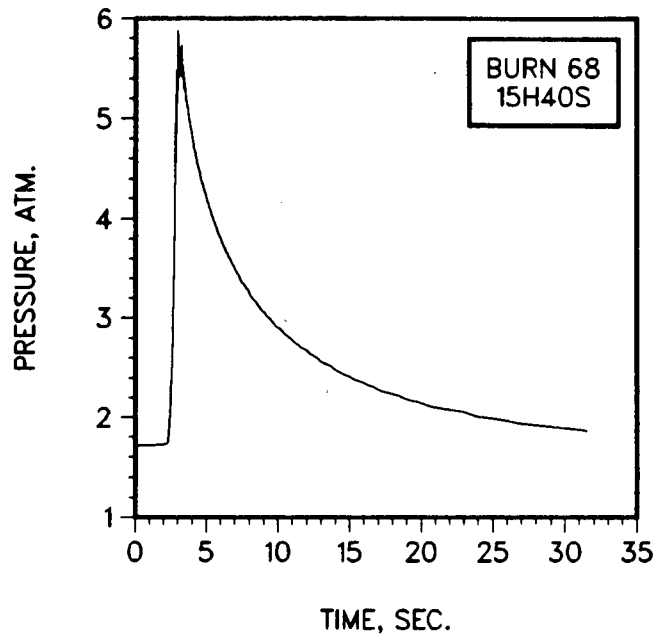
BURN 68
15H40S
PRESSURE, ATM.
TIME, SEC.

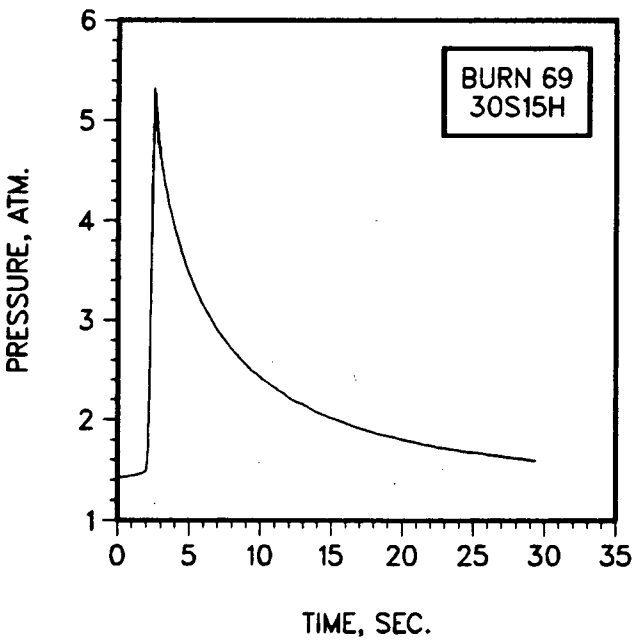
BURN 69
30S15H
PRESSURE, ATM.
TIME, SEC.

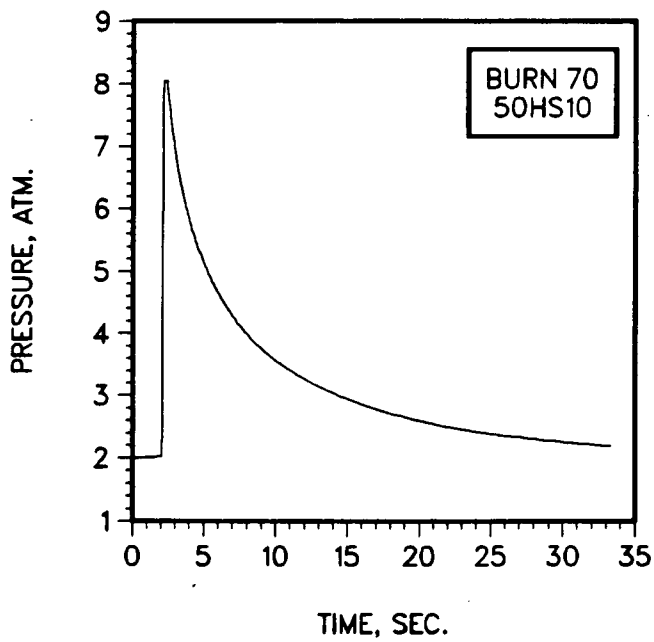
BURN 70
50HS10
PRESSURE, ATM.
TIME, SEC.

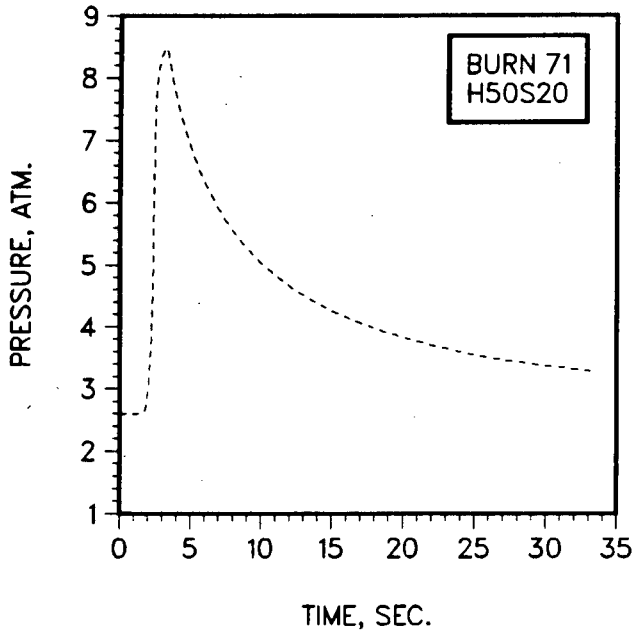
BURN 71
H50S20
PRESSURE, ATM.
TIME, SEC.

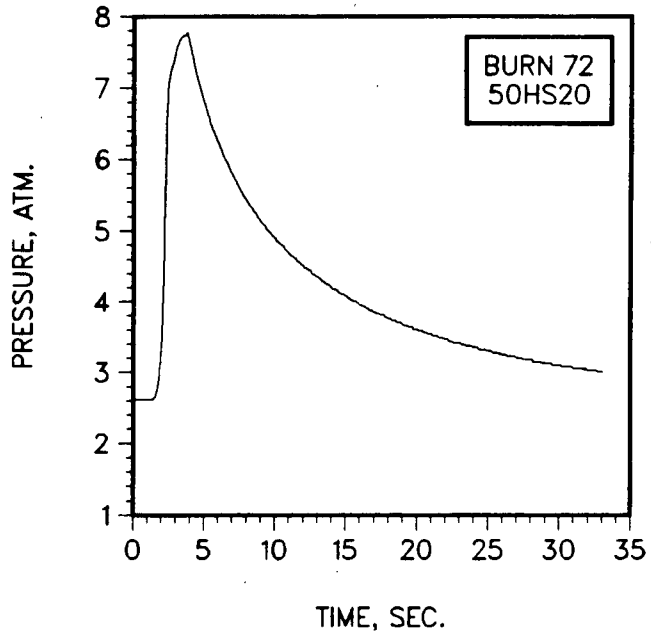
BURN 72
50HS20
PRESSURE, ATM.
TIME, SEC.

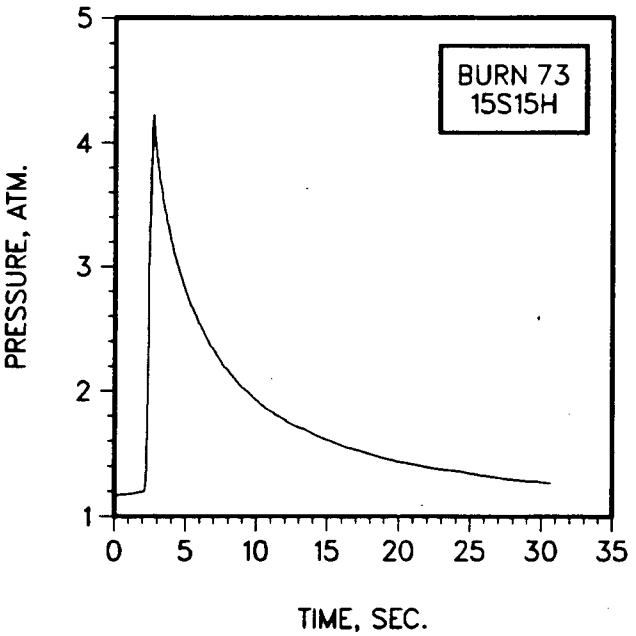
BURN 73
15S15H
PRESSURE, ATM.
TIME, SEC.

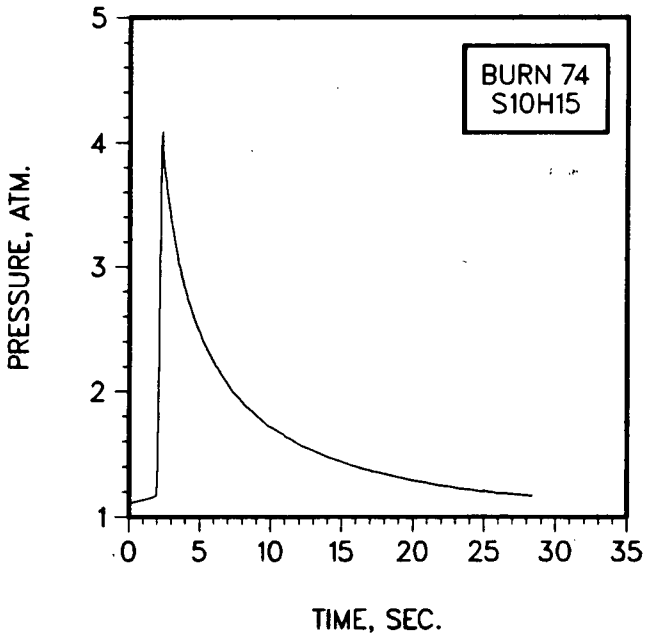
BURN 74
S10H15
PRESSURE, ATM.
TIME, SEC.

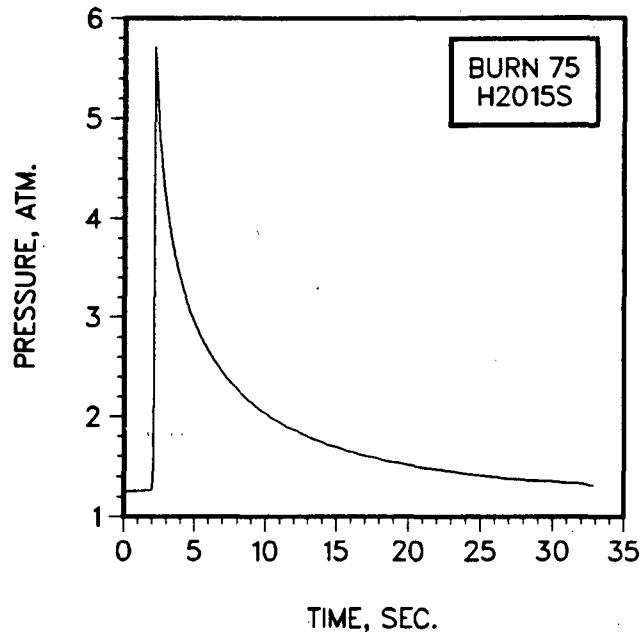
BURN 75
H2015S
PRESSURE, ATM.
TIME, SEC.
6
5
4
3
2
1
0
5
10
15
20
25
30
35

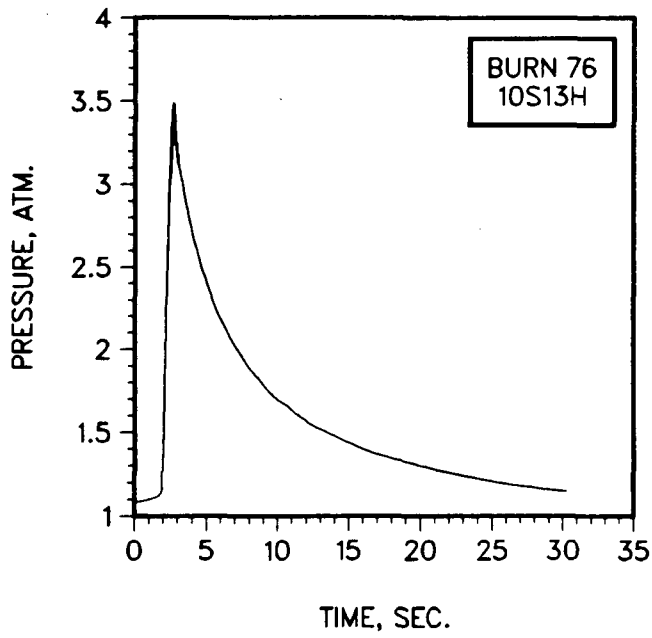
BURN 76
10S13H
PRESSURE, ATM.
TIME, SEC.
4
3.5
3
2.5
2
1.5
1
0
5
10
15
20
25
30
35

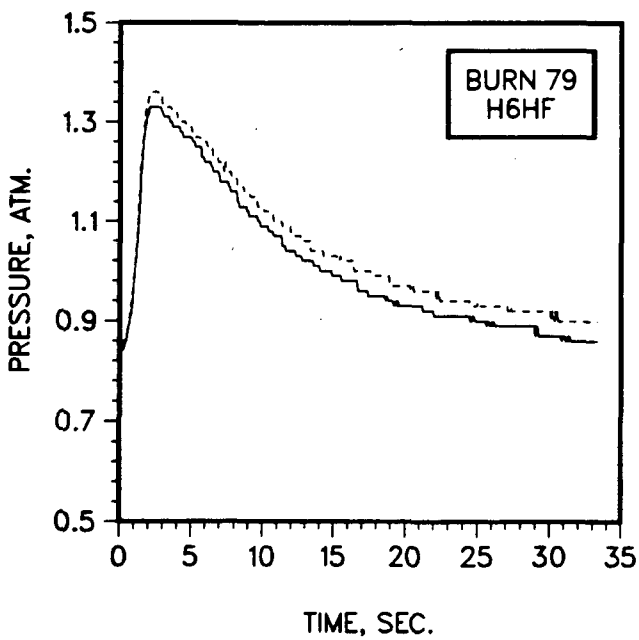
BURN 79
H6HF
PRESSURE, ATM.
TIME, SEC.
1.5
1.3
1.1
0.9
0.7
0.5
0
5
10
15
20
25
30
35

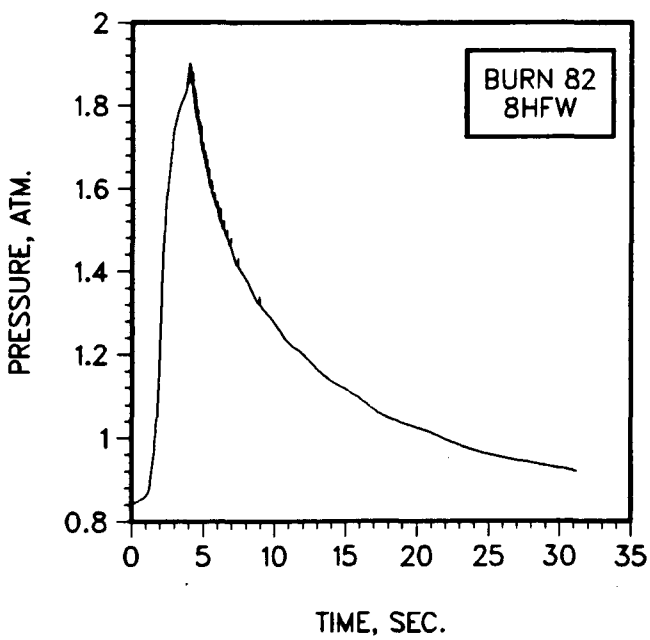
BURN 82
8HFW
PRESSURE, ATM.
TIME, SEC.
2
1.8
1.6
1.4
1.2
1
0.8
0
5
10
15
20
25
30
35

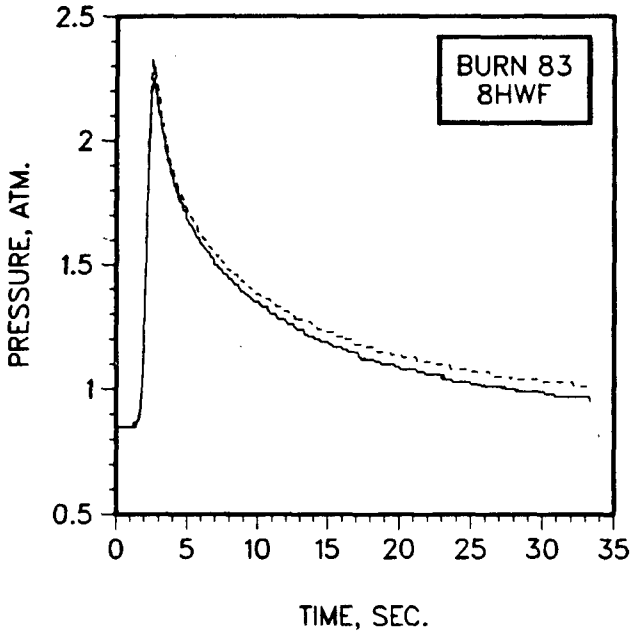
BURN 83
8HWF
PRESSURE, ATM.
TIME, SEC.

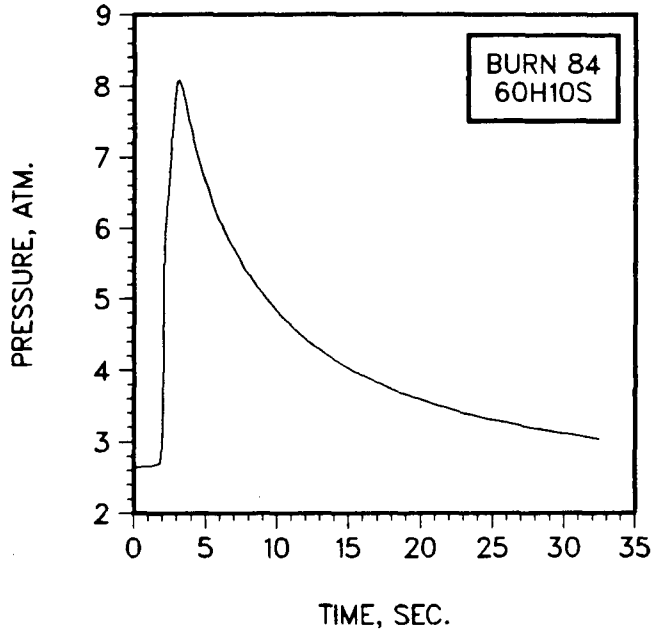
BURN 84
60H10S
PRESSURE, ATM.
TIME, SEC.

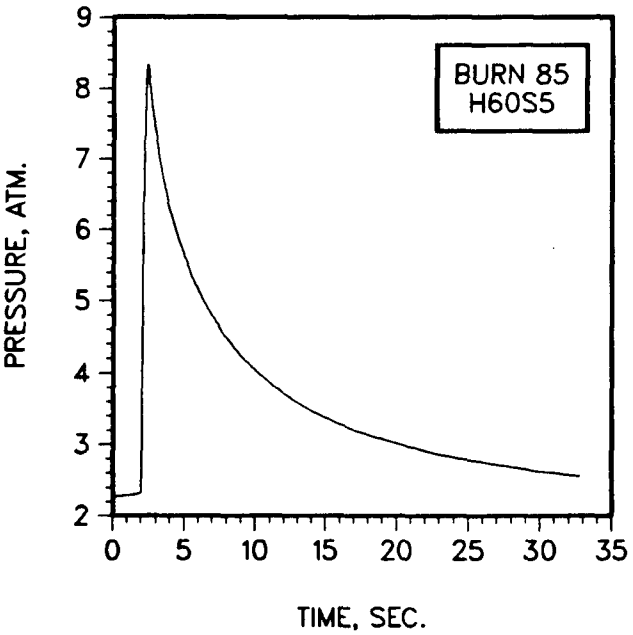
BURN 85
H60S5
PRESSURE, ATM.
TIME, SEC.

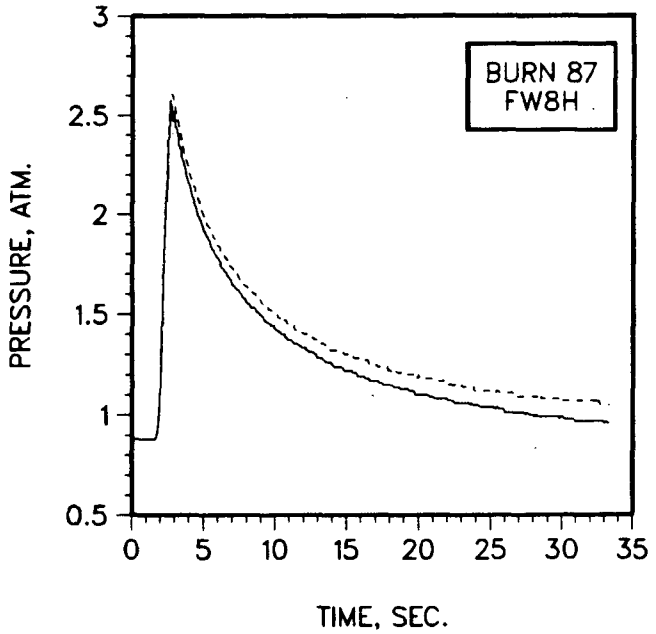
BURN 87
FW8H
PRESSURE, ATM.
TIME, SEC.

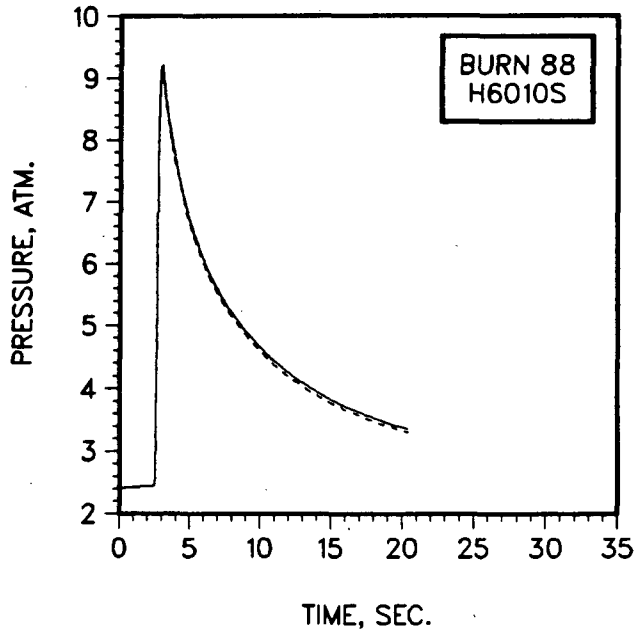
BURN 88
H6010S
PRESSURE, ATM.
TIME, SEC.

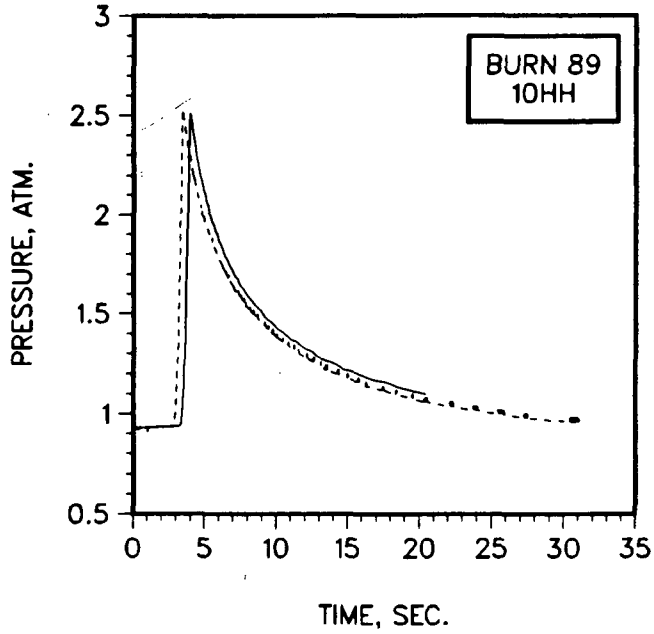
BURN 89
10HH
PRESSURE, ATM.
TIME, SEC.

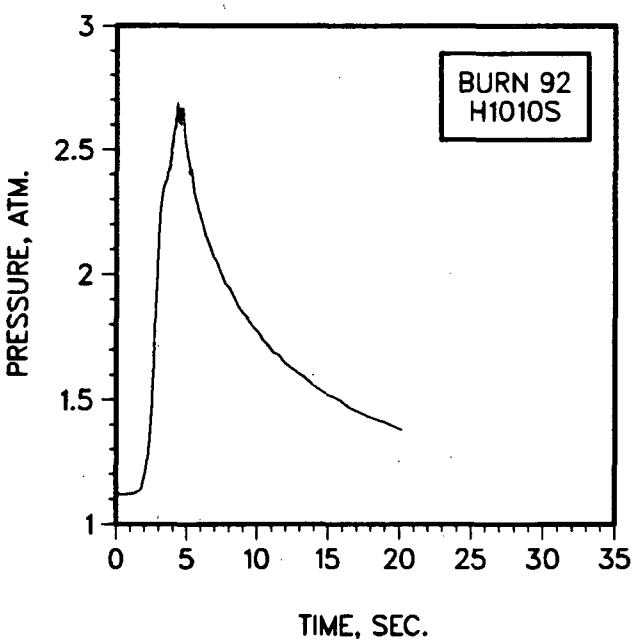
BURN 92
H1010S
PRESSURE, ATM.
TIME, SEC.

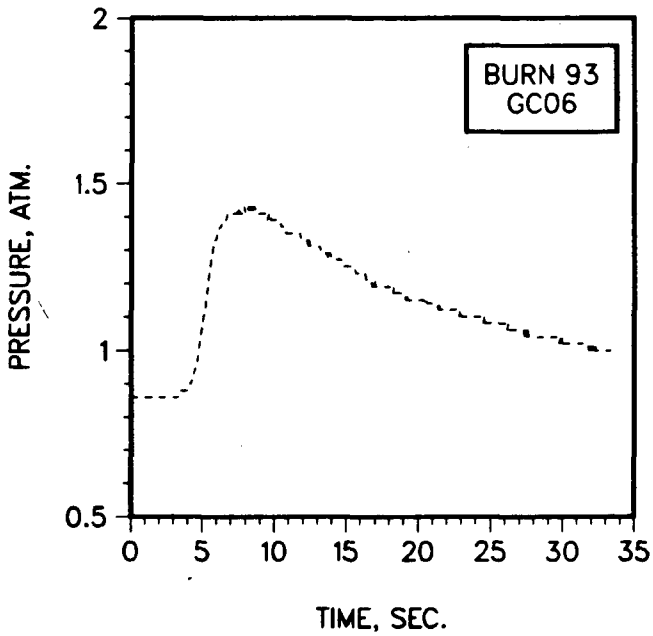
BURN 93
GC06
PRESSURE, ATM.
TIME, SEC.

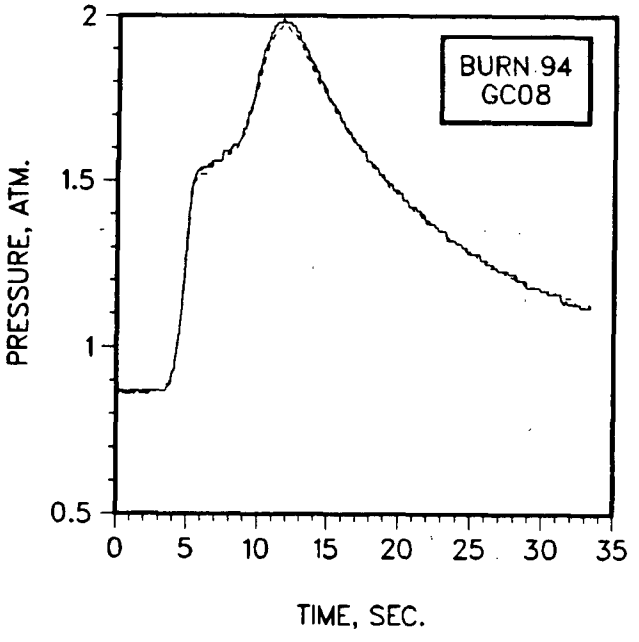
BURN 94
GC08
PRESSURE, ATM.
TIME, SEC.
2
1.5
1
0.5
0
5
10
15
20
25
30
35

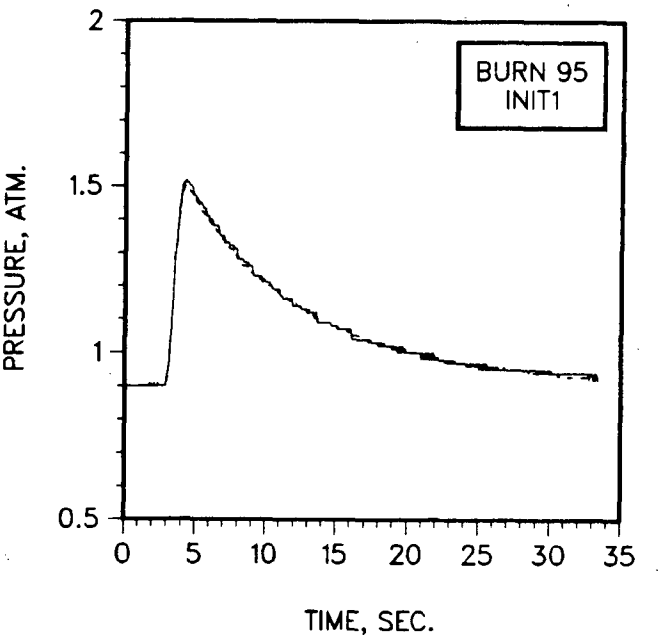
BURN 95
INIT1
PRESSURE, ATM.
TIME, SEC.
2
1.5
1
0.5
0
5
10
15
20
25
30
35

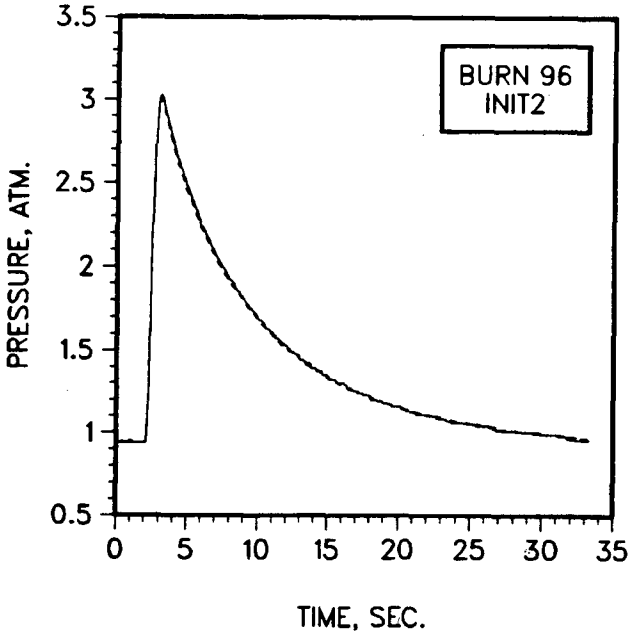
BURN 96
INIT2
PRESSURE, ATM.
TIME, SEC.
3.5
3
2.5
2
1.5
1
0.5
0
5
10
15
20
25
30
35

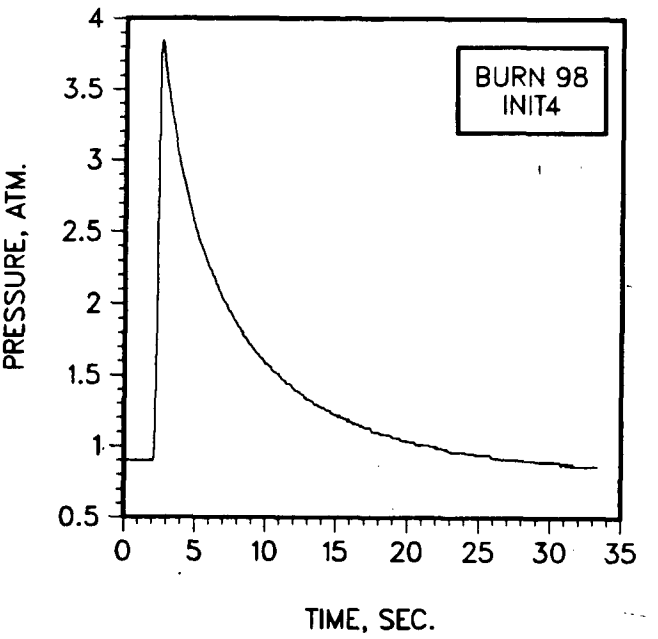
BURN 98
INIT4
PRESSURE, ATM.
TIME, SEC.
4
3.5
3
2.5
2
1.5
1
0.5
0
5
10
15
20
25
30
35

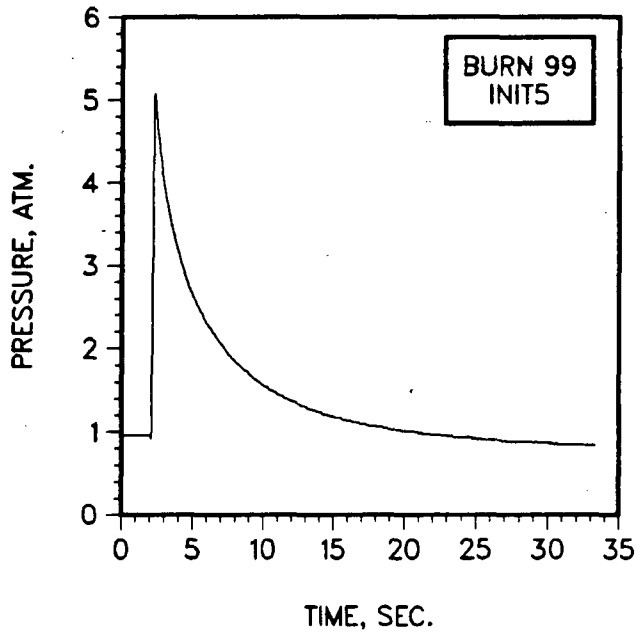
BURN 99
INIT5
PRESSURE, ATM.
TIME, SEC.
0
1
2
3
4
5
6
0
5
10
15
20
25
30
35

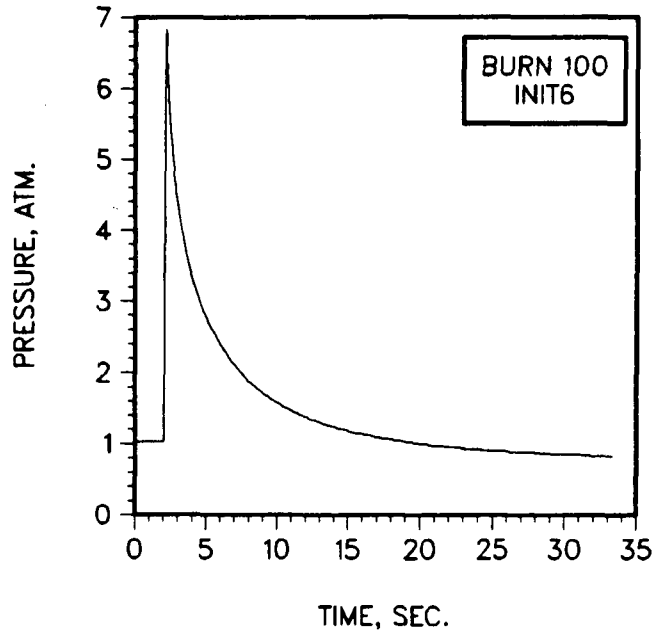
BURN 100
INIT6
PRESSURE, ATM.
TIME, SEC.
0
1
2
3
4
5
6
7
0
5
10
15
20
25
30
35

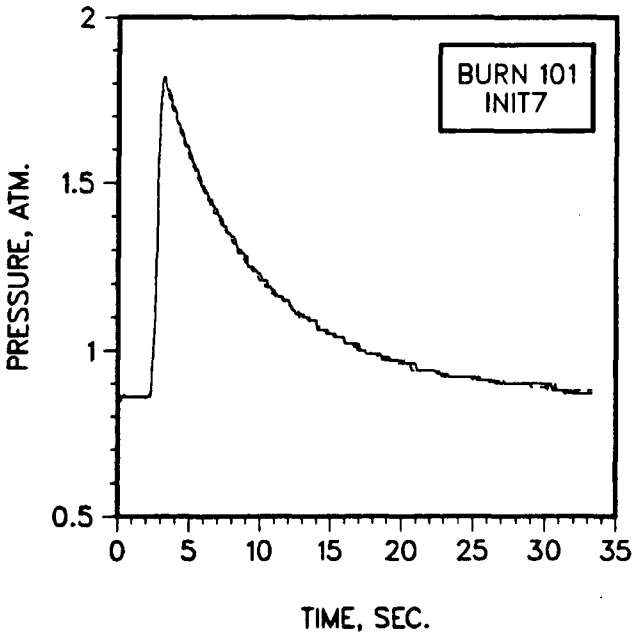
BURN 101
INIT7
PRESSURE, ATM.
TIME, SEC.
0.5
1
1.5
2
0
5
10
15
20
25
30
35

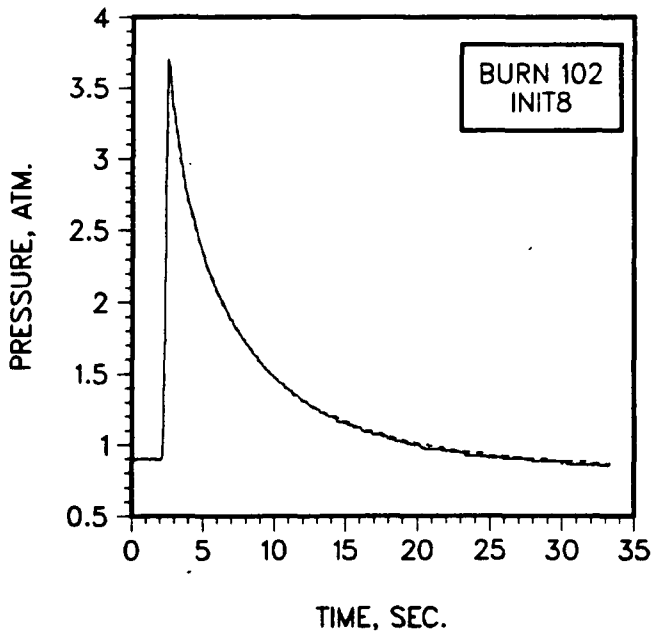
BURN 102
INIT8
PRESSURE, ATM.
TIME, SEC.
0.5
1
1.5
2
2.5
3
3.5
4
0
5
10
15
20
25
30
35

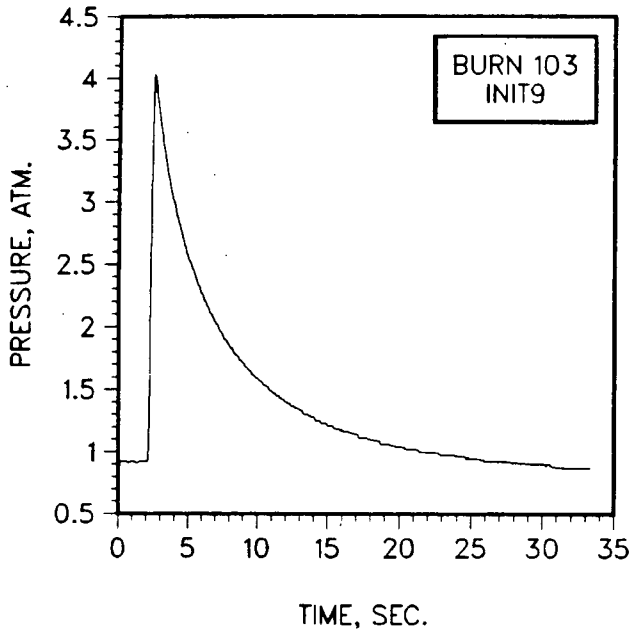
BURN 103
INIT9
PRESSURE, ATM.
TIME, SEC.

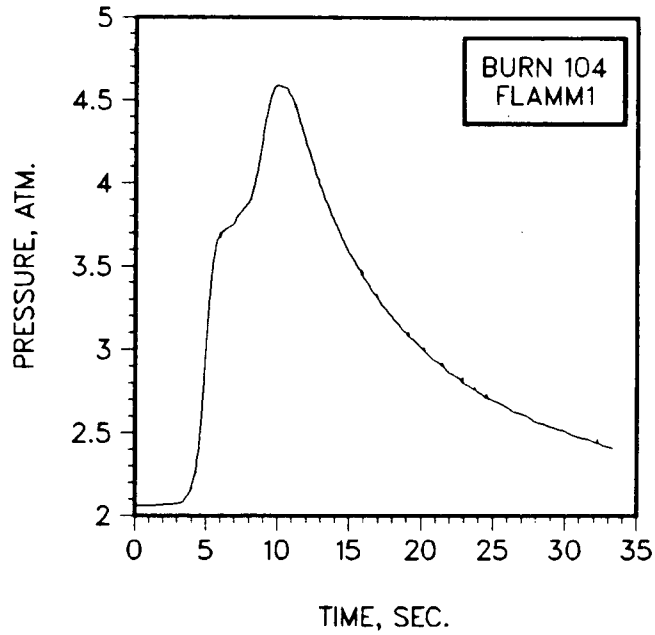
BURN 104
FLAMM1
PRESSURE, ATM.
TIME, SEC.

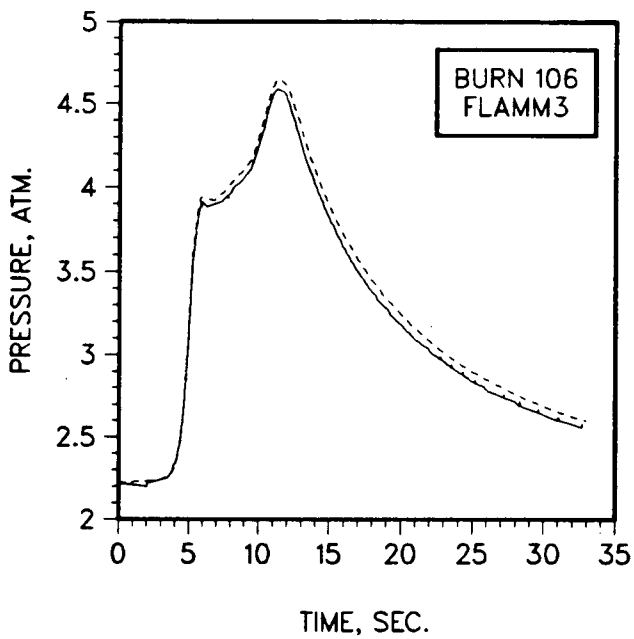
BURN 106
FLAMM3
PRESSURE, ATM.
TIME, SEC.

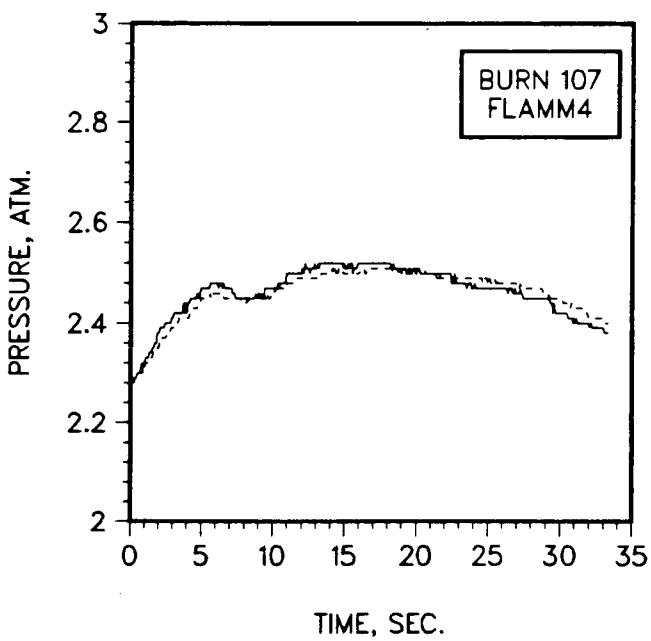
BURN 107
FLAMM4
PRESSURE, ATM.
TIME, SEC.

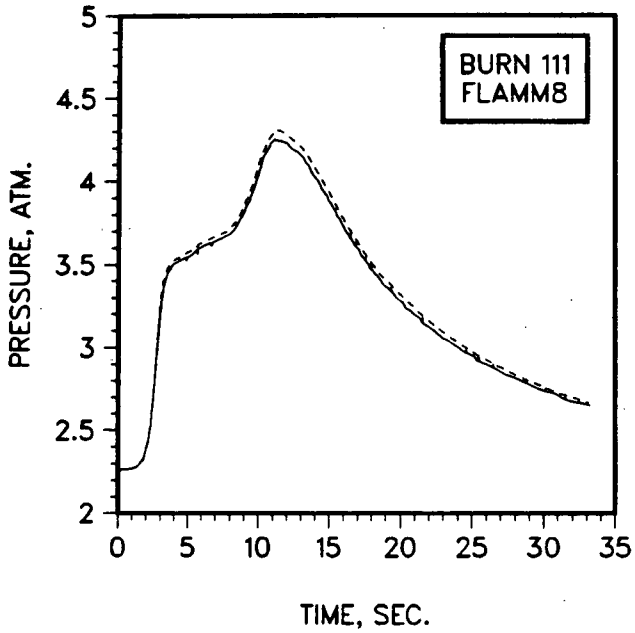
BURN 111
FLAMM8
PRESSURE, ATM.
TIME, SEC.

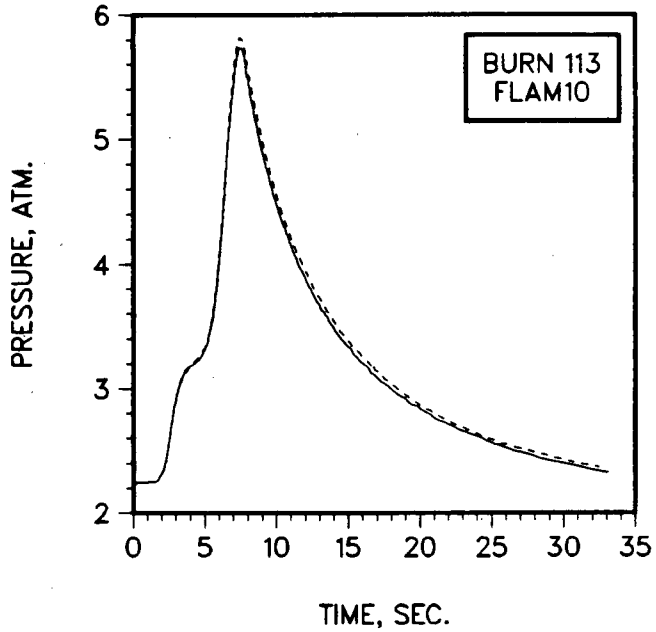
BURN 113
FLAM10
PRESSURE, ATM.
TIME, SEC.

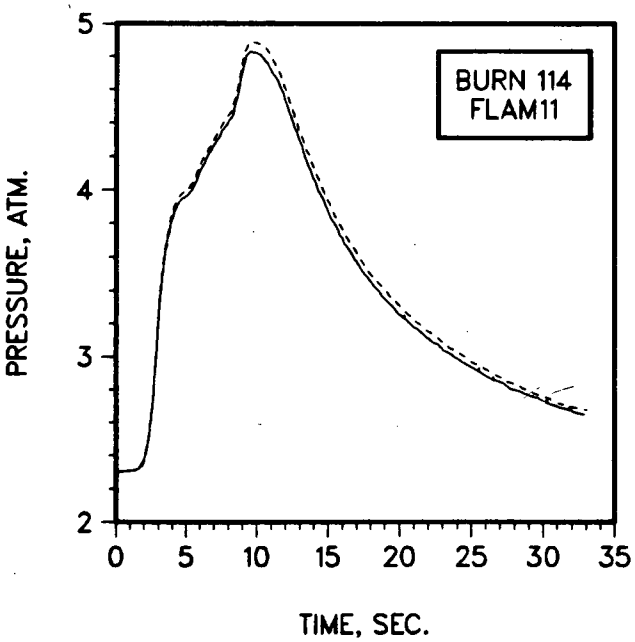
BURN 114
FLAM11
PRESSURE, ATM.
TIME, SEC.

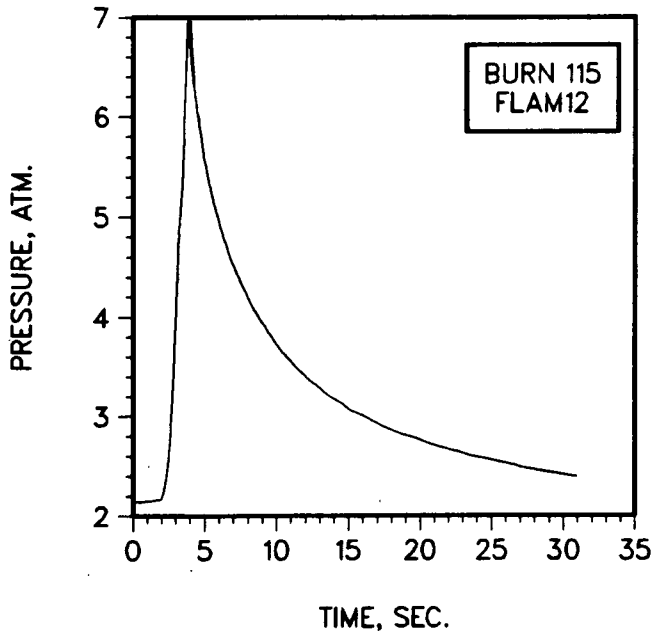
BURN 115
FLAM12
PRESSURE, ATM.
TIME, SEC.

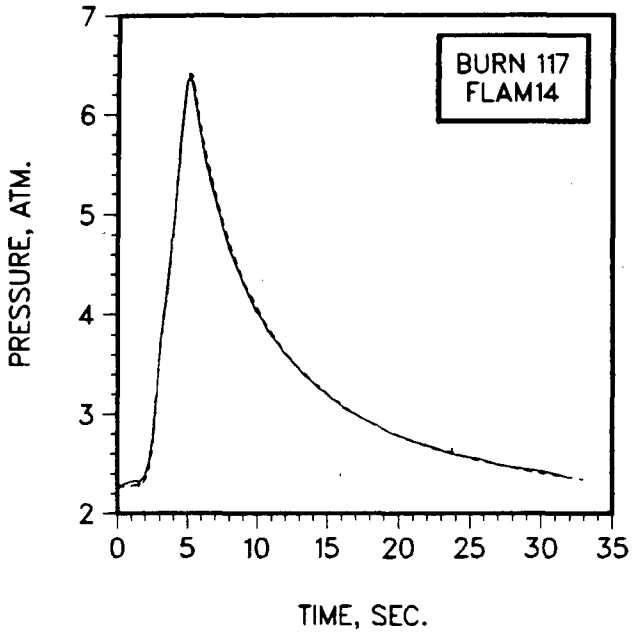
BURN 117
FLAM14
PRESSURE, ATM.
TIME, SEC.
7
6
5
4
3
2
0
5
10
15
20
25
30
35

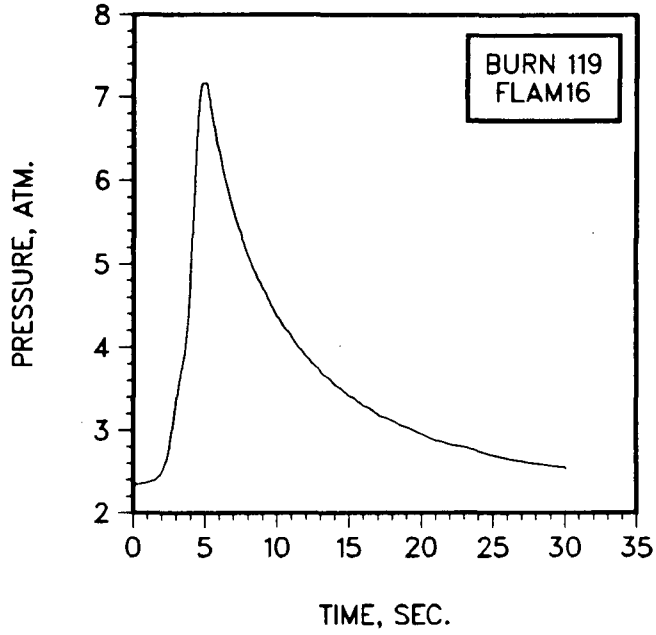
BURN 119
FLAM16
PRESSURE, ATM.
TIME, SEC.
8
7
6
5
4
3
2
0
5
10
15
20
25
30
35

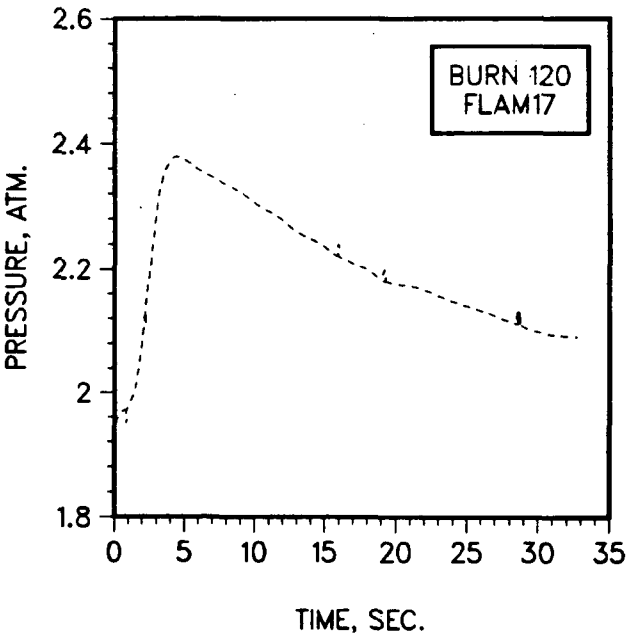
BURN 120
FLAM17
PRESSURE, ATM.
TIME, SEC.
2.6
2.4
2.2
2
1.8
0
5
10
15
20
25
30
35

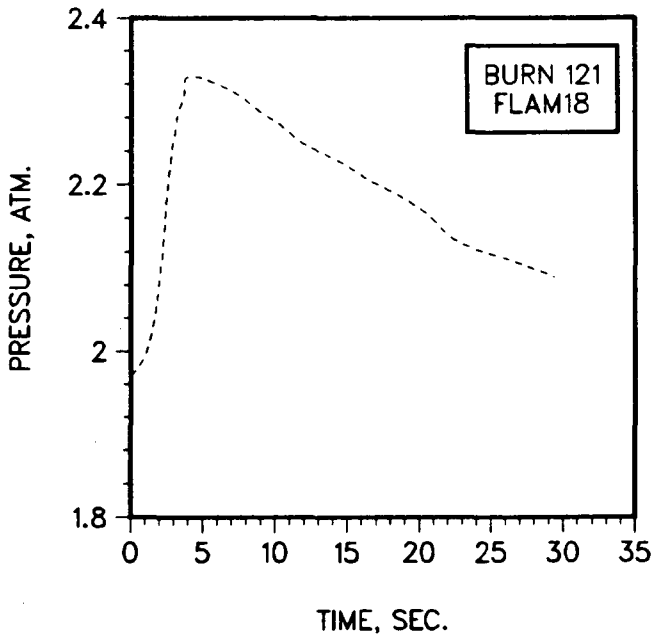
BURN 121
FLAM18
PRESSURE, ATM.
TIME, SEC.
2.4
2.2
2
1.8
0
5
10
15
20
25
30
35

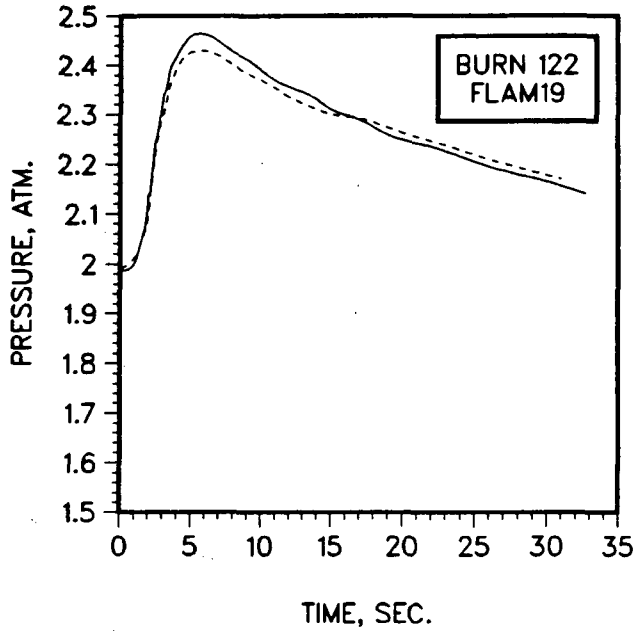
BURN 122
FLAM19
PRESSURE, ATM.
TIME, SEC.

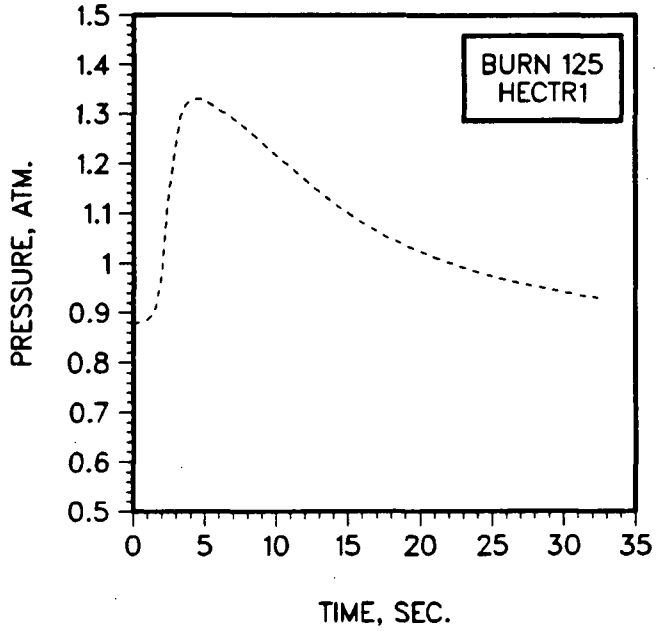
BURN 125
HECTR1
PRESSURE, ATM.
TIME, SEC.

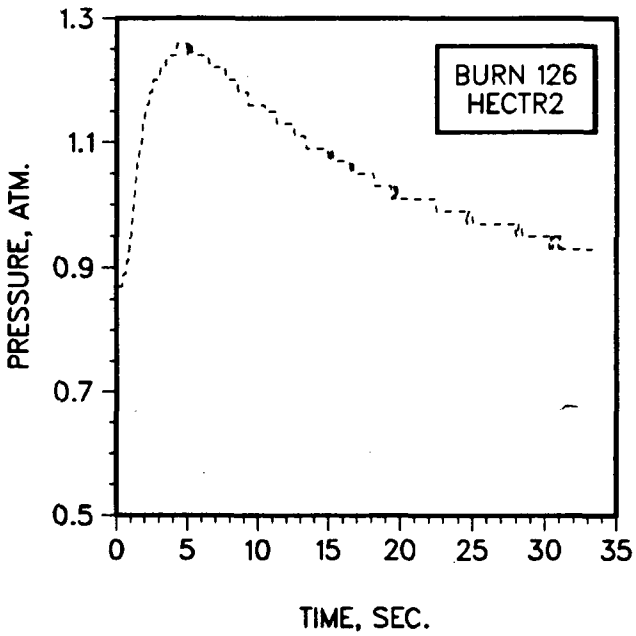
BURN 126
HECTR2
PRESSURE, ATM.
TIME, SEC.

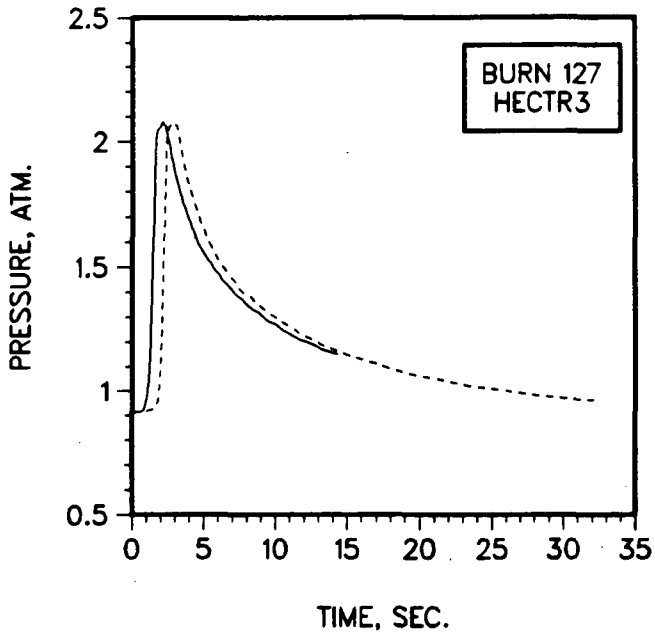
BURN 127
HECTR3
PRESSURE, ATM.
TIME, SEC.

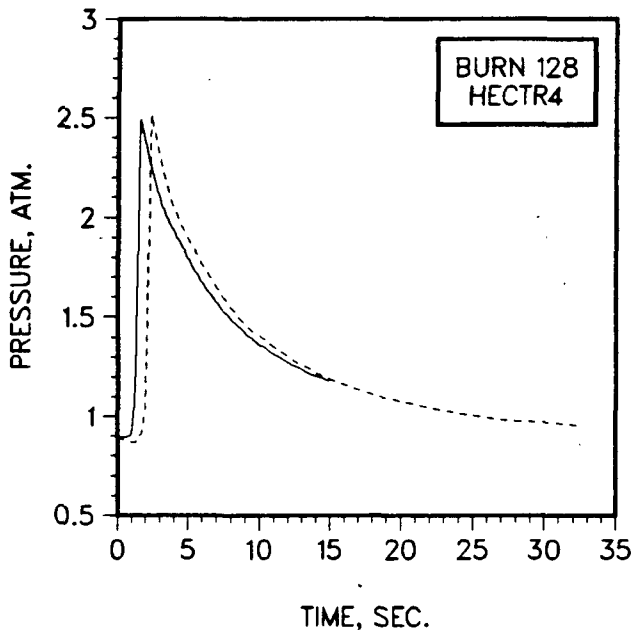
BURN 128
HECTR4
PRESSURE, ATM.
TIME, SEC.
3
2.5
2
1.5
1
0.5
0
5
10
15
20
25
30
35

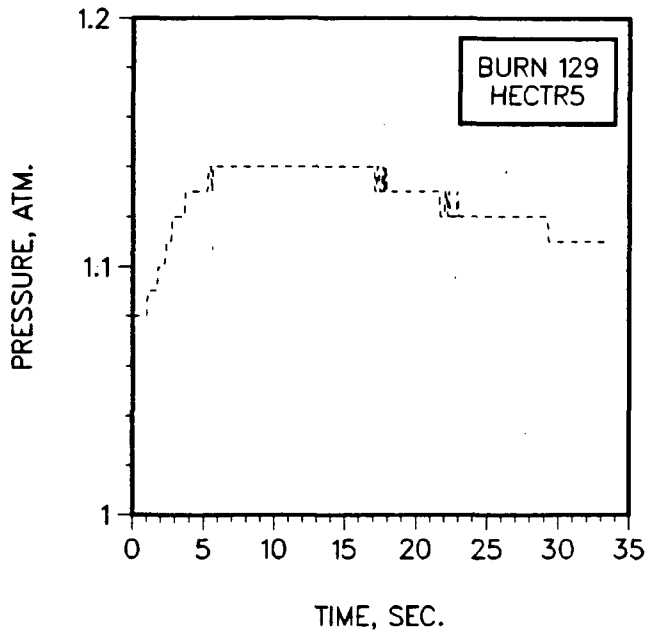
BURN 129
HECTR5
PRESSURE, ATM.
TIME, SEC.
1.2
1.1
1
0
5
10
15
20
25
30
35

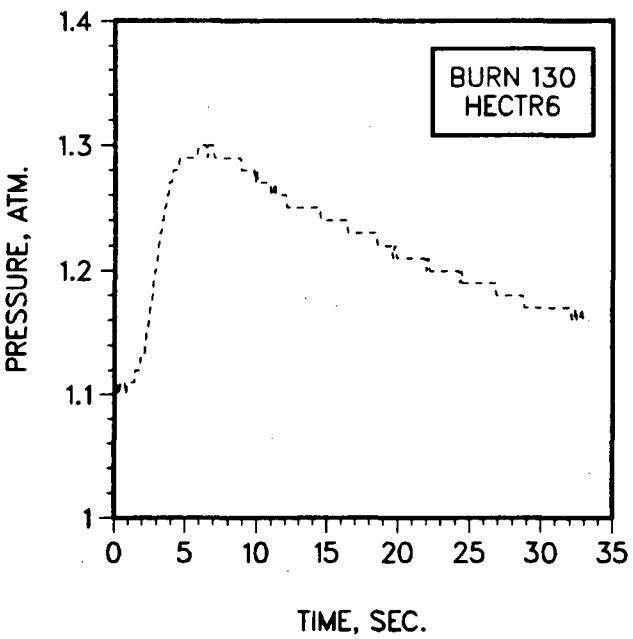
BURN 130
HECTR6
PRESSURE, ATM.
TIME, SEC.
1.4
1.3
1.2
1.1
1
0
5
10
15
20
25
30
35

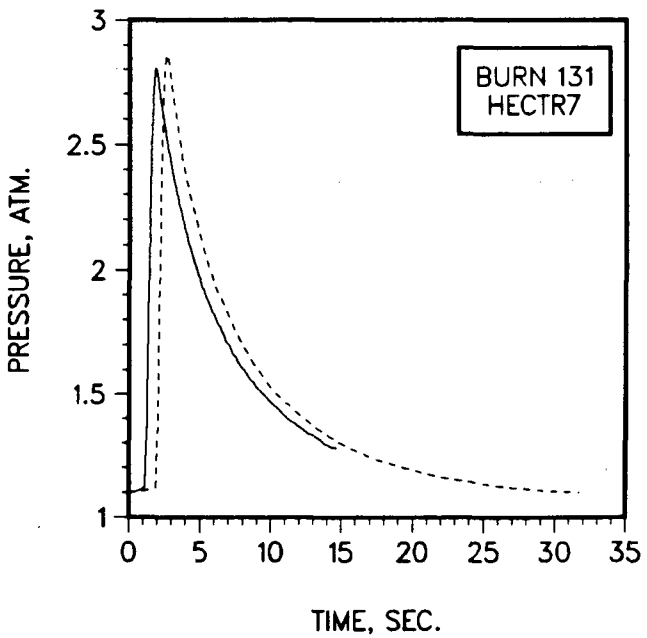
BURN 131
HECTR7
PRESSURE, ATM.
TIME, SEC.
3
2.5
2
1.5
1
0
5
10
15
20
25
30
35

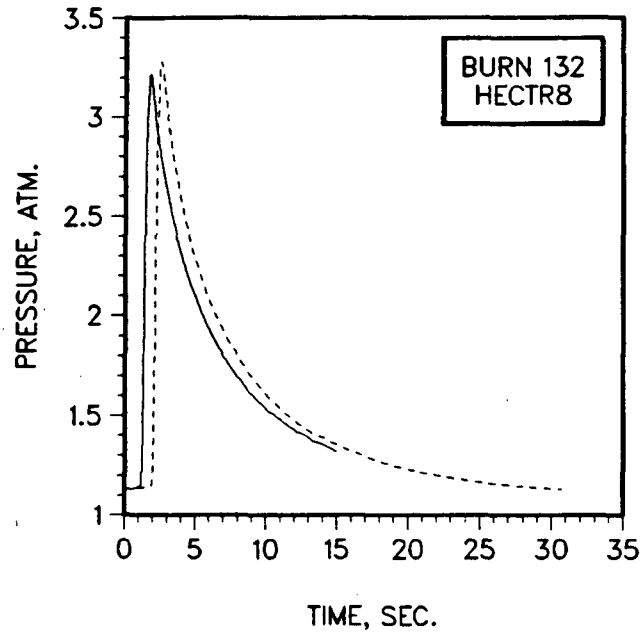
BURN 132
HECTR8
PRESSURE, ATM.
TIME, SEC.

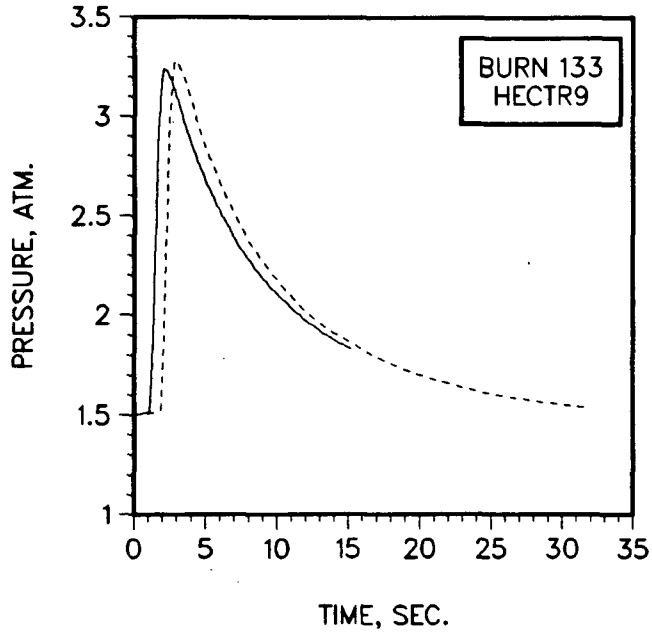
BURN 133
HECTR9
PRESSURE, ATM.
TIME, SEC.

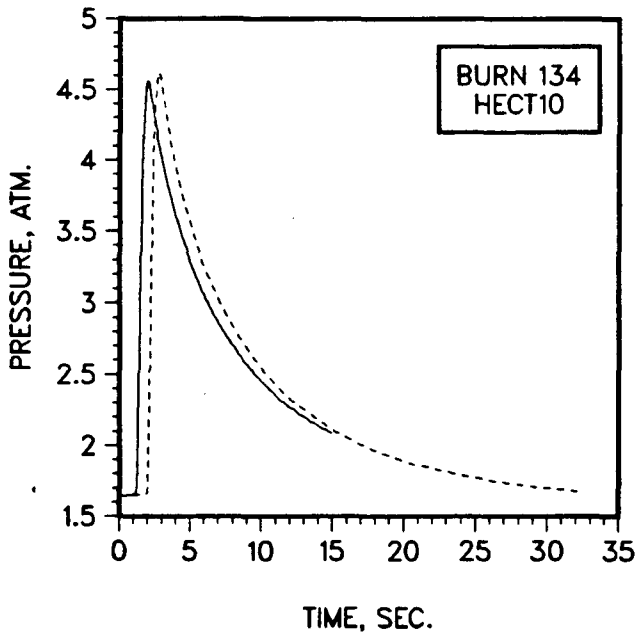
BURN 134
HECT10
PRESSURE, ATM.
TIME, SEC.

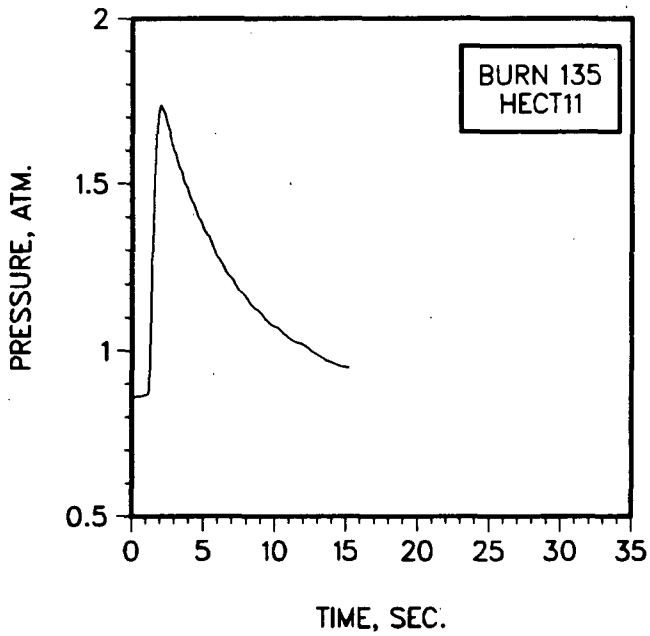
BURN 135
HECT11
PRESSURE, ATM.
TIME, SEC.

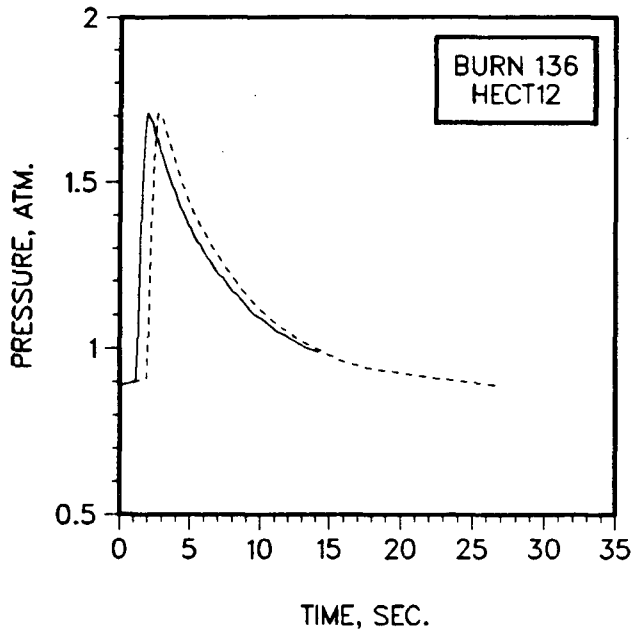
BURN 136
HECT12
PRESSURE, ATM.
TIME, SEC.
2
1.5
1
0.5
0
5
10
15
20
25
30
35

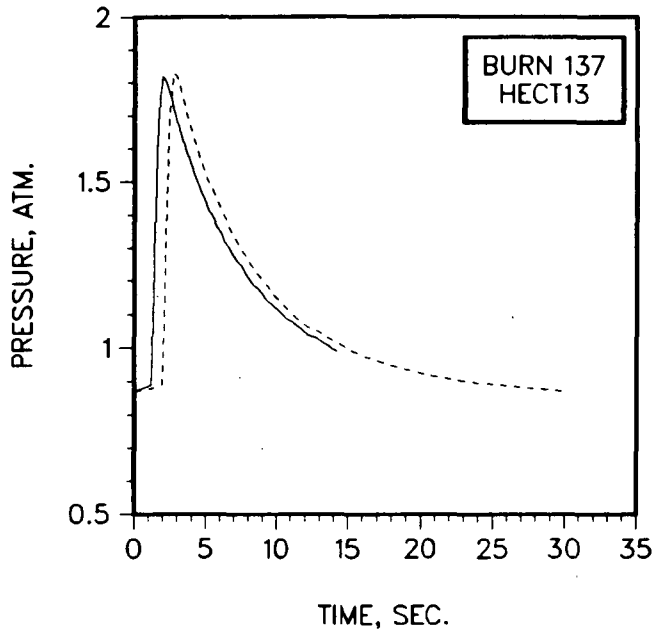
BURN 137
HECT13
PRESSURE, ATM.
TIME, SEC.
2
1.5
1
0.5
0
5
10
15
20
25
30
35

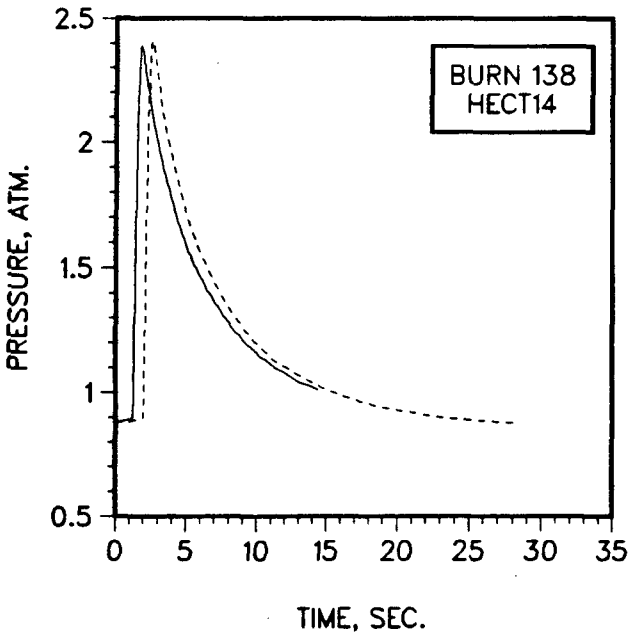
BURN 138
HECT14
PRESSURE, ATM.
TIME, SEC.
2.5
2
1.5
1
0.5
0
5
10
15
20
25
30
35

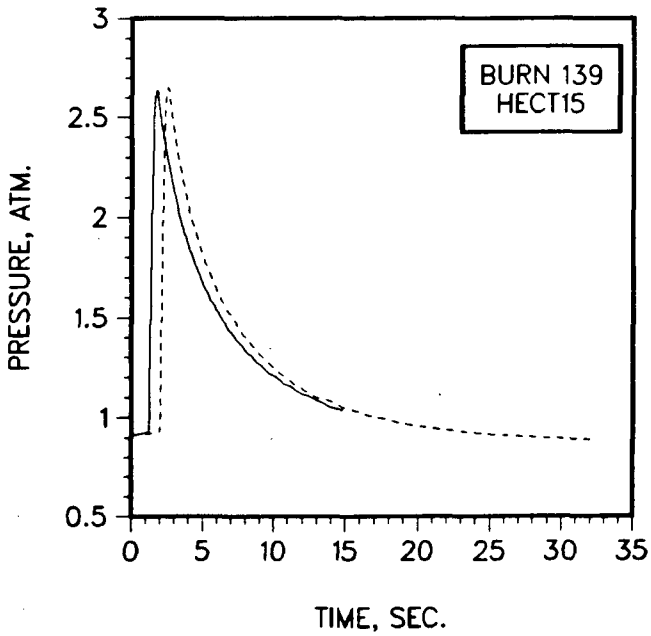
BURN 139
HECT15
PRESSURE, ATM.
TIME, SEC.
3
2.5
2
1.5
1
0.5
0
5
10
15
20
25
30
35

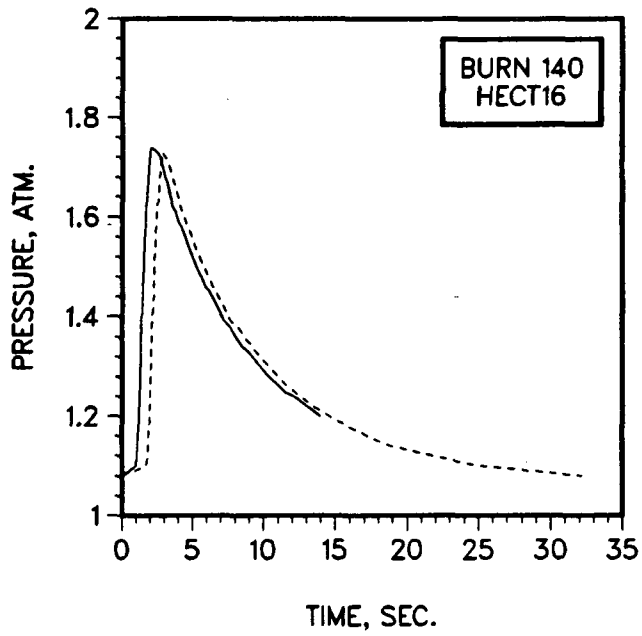
BURN 140
HECT16
PRESSURE, ATM.
TIME, SEC.
2
1.8
1.6
1.4
1.2
1
0
5
10
15
20
25
30
35

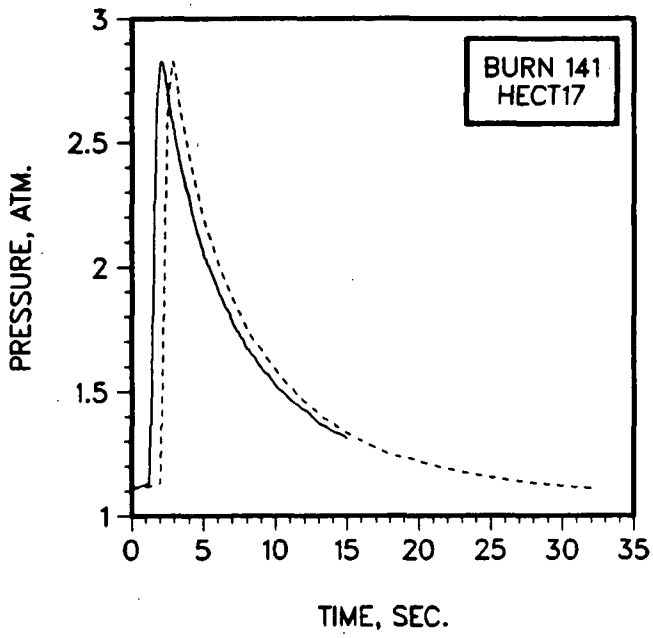
BURN 141
HECT17
PRESSURE, ATM.
TIME, SEC.
3
2.5
2
1.5
1
0
5
10
15
20
25
30
35

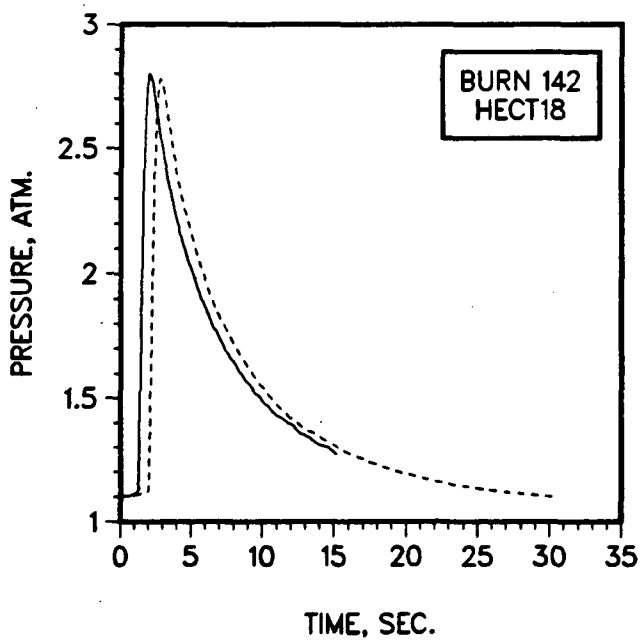
BURN 142
HECT18
PRESSURE, ATM.
TIME, SEC.
3
2.5
2
1.5
1
0
5
10
15
20
25
30
35

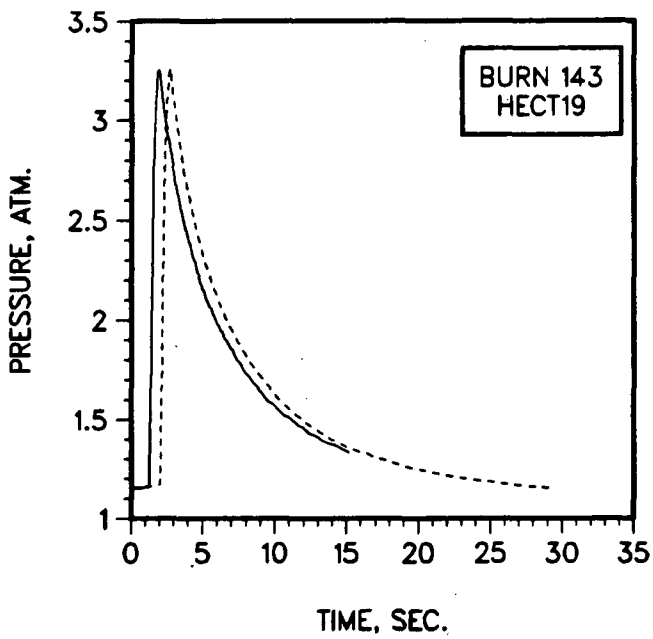
BURN 143
HECT19
PRESSURE, ATM.
TIME, SEC.
3.5
3
2.5
2
1.5
1
0
5
10
15
20
25
30
35

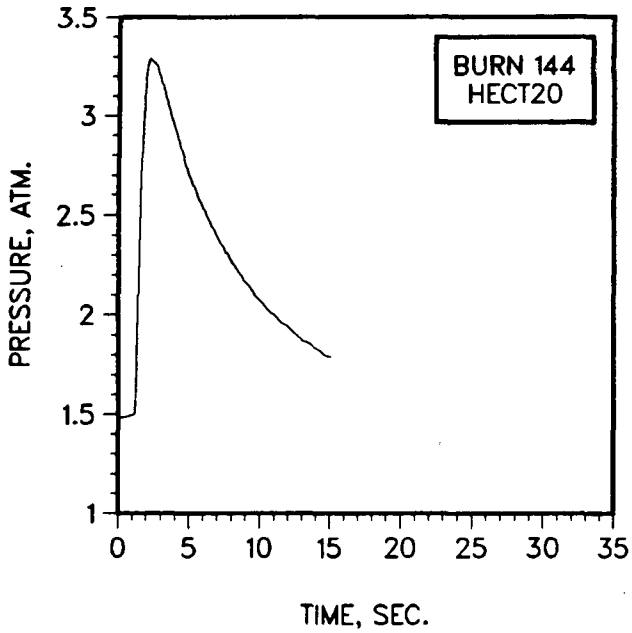
BURN 144
HECT20
PRESSURE, ATM.
TIME, SEC.
3.5
3
2.5
2
1.5
1
0
5
10
15
20
25
30
35

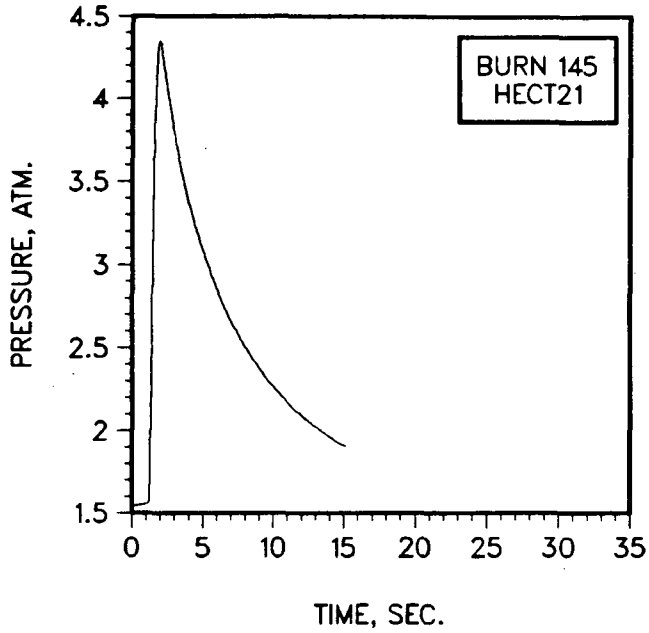
BURN 145
HECT21
PRESSURE, ATM.
TIME, SEC.
4.5
4
3.5
3
2.5
2
1.5
0
5
10
15
20
25
30
35

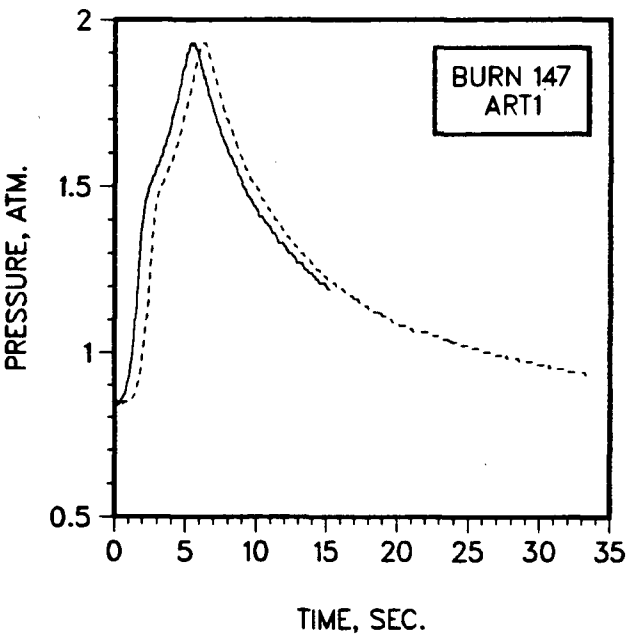
BURN 147
ART1
PRESSURE, ATM.
TIME, SEC.
2
1.5
1
0.5
0
5
10
15
20
25
30
35

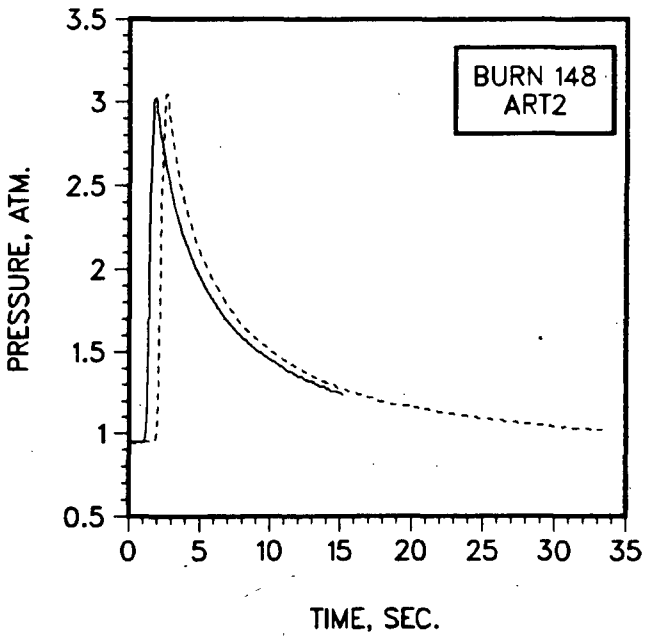
BURN 148
ART2
PRESSURE, ATM.
TIME, SEC.
3.5
3
2.5
2
1.5
1
0.5
0
5
10
15
20
25
30
35

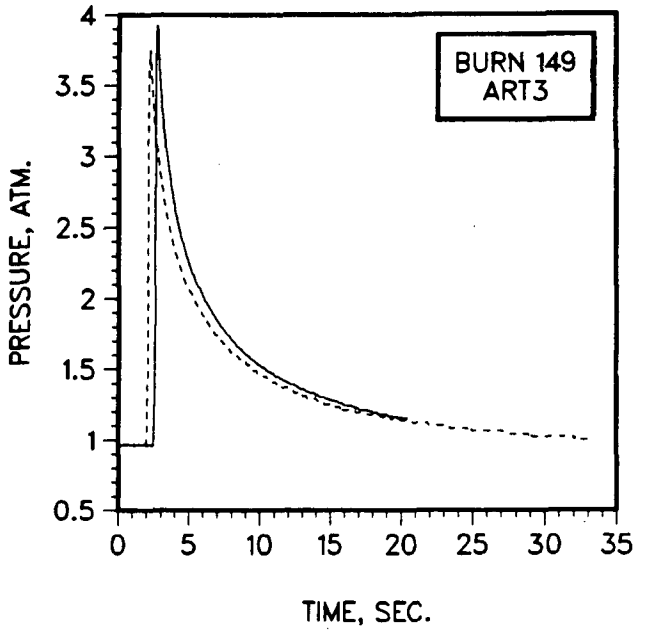
BURN 149
ART3
PRESSURE, ATM.
TIME, SEC.

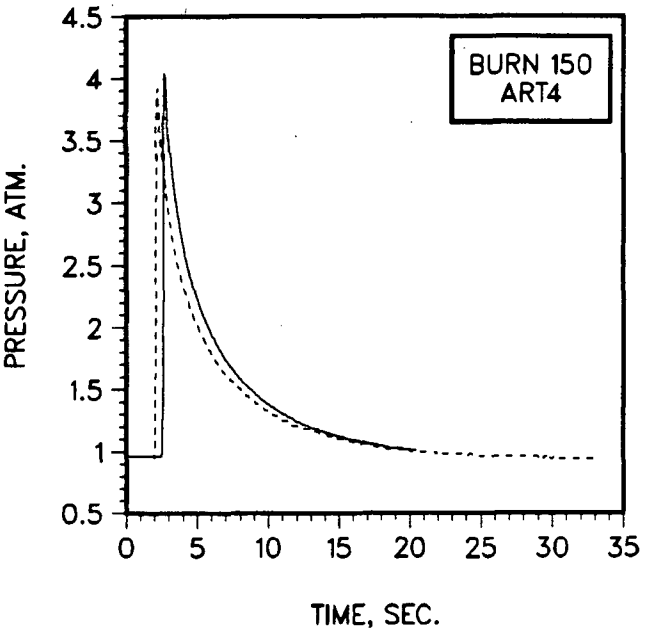
BURN 150
ART4
PRESSURE, ATM.
TIME, SEC.

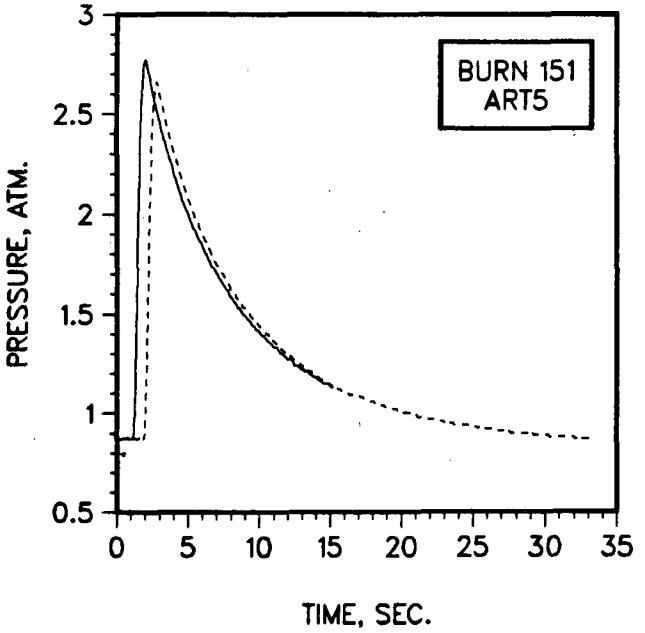
BURN 151
ART5
PRESSURE, ATM.
TIME, SEC.

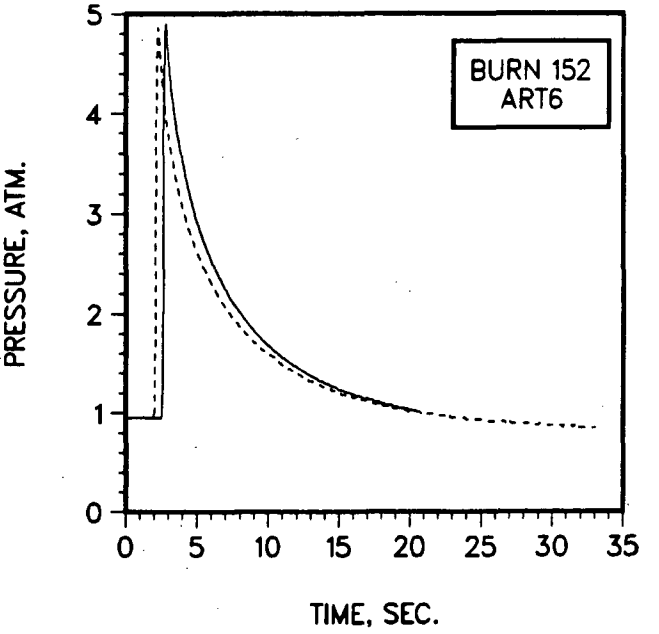
BURN 152
ART6
PRESSURE, ATM.
TIME, SEC.

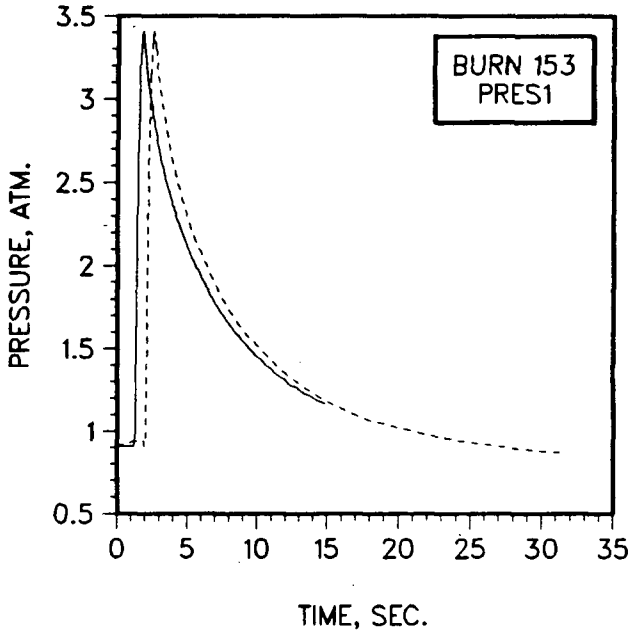
BURN 153
PRES1
PRESSURE, ATM.
TIME, SEC.

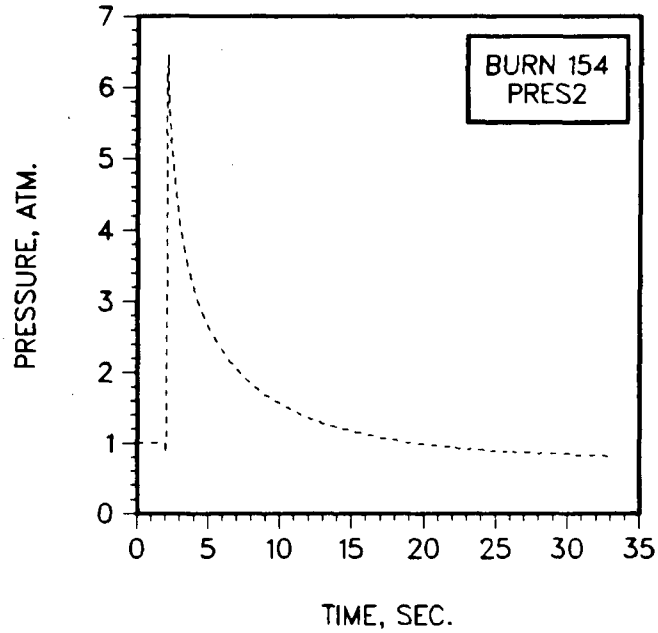
BURN 154
PRES2
PRESSURE, ATM.
TIME, SEC.

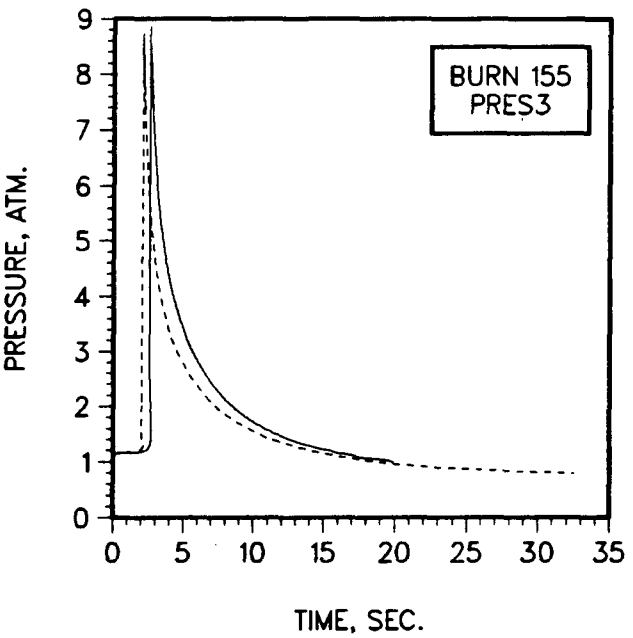
BURN 155
PRES3
PRESSURE, ATM.
TIME, SEC.

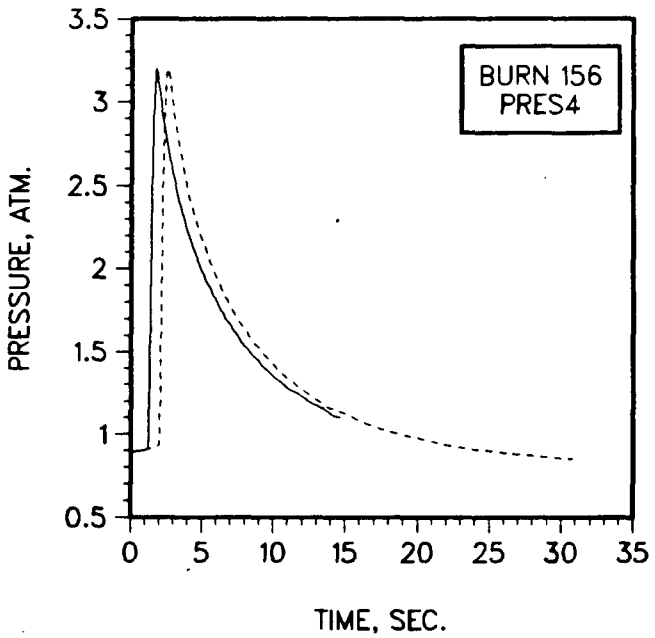
BURN 156
PRES4
PRESSURE, ATM.
TIME, SEC.

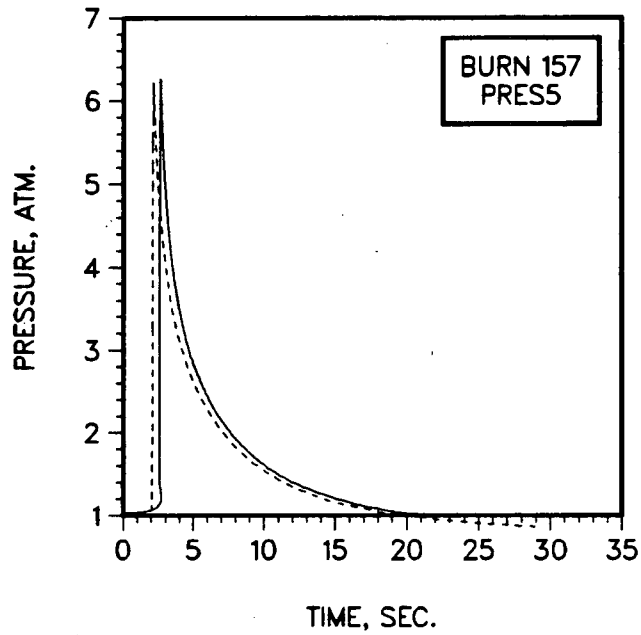
BURN 157
PRES5
PRESSURE, ATM.
TIME, SEC.

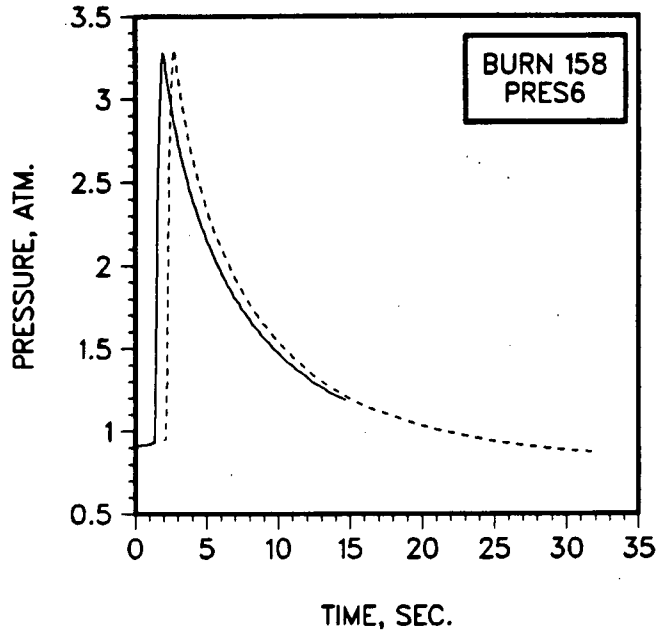
BURN 158
PRES6
PRESSURE, ATM.
TIME, SEC.

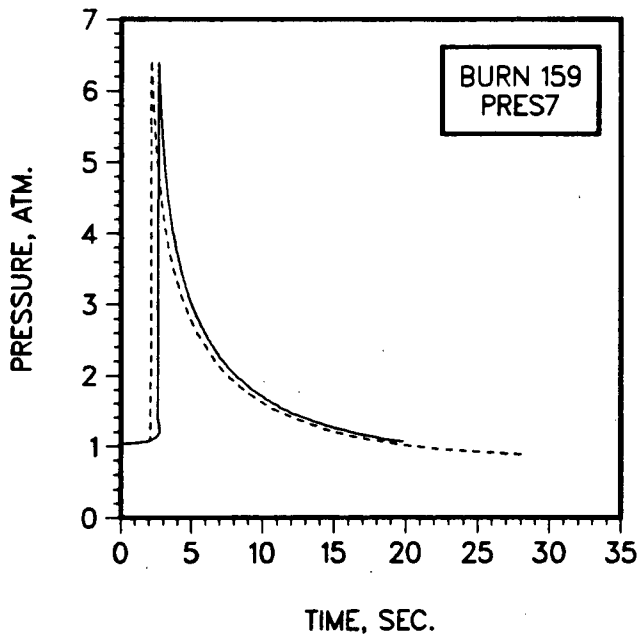
BURN 159
PRES7
PRESSURE, ATM.
TIME, SEC.

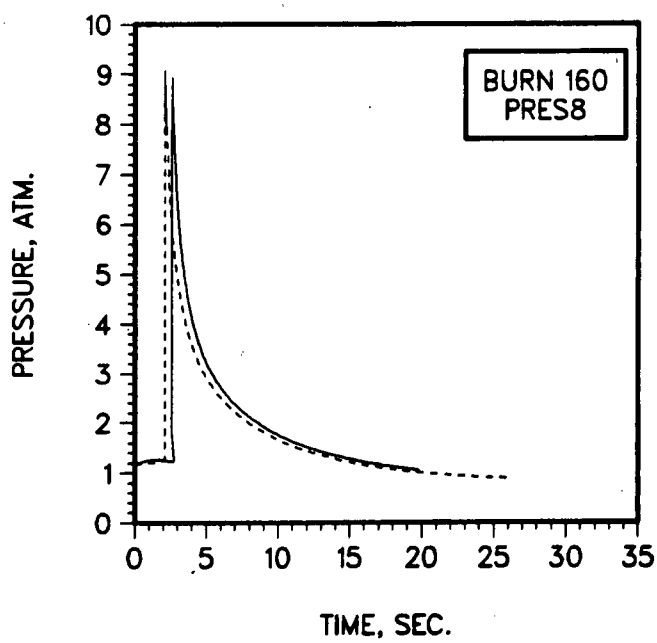
BURN 160
PRES8
PRESSURE, ATM.
TIME, SEC.

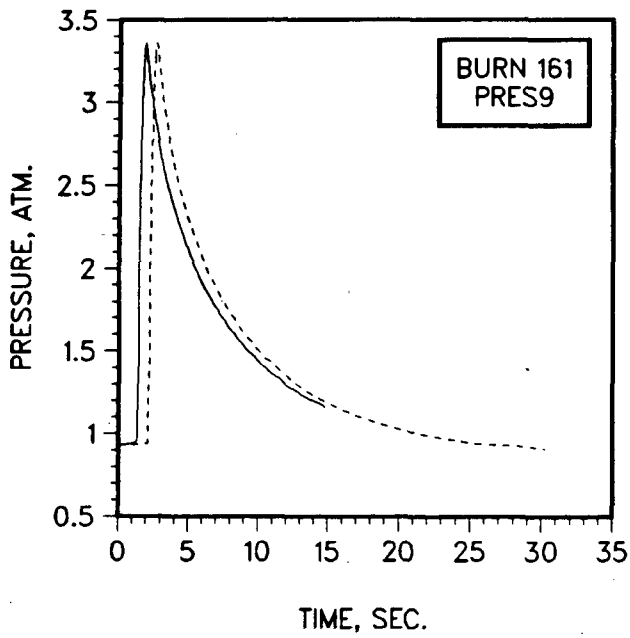
BURN 161
PRES9
PRESSURE, ATM.
TIME, SEC.

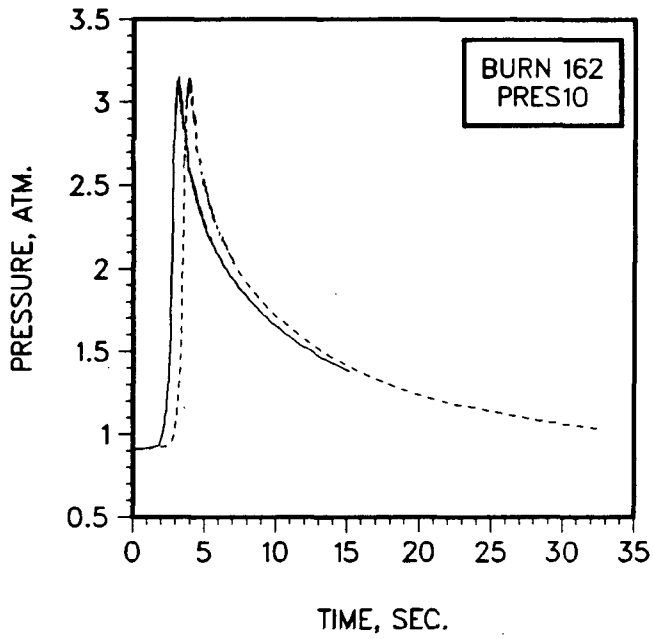
BURN 162
PRES10
PRESSURE, ATM.
TIME, SEC.

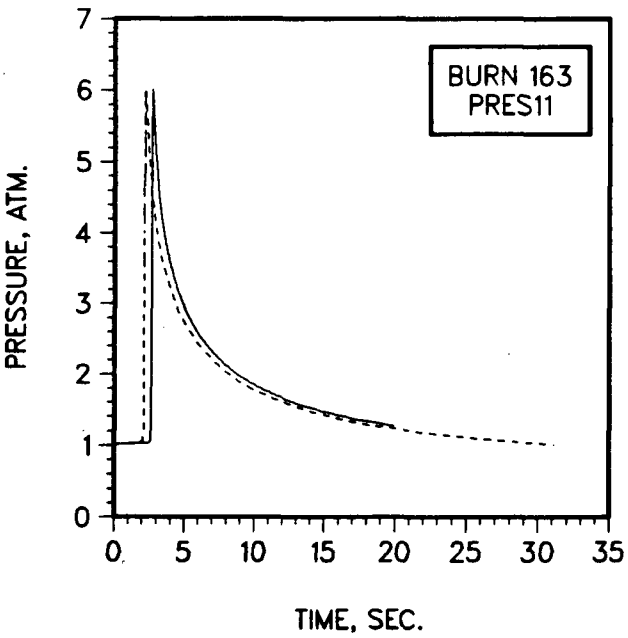
BURN 163
PRES11
PRESSURE, ATM.
TIME, SEC.

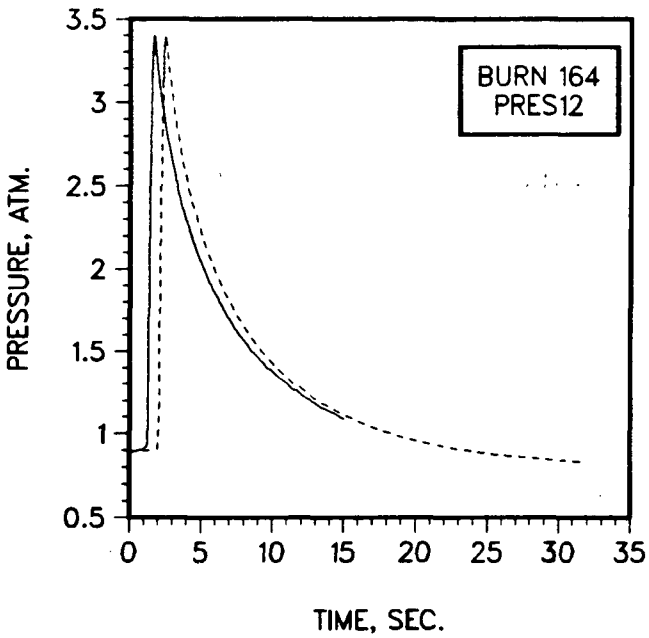
BURN 164
PRES12
PRESSURE, ATM.
TIME, SEC.

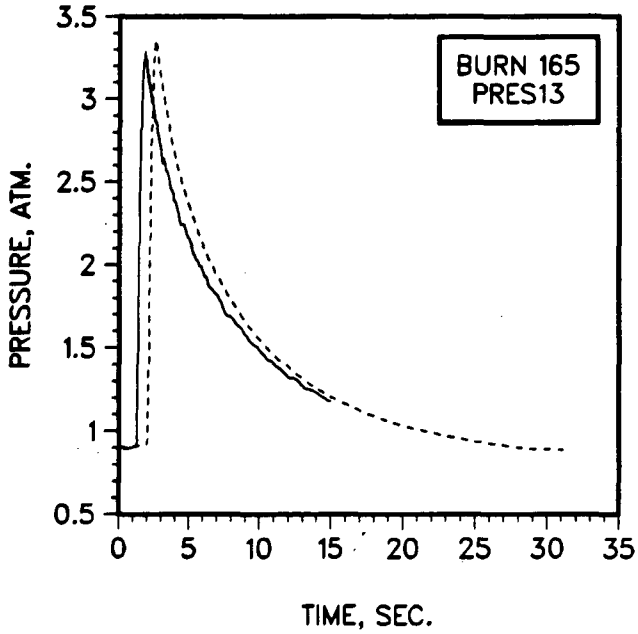
BURN 165
PRES13
PRESSURE, ATM.
TIME, SEC.

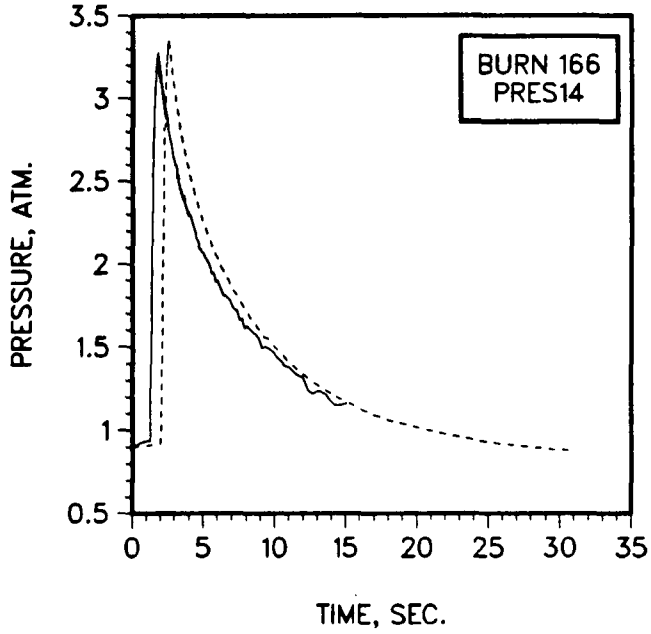
BURN 166
PRES14
PRESSURE, ATM.
TIME, SEC.

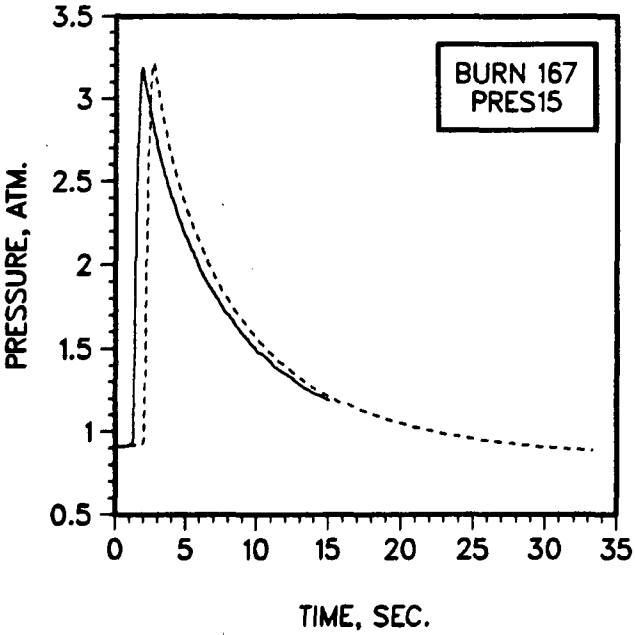
BURN 167
PRES15
PRESSURE, ATM.
TIME, SEC.

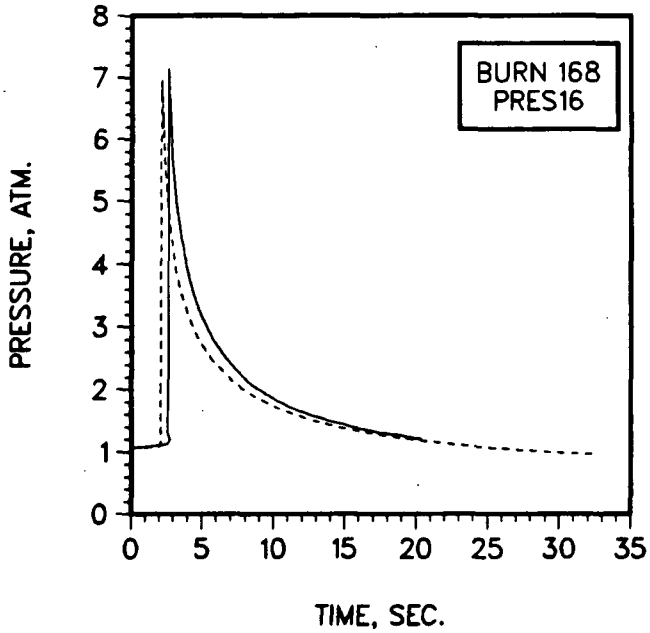
BURN 168
PRES16
PRESSURE, ATM.
TIME, SEC.

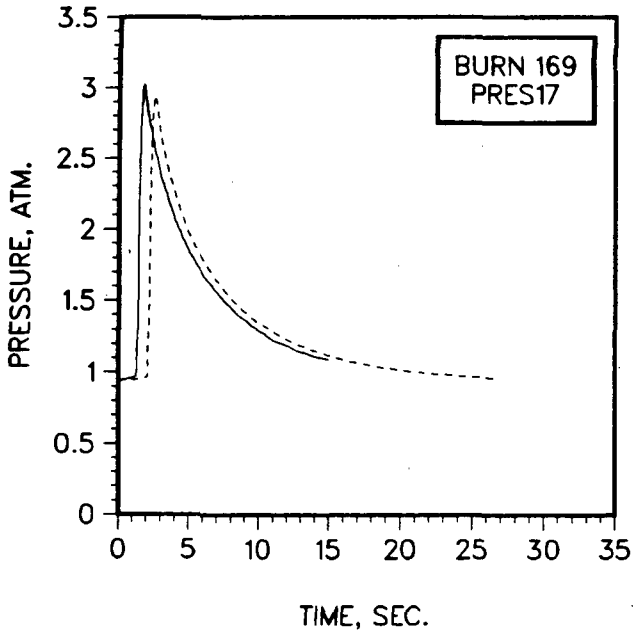
BURN 169
PRES17
PRESSURE, ATM.
TIME, SEC.
0
0.5
1
1.5
2
2.5
3
3.5
0
5
10
15
20
25
30
35

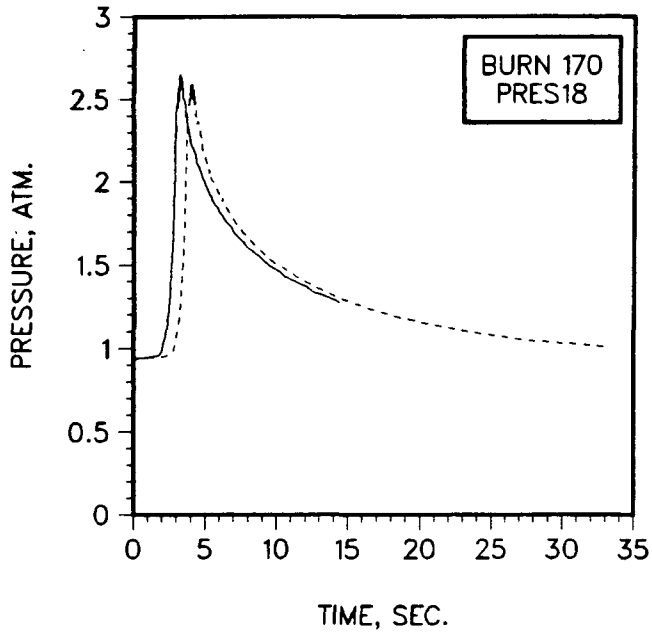
BURN 170
PRES18
PRESSURE, ATM.
TIME, SEC.
0
0.5
1
1.5
2
2.5
3
0
5
10
15
20
25
30
35

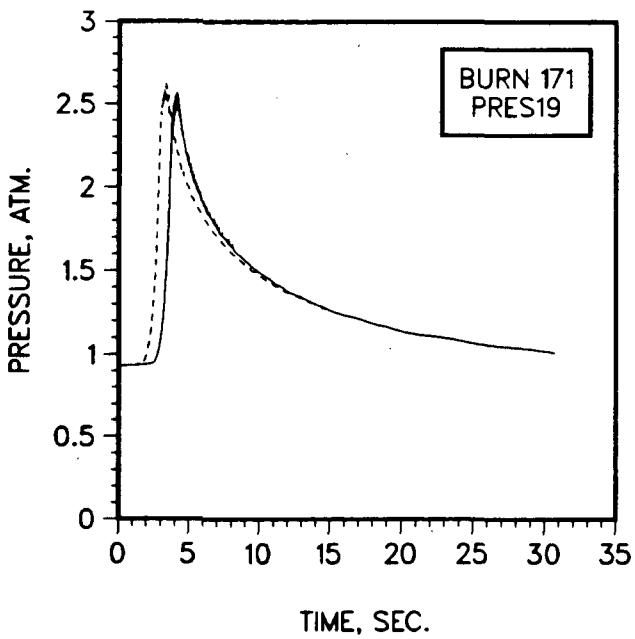
BURN 171
PRES19
PRESSURE, ATM.
TIME, SEC.
0
0.5
1
1.5
2
2.5
3
0
5
10
15
20
25
30
35

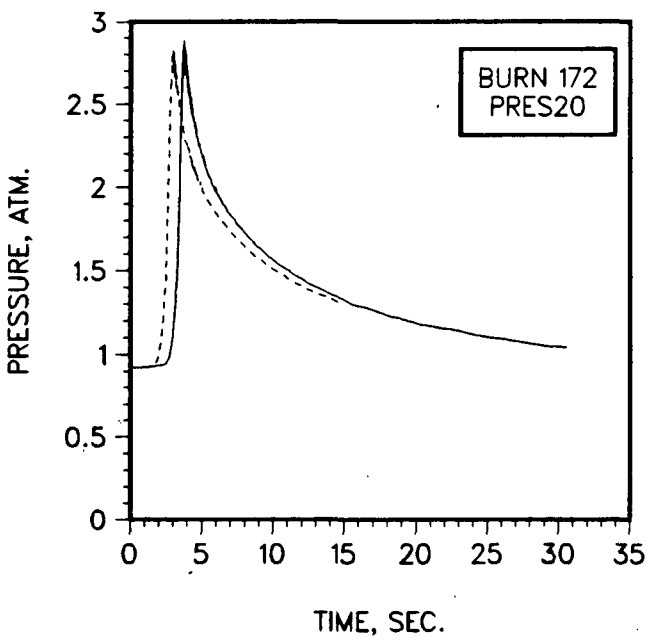
BURN 172
PRES20
PRESSURE, ATM.
TIME, SEC.
0
0.5
1
1.5
2
2.5
3
0
5
10
15
20
25
30
35

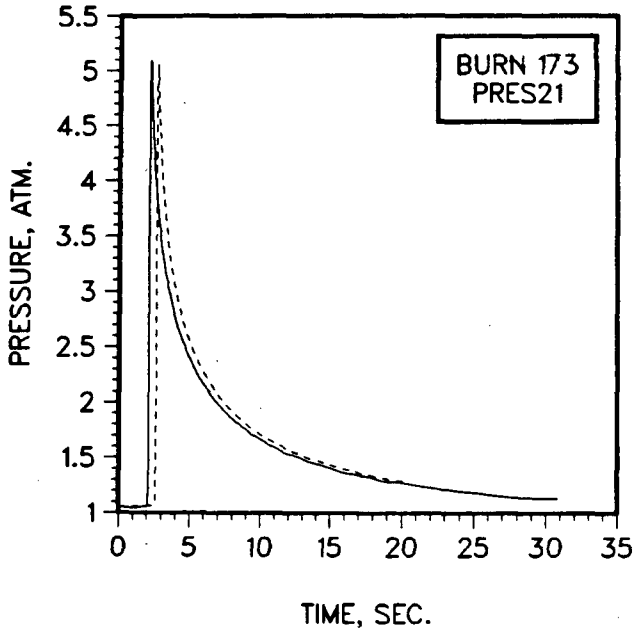
BURN 173
PRES21
PRESSURE, ATM.
TIME, SEC.
5.5
5
4.5
4
3.5
3
2.5
2
1.5
1
0
5
10
15
20
25
30
35

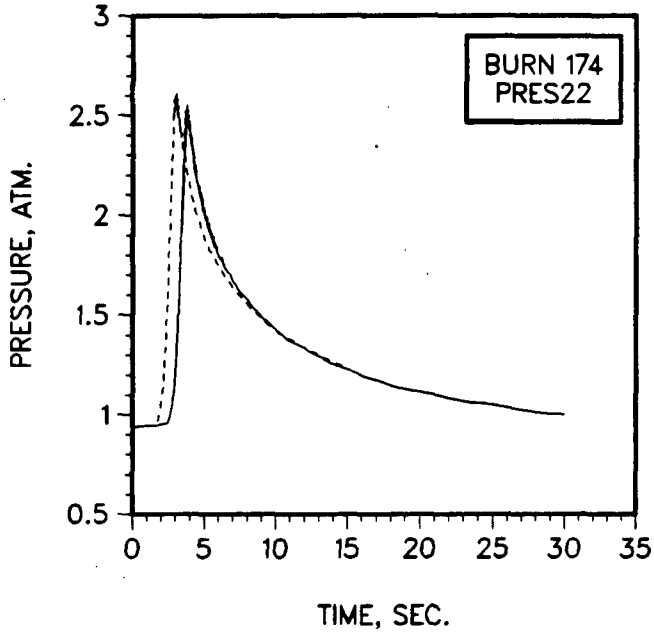
BURN 174
PRES22
PRESSURE, ATM.
TIME, SEC.
3
2.5
2
1.5
1
0.5
0
5
10
15
20
25
30
35

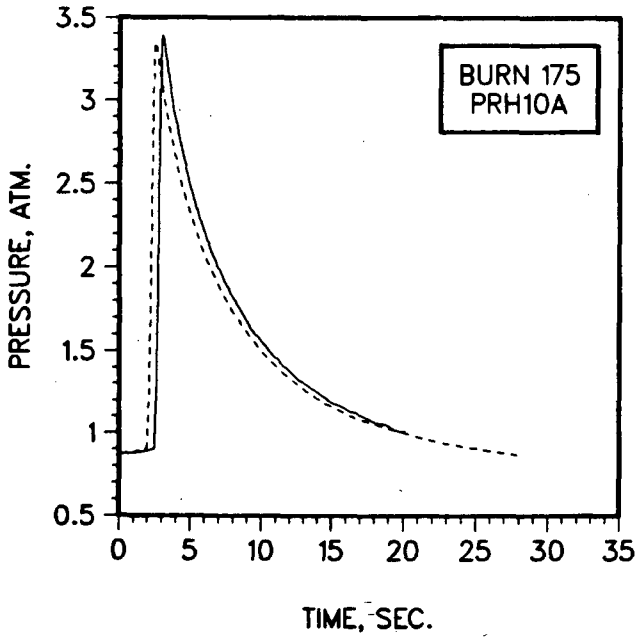
BURN 175
PRH10A
PRESSURE, ATM.
TIME, SEC.
3.5
3
2.5
2
1.5
1
0.5
0
5
10
15
20
25
30
35

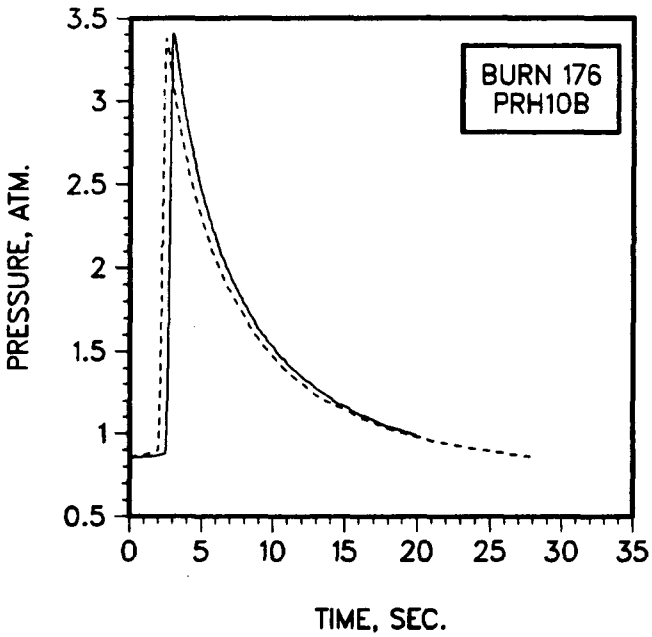
BURN 176
PRH10B
PRESSURE, ATM.
TIME, SEC.
3.5
3
2.5
2
1.5
1
0.5
0
5
10
15
20
25
30
35

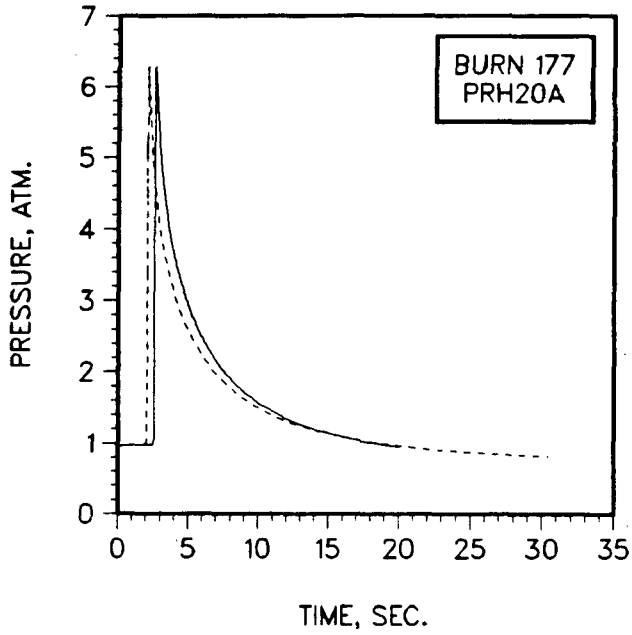
BURN 177
PRH20A
PRESSURE, ATM.
TIME, SEC.
0
1
2
3
4
5
6
7
0
5
10
15
20
25
30
35

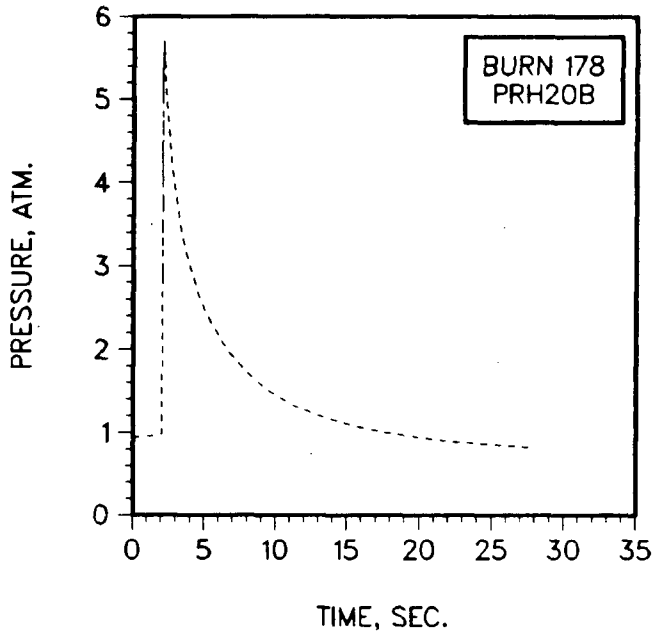
BURN 178
PRH20B
PRESSURE, ATM.
TIME, SEC.
0
1
2
3
4
5
6
0
5
10
15
20
25
30
35

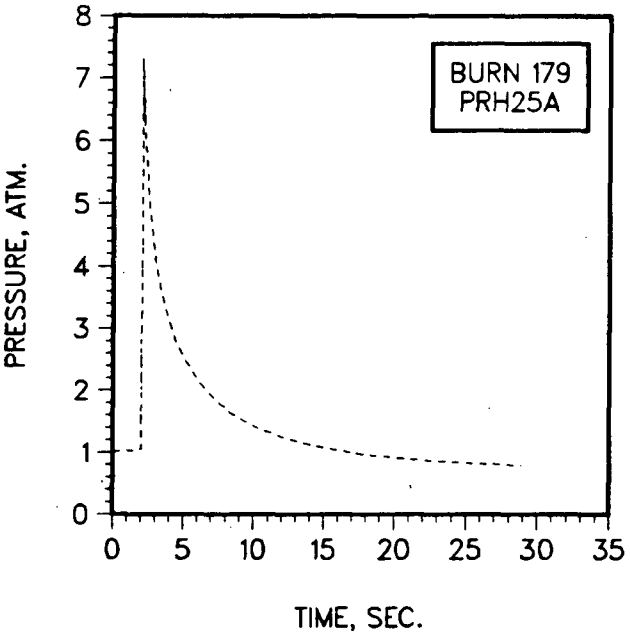
BURN 179
PRH25A
PRESSURE, ATM.
TIME, SEC.
0
1
2
3
4
5
6
7
8
0
5
10
15
20
25
30
35

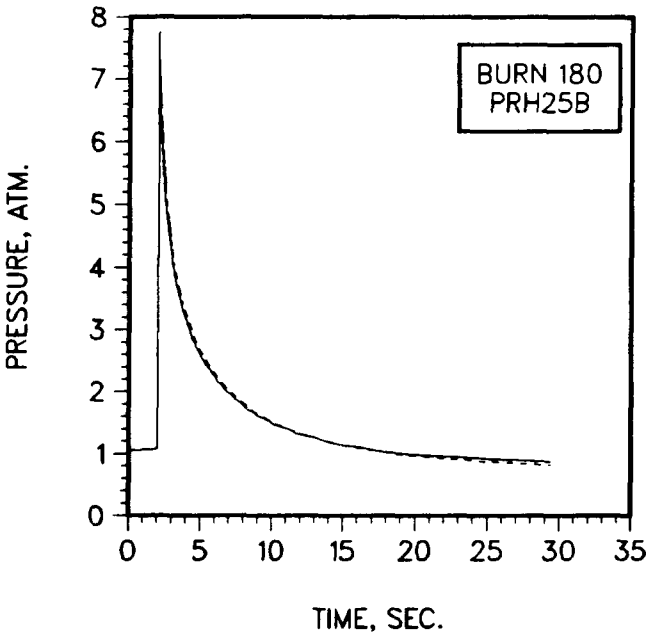
BURN 180
PRH25B
PRESSURE, ATM.
TIME, SEC.
0
1
2
3
4
5
6
7
8
0
5
10
15
20
25
30
35

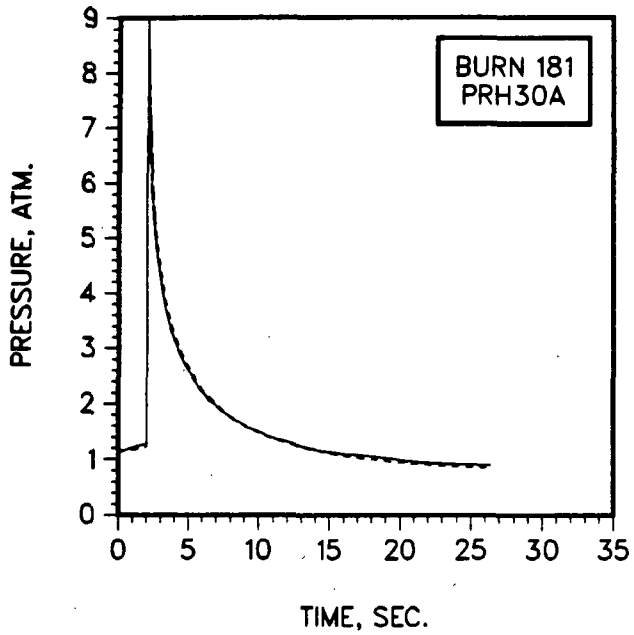
BURN 181
PRH30A
PRESSURE, ATM.
TIME, SEC.

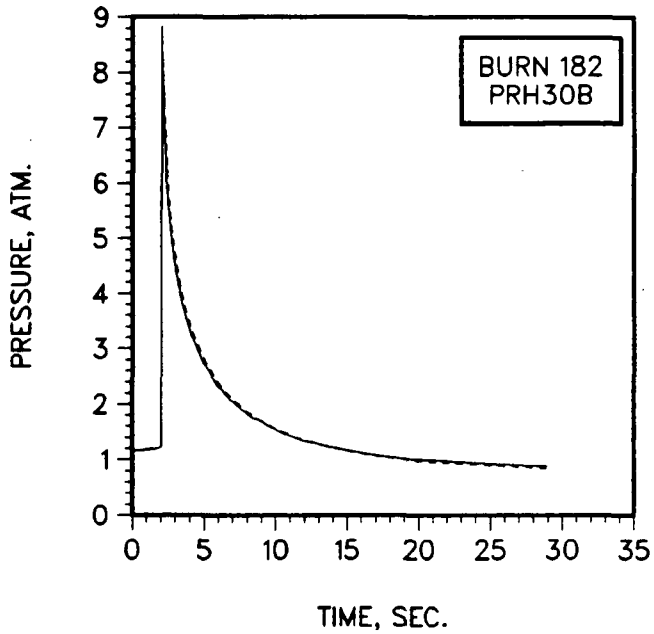
BURN 182
PRH30B
PRESSURE, ATM.
TIME, SEC.

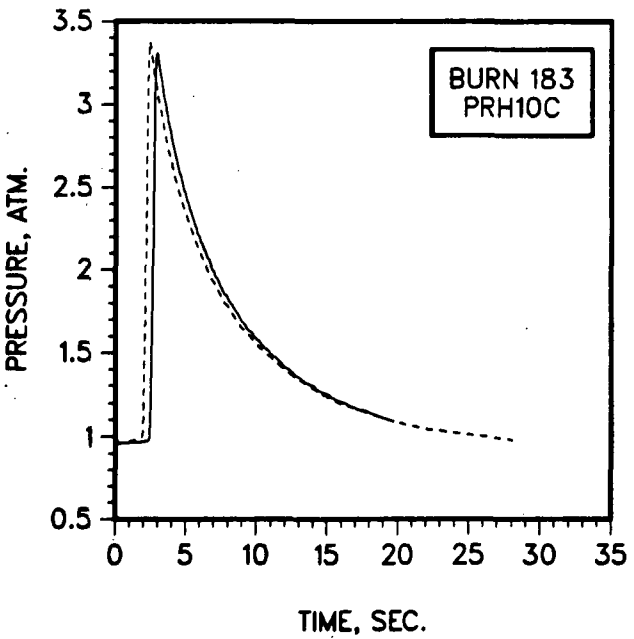
BURN 183
PRH10C
PRESSURE, ATM.
TIME, SEC.

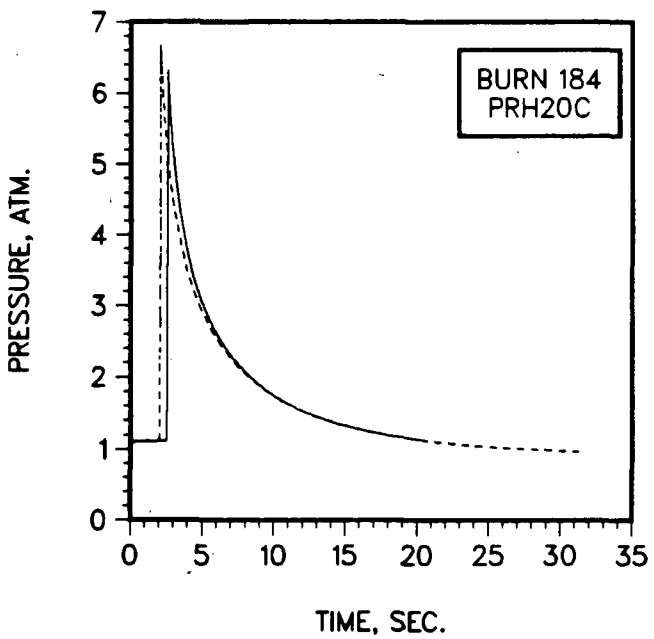
BURN 184
PRH20C
PRESSURE, ATM.
TIME, SEC.

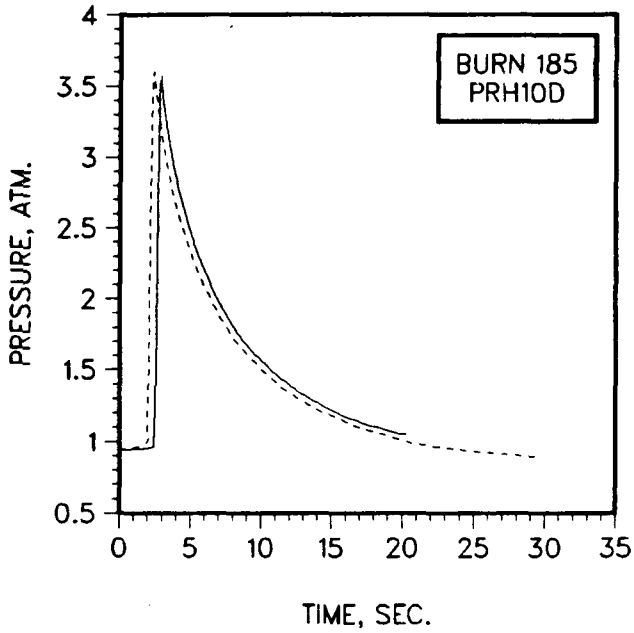
BURN 185
PRH10D
PRESSURE, ATM.
TIME, SEC.

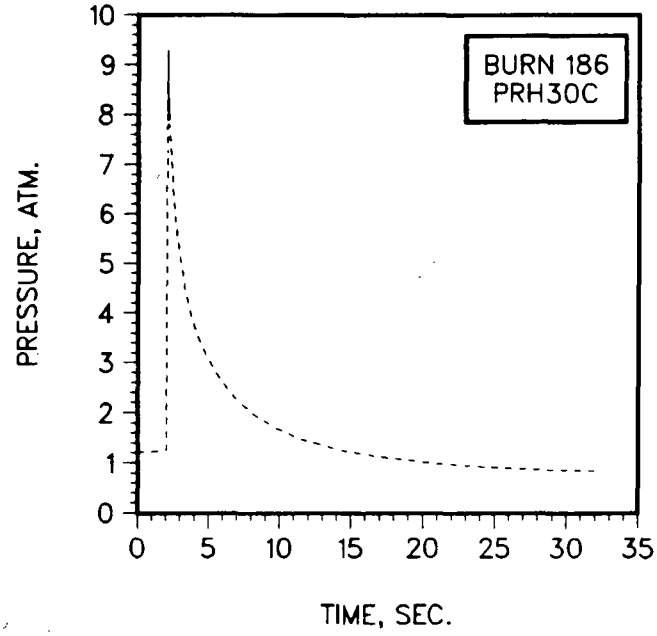
BURN 186
PRH30C
PRESSURE, ATM.
TIME, SEC.

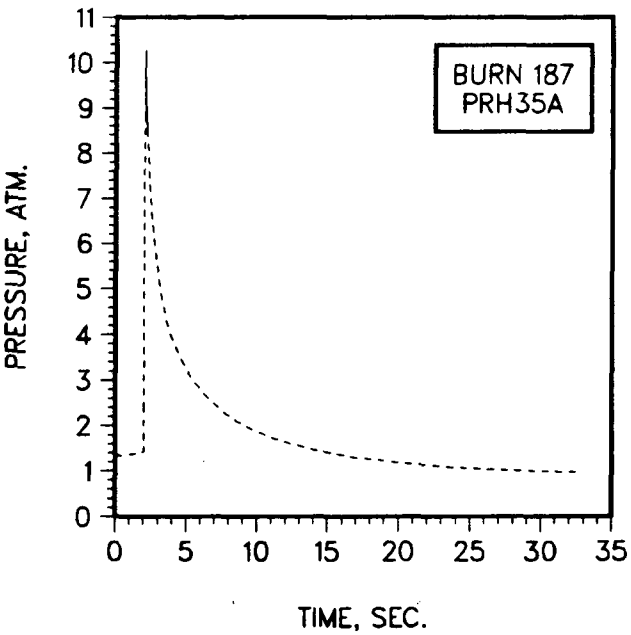
BURN 187
PRH35A
PRESSURE, ATM.
TIME, SEC.

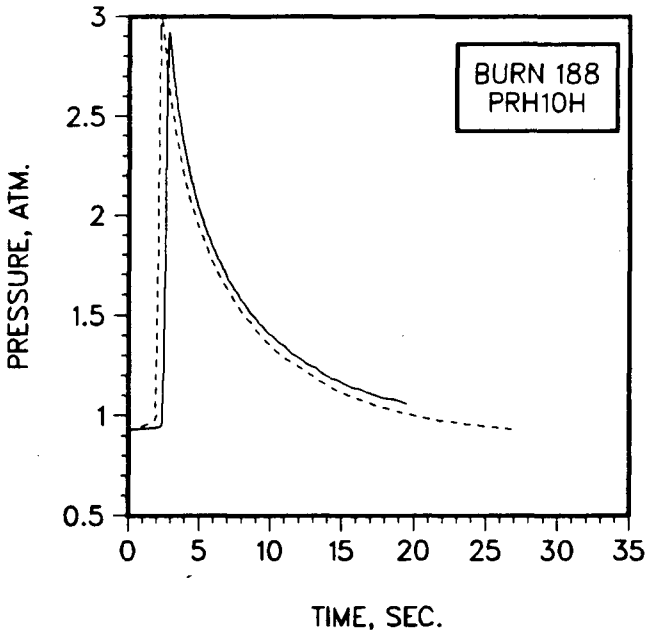
BURN 188
PRH10H
PRESSURE, ATM.
TIME, SEC.

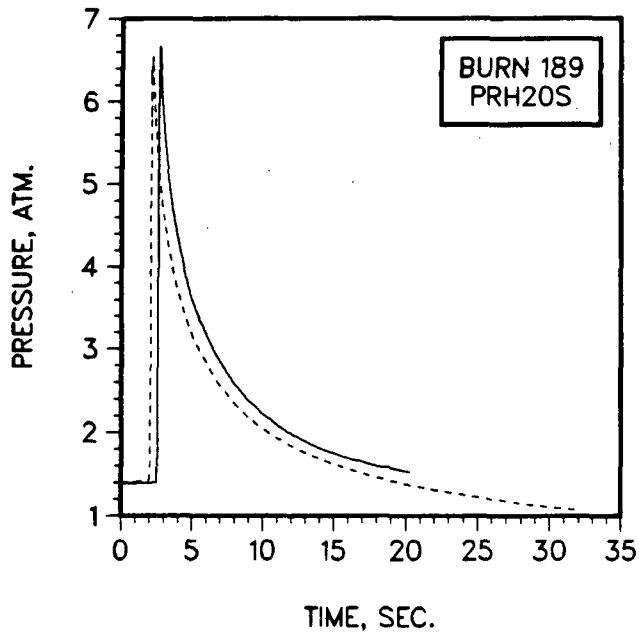
BURN 189
PRH20S
PRESSURE, ATM.
TIME, SEC.

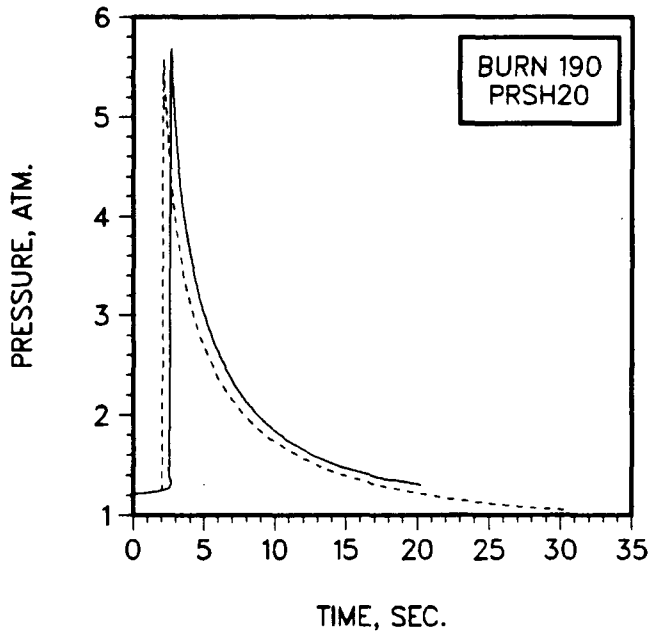
BURN 190
PRSH20
PRESSURE, ATM.
TIME, SEC.

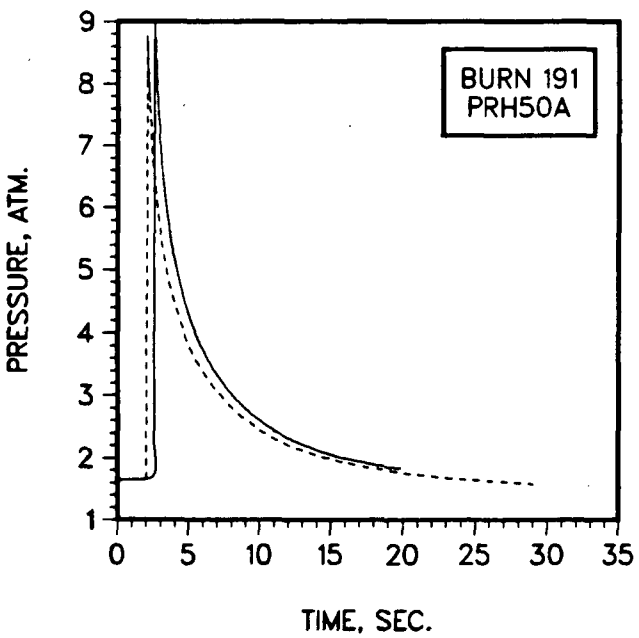
BURN 191
PRH50A
PRESSURE, ATM.
TIME, SEC.

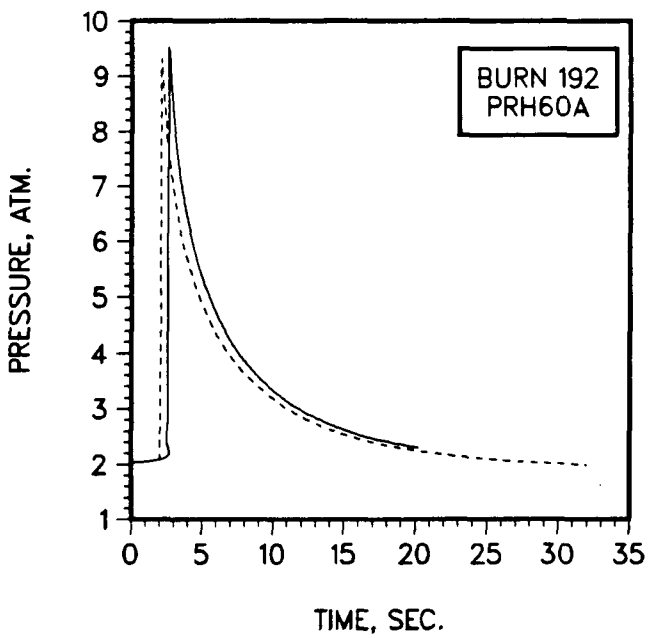
BURN 192
PRH60A
PRESSURE, ATM.
TIME, SEC.

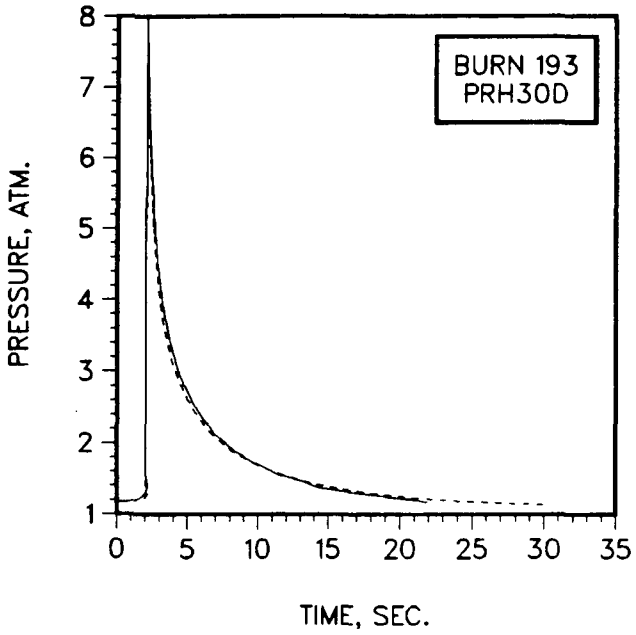
BURN 193
PRH30D
PRESSURE, ATM.
TIME, SEC.

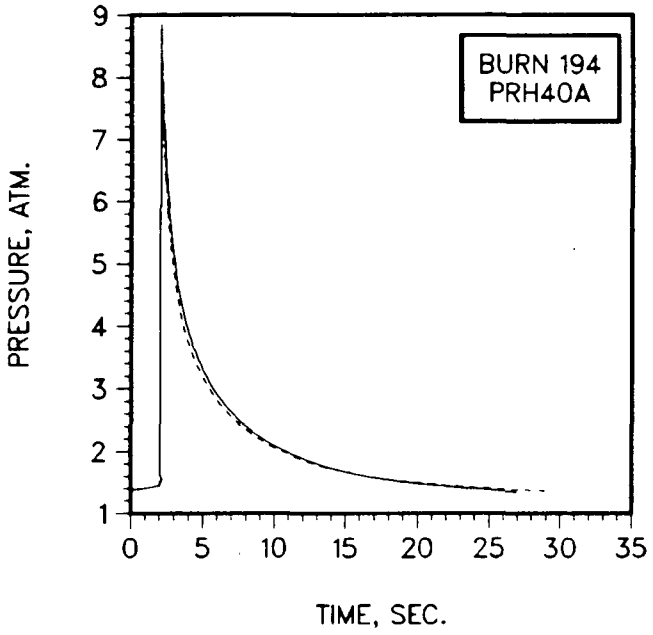
BURN 194
PRH40A
PRESSURE, ATM.
TIME, SEC.

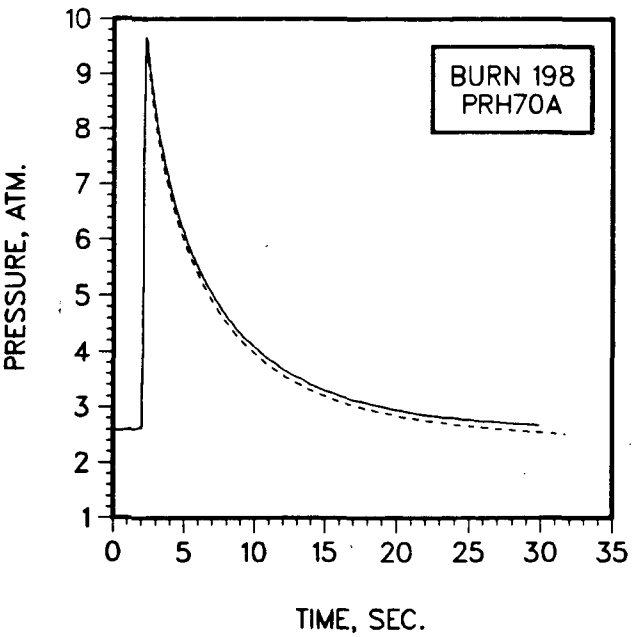
BURN 198
PRH70A
PRESSURE, ATM.
TIME, SEC.

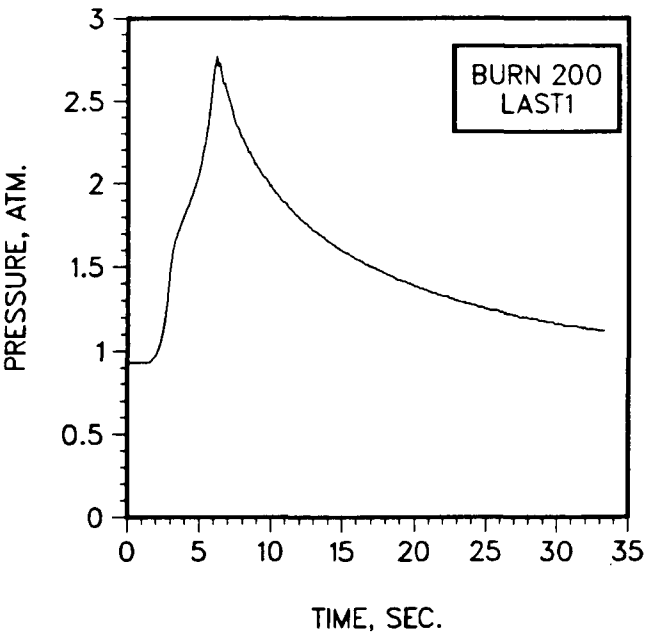
BURN 200
LAST1
PRESSURE, ATM.
TIME, SEC.

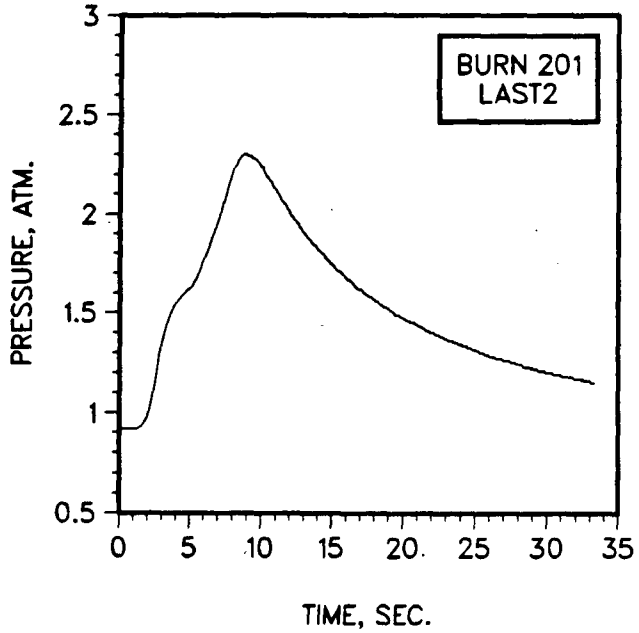
BURN 201
LAST2
PRESSURE, ATM.
TIME, SEC.

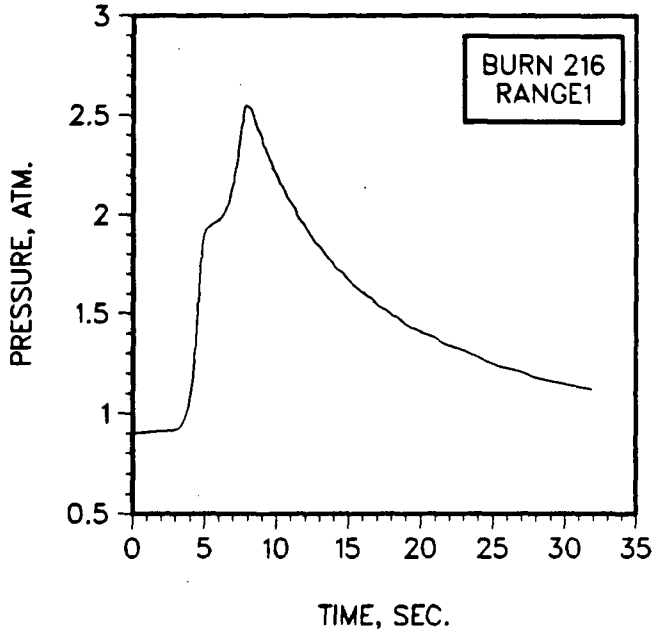
BURN 216
RANGE1
PRESSURE, ATM.
TIME, SEC.

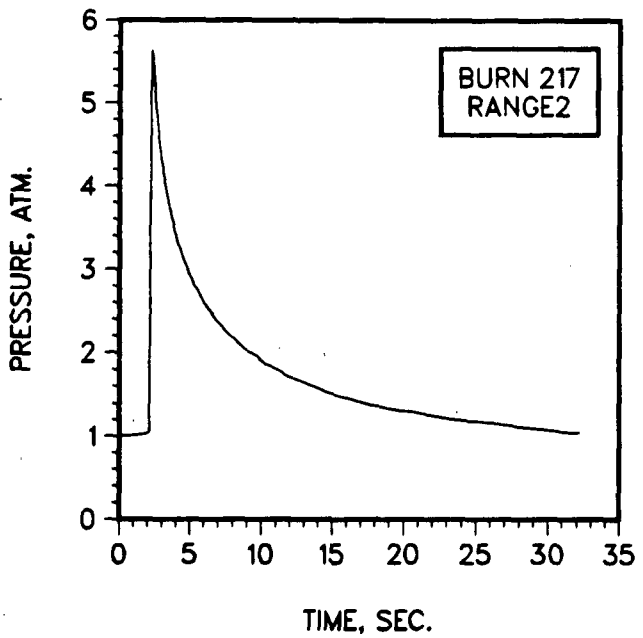
BURN 217
RANGE2
PRESSURE, ATM.
TIME, SEC.

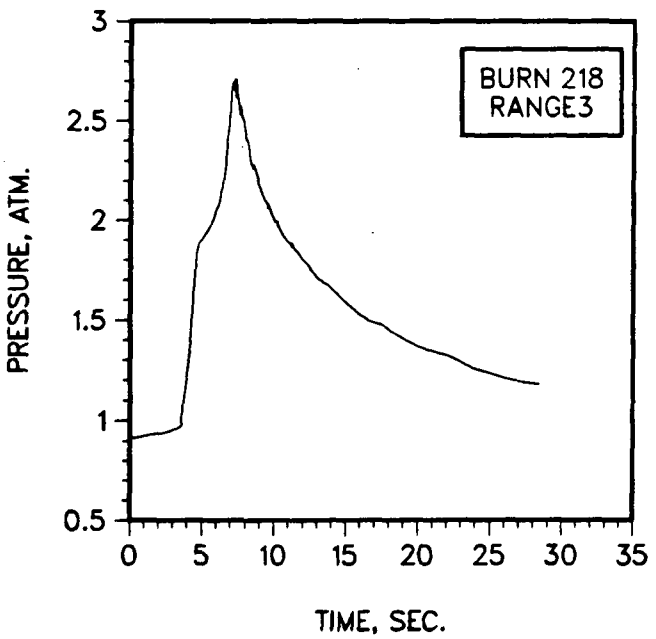
BURN 218
RANGE3
PRESSURE, ATM.
TIME, SEC.

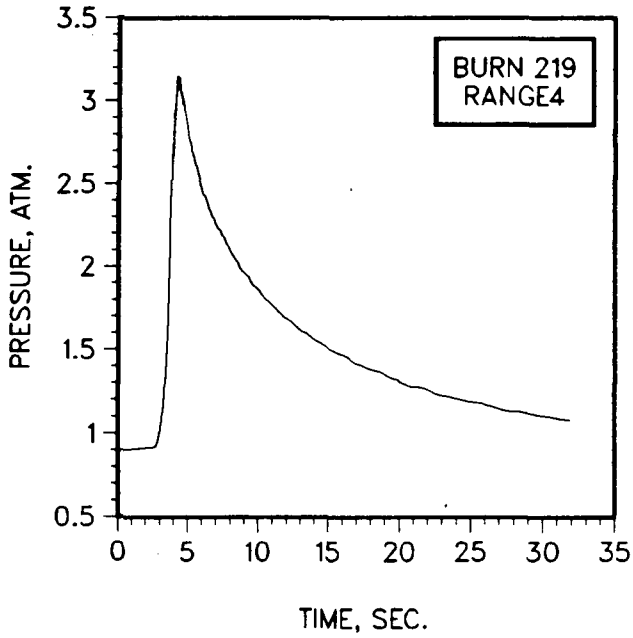
BURN 219
RANGE4
PRESSURE, ATM.
TIME, SEC.
3.5
3
2.5
2
1.5
1
0.5
0
5
10
15
20
25
30
35

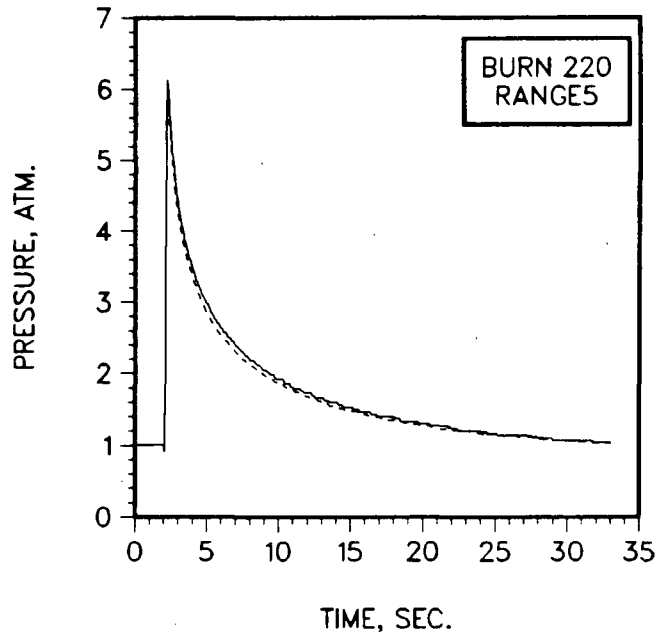
BURN 220
RANGE5
PRESSURE, ATM.
TIME, SEC.
7
6
5
4
3
2
1
0
5
10
15
20
25
30
35

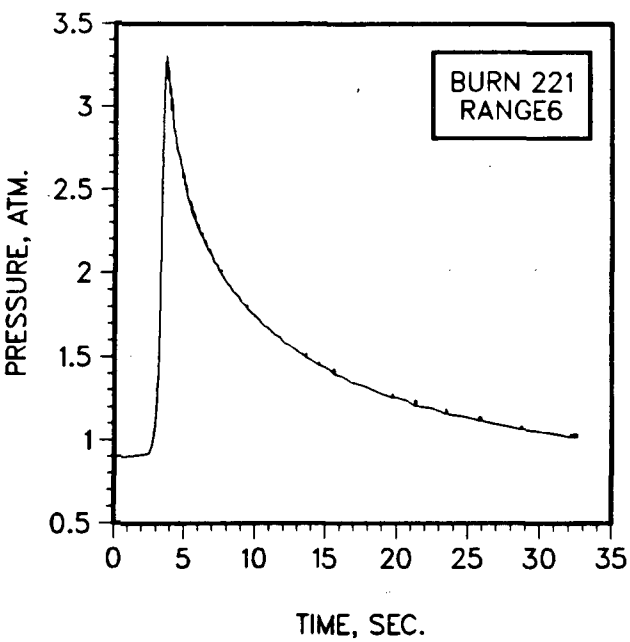
BURN 221
RANGE6
PRESSURE, ATM.
TIME, SEC.
3.5
3
2.5
2
1.5
1
0.5
0
5
10
15
20
25
30
35

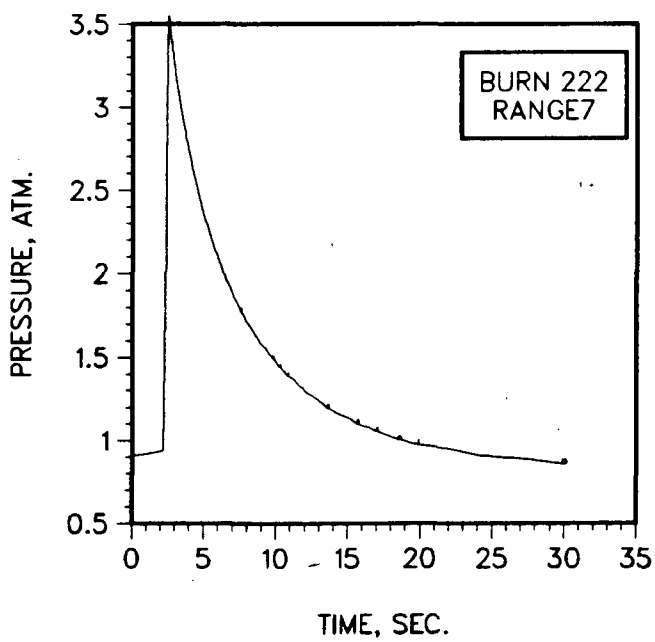
BURN 222
RANGE7
PRESSURE, ATM.
TIME, SEC.
3.5
3
2.5
2
1.5
1
0.5
0
5
10
15
20
25
30
35

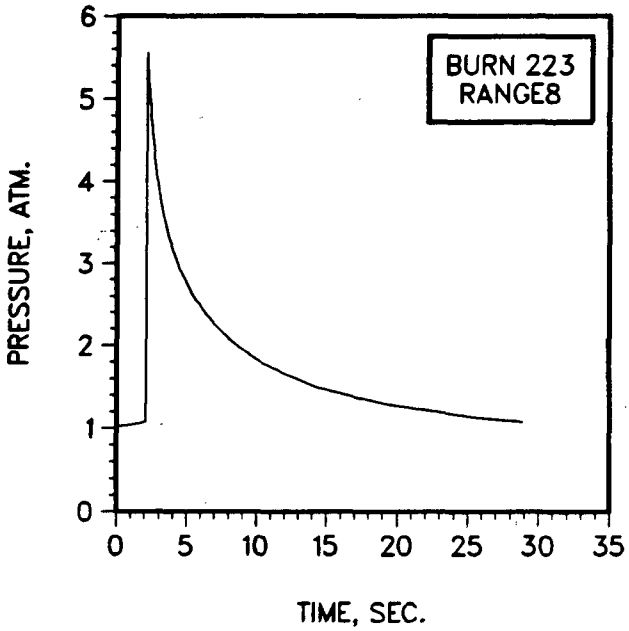
BURN 223
RANGE8
PRESSURE, ATM.
TIME, SEC.
0
1
2
3
4
5
6
0
5
10
15
20
25
30
35

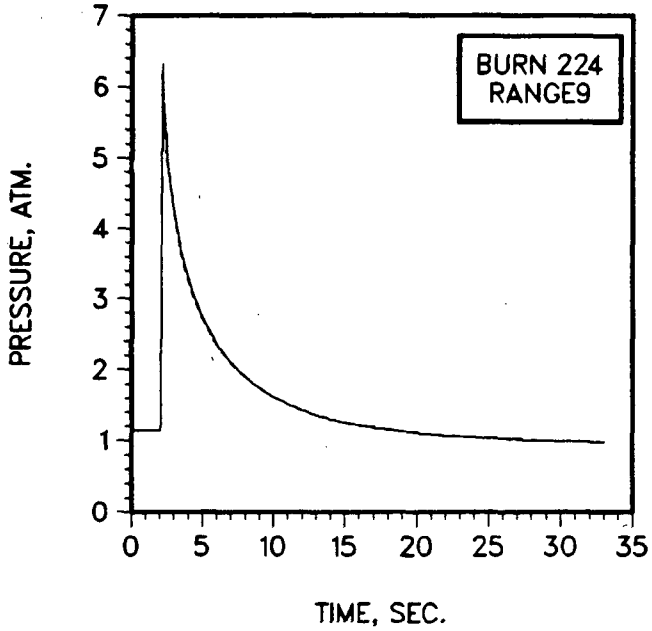
BURN 224
RANGE9
PRESSURE, ATM.
TIME, SEC.
0
1
2
3
4
5
6
7
0
5
10
15
20
25
30
35

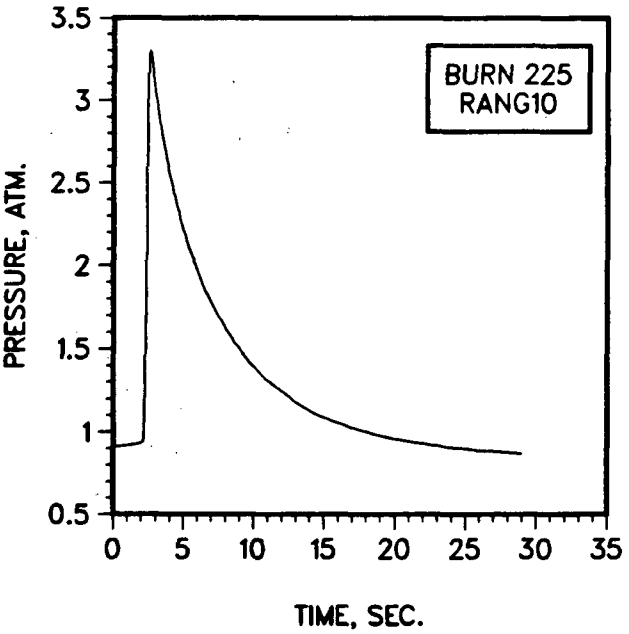
BURN 225
RANG10
PRESSURE, ATM.
TIME, SEC.
0.5
1
1.5
2
2.5
3
3.5
0
5
10
15
20
25
30
35

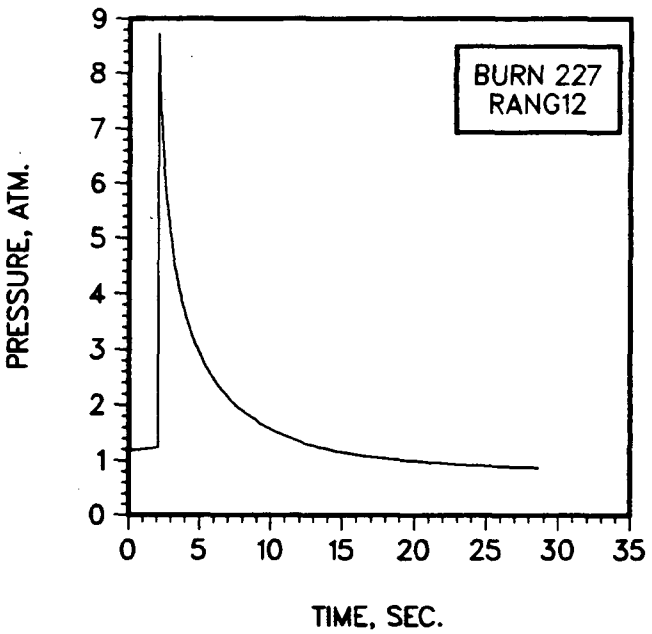
BURN 227
RANG12
PRESSURE, ATM.
TIME, SEC.
0
1
2
3
4
5
6
7
8
9
0
5
10
15
20
25
30
35

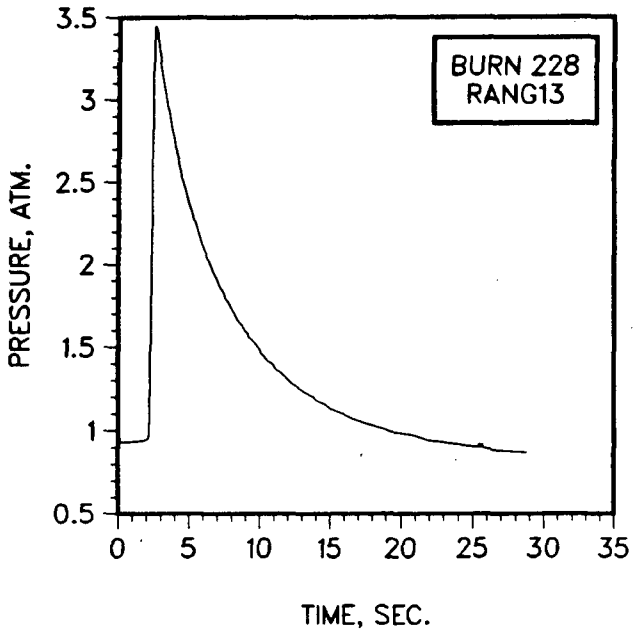
BURN 228
RANG13
PRESSURE, ATM.
TIME, SEC.

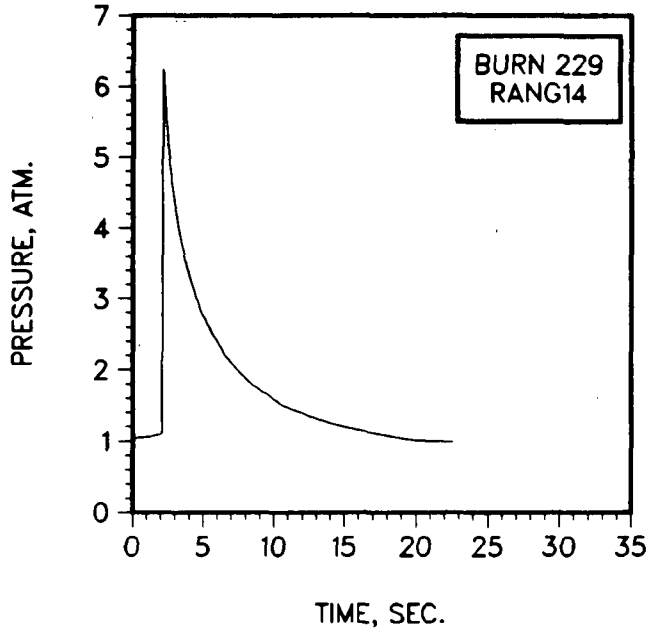
BURN 229
RANG14
PRESSURE, ATM.
TIME, SEC.

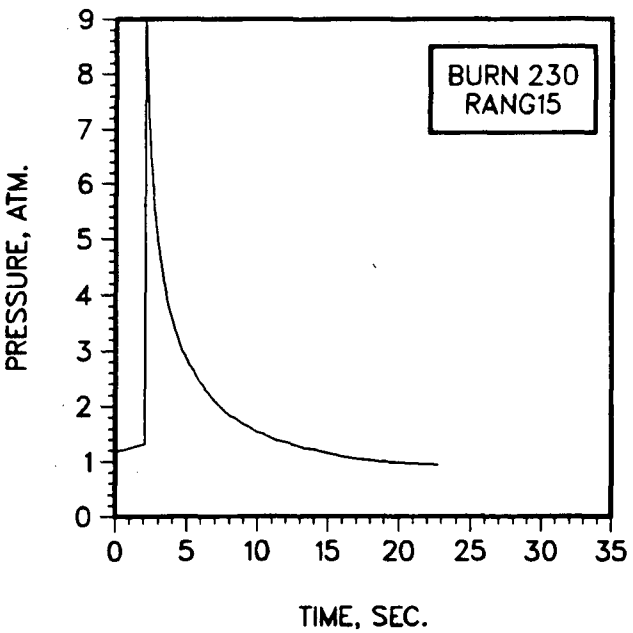
BURN 230
RANG15
PRESSURE, ATM.
TIME, SEC.

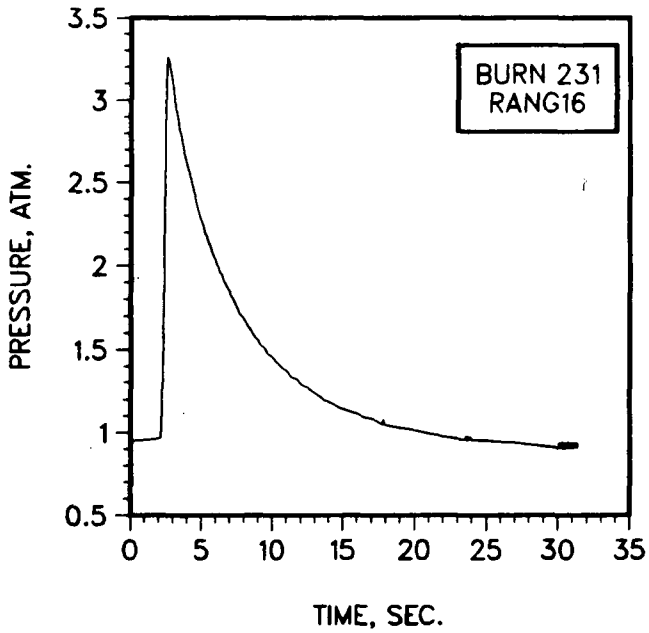
BURN 231
RANG16
PRESSURE, ATM.
TIME, SEC.

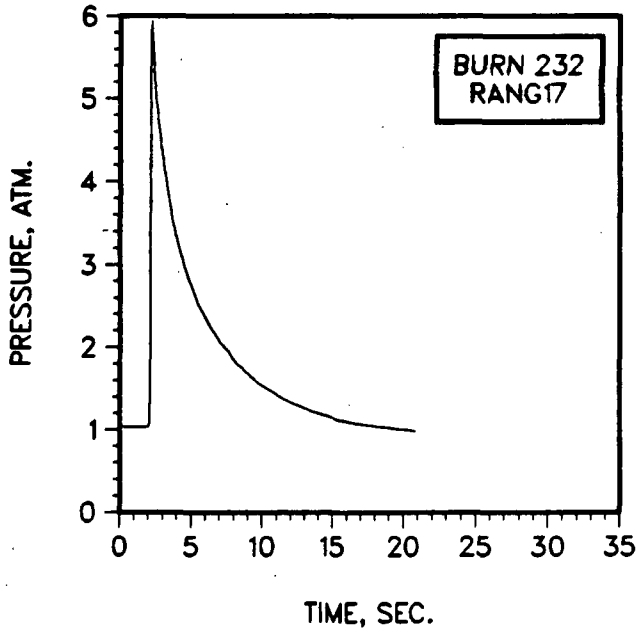
BURN 232
RANG17
PRESSURE, ATM.
TIME, SEC.
0
1
2
3
4
5
6
0
5
10
15
20
25
30
35

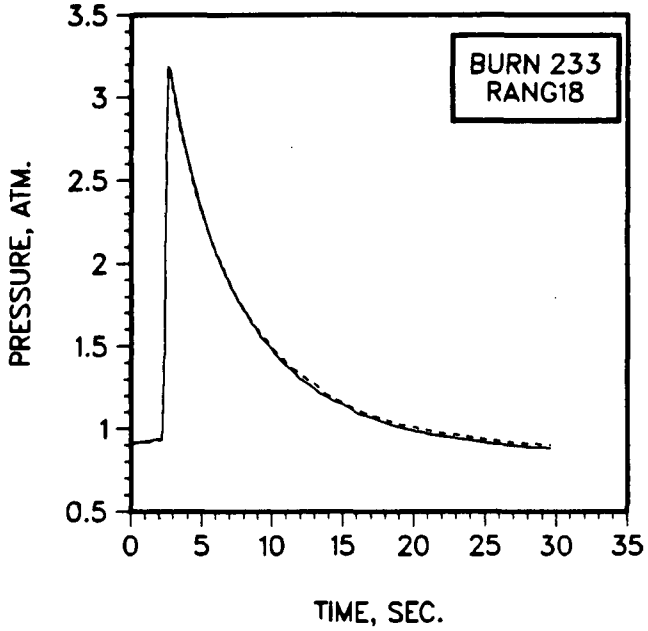
BURN 233
RANG18
PRESSURE, ATM.
TIME, SEC.
0.5
1
1.5
2
2.5
3
3.5
0
5
10
15
20
25
30
35

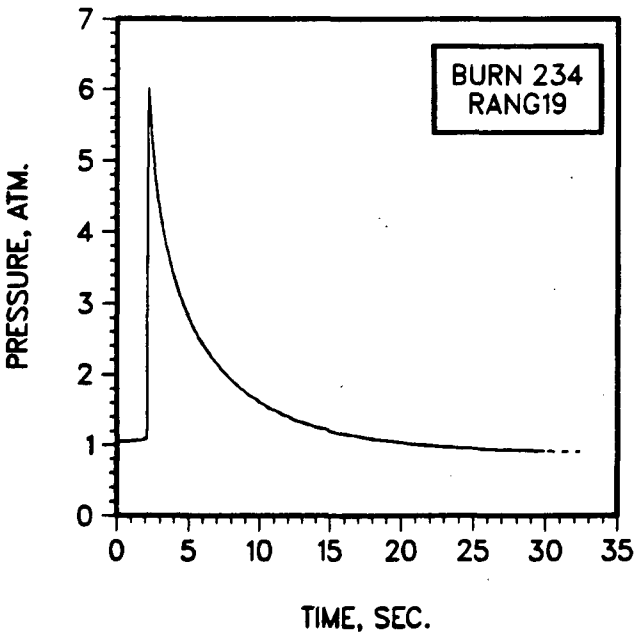
BURN 234
RANG19
PRESSURE, ATM.
TIME, SEC.
0
1
2
3
4
5
6
7
0
5
10
15
20
25
30
35

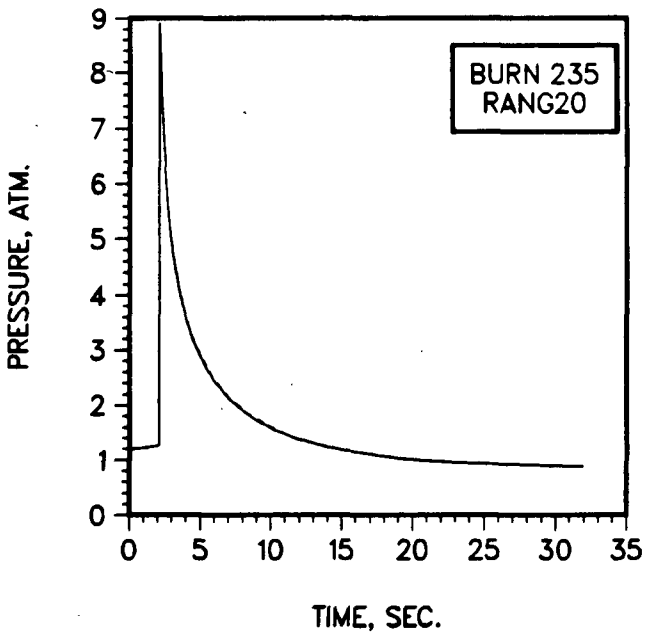
BURN 235
RANG20
PRESSURE, ATM.
TIME, SEC.
0
1
2
3
4
5
6
7
8
9
0
5
10
15
20
25
30
35

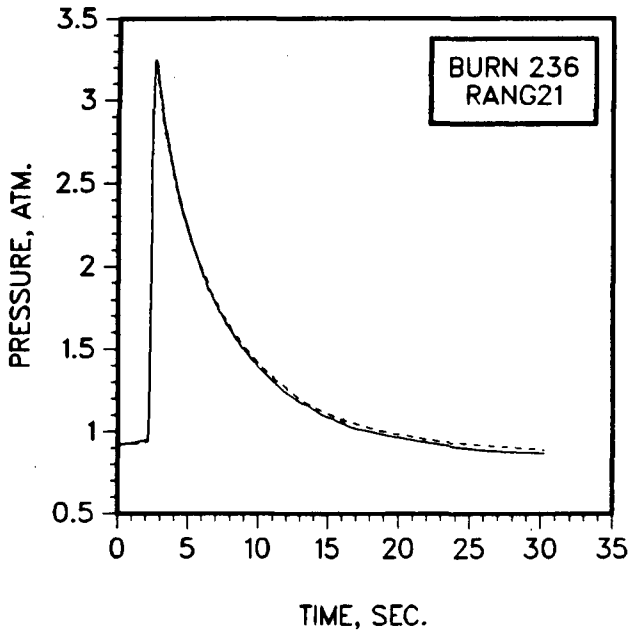
BURN 236
RANG21
PRESSURE, ATM.
TIME, SEC.
3.5
3
2.5
2
1.5
1
0.5
0
5
10
15
20
25
30
35

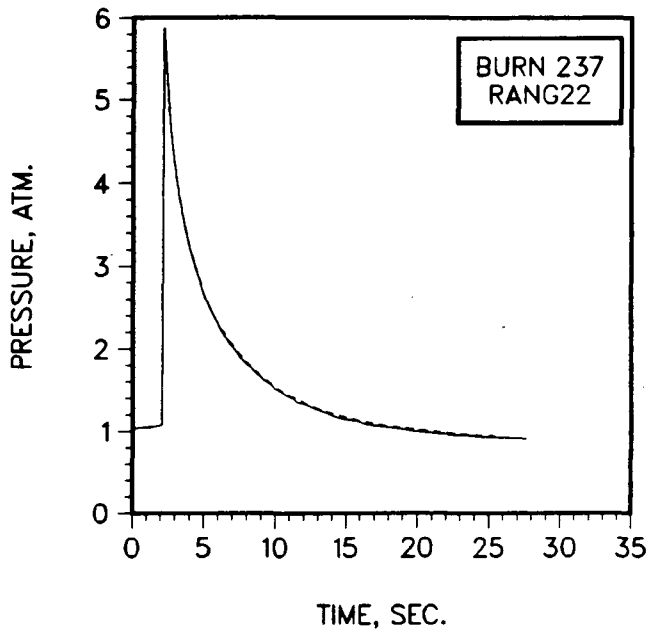
BURN 237
RANG22
PRESSURE, ATM.
TIME, SEC.
6
5
4
3
2
1
0
5
10
15
20
25
30
35

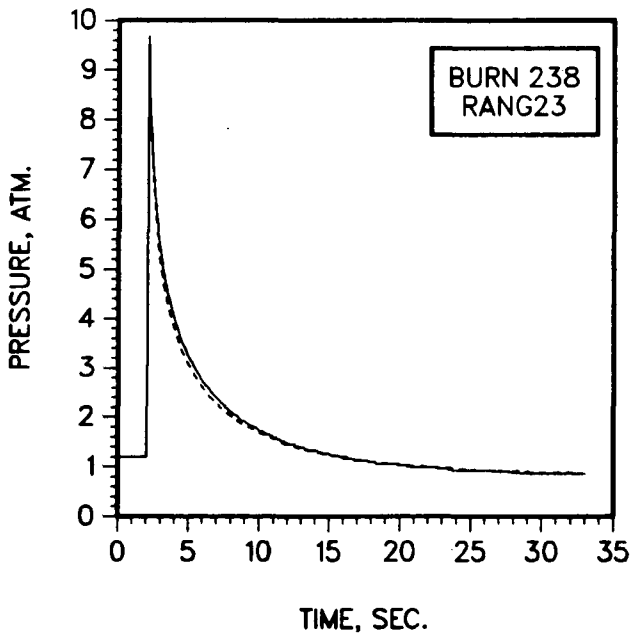
BURN 238
RANG23
PRESSURE, ATM.
TIME, SEC.
10
9
8
7
6
5
4
3
2
1
0
5
10
15
20
25
30
35

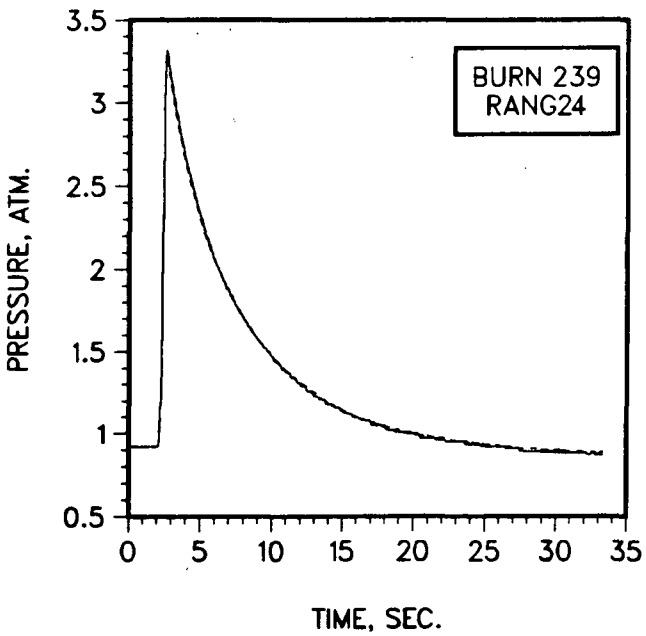
BURN 239
RANG24
PRESSURE, ATM.
TIME, SEC.
3.5
3
2.5
2
1.5
1
0.5
0
5
10
15
20
25
30
35

U. S. Government Printing Office
Receiving Branch (Attn: NRC Stock)
8610 Cherry Lane
Laurel, MD 20707
250 Copies for R3

U. S. Bureau of Mines
Pittsburgh Research Center
P. O. Box 18070
Pittsburgh, PA 15236
Attn: M. Hertzberg

U. S. Nuclear Regulatory Commission (3)
Office of Nuclear Regulatory Research
Washington, DC 20555
Attn: R. T. Curtis
J. T. Larkins
P. Worthington

U. S. Nuclear Regulatory Commission (3)
Office of Nuclear Regulatory Research
Washington, DC 20555
Attn: B. S. Burson
M. Silverberg
R. W. Wright

U. S. Nuclear Regulatory Commission (6)
Office of Nuclear Reactor Regulation
Washington, DC 20555
Attn: J. K. Long
J. F. Meyer
R. Palla
K. I. Parczewski
G. Quittschreiber
D. D. Yue

U. S. Nuclear Regulatory Commission (6)
Office of Nuclear Reactor Regulation
Washington, DC 20555
Attn: V. Benaroya
W. R. Butler
G. W. Knighton
T. M. Su
Z. Rosztoczy
C. G. Tinkler

U. S. Nuclear Regulatory Commission
Phillips Building
7920 Norfolk Avenue
Bethesda, MD 20014
Attn: C. J. Anderson

U. S. Department of Energy (2)
Operational Safety Division
Albuquerque Operations Office
P. O. Box 5400
Albuquerque, NM 87185
Attn: J. R. Roeder, Director
Dr. M. Peehs

Acurex Corporation
485 Clyde Avenue
Mountain View, CA 94042

American Electric Power Service Corp.
Room 1158-D
2 Broadway
New York, NY 10004
Attn: K. Vehstedt

Applied Sciences Association, Inc.
P. O. Box 2687
Palos Verdes Pen., CA 90274
Attn: D. Swanson

Argonne National Laboratory (2)
9700 South Cass Avenue
Argonne, IL 60439
Attn: H. M. Chung
R. P. Anderson

Battelle Columbus Laboratory (2)
505 King Avenue
Columbus, OH 43201
Attn: P. Cybulskis
R. Denning

Bechtel Power Corporation
P. O. Box 3965
San Francisco, CA 94119
Attn: R. Tosetti

Bechtel Power Corporation (2)
15740 Shady Grove Road
Gaithersburg, MD 20877
Attn: D. Ashton
D. Patton

Boeing
12517 SE 42nd Street
Bellevue, WA 98006
Attn: T. M. Murray

Brookhaven National Laboratory (2)
Upton, NY 11973
Attn: R. A. Bari
T. Pratt

Cleveland Electric Illuminating Co.
Perry Nuclear Plant
10 Center Road
North Perry, OH 44081
Attn: R. Stratman

Combustion Engineering Incorporated
1000 Prospect Hill Road
Windsor, CT 06095
Attn: J. D. Boyajian

Donald C. Cook Nuclear Station
Indiana & Michigan Electric Company
P. O. Box 458
Bridgman, MI 49106
Attn: D. Nelson

Duke Power Company (2)
P. O. Box 33189
Charlotte, NC 28242
Attn: F. G. Hudson
A. L. Sudduth

EG&G Idaho
Willow Creek Building, W-3
P. O. Box 1625
Idaho Falls, ID 83415
Attn: Server Sadik

Electric Power Research Institute (5)
3412 Hillview Avenue
Palo Alto, CA 94303
Attn: J. J. Haugh
R. Leyse
K. A. Nilsson
G. Thomas
L. B. Thompson

Factory Mutual Research Corporation
P. O. Box 688
Norwood, MA 02062
Attn: R. Zalosh

Fauske & Associates (2)
627 Executive Drive
Willowbrook, IL 60521
Attn: R. Henry
M. Plys

GPU Nuclear
100 Interpace Parkway
Parsippany, NJ 07054
Attn: J. E. Flaherty

General Electric Co.
175 Curtner Avenue
Mail Code N 1C157
San Jose, CA 95125
Attn: K. W. Holtzclaw

General Physics Corporation (8)
1000 Century Plaza
Columbia, MD 21044
Attn: S. B. Coon
G. J. Dickleman
E. E. Huff
C. Kupiec
W.J. Newell
J. M. Sutch
E. H. Trottier
J. N. Zerbo

General Public Utilities
Three Mile Island Nuclear Station
P. O. Box 480
Middletown, PA 17057
Attn: N. Brown

Indiana and Michigan Electric Company
P. O. Box 458
Bridgman, MI 49106
Attn: J. Dickson

Institute of Nuclear Power Operations (2)
1820 Water Place
Atlanta, GA 30339
Attn: S. Visner
E. Zebroski

Los Alamos National Laboratory (4)
P. O. Box 1663
Los Alamos, NM 87545
Attn: H. S. Cullingford
R. Gido
J. Carson Mark
G. Schott

Massachusetts Institute of Technology
Room 1-276
Cambridge, MA 02139
Attn: M. N. Fardis

University of Michigan
Department of Aerospace Engineering
Ann Arbor, MI 47109
Attn: Martin Sichel

Mississippi Power & Light (3)
P. O. Box 1640
Jckson, MS 39205
Attn: D. Bigbee
S. H. Hobbs
J. Richardson

New Mexico State University
Mechanical Engineering Department
Las Cruces, NM 88001
Attn: G. P. Mulholland

Northwestern University
Chemical Engineering Department
Evanston, IL 60201
Attn: S. G. Bankoff

NUS Corporation
4 Research Place
Rockville, MD 20850
Attn: R. Sherry

Offshore Power System (2)
8000 Arlington Expressway
Box 8000
Jacksonville, FL 32211
Attn: G. M. Fuls
D. H. Walker

Pennsylvania Power and Light
Susquehanna SES
P. O. Box 467
Berwick, PA 18603
Attn: R. DeVore

Power Authority State of NY (2)
10 Columbus Circle
New York, NY 10019
Attn: R. E. Deem
S. S. Iyer

Purdue University
School of Nuclear Engineering
West Lafayette, IN 47907
Attn: T. G. Theofanous

Sandia National Laboratories (20)
Organization 6427
P.O. Box 5800
Albuquerque, NM 87185
Attn: G. Shaw

Sandia National Laboratories (6)
Livermore, CA 94550
Attn: W. T. Ashurst, 8523
K. D. Marx, 8523
W. J. McLean, 8360
M. A. Pound, 8024
B. R. Sanders, 8523
P. K. Barr, 8363

Stone & Webster Engineering Corporation
245 Summer Street/9
Boston, MA 02143
Attn: G. Brown

Dr. Roger Strehlow
505 South Pine Street
Champaign, IL 61820

TVA
400 Commerce
W9C157-CD
Knoxville, TN 37902
Attn: Wang Lau

Technology for Energy Corporation (2)
10770 Dutchtown Road
Knoxville, TN 37922
Attn: J. Carter
E. L. Fuller

Thompson Associates
639 Massachusetts Avenue
Third Floor
Cambridge, MA 02139
Attn: Timothy Woolf

UCLA
Nuclear Energy Laboratory
405 Hilgard Avenue
Los Angeles, CA 90024
Attn: I. Catton

Virginia Electric & Power Company (3)
Northanna Power Station
P. O. Box 402
Mineral, VA 23117
Attn: A. Hogg
A. K. White
E. L. Wilson

Virginia Electric & Power Company
P. O. Box 26666
James River Plaza
Richmond, VA 23261
Attn: R. Garner

Westinghouse Corporation (3)
P. O. Box 355
Pittsburgh, PA 15230
Attn: N. Liparulo
J. Olhoeft
V. Srinivas

Westinghouse Electric Corporation
Monroeville Nuclear Center
Monroeville, PA 15146
Attn: P. Lain

Westinghouse Hanford Company (3)
P. O. Box 1970
Richland, WA 99352
Attn: G. R. Bloom
L. Muhlstein
R. D. Peak

University of Wisconsin
Nuclear Engineering Department
1500 Johnson Drive
Madison, WI 53706
Attn: M. L. Corradini

Zion Nuclear Power Station
Commonwealth Edison Company
Shiloh Blvd. and Lake Michigan
Zion, IL 60099
Attn: C. Schultz

Director of Research, Science & Education
CEC
Rue De La Loi 200
1049 Brussels
BELGIUM
Attn: B. Tolley

AEC, Ltd. (2)
Whiteshell Nuclear Research Establishment
Pinawa, Manitoba
CANADA
Attn: D. Liu
H. Tamm

McGill University (3)
315 Querbes
Outremont, Quebec
CANADA H2V 3W1
Attn: John H. S. Lee

Battelle Institut E. V.
Am Roemerhof 35
6000 Frankfurt am Main 90
FEDERAL REPUBLIC OF GERMANY
Attn: Dr. Werner Baukal

Gesellschaft fur Reaktorsicherheit (GRS)
Postfach 101650
Glockengasse 2
5600 Koeln 1
FEDERAL REPUBLIC OF GERMANY
Attn: Dr. M. V. Banaschik

Gesellschaft fur Reaktorsicherheit (GRS mbH) (2)
8046 Garching
FEDERAL REPUBLIC OF GERMANY
Attn: E. F.Hicken
H. L. Jahn

Kernforschungszentrum Karlsruhe (3)
Postfach 3640
75 Karlsruhe
FEDERAL REPUBLIC OF GERMANY
Attn: Dr. S. Hagen
Dr. J. P. Hosemann
Dr. M. Reimann

Kraftwerk Union
Hammerbacherstrasse 12 & 14
Postfach 3220
D-8520 Erlangen 2
FEDERAL REPUBLIC OF GERMANY
Attn: Dr. K. Hassman

Technische Universitaet Muenchen
D-8046 Garching
FEDERAL REPUBLIC OF GERMANY
Attn: Dr. H. Karwat

CNEN NUCLIT
Rome
ITALY
Attn: A. Morici

Swedish State Power Board
El-Och Vaermeteknik
SWEDEN
Attn: Eric Ahlstroem

AERE Harwell (2)
Didcot
Oxfordshire OX11 ORA
UNITED KINGDOM
Attn: J. Gittus, AETB
J. R. Matthews, TPD

Berkeley Nuclear Laboratory
Berkeley GL 139PB
Gloucestershire
UNITED KINGDOM
Attn: J. E. Antill

British Nuclear Fuels, Ltd
Building 396
Springfield Works
Salwick, Preston
Lancs
UNITED KINGDOM
Attn: W. G. Cunliffe

National Nuclear Corp. Ltd.
Cambridge Road
Whetestone, Leicester, LE83LH
UNITED KINGDOM
ATTN: R. MAY

Simon Engineering Laboratory
University of Manchester
M139PL
UNITED KINGDOM
Attn: Prof. W. B. Hall

Anthony R. Taig
GDCD/CEGB
Barnwood, Gloucester
Gloucestershire
UNITED KINGDOM

UKAEA Safety & Reliability Directorate
Wigshaw Lane, Culcheth
Warrington WA34NE
Cheshire
UNITED KINGDOM (3)
Attn: J. G. Collier
S. F. Hall

UKAEA AEE Winfrith
214/A32
Dorchester
Dorset DT2 8DH
UNITED KINGDOM
Attn: A. J. Wickett

Sandia Distribution:
1131 W. B. Benedick
1512 J. C. Cummings
1513 A. C. Ratzel
6400 A. W. Snyder
6410 J. W. Hickman
6411 A. S. Benjamin
6412 A. L. Camp
6414 D. M. Ericson, Jr.
6415 F. E. Haskin
6415 S. E. Dingman
6420 J. V. Walker
6421 P. S. Pickard
6422 D. A. Powers
6422 W. W. Tarbell
6423 K. Bolt
6425 W. J. Camp
6427 M. Berman
6427 J. T. Hitchcock
6427 B. W. Marshall, Jr. (15)
6427 L. S. Nelson
6427 M. P. Sherman
6427 D. W. Stamps
6427 S. R. Tieszen
6427 C. C. Wong
6440 D. A. Dahlgren
6442 W. A. von Riesemann
6444 R. K. Byers
6444 W. H. Schmidt
6445 V. J. Dandini
6449 K. D. Bergeron
3141 C. M. Ostrander (5)
3151 W. L. Garner

NRC FORM 335 (2 84) NRCM 1102, 3201, 3202

U.S. NUCLEAR REGULATORY COMMISSION

BIBLIOGRAPHIC DATA SHEET

SEE INSTRUCTIONS ON THE REVERSE

1 REPORT NUMBER (Assigned by TIDC, add Vol No., if any)

NUREG/CR-3468
SAND84-0383

2 TITLE AND SUBTITLE

Hydrogen:Air:Steam Flammability Limits and Combustion Characteristics in the FITS Vessel

3 LEAVE BLANK

4 DATE REPORT COMPLETED

MONTH: August YEAR: 1986

5 AUTHOR(S)

Billy W. Marshall, Jr.

6 DATE REPORT ISSUED

MONTH: December YEAR: 1986

7 PERFORMING ORGANIZATION NAME AND MAILING ADDRESS (Include Zip Code)

Sandia National Laboratories
Division 6427
P.O. Box 5800
Albuquerque, NM 87185

8 PROJECT/TASK/WORK UNIT NUMBER

9 FIN OR GRANT NUMBER

A1246

10 SPONSORING ORGANIZATION NAME AND MAILING ADDRESS (Include Zip Code)

Division of Reactor System Safety
Accident Evaluation Branch
Office of Nuclear Regulatory Research
U.S. Nuclear Regulatory Research
Washington, DC 20555

11a TYPE OF REPORT

Technical

b PERIOD COVERED (Inclusive dates)

12 SUPPLEMENTARY NOTES

13 ABSTRACT (200 words or less)

Experimentally observed flammability limits of hydrogen:air:steam mixtures in both turbulent and quiescent environments were measured and a correlation developed that describes the three-component flammability limit. The combustion pressure data measured for the hydrogen:air:steam tests indicate that the addition of steam reduces the normalized peak combustion pressure (P_{max}/P_o) as compared to equivalent hydrogen:air burns. Turbulence was found to affect the extent of combustion and other combustion characteristics of the lean hydrogen burns (i.e., ≤10% hydrogen by volume) where bouyancy governs flame propagation.

The experimentally measured pressure decays were used to infer the "global" heat transfer characteristics during the postcombustion cooling phase. Convection was found to dominate the time-integrated heat transfer of the leaner (<10%) hydrogen:air burns, accounting for 50 to 70% of the postcombustion heat transfer. Radiation was slightly more prevalent than convection for the hydrogen:air burns near stoichiometry. When moderate quantities of steam were added to the environment, radiation became the dominant postcombustion cooling mechanism due to the increase in bulk gas emittance. If richer steam concentrations were added to the environment, radiation and convection appear to be equally important heat transfer mechanisms.

14 DOCUMENT ANALYSIS - a KEYWORDS/DESCRIPTORS

Flammability, Flammability Limits, Deflagration, Combustion, Hydrogen Combustion, Reactor Safety

b IDENTIFIERS/OPEN ENDED TERMS

15 AVAILABILITY STATEMENT

GPO/NTIS

16 SECURITY CLASSIFICATION

(This page) Unclassified

(This report) Unclassified

17 NUMBER OF PAGES

18 PRICE

☆ U.S. GOVERNMENT PRINTING OFFICE: 1987—773-049/41029